

GDS-80

The BioWare gene gun, which has been mentioned in this book, is the same product as Wealtec GDS-80, and it has been tested in many aspects of applications. For instances, to deliver DNA into the cultured cells, epidermal cells of live mice, plant cells, and so on. Each of them has different optimal conditions, and has been announced on many different popular academic journals which were authorized to be listed here. Users can find their references in this reference book which are suitable for their experiments. The papers which listed here are in different kinds of experiment topics as followed.

Incubated Cell Line

- Chang ML, Chen JC, Yeh CT, Chang MY, Liang CK, Chiu CT, Lin DY, and Liaw YF. (2008) Gene gun bombardment with DNA-coated gold particles is a potential alternative to hydrodynamics-based transfection for delivering genes into superficial hepatocytes. *Hum Gene Ther.* 19(4):391-5.
- Cheng WF, Chang MC, Sun WZ, Lee CN, Lin HW, Su YN, Hsieh CY, and Chen CA. (2008) Connective tissue growth factor linked to the E7 tumor antigen generates potent antitumor immune responses mediated by an antiapoptotic mechanism. *Gene Ther.* 15(13):1007-16
- Cheng WF, Hung CF, Chen CA, Lee CN, Su YN, Chai CY, Boyd DA, Hsieh CY, and Wu TC. (2005) Characterization of DNA vaccines encoding the domains of calreticulin for their ability to elicit tumor-specific immunity and antiangiogenesis. *Vaccine.* 23(29):3864-74.
- Cheng WF, Lee CN, Chang MC, Su YN, Chen CA, and Hsieh CY. (2005) Antigen-specific CD8⁺ T lymphocytes generated from a DNA vaccine control tumors through the Fas-FasL pathway. *Mol Ther.* 12(5):960-8.
- Cheng WP, Hung HF, Wang BW, and Shyu KG. (2008) The molecular regulation of GADD153 in apoptosis of cultured vascular smooth muscle cells by cyclic mechanical stretch. *Cardiovasc Res.* 77(3):551-9.
- Chen SC, Wang BW, Wang DL, and Shyu KG. (2008) Hypoxia induces discoidin domain receptor-2 expression via the p38 pathway in vascular smooth muscle cells to increase their migration. *Biochem Biophys Res Commun.* 374(4):662-7.

- Hsieh CY, Chen CA, Huang CY, Chang MC, Lee CN, Su YN, and Cheng WF. (2007) IL-6-encoding tumor antigen generates potent cancer immunotherapy through antigen processing and anti-apoptotic pathways. *Mol Ther.* 15(10):1890-7.
- Tu CF, Lin CC, Chen MC, Ko TM, Lin CM, Wang YC, and Lai MD. (2007) Autologous neu DNA vaccine can be as effective as xenogenic neu DNA vaccine by altering administration route. *Vaccine.* 25(4):719-28.
- Wang BW, Chang H, Kuan P, and Shyu KG. (2008) Angiotensin II activates myostatin expression in cultured rat neonatal cardiomyocytes via p38 MAP kinase and myocyte enhance factor 2 pathway. *J Endocrinol.* 197(1):85-93.
- Wang BW, Hung HF, Chang H, Kuan P, and Shyu KG. (2007) Mechanical stretch enhances the expression of resistin gene in cultured cardiomyocytes via tumor necrosis factor-alpha. *Am J Physiol Heart Circ Physiol.* 293(4):H2305-12.

Living Animals

- Lin CC, Yen MC, Lin CM, Huang SS, Yang HJ, Chow NH, and Lai MD. (2008) Delivery of noncarrier naked DNA vaccine into the skin by supersonic flow induces a polarized T helper type 1 immune response to cancer. *J Gene Med.* 10(6):679-89.

Plant Cells

- Kao CY, Huang SH, and Lin CM. (2008) A low-pressure gene gun for genetic transformation of maize. *Plant Biotechnol Rep.* 2:267-270.

Technical Report

Gene Gun Bombardment with DNA-Coated Gold Particles Is a Potential Alternative to Hydrodynamics-Based Transfection for Delivering Genes into Superficial Hepatocytes

MING-LING CHANG,¹ JENG-CHANG CHEN,² CHAU-TING YEH,¹ MING-YU CHANG,³
CHUN-KAI LIANG,¹ CHENG-TANG CHIU,¹ DENG-YN LIN,¹ and YUN-FAN LIAW¹

ABSTRACT

Although *in vivo* nonviral gene delivery to the liver is critical for hepatic gene therapy, there are a number of technical obstacles. Enhanced green fluorescent protein (EGFP)-encoding DNA was coated onto gold particles (gold-DNA), dissolved in phosphate-buffered saline (pure DNA), and prepared as a polymer adjuvant (jetPEI)-galactosidase solution (polymer-DNA). Murine liver transfection was attempted by nonviral approaches, which included hydrodynamics-based transfection (HBT) of pure DNA, transport and transhepatic injection of polymer-DNA, and gene gun bombardment with pure DNA, gold-DNA, and polymer-DNA. Only HBT and gene gun bombardment yielded significant numbers of EGFP⁺ hepatocytes. With the exception of the edge of the liver, HBT had a whole-liver transfection rate of 20% under optimized conditions. HBT resulted in marked hepatic infarctions, most prominently at the edge of the liver. For gene gun bombardment, the transfection rate was pressure dependent and limited to 15% for gold-DNA. Triple or quadruple bombardment at 30 psi resulted in a transfection rate comparable to that of a single bombardment at higher pressure, but was associated with minimal scattered hepatic necrosis. The EGFP⁺ hepatocytes were located mainly in the superficial layers. We conclude that both HBT and gene gun bombardment yielded efficient murine hepatocyte transfection *in vivo*. Severe hepatic infarction impedes foreign gene expression in the superficial hepatocytes after HBT. Repeated bombardment with gold-DNA, using an accelerated particle gene gun at 30 psi, is a potential alternative to HBT for delivering genes to superficial hepatocytes *in vivo*, although gold-related hepatic necrosis is a persistent problem.

INTRODUCTION

In vivo gene delivery to the liver is critical for both experimental and clinical applications. At present, there are two main modes for gene delivery: viral and nonviral (Dobson, 2006). Viral vectors confer more effective expression than synthetic molecular gene vectors, albeit at the expense of infection and immunogenicity (Azzam and Domb, 2004). To lessen the potential biohazards of viral vectors, naked DNA is considered

attractive because it can be manipulated by standard recombinant DNA techniques and delivered by both chemical and physical means. However, chemical approaches such as circulating cationic vectors can attract serum proteins, leading to dynamic changes in their physicochemical properties and diminished transfection efficiency (Nishikawa and Huang, 2001). Physical approaches to gene transfer have improved and become as effective as viral vectors (Wells, 2004). Hydrodynamics-based transfection (HBT) of hepatocytes has been reported to produce

¹Liver Research Center and Department of Hepatogastroenterology, Chang Gung Memorial Hospital, Taoyuan, Taiwan; and Chang Gung University, Taoyuan, Taiwan 33305.

²Department of Surgery, Chang Gung Children's Hospital, Taoyuan, Taiwan 33305.

³Division of Pediatric Critical Care and Emergency Medicine, Chang Gung Children's Hospital, Taoyuan, Taiwan 33305.

a satisfactory transfection efficiency in mice (Wolff and Budker, 2005). Notably, gene guns can be used for difficult-to-transfect cells and particular *in situ* approaches (Johnston and Tang, 1994). However, whether gene guns are effective for liver transfection is uncertain. We examined the effectiveness of murine liver transfection by gene gun bombardment with enhanced green fluorescent protein (EGFP)-encoding DNA and compared the results with those obtained by other chemical or physical approaches.

MATERIALS AND METHODS

Mice

Eight-week-old male FVB/N mice were purchased from the Animal Center of the National Science Council (Taipei, Taiwan). For each transfection method, 30 mice were used. The use of animals in this study was approved by the Animal Care and Use Committee at Chang Gung Memorial Medical Center (Taoyuan, Taiwan).

Preparation of DNA

EGFP plasmid (PEGFP-C1, 4.7 kDa) was purchased from Clontech (Mountain View, CA). The plasmid was cloned and purified with an EndoFree plasmid kit (Qiagen, Valencia, CA). Naked EGFP DNA was dissolved at 1 $\mu\text{g}/\mu\text{l}$ in phosphate-buffered saline (PBS) (pure DNA). EGFP DNA-coated gold particles (gold-DNA) were prepared by adding 5 mg of Biolistic 1.0- μm gold particles (Bio-Rad, Hercules, CA) to 5 μl of 1- $\mu\text{g}/\mu\text{l}$ plasmid solution, 20 μl of 0.1 M spermidine (Sigma-Aldrich, St. Louis, MO), and 20 μl of 0.5 M CaCl_2 (Sigma-Aldrich). After several washes, the precipitate was dissolved in 100% alcohol for bombardment. The EGFP DNA-jetPEI-Gal solution (polymer-DNA) was prepared according to the manufacturer's protocol (Polyplus Transfection, New York, NY). The ratio of nitrogen residues on jetPEI to phosphates on the DNA backbone (N:P ratio) ranged from 5 to 10 for 0.31 to 0.62 μg of DNA.

Gene gun transfection with pure DNA, gold-DNA, and polymer-DNA

After general anesthesia by intraperitoneal injection of ketamine and diphenhydramine (Benadryl; Pfizer, New York, NY), the mice underwent midline laparotomy, to exposure the liver for gene gun bombardment. *In situ* liver transfections were performed with the low pressure-accelerated particle gene gun (Bioware Technologies, Taipei, Taiwan). A 1-cm-thick rubber ring was placed on the shooting end of gene gun. Briefly, gold-DNA (5–20 μl) was bombarded into mouse liver at pressures of 20–45 psi. Alternatively, pure DNA (5–20 μl) was bombarded into mouse liver at pressures of 20–45 psi. For polymer-DNA bombardment, DNA-jetPEI-Gal solution (5 μl) was bombarded into mouse liver. The mouse abdomen was closed carefully after bombardment.

Intravenous or direct liver injection of polymer-DNA

Mouse liver was exposed as described above. EGFP DNA-jetPEI-Gal solution (N:P ratio, 5–10) was used for *in*

vivo transfection via the portal vein (100 to 400 μl for 10 min) or direct injected into the right lobe of the liver (20 to 100 μl for 3 min). Tail vein injection was also performed (400 μl for 10 min) without laparotomy.

Hydrodynamics-based transfection

Five to 250 μg of EGFP DNA was injected via the tail vein in a volume of saline equivalent to 8% of the body mass of the mouse (e.g., 1.6 ml for a 20-g mouse). The entire volume was delivered within 5 sec.

Transfection rate evaluation

Mice were killed 48 hr or 7 days after transfection, and their livers were harvested. The livers were either cryofixed or fixed in 4% buffered paraformaldehyde (PFA). Unless otherwise indicated, transfection rates were evaluated 48 hr after transfection.

Cryofixation was performed by immersion of tissues in ice-cold isopentane for 3 min, followed by freezing at -80°C . Fixed frozen samples were mounted in Tissue-Tek O.C.T. 4583 compound (Sakura Finetek USA, Torrance, CA). Samples were sectioned sequentially on a Jung Frigocut 2800N (Leica, Deerfield, IL) at a cutting interval of 6 μm . Samples fixed in 4% PFA were subjected to hematoxylin and eosin (H&E) staining. Sections were examined by either fluorescence microscopy or light microscopy. EGFP⁺ hepatocytes were observed at $\times 20$ magnification under the fluorescence microscope. The transfection rate was defined as the number of EGFP⁺ hepatocytes divided by the total number of hepatocytes within the same field on three randomized occasions. Mice transfected with DNA-free PBS (with or without gold) of the same volume were used as negative controls.

Hepatic inflammation evaluation

Forty-eight hours after transfection, the serum alanine aminotransferase (ALT) levels of the mice were measured with a Vitros DT60 II chemistry system (Johnson & Johnson, New Brunswick, NJ).

Statistical analysis

Independent sample *t* testing was used to compare the means obtained for two different bombardment pressures or repetitions. One-way analysis of variance (ANOVA) was used to test the equality of the means among the three DNA groups. Differences were regarded as significant for $p < 0.05$.

RESULTS

Gene gun transfection with pure DNA, gold-DNA, and polymer-DNA

Mice transfected with the EGFP plasmid by gene gun bombardment did not have significant numbers of EGFP⁺ hepatocytes unless a pressure of 30 psi was used (Figs. 1A and 2). With respect to transfection rate, gold-DNA compared favorably with pure DNA and polymer-DNA (Fig. 2). However, liver laceration increased abruptly at pressures above 30 psi, ac-

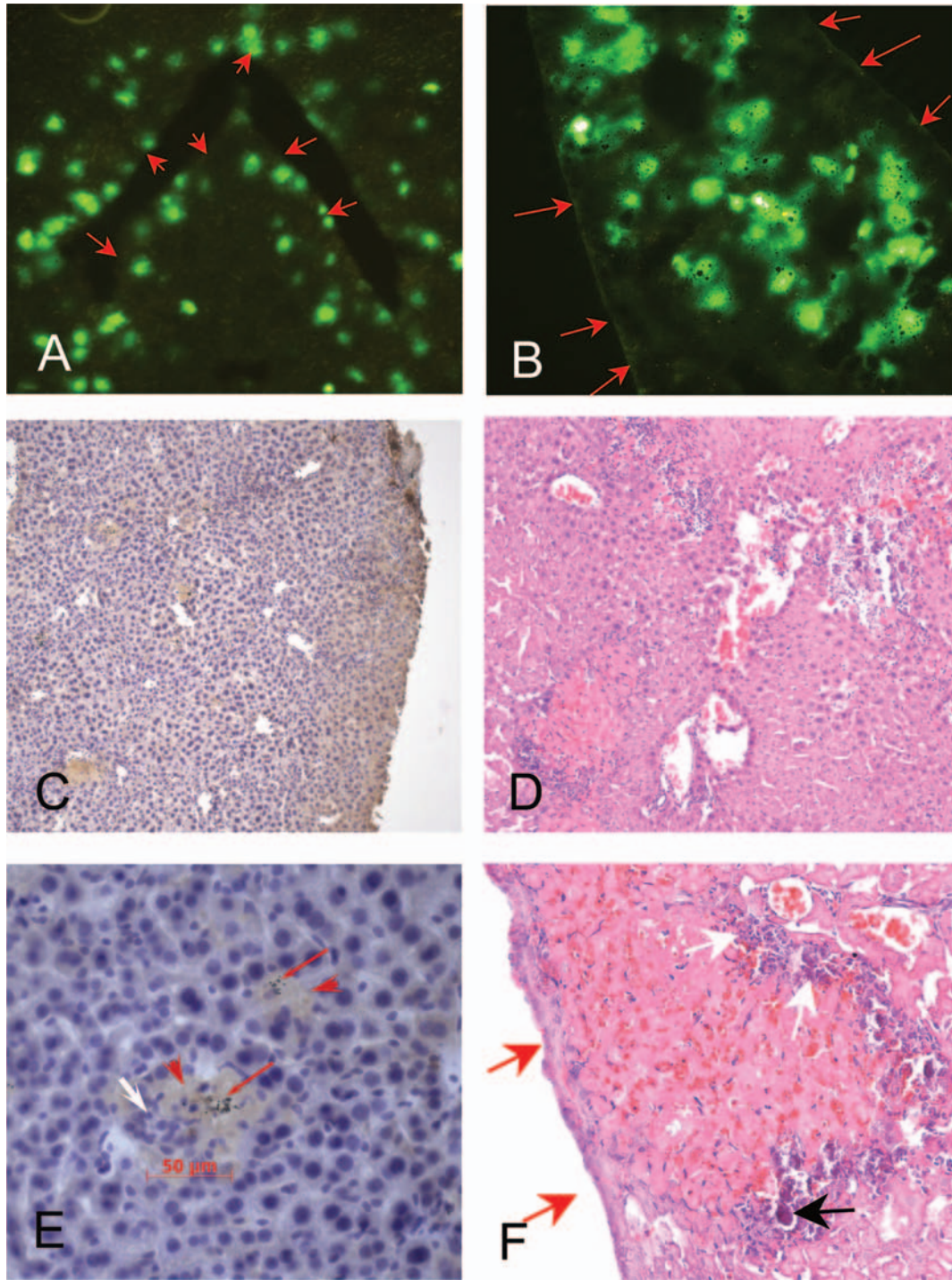


FIG. 1. (A and B) EGFP⁺ hepatocytes are shown (original magnification, $\times 20$) after gene gun bombardment with gold-DNA (A) at a pressure of 30 psi, and after HBT with injection of 10 μg of DNA within 4 sec (B). The edge of the liver is indicated by red arrows. (C and E) H&E staining of mouse liver after gold-DNA bombardment; a low-power field (C, $\times 100$) and a high-power field (E, $\times 400$) are shown. Gold particles (red arrows) and inflammatory cells (white arrow) are scattered in an area of necrotic hepatocytes (red arrowheads). (D and F) H&E staining of mouse liver after HBT; a low-power field (D, $\times 100$) and a high-power field (F, $\times 400$) are shown. Diffuse infarctions in the hepatic parenchyma are evident (D). A representative confluent hepatic infarction (F, red arrows) is located underneath the edge of the liver. Infiltrating inflammatory cells (F, white arrows) and calcification (F, black arrow) are associated with the infarction.

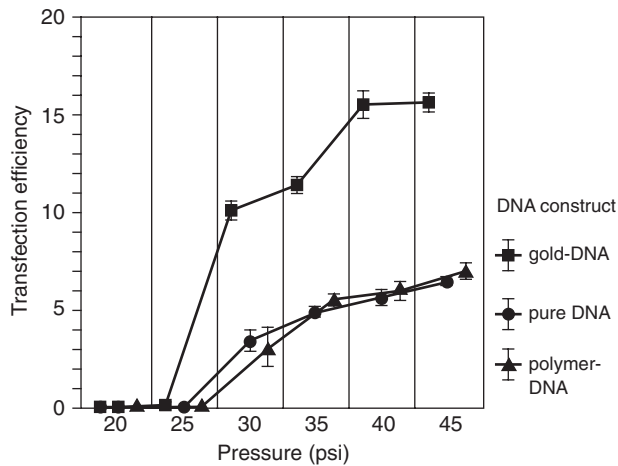


FIG. 2. Relationships between the transfection rate and bombardment pressure for three DNA preparations. In terms of transfection efficiency, gold-DNA compares favorably with pure DNA and polymer-DNA at a pressure of :30 psi ($p < 0.001$, one-way ANOVA). For each DNA preparation, significant differences were observed for 25 versus 30 psi, 30 versus 35 psi, 35 versus 40 psi, and 40 versus 45 psi ($p < 0.001$ – 0.044 , t test), but not for 40 versus 45 psi in the gold-DNA group ($p = 0.754$, t test).

counting for a mortality rate of more than 35%. The maximal transfection rate achieved by a single bombardment was approximately 15% for gold-DNA and 5–6% for pure DNA or polymer-DNA (Fig. 2). At 30 psi, the transfection rates reached a plateau at approximately 6.2, 5.9, and 15% for pure DNA, polymer-DNA, and gold-DNA, respectively, with three or four bombardments (Fig. 3). The mortality rate after triple bombardment at 30 psi was negligible and ranged from 0 to 3.3%. Further repetitions of bombardment led to mortality due to gross liver laceration. Regardless of the composition of the DNA solution, EGFP⁺ hepatocytes after bombardment were located mainly in the superficial layers (depth of 10–60 μ m, one to three cell layers) of the liver. Despite the better transfection rate obtained for gold-DNA, H&E staining of bombarded liver tissues revealed several necrotic spots with deposition of gold particles (Fig. 1C and E), indicating liver injury at the bombardment site, probably caused by the gold particles. The ALT levels of the mice were 249 ± 75 U/liter (normal range, 15–84 U/liter). One week after bombardment with gold-DNA, the transfection rate decreased to 9.7%.

Intravenous and direct liver injection of polymer-DNA

None of the transfections with polymer-DNA generated EGFP⁺ hepatocytes.

Hydrodynamics-based transfection

The immediate mortality rate was 6.6%, despite cardiopulmonary resuscitation for more than 10 min. The highest transfection rate for HBT was about 20% under optimized conditions of :10 μ g of DNA injected within 4 sec. EGFP⁺ hepatocytes were evenly distributed over the whole liver but

were scarce at the edge of the liver (Fig. 1B, arrows). H&E staining revealed remarkable hepatic infarctions in both control and experimental animals. At the edge of the liver, confluent infarctions were impressive and formed broad bands (Fig. 1D and F). The ALT levels of mice were 588 ± 135 U/liter. One week after HBT, the transfection rate decreased to 11.8%.

DISCUSSION

The chemical approach with jetPEI-Gal injection in FVB/N mice was unsatisfactory, as it gave minimal transfection rates regardless of the injection route. Successful *in vivo* transfections by jetPEI injection have been reported in the lung (Zou *et al.*, 2000). Although jetPEI-Gal was chosen over jetPEI for use in the current study, because of its higher affinity for hepatocytes (Robaczewska *et al.*, 2001), our data indicate that the liver represents a more robust barrier for polymer-adjutant transfection than the lung.

HBT yielded the highest transfection rate of all the nonviral DNA delivery methods. This is comparable to the results of previous studies (Zhang *et al.*, 1999; Yang *et al.*, 2002). However, rapid injection of a large volume via the tail vein usually causes transient heart dysfunction (Zhang *et al.*, 2004) and may lead to animal loss. Clinical application is not feasible, because humans lack a homolog for the tail vein. Furthermore, HBT leads to increased venous pressure (Zhang *et al.*, 2004) and subsequent hepatic infarction. The infarctions had a tendency to be confluent at the liver edge, where perfusion is sparser than elsewhere. Thus, it does not guarantee foreign gene expression in the superficial hepatocytes.

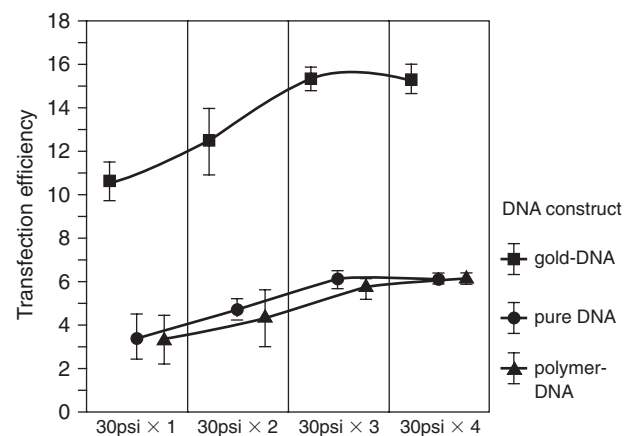


FIG. 3. Transfection rates in relation to number of bombardment repetitions at a pressure of 30 psi. For the same number of bombardment repetitions, gold-DNA gives superior transfection rates compared with pure DNA and polymer-DNA ($p < 0.001$, one-way ANOVA). A significant increase in transfection rate is observed for bombardment performed up to three times for each DNA group ($p < 0.001$ – 0.032 , t test), with the exception of polymer-DNA bombardment carried out once and twice ($p = 0.075$, t test). The transfection rates for three and four bombardment repetitions are not significantly different for each group ($p = 0.55$ – 1.0 , t test).

The original application of the gene gun was for skin vaccination, which induces DNA expression in the most superficial layers of the skin (Johnston and Tang, 1994; Peachman *et al.*, 2003). Thus, cell sampling for gene gun bombardment should focus on the superficial cells. GFP⁺ hepatocytes were most prominent in the first three layers. In comparison with the skin, the liver is too fragile to bear the bombardment pressure required for *in situ* transfection. Therefore, the pressure must be adjusted by weighing transfection efficiency against possible liver tearing. Triple bombardment at a tolerable pressure of 30 psi has been shown to yield a transfection efficiency comparable to that obtained from a single bombardment at higher pressure, which usually causes gross liver laceration. However, unpredictable location of gene transfer usually ensues from a direct strike (our unpublished data). Therefore, a rubber ring was placed at the opening of the gene gun. It ensures good guidance, allowing constant focusing and an attenuated blast effect. Among the various DNA preparations, gold-DNA bombardment had the highest transfection rate, although it was associated with gold particle-related necrosis. Nevertheless, the level of injury, determined by histological examination and the serum ALT level, was less severe than that caused by HBT. Gene gun bombardment is comparable with HBT in terms of stability, with a 20% decrease in the transfection rate after 1 week.

In conclusion, gene gun bombardment of the liver with gold-DNA is a potentially useful alternative to HBT for the transfection of superficial hepatocytes, particularly because it does not induce severe hepatic injury. Its application could potentially be extended to other animals, regardless of the presence or absence of a tail vein; however, its application is limited to superficial cells and animals that can tolerate laparotomy.

ACKNOWLEDGMENTS

Financial support was provided by the National Science Council, Taiwan (93-2314-B-182A-148, 94-2314-B-182A-185, and 95-3112-B-182A-002) and by Chang Gung Memorial Hospital, Taoyuan, Taiwan (CMRPG 33014, CMRPG 340341, and SMRPG 350081). Professor Pei-Jer Chen (Hepatitis Research Center, National Taiwan University Hospital, Taipei, Taiwan) provided helpful discussion.

AUTHOR DISCLOSURE STATEMENT

No competing financial interests exist.

REFERENCES

- AZZAM, T., and DOMB, A.J. (2004). Current developments in gene transfection agents. *Curr. Drug Deliv.* **1**, 165–193.
- DOBSON, J. (2006). Gene therapy progress and prospects: Magnetic nanoparticle-based gene delivery. *Gene Ther.* **13**, 283–287.
- JOHNSTON, S.A., and TANG, D.C. (1994). Gene gun transfection of animal cells and genetic immunization. *Methods Cell Biol.* **43**, 353–365.
- NISHIKAWA, M., and HUANG, L. (2001). Nonviral vectors in the new millennium: Delivery barriers in gene transfer. *Hum. Gene Ther.* **12**, 861–870.
- PEACHMAN, K.K., RAO, M., and ALVING, C.R. (2003). Immunization with DNA through the skin. *Methods* **31**, 232–242.
- ROBACZEWSKA, M., GUERRET, S., REMY, J.S., CHEMIN, I., OFFENSPERGER, W.B., CHEVALLIER, M., BEHR, J.P., PODHAJSKA, A.J., BLUM, H.E., TREPO, C., and COVA, L. (2001). Inhibition of hepadnaviral replication by polyethylenimine-based intravenous delivery of antisense phosphodiester oligodeoxynucleotides to the liver. *Gene Ther.* **8**, 874–881.
- WELLS, D.J. (2004). Gene therapy progress and prospects: electroporation and other physical methods. *Gene Ther.* **11**, 1363–1366.
- WOLFF, J.A., and BUDKER, V. (2005). The mechanism of naked DNA uptake and expression. *Adv. Genet.* **54**, 3–20.
- YANG, P.L., ALTHAGE, A., CHUNG, J., and CHISARI, F.V. (2002). Hydrodynamic injection of viral DNA: A mouse model of acute hepatitis B virus infection. *Proc. Natl. Acad. Sci. U.S.A.* **99**, 13825–13830.
- ZHANG, G., BUDKER, V., and WOLFF, J.A. (1999). High levels of foreign gene expression in hepatocytes after tail vein injections of naked plasmid DNA. *Hum. Gene Ther.* **10**, 1735–1737.
- ZHANG, G., GAO, X., SONG, Y.K., VOLLMER, R., STOLZ, D.B., GASIOROWSKI, J.Z., DEAN, D.A., and LIU, D. (2004). Hydrodilation as the mechanism of hydrodynamic delivery. *Gene Ther.* **11**, 675–682.
- ZOU, S.M., ERBACHER, P., REMY, J.S., and BEHR, J.P. (2000). Systemic linear polyethylenimine (L-PEI)-mediated gene delivery in the mouse. *J. Gene Med.* **2**, 128–134.

Address reprint requests to:

*Dr. Ming-Ling Chang
Liver Research Unit and Department of
Hepatogastroenterology
Chang Gung Memorial Hospital
No. 5, Fu Hsing Street
Kuei Shan, Taoyuan, Taiwan 33305*

E-mail: mlchang8210@gmail.com

Received for publication November 14, 2007; accepted after revision January 15, 2008.

Published online: March 21, 2008.

ORIGINAL ARTICLE

Connective tissue growth factor linked to the E7 tumor antigen generates potent antitumor immune responses mediated by an antiapoptotic mechanism

W-F Cheng^{1,2}, M-C Chang², W-Z Sun³, C-N Lee², H-W Lin², Y-N Su¹, C-Y Hsieh² and C-A Chen²

¹Graduate Institute of Clinical Medicine, College of Medicine, National Taiwan University, Taipei, Taiwan; ²Department of Obstetrics and Gynecology, College of Medicine, National Taiwan University, Taipei, Taiwan and ³Department of Anesthesiology, College of Medicine, National Taiwan University, Taipei, Taiwan

A novel method for generating an antigen-specific cancer vaccine and immunotherapy has emerged using a DNA vaccine. However, antigen-presenting cells (APCs) have a limited life span, which hinders their long-term ability to prime antigen-specific T cells. Connective tissue growth factor (CTGF) has a role in cell survival. This study explored the intradermal administration of DNA encoding CTGF with a model tumor antigen, human papilloma virus type 16 E7. Mice vaccinated with CTGF/E7 DNA exhibited a dramatic increase in E7-specific CD4⁺ and CD8⁺ T-cell precursors. They also showed an impressive antitumor effect against E7-expressing

tumors compared with mice vaccinated with the wild-type E7 DNA. The delivery of DNA encoding CTGF and E7 or CTGF alone could prolong the survival of transduced dendritic cells (DCs) *in vivo*. In addition, CTGF/E7-transduced DCs could enhance a higher number of E7-specific CD8⁺ T cells than E7-transduced DCs. By prolonging the survival of APCs, DNA vaccine encoding CTGF linked to a tumor antigen represents an innovative approach to enhance DNA vaccine potency and holds promise for cancer prophylaxis and immunotherapy. Gene Therapy advance online publication, 20 March 2008; doi:10.1038/gt.2008.25

Keywords: connective tissue growth factor; DNA vaccine; immunotherapy; HPV16; E7 antigen

Introduction

Cervical cancer is the most frequent neoplasm and has the fifth highest mortality rate among the malignancies in women.^{1–3} Each year it affects half a million women worldwide and cause about 200 000 deaths. Human papilloma viruses (HPVs) have been consistently implicated in causing cervical cancer, especially the high-risk types.^{3–6} An international study revealed that around 50% of cervical cancer cases contained HPV type 16 (HPV16) in their specimens.³ HPV infection precedes cervical intraepithelial neoplasia and thus infection with HPV16 produces the highest risk of developing cervical cancer.³

An ideal cancer treatment should be able to eradicate systemic tumors at multiple sites in the body and should have the ability to discriminate between neoplastic and non-neoplastic cells. The present available forms of treatment for cervical cancer, for example surgery, radiation therapy and chemotherapy,^{7,8} are all cytoreductive treatment modalities. This means that in addition to cancerous cells, healthy cells are also

destroyed in the process. In this regard, antigen-specific cancer immunotherapy would be an attractive approach for cancer treatment.^{9,10}

Intradermal administration of DNA vaccines using a gene gun can be used to efficiently deliver genes of interest into professional antigen-presenting cells (APCs) *in vivo* for cancer vaccine and immunotherapy.¹¹ The skin contains numerous bone marrow-derived APCs (called Langerhans cells) that are able to move through the lymphatic system from the site of injection to draining lymph nodes, where they prime antigen-specific T cells.¹² Previously, the gene gun approach was used to test strategies capable of routing model antigens to desired subcellular compartments such as endosome and centrosome, and enhance antigen processing and presentation to T cells.^{13–15}

Connective tissue growth factor (CTGF) is a cysteine-rich protein originally identified in a conditioned medium of human umbilical vein endothelial cells.¹⁶ Recently, CTGF has been shown to inhibit apoptosis of chicken embryo fibroblasts¹⁷ and human rhabdomyosarcoma cells.¹⁸ It has also been demonstrated to promote endothelial cell survival.¹⁹ CTGF could promote differentiation through a p38 mitogen-activated protein kinase and proliferation through a p44/42 MAPK/extracellular-signal regulated kinase in chondrocytes.²⁰ CTGF can also promote the acquisition of the apoptosis-resistant phenotype that may be similar to those of IGF-II in skeletal myoblasts.^{21,22}

Correspondence: Professor C-A Chen, Department of Obstetrics and Gynecology, College of Medicine, National Taiwan University, 7 Chung-Shan South Road, Taipei 100, Taiwan.

E-mail: chianchen@ntu.edu.tw

Received 13 April 2007; revised 8 January 2008; accepted 8 January 2008

In this study, we tested CTGF, the potential anti-apoptotic molecule, for its ability to enhance survival of dendritic cells (DCs) and E7-specific CD8⁺ T-cell immune responses, when linked to E7 DNA. We chose HPV16 E7 as a model antigen, because HPVs, particularly HPV16, are associated with a majority of cervical cancers, while E7 is essential for the induction and maintenance of cellular transformation. Effective vaccines against E7 can potentially be used to control HPV infections and HPV-associated lesions. By examining E7-specific immune responses, antitumor effects, survival of DNA-transfected DCs and the ability of DNA-transfected DCs to activate an E7-specific T cell line, we demonstrated that a CTGF/E7 chimeric DNA vaccine could generate a dramatic increase in E7-specific CD4⁺ and CD8⁺ T-cell precursors. It also has an impressive antitumor effect against E7-expressing tumors by prolonging the survival of transduced DCs *in vivo*. An antiapoptotic strategy could increase the immunologic responses and create a more potent antitumor effect.

Results

Vaccination with DNA encoding CTGF linked to E7 significantly enhanced the E7-specific T-cell immunities

To determine whether CTGF could enhance E7-specific T-cell-mediated immune responses in mice when linked to the E7 DNA vaccine, we performed intracellular cytokine staining with flow cytometry analysis to characterize E7-specific CD4⁺ and CD8⁺ T-cell precursors. The representative figures of E7-specific CD8⁺ T precursors in various vaccinated groups by flow cytometry analysis are shown in Figure 1a.

Figure 1b shows that vaccination with CTGF/E7 DNA generated higher frequencies of E7-specific interferon (IFN)- γ -secreting CD8⁺ T-cell precursors when compared to mice vaccinated with the other DNA-vaccinated groups (14.1 \pm 2.1 for the 'naïve' group, 15.0 \pm 1.4 for the 'no insert' group, 15.0 \pm 2.8 for the 'wild-type E7' group, 12.0 \pm 2.1 for the 'CTGF' group, 844.0 \pm 35.5 for the 'CTGF/E7' group, $P < 0.01$). Mice vaccinated with

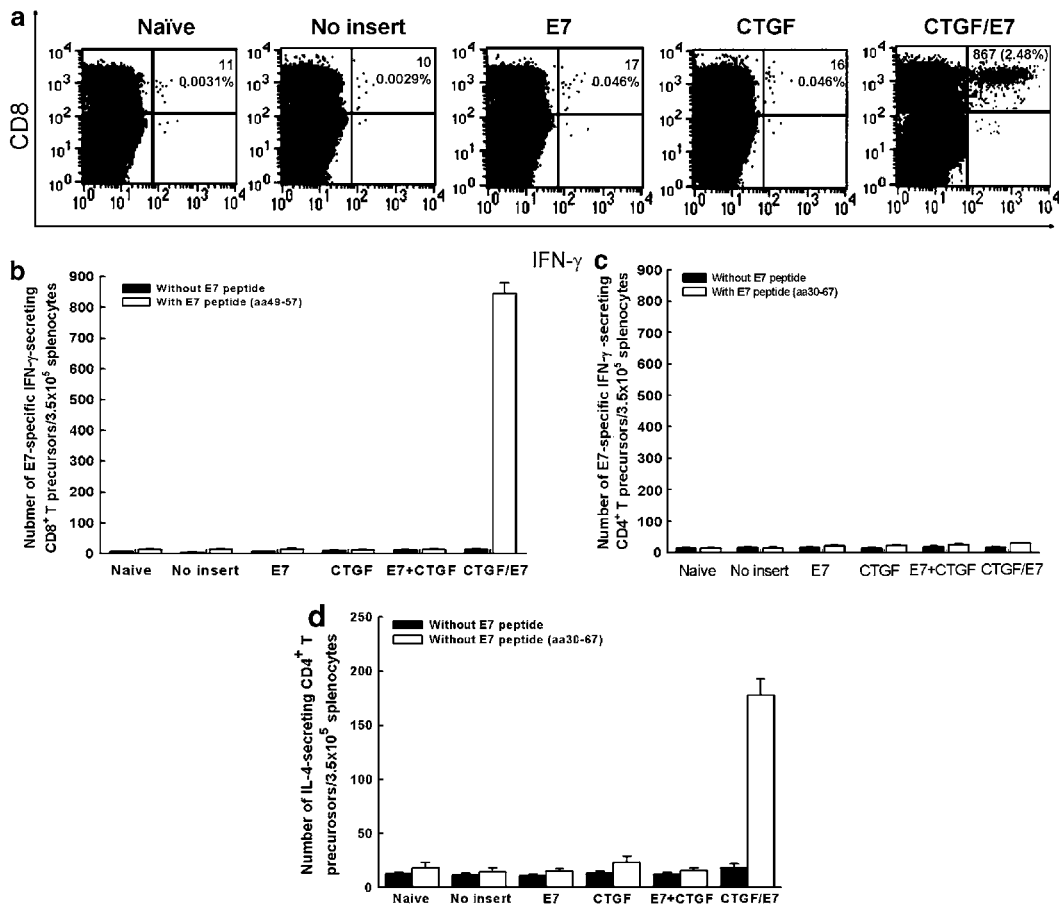


Figure 1 E7-specific immunological profiles of vaccinated mice using intracellular cytokine staining and ELISA. (a) Representative figures of E7-specific IFN- γ -secreting CD8⁺ T cells in mice vaccinated with DNA encoding no insert, E7, CTGF or CTGF/E7. (b) Bar graph depicting the number of antigen-specific IFN- γ -secreting CD8⁺ T-cell precursors/ 3.5×10^5 splenocytes (mean \pm s.d.). (c) Bar graph depicting the number of E7-specific IFN- γ -secreting CD4⁺ T-cell precursors/ 3.5×10^5 splenocytes (mean \pm s.d.). (d) Bar graphs depicting the number of E7-specific IL-4-secreting CD4⁺ T-cell precursors/ 3.5×10^5 splenocytes (mean \pm s.d.). The data collected from all of the above experiments are from one representative experiment of two performed. CTGF, connective tissue growth factor; ELISA, enzyme-linked immunosorbent assay; IFN, interferon; IL, interleukin.

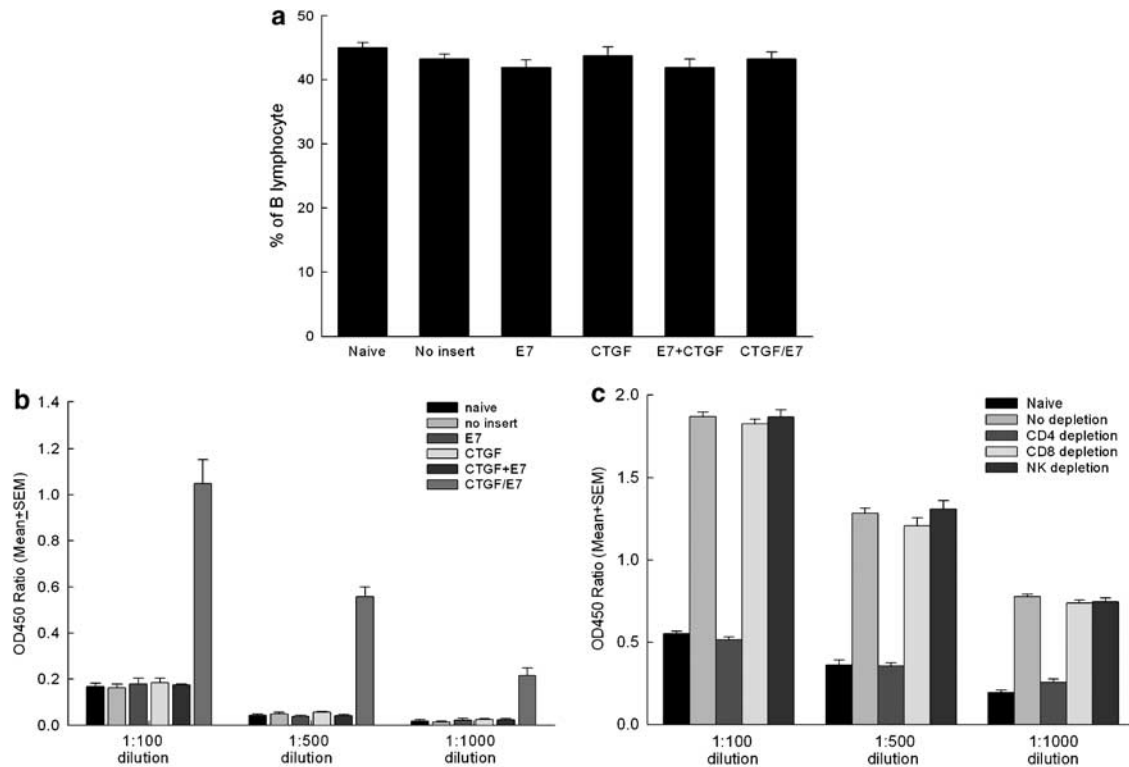


Figure 2 Percentages of B lymphocytes and E7-specific immunological profiles of vaccinated mice with or without respective antibody depletion. (a) Percentages of B lymphocytes in various DNA-vaccinated groups. (b) ELISA demonstrates E7-specific antibodies in mice vaccinated with various DNA vaccines. (c) ELISA demonstrates E7-specific antibodies in mice vaccinated with CTGF/E7 DNA with *in vivo* antibody depletion. The data collected from all of the above experiments are from one representative experiment of the two performed. CTGF, connective tissue growth factor; ELISA, enzyme-linked immunosorbent assay.

various DNA vaccines did not show significantly different numbers of E7-specific IFN- γ -secreting CD4⁺ T-cell precursors ($P > 0.05$) (Figure 1c). However, mice vaccinated with CTGF/E7 DNA vaccine revealed significantly higher numbers of E7-specific interleukin-4-secreting CD4⁺ T-cell precursors than the other groups (18.0 ± 5.0 for the naive group, 14.5 ± 3.5 for the no insert group, 15.0 ± 2.8 for the wild-type E7 group, 23.0 ± 6.0 for the CTGF group, 178.0 ± 15.0 for the CTGF/E7 group, $P < 0.01$) (Figure 1d).

We also evaluated whether the CTGF/E7 DNA vaccine would influence the percentages of B lymphocytes. No difference in the percentages of B lymphocytes could be observed between the naive and DNA-vaccinated groups (Figure 2a).

Enzyme-linked immunosorbent assay (ELISA) was carried out to determine whether CTGF/E7 DNA could enhance the E7-specific antibody response in vaccinated mice. The titers of anti-E7 antibodies generated by CTGF/E7 DNA vaccine were significantly higher than those by the other DNA vaccines (0.167 ± 0.015 for the naive group, 0.163 ± 0.016 for the no insert group, 0.179 ± 0.025 for the wild-type E7 group, 0.184 ± 0.020 for the CTGF group, 0.176 ± 0.021 for E7 mixed with the CTGF group, 1.048 ± 0.104 for the CTGF/E7 group, 1:100 dilution, $P < 0.01$) (Figure 2b). However, the titers of anti-E7 antibodies in mice vaccinated with CTGF/E7 DNA vaccine with CD4 depletion group (0.532 ± 0.018 , 1:100 dilution) significantly decreased as compared with those with CD8-depletion group (1.829 ± 0.028 , 1:100 dilution), NK1.1-depletion group (1.827 ± 0.043 , 1:100 dilution),

or without antibody-depletion group (1.872 ± 0.028 , 1:100 dilution, $P < 0.01$, one-way analysis of variance) (Figure 2c).

Our results reveal that the physical linkage of CTGF to E7 could enhance the E7-specific helper and cytotoxic T-cell immunities and E7-specific antibody responses.

Vaccination with CTGF/E7 DNA enhanced tumor protection in mice challenged with an E7-expressing tumor cell line

To determine whether the observed enhancement of E7-specific CD8⁺ T-cell response translated into a significant E7-specific protective antitumor effect, we performed an *in vivo* tumor-protection experiment. As shown in Figure 3a, when challenged with TC-1 tumor cells, 100% of mice receiving CTGF/E7 DNA vaccination remained tumor-free even 60 days after the challenge. In comparison, all mice vaccinated with the wild-type E7 DNA developed tumors within 14 days. Thus, CTGF may protect vaccinated mice against a lethal challenge with E7-expressing tumor cells, when it is linked to the E7 antigen in a DNA vaccine.

Treatment with CTGF/E7 led to a significant reduction of pulmonary tumor nodules in vaccinated mice

We further assessed the therapeutic potential of each vaccine by performing an *in vivo* tumor treatment experiment using the lung hematogenous spread model described by Liao *et al.*²³ The representative pulmonary tumor nodules are shown in Figure 3b. As shown in

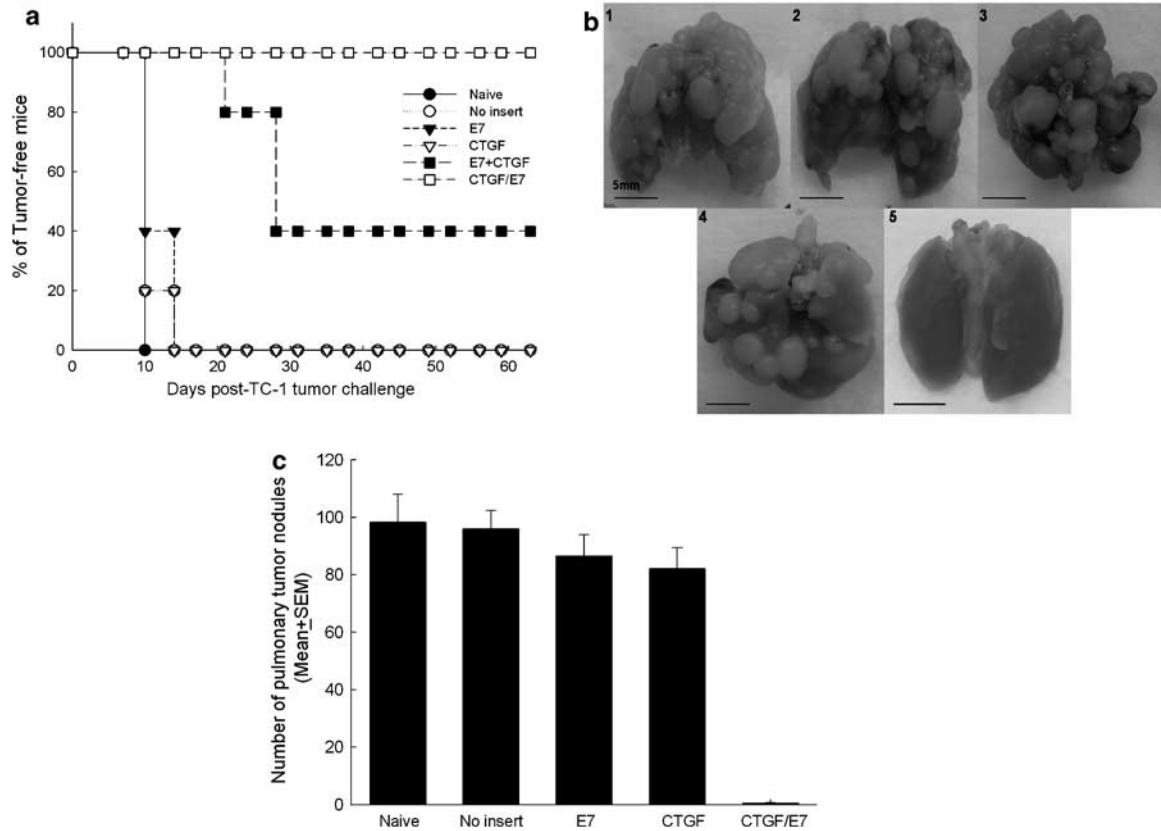


Figure 3 *In vivo* tumor protection and treatment experiments in mice. (a) *In vivo* tumor protection experiments. Mice were vaccinated with various DNA vaccines and then were challenged with TC-1 tumor cells. Note that 100% of mice receiving CTGF/E7 remained tumor-free even 60 days after TC-1 challenge. All mice vaccinated with wild-type E7 DNA developed tumors within 14 days of challenge. (b) Representative figures of pulmonary tumor nodules in mice of treatment experiments. 1: naïve group, 2: no insert group, 3: E7 group, 4: CTGF group, 5: CTGF/E7 group. (c) Mean pulmonary tumor nodules of each vaccinated group in tumor treatment experiments. Note: mice treated with DNA encoding CTGF/E7 showed significantly lower numbers of pulmonary tumor nodules than mice treated with DNA encoding E7, no insert or CTGF. CTGF, connective tissue growth factor.

Figure 3c, mice treated with CTGF/E7 (0.4 ± 0.2) exhibited significantly fewer pulmonary tumor nodules than mice treated with the other DNA vaccines (98.2 ± 9.8 for the naïve group, 96.0 ± 6.4 for the no insert group, 86.6 ± 7.4 for the wild-type E7 group, 82.2 ± 7.3 for the CTGF group, $P < 0.001$).

These data indicate that CTGF when linked to the E7 antigen could generate more potent preventive and therapeutic effects than the wild-type E7 DNA constructs in both subcutaneous and lung hematogenous spread models.

Only CD8⁺ T cells were essential for the antitumor effect generated by CTGF/E7 DNA

To determine the subset of lymphocytes important for the antitumor effect, we performed *in vivo* antibody-depletion experiments.¹³ As shown in Figure 4, all naïve mice and mice depleted of CD8⁺ T cells grew tumors within 14 days after the tumor challenge. In contrast, all of the nondepleted mice and all of the vaccinated mice depleted of CD4⁺ T cells or NK1.1 cells remained tumor-free even 60 days after the tumor challenge.

These results suggest that CD8⁺ T cells are important and essential for the antitumor immunity generated by the CTGF/E7 DNA vaccine.

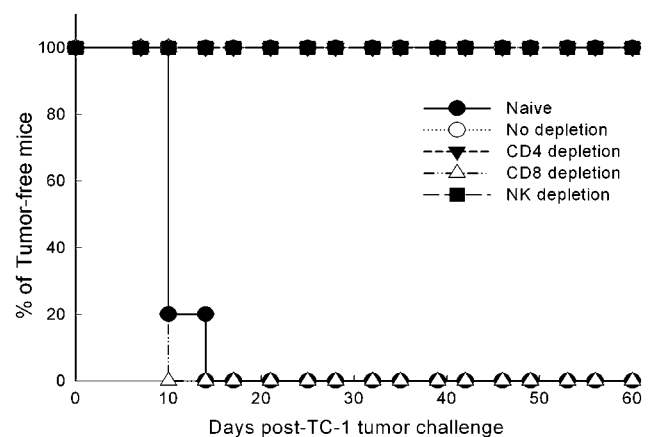


Figure 4 *In vivo* antibody depletion experiments of mice vaccinated with CTGF/E7 DNA vaccine. Mice were vaccinated with CTGF/E7 DNA vaccine, injected with CD4, CD8 or NK1.1 antibody, and challenged with TC-1 tumor cells. Note: all of the CTGF/E7-vaccinated mice depleted with CD8⁺ T lymphocytes and naïve mice got tumorigenesis within 14 days after TC-1 tumor challenge. All of the CTGF/E7-vaccinated mice depleted of CD4⁺ T lymphocytes or NK1.1⁺ cells were tumor-free after 60 days of TC-1 tumor challenge. The data collected from all of the above experiments are from one representative experiment of the two performed. CTGF, connective tissue growth factor.

Protein expression levels are similar between cells transfected with wild-type E7 or CTGF/E7 chimeric DNA

We then evaluated whether CTGF/E7 chimeric DNA would influence the E7 protein expression. Cell transfection experiments and immunoblotting were performed. As shown in Figure 5, the protein expression levels

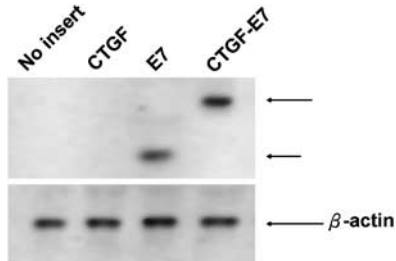


Figure 5 The protein expression levels of respective constructs in 293 transfected D^hK^b cells. The E7 or chimeric E7 protein expression levels in respective constructs are shown. Note: the E7 (short arrow) or CTGF/E7 (long arrow) protein expression level in E7 or CTGF/E7 DNA-transfected 293 D^hK^b cells was not significantly different. CTGF, connective tissue growth factor.

between cells transfected with wild-type E7 DNA or chimeric CTGF/E7 DNA were not significantly different or altered. Our results indicated that when linked to E7, CTGF would not alter the E7 protein expression.

Improved survival of DNA-transfected DCs in inguinal lymph nodes of mice vaccinated with CTGF/E7/GFP DNA

To find out whether the *in vivo* antiapoptotic phenomenon of CTGF/E7 DNA could also be observed *in vivo* to enhance the E7-specific immunity, we used green fluorescent protein (GFP) linked to E7 as a fluorescent tag to identify DNA-transfected DCs in the inguinal lymph nodes. Inguinal lymph nodes were collected from vaccinated mice at 1 and 5 days after gene gun vaccination. CD11⁺ cells with DC size and granular characteristics were gated as DCs, as reported previously.²² As shown in Figure 6a, there was no significant difference in numbers of CD11c and GFP-positive cells in the inguinal lymph nodes at day 1 after vaccination with various DNA constructs. On day 5 after gene gun vaccination, however, a greater percentage of GFP⁺CD11c⁺ cells was observed in lymph nodes of

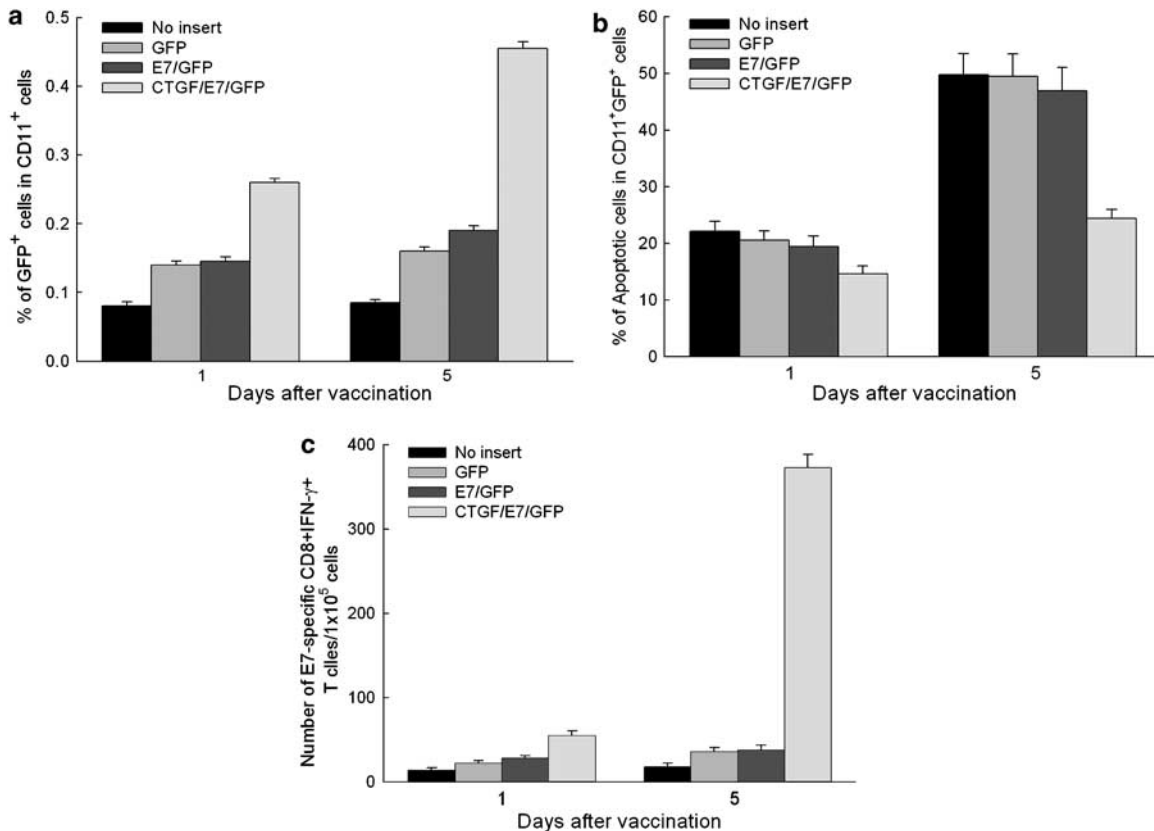


Figure 6 Characterization of DNA-transfected CD11c-enriched cells and activation of E7-specific CD8⁺ T cells by CD11c-enriched cells isolated from the inguinal lymph nodes of vaccinated mice. Mice were immunized with pcDNA3-GFP, E7/GFP or CTGF/E7/GFP DNA. The percentage of apoptotic cells was determined by staining with annexin V followed by flow cytometry analysis using the CD11c⁺GFP⁺ cells. (a) Bar graph depicting the percentage of CD11c⁺GFP⁺ monocytes among the gated monocytes (mean ± s.e.m.). (b) Bar graph depicting the percentage of apoptotic cells in CD11c⁺GFP⁺ cells (mean ± s.e.m.). (c) Numbers of IFN- γ -secreting E7-specific CD8⁺ T cells stimulated by CD11c-enriched cells isolated from the inguinal lymph nodes of vaccinated mice. Mice were immunized and CD11c⁺ cells were enriched, incubated with an E7-specific CD8⁺ T cell line and intracellular cytokine staining and flow cytometry analysis were performed to determine the number of E7-specific IFN- γ -secreting CD8⁺ T cells. The data collected from all of the above experiments are from one experiment representative of the two performed. CTGF, connective tissue growth factor; IFN, interferon.

CTGF/E7/GFP DNA-vaccinated mice as compared with lymph nodes collected from mice vaccinated with E7/GFP or only GFP DNA constructs (0.085 ± 0.005 for the naïve group, 0.160 ± 0.006 for the GFP group, 0.190 ± 0.007 for the E7/GFP group, $0.455 \pm 0.010\%$ for the CTGF/E7/GFP, $P < 0.001$, one-way analysis of variance) (Figure 6a).

We further assayed for the apoptotic cells in GFP⁺CD11c⁺ cells derived from the draining lymph nodes of various vaccinated mice by staining for annexin V followed by flow cytometry analysis. As shown in Figure 6b, at day 5, mice vaccinated with DNA encoding CTGF/E7/GFP DNA demonstrated a significantly lower percentage of apoptotic cells when compared with mice vaccinated with E7/GFP or GFP only (49.8 ± 3.7 for the naïve group, 49.5 ± 3.9 for the GFP group, 46.9 ± 4.2 for the E7/GFP group, $24.4 \pm 1.7\%$ for the CTGF/E7/GFP, $P < 0.001$, one-way analysis of variance).

Our results suggest that the administration of CTGF/E7/GFP DNA, which generated an antiapoptotic function, prolonged the survival of DNA-transfected DCs *in vivo*.

CD11c-enriched cells from mice vaccinated with CTGF/E7/GFP DNA enhanced the activation of an E7-specific CD8⁺ T cell line

We evaluated whether these CTGF/E7-transfected CD11c-enriched cells with prolonged life span from the inguinal lymph nodes of the CTGF/E7/GFP DNA-vaccinated mice had the ability to stimulate INF- γ secretion from an E7-specific CD8⁺ T cell line. These CD11c-enriched cells were isolated 1 or 5 days after the last DNA vaccination and were incubated with an E7-specific T cell line. As shown in Figure 6c, CD11c-enriched cells isolated from mice vaccinated with CTGF/E7/GFP DNA were more effective in activating the E7-specific CD8⁺ T cell line to secrete INF- γ compared with E7/GFP or GFP-only DNA vaccine, particularly at day 5 (18.0 ± 4.2 for the no insert group, 36.0 ± 4.9 for the GFP group, 38.0 ± 5.6 for the E7/GFP group, 373.0 ± 15.5 for the CTGF/E7/GFP, $P < 0.001$).

These *in vivo* results are consistent with the notion that DNA-transfected DCs from mice vaccinated with CTGF/E7/GFP DNA could enhance the activation of E7-specific CD8⁺ T cells via the antiapoptotic function of CTGF.

Discussion

In this study, we demonstrated that linking of HPV16 E7 antigen to CTGF DNA can significantly enhance the potency of an E7-expressing DNA vaccine. CTGF/E7 DNA elicited strong E7-specific CD8⁺ T-cell immune responses (Figure 1b), generated a significant CD8⁺ T-cell-dependent protective effect against subcutaneous HPV16 E7-expressing tumors (Figures 3a and 4), and was useful in the treatment of lethal pulmonary tumor nodules (Figure 3c). DC life could be prolonged by inhibiting apoptosis using CTGF/E7 DNA, and not wild-type E7 DNA, resulting in an increased quantity of longer-lived DCs in the draining lymph nodes (Figure 6). Thus, our data supported our hypothesis that linking of CTGF to E7 creates a better vaccine than either E7 or CTGF via the antiapoptotic mechanism.

CTGF/E7 chimeric DNA vaccine enhances antigen-specific T-cell immunity by an antiapoptotic mechanism. Our *in vivo* observations showed that *in vivo* CTGF/E7-transfected DCs had longer life spans than *in vivo* E7-transfected DCs (Figure 6b). In addition, these CTGF/E7-transfected DCs stimulated higher numbers of E7-specific CD8⁺ T cells than E7-transfected DCs *in vivo* (Figure 6c). Our explanation is that the CTGF/E7 chimeric molecule may create larger numbers of APCs *in vivo* by its antiapoptotic function than wild-type E7 did. These E7-specific APCs transfected by CTGF/E7 enhanced higher E7-specific T-cell immunity and generated potent preventive and therapeutic effects of the E7-specific tumor. Many molecules, such as Bcl-2, Bcl-XL or serine protease inhibitor-6 successfully enhance antigen-specific immunity by their antiapoptotic ability.^{24,25} However, Bcl-2 and Bcl-XL have been shown to be oncogenes, which are not suitable for transduction to enhance immune responses *in vivo*.

Connective tissue growth factor secreted by fibroblasts for multiple purposes is more likely to be utilized in clinical applications for its antiapoptotic strategy.²⁶ Its presence has been shown to be a survival factor for different cell types.^{27,28} Previous studies have demonstrated that CTGF may also be a useful therapeutic agent in human rhabdomyosarcoma.¹⁸ Disrupting CTGF expression using CTGF-neutralizing antibodies could enhance the apoptosis of rhabdomyosarcoma cells and inhibit the angiogenesis. This evidence suggests that CTGF may have a key role in tumor progression because of its antiapoptotic function. CTGF's ability to inhibit apoptosis in tumor cells may be one of the safety concerns that make the CTGF/E7 chimeric DNA vaccine recommendable. Our results revealed that mice vaccinated with CTGF DNA only would not promote tumorigenesis as compared with those vaccinated with wild-type E7 DNA or naïve mice in the tumor treatment experiments (Figure 3c). This implies that a CTGF/E7 chimeric DNA vaccine can generate potent antitumor effects, and not tumorigenic effects.

E7-specific antibody titers were significantly enhanced by CTGF/E7 vaccination. CTGF/E7 DNA vaccine could enhance the antibody response and interleukin-4-secreting CD4⁺ helper T-cell precursors in vaccinated mice (Figures 1d and 2b). CTGF can be secreted into the stroma to work for the endocrine or paracrine functions as a chemotactic and mitogenic factor on fibroblasts to induce wound healing.²⁹ It seems that the CTGF/E7 chimeric protein could enhance the anti-E7 antibody responses via the Th2 cell pathway in our observation. Although the overall percentages of B cells was not altered between vaccinated groups (Figure 2a), we still cannot rule out the possibility that the percentage of antibody-secreting plasma cells may be enhanced by the CTGF/E7 vaccine. It would be interesting to pursue further research to find out how CTGF enhances humoral immunity. Although antibody-mediated responses have not been shown to have an important role in controlling HPV-associated malignancies, antigen-specific antibodies are significant in other tumor models, such as the breast cancer model with the HER-2/neu antigen. So the chimeric CTGF vaccine strategy may be used to generate antibodies that perform on tumor cells.

Our *in vivo* antibody-depletion experiment was consistent with the concept that CD8⁺ T cells are the key

players in gene gun-mediated CTGF/E7 DNA vaccination (Figure 4). Our data showed that CD8⁺ T cells are required in the effector phase of antitumor immunity. In contrast, the depletion of CD4⁺ or NK1.1⁺ cells did not decrease antitumor immunity generated by CTGF/E7 DNA. Such phenomena could also be observed in the other E7-chimeric DNA molecules, such as calreticulin/E7, E7/HSP70, VP22/E7 or γ -tubulin/E7,^{13,15,30,31} although they enhanced antigen-specific immunity in different ways.

DNA vaccine with combined strategies generates significantly higher antitumor immunity than those with a single strategy. Previous studies have demonstrated that vaccination with DCs transfected with BAK/BAX short interfering RNA can generate a stronger therapeutic antitumor effect in vaccinated mice compared with a control short interfering RNA.³² These data indicate that administering antigen peptide-loaded DCs transfected with BAK/BAX short interfering RNA prolongs the life of the DCs and enhances antigen-specific CD8 cytotoxic killing effects. In this study, we also observed that mice vaccinated with DNA encoding E7/GFP mixed with DNA encoding CTGF demonstrate a significantly lower percentage of apoptotic cells in CD11c⁺ GFP⁺ cells derived from the draining lymph nodes. Our results suggest that the increase in the number of antigen-expressing DCs in lymph nodes may contribute to the enhancement of E7-specific T-cell activation. However, such qualitative changes may result in vaccination with DNA encoding antiapoptotic factors. Mice vaccinated with calreticulin/E7 combined with CTGF DNA have significantly enhanced antitumor effects compared with those vaccinated with calreticulin/E7 only (data not shown). These data indicate that the antitumor effects of DNA vaccine are more potent when combined with different strategies.

In summary, this study demonstrates that linkage of CTGF to the HPV16 E7 antigen can significantly elicit strong E7-specific CD8⁺ T-cell immune responses and generates significant CD8⁺ T-cell-dependent protective effects against subcutaneous HPV16 E7-expressing tumors that can effectively treat lethal pulmonary tumor nodules. CTGF/E7 chimeric DNA may prolong the life span of CTGF/E7-transfected DCs to induce higher numbers of E7-specific T-cell precursors *in vivo*. The antiapoptosis strategy can also be synergistically applied in combination with other DNA vaccines. The promising results of this study will encourage the application of the combined strategies to target other cancers or infectious diseases with known antigens.

Materials and methods

Plasmid DNA constructs and preparation

To generate pcDNA3-CTGF, CTGF was first amplified by PCR using human placenta cDNA as the template and a set of primers: 5'-CCGCTCGAGAGGAGCCCAGCTATGAAGTC-3' and 5'-CCGGAATTCGACCAGAAGAAGGAATGCC-3'. The amplified product was then cloned into the *XhoI/EcoRI* sites of pcDNA3 vector (Invitrogen Corp., Carlsbad, CA, USA). To generate pcDNA3-CTGF/E7, E7 was generated as described in a previous study²³ and cloned into the *HindIII* sites of pcDNA3-CTGF to generate pcDNA3-CTGF/E7. To generate pcDNA3-

CTGF/E7/GFP, pcDNA3-CTGF/E7 was first digested by the restriction enzyme *HindIII*. The GFP fragment was obtained from plasmid pcDNA3-E7/GFP by *EcoRI/NotI* digestion. The DNA fragment was then filled in and ligated into CTGF/E7 to generate the desired plasmid, which was confirmed by sequencing.

Cell line

The production and maintenance of TC-1 tumor cells have already been described in a previous study.³³ In brief, HPV16 E6, E7 and *ras* oncogene were used to transform primary C57BL/6 lung epithelial cells from mice to generate TC-1. On the day of tumor challenge, tumor cells were collected by trypsinization, washed twice with 1 × Hanks buffered salt solution, and resuspended in the buffer to the concentration designated for injection.

A human embryonic kidney 293 cell line expressing the D^b and K^b (293 D^bK^b cells), two C57BL/6 mouse MHC class I molecules) for various cell transfection and *in vitro* immunological experiments have been described in a previous study.¹³ 293 D^bK^b cells were maintained in RPMI-1640, supplemented with 10% (v/v) fetal bovine serum, 50 U ml⁻¹ penicillin/streptomycin, 2 mM L-glutamine, 1 mM sodium pyruvate and 2 mM non-essential amino acids.

Immunoblotting

293 D^bK^b cells transfected with various DNA were lysed in an immunoprecipitation assay buffer containing 137 mM NaCl, 2.7 mM KCl, 1 mM MgCl₂, 1 mM CaCl₂, 1% NP40, 10% glycerol, 1 mg/ml BSA, 20 mM Tris pH 8.0 and 2 mM orthovanadate, and were analyzed as described previously.⁵ Briefly, 50 μ g of cell lysates were resolved on an SDS-containing 12% polyacrylamide gel. They were transferred to polyvinylidene difluoride nylon membranes (Millipore, Bedford, MA, USA) and probed with antibodies specific to E7 (Zymed, San Francisco, CA, USA) or β -actin (Chemicon International Inc., Temecula, CA, USA). The membrane was then probed with either horseradish peroxidase-conjugated goat-anti-mouse or goat-anti-rabbit antibody. The specific bands were visualized by an ECL (enhanced chemiluminescence) western blot system (Amersham, Buckinghamshire, England).

Mice

Six- to 8-week-old female C57BL/6J mice were purchased and kept in the animal facility of the school of Medicine, National Taiwan University. All of the animal procedures were performed according to approved protocols and in accordance with recommendations for the proper use and care of laboratory animals. In all the following experiments, the mice were divided into groups of five mice each.

DNA vaccination

Preparation of DNA-coated gold particles and gene gun particle-mediated DNA vaccinations were performed using a helium-driven gene gun, according to a protocol we used in previous research.¹⁴ Respective DNA-coated gold particles were delivered to the shaved abdominal region of mice with a 50 psi discharge pressure of helium.

Intracellular cytokine staining and flow cytometry analysis

In the first experiment, the mice were immunized with 2 μg of the various DNA vaccines and received a booster with the same regimen 1 week later. Splenocytes were harvested 1 week after the last vaccination. Before intracellular cytokine staining, 3.5×10^5 pooled splenocytes from each vaccination group were incubated for 16 h with either 1 $\mu\text{g ml}^{-1}$ of E7 peptide (aa 49–57) containing an MHC class I epitope³⁴ for detecting E7-specific CD8⁺ T-cell precursors or 10 $\mu\text{g ml}^{-1}$ of E7 peptide (aa 30–67) containing an MHC class II epitope³⁵ for detecting E7-specific CD4⁺ T-cell precursors. Golgi-stop (Pharmingen, San Diego, CA, USA) was added 6 h before harvesting the cells, which were first stained with PE-CD8 or CD4 antibody (Pharmingen), and then subjected to intracellular cytokine staining using the Cytofix/Cytoperm kit, according to the manufacturer's instructions (Pharmingen). Intracellular cytokine staining for fluorescein isothiocyanate-IFN- γ (Pharmingen), interleukin-4 (Biolegend, San Diego, CA) or immunoglobulin isotype control antibody (rat IgG1) (Pharmingen), as well as flow cytometry analysis, were performed using conditions described previously.³⁶

In the second experiment, the splenocytes were stained first with fluorescein isothiocyanate-CD3 and PE-CD19 antibodies (Pharmingen) and analyzed as already described to identify the percentages of B lymphocytes (CD3(-)CD19(+)).

Enzyme-linked immunosorbent assay for anti-E7 antibody

In the first experiment, mice were immunized with 2 μg of the various DNA vaccines and received a booster with the same regimen 1 week later. Sera were prepared from the mice 14 days after their last immunization. To detect HPV16 E7-specific antibodies in the sera, direct ELISA was used as described previously.³⁷ The ELISA plate was read with a standard ELISA reader at 450 nm.

In the second experiment, mice were immunized with 2 μg of the CTGF/E7 DNA vaccine with a gene gun, boosted 1 week later, and received respective antibody to deplete the CD4, CD8 and NK1.1 lymphocytes. The monoclonal antibody GK1.5 was used for CD4 depletion,³⁸ 2.43 was used for CD8 depletion³⁹ and PK136 was used for NK1.1 depletion.⁴⁰ Depletion was terminated on day 14 after the last immunization. Sera were prepared from the mice 14 days after their last immunization. To detect HPV16 E7-specific antibodies in the sera, direct ELISA was used as described above.

In vivo tumor protection experiments

For the first tumor protection experiments, the mice either received no vaccination or were immunized with 2 μg per mouse of various DNA vaccines with a gene gun. At 1 week later, the mice were boosted with the same regimen as the first vaccination. One week after the last vaccination, they were subcutaneously challenged with 5×10^4 cells per mouse of TC-1 tumor cells in the right leg. The mice were monitored for evidence of tumor growth by palpation and inspection twice a week until they were sacrificed on day 60.

In vivo antibody depletion experiments

In vivo antibody depletions were performed as in a previous study.⁴¹ Briefly, the mice were vaccinated with 2 μg per mouse of CTGF/E7 DNA with a gene gun, boosted 1 week later and challenged with 5×10^4 cells per mouse of TC-1 tumor cells. Injection of respective antibody was started 1 week before tumor challenge and terminated on day 40 after the tumor challenge. The mice were monitored for evidence of tumor growth by palpation and inspection twice a week until they were killed on day 60.

In vivo tumor treatment experiments

For the first *in vivo* tumor treatment experiment, the mice were injected with 5×10^4 cells per mouse of TC-1 tumor cells via the tail vein as described earlier.⁴² Two days after tumor challenge, the each mouse received 16 μg of no insert DNA, E7 DNA, CTGF DNA or CTGF/E7 DNA by a gene gun. This was followed by a booster with the same regimen every 7 days for 4 weeks (a total 64 μg DNA). Mice receiving no vaccination were used as a negative control. The mice were sacrificed and their lungs were explanted on day 28. Pulmonary tumor nodules in each mouse were evaluated and counted by experimenters who were blind to the sample identities.

In vitro apoptotic assays

293 D^bK^b cells were cultured and transfected with GPT only, E7/GFP, CTGF/GFP or CTGF/E7/GFP DNA for *in vitro* apoptotic assays, as described above. 293 D^bK^b cells were collected 24 or 48 h after transfection. The cells were stained with annexin V-fluorescein isothiocyanate and propidium iodide, according to the manufacturer's protocol. To determine the percentage of apoptotic 293 D^bK^b cells, annexin V staining was performed after gating around a population of GFP⁺ cells. The percentage of apoptotic cells was analyzed using flow cytometry analysis by gating annexin V (+) cells.

Preparation of CD11c⁺ cells in the inguinal lymph nodes from vaccinated mice

C57BL/6J mice received multiple inoculations of non-overlapping intradermal administration with a gene gun on the abdominal region. Gold particles used for each inoculation were coated with 1 μg of pcDNA3 encoding GFP, E7/GFP or CTGF/E7 DNA. The pcDNA3 with no insert was used as a negative control. Inguinal lymph nodes were harvested from vaccinated mice 1 or 5 days after vaccination with a gene gun. A single-cell suspension from isolated inguinal lymph nodes was prepared.

CD11c⁺ cells were enriched from lymph nodes using CD11c (N418) micro-beads (Miltenyi Biotec, Auburn, CA, USA). The percentage of CD11c⁺ cells was characterized by flow cytometry analysis using PE-conjugated anti-CD11c antibody (Pharmingen). GFP-positive cells were analyzed by flow cytometry analysis using a previously described protocol.²⁵

Data are expressed as the percentage of CD11c⁺GFP⁺ cells among gated monocytes. Detection of apoptotic cells in the CD11c⁺GFP⁺ cells was performed using annexin V-PE apoptosis detection Kit-I (BD Bioscience, San Diego, CA, USA) according to the manufacturer's protocol. The percentage of apoptotic cells was analyzed

using flow cytometry analysis by gating CD11c⁺GFP⁺ cells.

Activation of E7-specific CD8⁺ T cell line by CD11c-enriched cells

Mice were vaccinated and CD11c⁺-enriched cells were collected as described above. CD11c-enriched cells (2×10^4) were incubated with 2×10^6 of the E7-specific CD8⁺ T cell line for 16 h. The cells were then stained for both surface CD8 and intracellular IFN- γ and analyzed with flow cytometry analysis as described above.

Statistical analysis

All data were expressed as mean \pm s.e.m. or mean \pm s.d. and were representative of at least two different experiments. Data for intracellular cytokine staining with flow cytometry analysis and tumor treatment experiments were evaluated by analysis of variance. Comparisons between individual data points were made using the Student's *t*-test. In the tumor protection experiment, the principal outcome of interest was the time it took for the tumor to develop. The event time distributions for different mice were compared using the Kaplan and Meier and log-rank analyses. A *P*-value <0.05 was considered statistically significant.

Acknowledgements

This study was supported by grants from the National Science Committee of Taiwan (NSC95-2314-B002-285). We would like to thank Dr TC Wu (Johns Hopkins Medical Institutes, Baltimore, MD, USA) for plasmid pcDNA3-E7/GFP and TC-1 tumor cells.

References

- Smith HO, Tiffany MF, Qualls CR, Key CR. The rising incidence of adenocarcinoma relative to squamous cell carcinoma of the uterine cervix in the United States—a 24-year population-based study. *Gynecol Oncol* 2000; **78**: 97–105.
- Mohar A, Frias-Mendivil M. Epidemiology of cervical cancer. *Cancer Invest* 2000; **18**: 584–590.
- Bosch FX, Manos MM, Munoz N, Sherman M, Jansen AM, Peto J et al. Prevalence of human papillomavirus in cervical cancer: a worldwide perspective. International biological study on cervical cancer (IBSCC) Study Group. *J Natl Cancer Inst* 1995; **87**: 796–802.
- Heard I, Tassie JM, Schmitz V, Mandelbrot L, Kazatchkine MD, Orth G. Increased risk of cervical disease among human immunodeficiency virus-infected women with severe immunosuppression and high human papillomavirus load. *Obstet Gynecol* 2000; **96**: 403–409.
- Chen CH, Ji H, Suh KW, Choti MA, Pardoll DM, Wu TC. Gene gun-mediated DNA vaccination induces antitumor immunity against human papillomavirus type 16 E7-expressing murine tumor metastases in the liver and lungs. *Gene Ther* 1999; **6**: 1972–1981.
- Chen TM, Chen YH, Wu CC, Chen CA, Chang CF, Hsieh CY. Factors influencing tumor cell kinetics in cervical cancer. *J Cancer Res Clin Oncol* 1996; **122**: 504–508.
- Lin HH, Cheng WF, Chan KW, Chang DY, Chen CK, Huang SC. Risk factors for recurrence in patients with stage IB, IIA, and IIB cervical carcinoma after radical hysterectomy and postoperative pelvic irradiation. *Obstet Gynecol* 1996; **88**: 274–279.
- Chang TC, Lai CH, Hong JH, Hsueh S, Huang KG, Chou HH et al. Randomized trial of neoadjuvant cisplatin, vincristine, bleomycin, and radical hysterectomy versus radiation therapy for bulky stage IB and IIA cervical cancer. *J Clin Oncol* 2000; **18**: 1740–1747.
- Boon T, Cerottini JC, Van den Eynde B, van der Bruggen P, Van Pel A. Tumor antigens recognized by T lymphocytes. *Annu Rev Immunol* 1994; **12**: 337–365.
- Chen CH, Wu TC. Experimental vaccine strategies for cancer immunotherapy. *J Biomed Sci* 1998; **5**: 231–252.
- Condon C, Watkins SC, Celluzzi CM, Thompson K, Falo Jr LD. DNA-based immunization by *in vivo* transfection of dendritic cells. *Nat Med* 1996; **2**: 1122–1128.
- Porgador A, Irvine KR, Iwasaki A, Barber BH, Restifo NP, Germain RN. Predominant role for directly transfected dendritic cells in antigen presentation to CD8⁺ T cells after gene gun immunization. *J Exp Med* 1998; **188**: 1075–1082.
- Cheng WF, Hung CF, Chai CY, Hsu KF, He L, Ling M et al. Tumor-specific immunity and antiangiogenesis generated by a DNA vaccine encoding calreticulin linked to a tumor antigen. *J Clin Invest* 2001; **108**: 669–678.
- Cheng WF, Hung CF, Chen CA, Lee CN, Su YN, Chai CY et al. Characterization of DNA vaccines encoding the domains of calreticulin for their ability to elicit tumor-specific immunity and antiangiogenesis. *Vaccine* 2005; **23**: 3864–3874.
- Hung CF, Cheng WF, He L, Ling M, Juang J, Lin CT et al. Enhancing major histocompatibility complex class I antigen presentation by targeting antigen to centrosomes. *Cancer Res* 2003; **63**: 2393–2398.
- Bradham DM, Igarashi A, Potter RL, Grotendorst GR. Connective tissue growth factor: a cysteine-rich mitogen secreted by human vascular endothelial cells is related to the SRC-induced immediate early gene product CEF-10. *J Cell Biol* 1991; **114**: 1285–1294.
- Gygi D, Zumstein P, Grossenbacher D, Altwegg L, Luscher TF, Gehring H et al. Human connective tissue growth factor expressed in *Escherichia coli* is a non-mitogenic inhibitor of apoptosis. *Biochem Biophys Res Commun* 2003; **311**: 685–690.
- Croci S, Landuzzi L, Astolfi A, Nicoletti G, Rosolen A, Sartori F et al. Inhibition of connective tissue growth factor (CTGF/CCN2) expression decreases the survival and myogenic differentiation of human rhabdomyosarcoma cells. *Cancer Res* 2004; **64**: 1730–1736.
- Babic AM, Chen CC, Lau LF. Fisp12/mouse connective tissue growth factor mediates endothelial cell adhesion and migration through integrin α v β 3, promotes endothelial cell survival, and induces angiogenesis *in vivo*. *Mol Cell Biol* 1999; **19**: 2958–2966.
- Yosimichi G, Nakanishi T, Nishida T, Hattori T, Takano-Yamamoto T, Takigawa M. CTGF/Hcs24 induces chondrocyte differentiation through a p38 mitogen-activated protein kinase (p38MAPK), and proliferation through a p44/42 MAPK/extracellular-signal regulated kinase (ERK). *Eur J Biochem* 2001; **268**: 6058–6065.
- Igarashi A, Hayashi N, Nashiro K, Takehara K. Differential expression of connective tissue growth factor gene in cutaneous fibrohistiocytic and vascular tumors. *J Cutan Pathol* 1998; **25**: 143–148.
- Shakunaga T, Ozaki T, Ohara N, Asaumi K, Doi T, Nishida K et al. Expression of connective tissue growth factor in cartilaginous tumors. *Cancer* 2000; **89**: 1466–1473.
- Liao CW, Chen CA, Lee CN, Su YN, Chang MC, Syu MH et al. Fusion protein vaccine by domains of bacterial exotoxin linked with a tumor antigen generates potent immunogenic responses and antitumor effects. *Cancer Res* 2005; **65**: 9089–9098.
- Kim TW, Hung CF, Boyd DA, He L, Lin CT, Kaiserman D et al. Enhancement of DNA vaccine potency by coadministration of a

- tumor antigen gene and DNA encoding serine protease inhibitor-6. *Cancer Res* 2004; **64**: 400–405.
- 25 Kim TW, Hung CF, Ling M, Juang J, He L, Hardwick JM *et al*. Enhancing DNA vaccine potency by coadministration of DNA encoding antiapoptotic proteins. *J Clin Invest* 2003; **112**: 109–117.
- 26 Yang F, Tuxhorn JA, Ressler SJ, McAlhany SJ, Dang TD, Rowley DR. Stromal expression of connective tissue growth factor promotes angiogenesis and prostate cancer tumorigenesis. *Cancer Res* 2005; **65**: 8887–8895.
- 27 Schutze N, Noth U, Schneidereit J, Hendrich C, Jakob F. Differential expression of CCN-family members in primary human bone marrow-derived mesenchymal stem cells during osteogenic, chondrogenic and adipogenic differentiation. *Cell Commun Signal* 2005; **3**: 5–16.
- 28 Heuer H, Christ S, Friedrichsen S, Brauer D, Winckler M, Bauer K *et al*. Connective tissue growth factor: a novel marker of layer VII neurons in the rat cerebral cortex. *Neuroscience* 2003; **119**: 43–52.
- 29 Steffen CL, Ball-Mirith DK, Harding PA, Bhattacharyya N, Pillai S, Brigstock DR. Characterization of cell-associated and soluble forms of connective tissue growth factor (CTGF) produced by fibroblast cells *in vitro*. *Growth Factors* 1998; **15**: 199–213.
- 30 Chen CH, Wang TL, Hung CF, Yang Y, Young RA, Pardoll DM *et al*. Enhancement of DNA vaccine potency by linkage of antigen gene to an HSP70 gene. *Cancer Res* 2000; **60**: 1035–1042.
- 31 Hung CF, Cheng WF, Chai CY, Hsu KF, He L, Ling M *et al*. Improving vaccine potency through intercellular spreading and enhanced MHC class I presentation of antigen. *J Immunol* 2001; **166**: 5733–5740.
- 32 Peng S, Kim TW, Lee JH, Yang M, He L, Hung CF *et al*. Vaccination with dendritic cells transfected with BAK and BAX siRNA enhances antigen-specific immune responses by prolonging dendritic cell life. *Hum Gene Ther* 2005; **16**: 584–593.
- 33 Lin K-Y, Guarnieri FG, Staveley-O'Carroll KE, Levitsky HI, August T, Pardoll DM *et al*. Treatment of established tumors with a novel vaccine that enhances major histocompatibility class II presentation of tumor antigen. *Cancer Res* 1996; **56**: 21–26.
- 34 Feltkamp MC, Smits HL, Vierboom MP, Minnaar RP, de Jongh BM, Drijfhout JW *et al*. Vaccination with cytotoxic T lymphocyte epitope-containing peptide protects against a tumor induced by human papillomavirus type 16-transformed cells. *Eur J Immunol* 1993; **23**: 2242–2249.
- 35 Tindle RW, Fernando GJ, Sterling JC, Frazer IH. A 'public' T-helper epitope of the E7 transforming protein of human papillomavirus 16 provides cognate help for several E7 B-cell epitopes from cervical cancer-associated human papillomavirus genotypes. *Proc Natl Acad Sci USA* 1991; **88**: 5887–5891.
- 36 Cheng WF, Hung CF, Hsu KF, Chai CY, He L, Polo JM *et al*. Cancer immunotherapy using Sindbis virus replicon particles encoding a VP22-antigen fusion. *Hum Gene Ther* 2002; **13**: 553–568.
- 37 Cheng WF, Hung CF, Hsu KF, Chai CY, He L, Ling M *et al*. Enhancement of sindbis virus self-replicating RNA vaccine potency by targeting antigen to endosomal/lysosomal compartments. *Hum Gene Ther* 2001; **12**: 235–252.
- 38 Dialynas DP, Quan ZS, Wall KA, Pierres A, Quintans J, Loken MR *et al*. Characterization of the murine T cell surface molecule, designated L3T4, identified by monoclonal antibody GK1.5: similarity of L3T4 to the human Leu-3/T4 molecule. *J Immunol* 1983; **131**: 2445–2451.
- 39 Sarmiento M, Glasebrook AL, Fitch FW. IgG or IgM monoclonal antibodies reactive with different determinants on the molecular complex bearing Lyt 2 antigen block T cell-mediated cytotoxicity in the absence of complement. *J Immunol* 1980; **125**: 2665–2772.
- 40 Koo GC, Dumont FJ, Tutt M, Hackett Jr J, Kumar V. The NK-1.1(–) mouse: a model to study differentiation of murine NK cells. *J Immunol* 1986; **137**: 3742–3747.
- 41 Cheng WF, Hung CH, Chai CY, Hsu KF, He L, Ling M *et al*. Enhancement of sindbis virus self-replicating RNA vaccine potency by linkage of herpes simplex virus type 1 VP22 protein to antigen. *J Virol* 2001; **75**: 2368–2376.
- 42 Ji H, Chang EY, Lin KY, Kurman RJ, Pardoll DM, Wu TC. Antigen-specific immunotherapy for murine lung metastatic tumors expressing human papillomavirus type 16 E7 oncoprotein. *Int J Cancer* 1998; **78**: 41–45.

Characterization of DNA vaccines encoding the domains of calreticulin for their ability to elicit tumor-specific immunity and antiangiogenesis

Wen-Fang Cheng^{a,1}, Chien-Fu Hung^{b,1}, Chi-An Chen^a, Chien-Nan Lee^a, Yi-Ning Su^c,
Chee-Yin Chai^d, David A.K. Boyd^b, Chang-Yao Hsieh^{a,2}, T.-C. Wu^{b,e,f,g,*}

^a Department of Obstetrics and Gynecology, National Taiwan University Hospital, Taipei, Taiwan

^b Department of Pathology, The Johns Hopkins University School of Medicine, Ross 512,
720 Rutland Avenue, Baltimore, MD 21205, USA

^c Genetic Medicine, National Taiwan University Hospital, Taipei, Taiwan

^d Department of Pathology, School of Medicine, Kaohsiung Medical University, Kaohsiung, Taiwan

^e Department of Obstetrics and Gynecology, Johns Hopkins Medical Institutions, Baltimore, MD, USA

^f Department of Molecular Microbiology and Immunology, Johns Hopkins Medical Institutions, Baltimore, MD, USA

^g Department of Oncology, Johns Hopkins Medical Institutions, Baltimore, MD, USA

Received 22 June 2004; received in revised form 20 October 2004; accepted 25 October 2004

Available online 24 November 2004

Abstract

Antigen-specific cancer immunotherapy and antiangiogenesis are feasible strategies for cancer therapy because they can potentially treat systemic tumors at multiple sites in the body while discriminating between neoplastic and non-neoplastic cells. We have previously developed a DNA vaccine encoding calreticulin (CRT) linked to human papillomavirus-16 E7 and have found that this vaccine generates strong E7-specific antitumor immunity and antiangiogenic effects in vaccinated mice. In this study, we characterized the domains of CRT to produce E7-specific antitumor immunity and antiangiogenic effects by generating DNA vaccines encoding each of the three domains of CRT (N, P, and C domains) linked to the HPV-16 E7 antigen. We found that C57BL/6 mice vaccinated intradermally with DNA encoding the N domain of CRT (NCRT), the P domain of CRT (PCRT), or the C domain of CRT (CCRT) linked with E7 exhibited significant increases in E7-specific CD8⁺ T cell precursors and impressive antitumor effects against E7-expressing tumors compared to mice vaccinated with wild-type E7 DNA. In addition, the N domain of CRT also showed antiangiogenic properties that might have contributed to the antitumor effect of NCRT/E7. Thus, the N domain of CRT can be linked to a tumor antigen in a DNA vaccine to generate both antigen-specific immunity and antiangiogenic effects for cancer therapy.

© 2004 Published by Elsevier Ltd.

Keywords: Calreticulin; DNA vaccine; NCRT; CCRT; PCRT; HPV-16; E7 antigen

1. Introduction

Antigen-specific cancer immunotherapy and antiangiogenesis are feasible strategies for cancer therapy because they

are able to treat systemic tumors at multiple sites in the body while discriminating between neoplastic and non-neoplastic cells. Activation of antigen-specific T cell-mediated immune responses allows for killing of tumors associated with a specific antigen [1,2] while inhibition of angiogenesis controls neoplastic growth by sequestering neoplastic cells from an adequate blood supply [3,4]. Therefore, an innovative approach that combines both mechanisms will likely generate the most potent antitumor effect.

We have previously combined tumor-specific immunity and antiangiogenesis in an innovative DNA vaccine strategy

* Corresponding author. Tel.: +1 410 614 3899; fax: +1 443 287 4295.

E-mail addresses: cyhsieh@ha.mc.ntu.edu.tw (C.-Y. Hsieh),
wutc@jhmi.edu (T.-C. Wu).

¹ Wen-Fang Cheng and Chien-Fu Hung are equal contributors to this article.

² Tel.: 886 2 2312 3456; fax: 886 2 2393 4197.

encoding calreticulin (CRT) linked to model antigen HPV-16 E7 [5]. CRT is an abundant 46 kDa Ca^{2+} -binding protein located in the endoplasmic reticulum (ER) [6]. The protein has been shown to associate with peptides delivered into the ER by transporters associated with antigen processing (TAP-1 and TAP-2) [7] and with MHC class I- β 2 microglobulin molecules to aid in antigen presentation [8]. Previous studies have shown that CRT can be complexed with peptides in vitro to elicit peptide-specific CD8^+ T cell responses through exogenous administration [9]. Recently, full-length calreticulin has been reported to be an endothelial cell inhibitor and exerts antitumor effects in vivo via antiangiogenesis [10–12].

The CRT protein is composed of three domains, the N domain, P domain and C domain. The N domain (residues 1–180), also known as vasostatin, is extremely conserved among calreticulins from different species [13]. The N domain interacts with the DNA-binding domain of the glucocorticoid receptor in vitro [14], with rubella virus RNA [15], with α -integrin [16], and with protein disulphide-isomerase (PDI) and ER protein 57 (ERp57) [17]. The N domain of calreticulin also inhibits proliferation of endothelial cells and suppresses angiogenesis [10]. The P domain (residues 181–280) is rich in proline and contains two sets of three sequence repeats. This region of the protein binds Ca^{2+} with high affinity [18]. The P domain is thought to be critical for the lectin-like chaperone activity of calreticulin [19]. The P domain of calreticulin also interacts with PDI [17] and perforin [20,21]. The C-terminal region of the protein is highly acidic and terminates with the KDEL ER retrieval sequence [22]. This C domain of CRT binds to calcium [18] and to blood-clotting factors [23] and inhibits injury-induced restenosis [24].

In the present study, we investigated DNA vaccines encoding each of the N, P, and C domains of calreticulin chimerically linked to HPV-16 E7 for their abilities to elicit antigen-specific CD8^+ T cell responses and antitumor immunity in vaccinated mice. We found that C57BL/6 mice vaccinated intradermally with NCRT/E7, PCRT/E7 or CCRT/E7 DNA exhibited significant increases in E7-specific CD8^+ T cell precursors and impressive antitumor effects against E7-expressing tumors compared with mice vaccinated with wild-type E7 DNA. We also determined that the N domain of calreticulin (NCRT) resulted in antiangiogenic antitumor effects. Thus, cancer therapy using NCRT linked to a tumor antigen holds promise for treating tumors through a combination of antigen-specific immunotherapy and antiangiogenesis.

2. Materials and methods

2.1. Plasmid DNA constructs and preparation

The generation of pcDNA3-E7 has been described previously [5,25]. The generation of pcDNA3-CRT has also been described previously [5]. There is more than 90% homology between rabbit, human, mouse, and rat CRT [26]. For the gen-

eration of pcDNA3-NCRT, DNA encoding the N domain of CRT, NCRT was first amplified with PCR by using rabbit CRT cDNA as the template [27] and a set of primers, 5'-CCGG-TCTAGAATGCTGCTCCCTGTGCCGCT-3' and 5'-CCCGAATTCGTTGTCCGGCCGCACGATCA-3'. The amplified product was further cloned into the *Xba*I/*Eco*RI site of pcDNA3 (Invitrogen Corp., Carlsbad, CA, USA). For the generation of pcDNA3-PCRT, DNA encoding the P domain of CRT was first amplified with PCR using rabbit CRT cDNA as the template and a set of primers, 5'-TGCTCTAGAACGTATGAGGTGAAGATTGA-3' and 5'-CCGGAATTCGGGGTTCTGAATCACCGGC-3'. The amplified product was further cloned into the *Xba*I/*Eco*RI site of pcDNA3. For the generation of pcDNA3-CCRT, DNA encoding the C domain of CRT was first amplified with PCR using rabbit CRT cDNA as the template and a set of primers, 5'-TGCTCTAGAGAGTACAAGGGTGAGTGGAAGC-3' and 5'-CCGGAATTCAGCTCGTCCCTTGGCCTGGC-3'. The completed product was then cloned into the *Xba*I/*Eco*RI site of pcDNA3. For the generation of pcDNA3-NCRT/E7, PCRT/E7, and CCRT/E7, E7 was first amplified with pcDNA3-E7 as a template and a set of primers, 5'-GGGGAATTCATGGAGATACACCTA-3' and 5'-GGTGGATCCTTGAGAACAGATGG-3', and then cloned it into the *Eco*RI/*Bam*HI sites of pcDNA3-NCRT, pcDNA3-PCRT, or pcDNA3-CCRT to generate pcDNA3-NCRT/E7, pcDNA3-PCRT/E7, or pcDNA3-CCRT/E7.

2.2. Cell line

The production and maintenance of TC-1 cells have been described previously [28]. In brief, HPV-16 E6, E7 and *ras* oncogene were used to transform primary C57BL/6 mice lung epithelial cells to generate TC-1.

2.3. DNA vaccination

Preparation of DNA-coated gold particles and gene gun particle-mediated DNA vaccinations were performed using a helium-driven gene gun according to a protocol described previously with some modifications [25]. Gene gun particle-mediated DNA vaccinations were performed using a Low Pressure-accelerated Gene Gun (BioWare Technologies Co. Ltd., Taipei, Taiwan). The gold particles (Bio-Rad 1652263) were weighted and suspended in 70% ethanol. This suspension was vortexed vigorously and then centrifuged to collect the particles. After washing by distilled water three times, the collected particles were resuspended in DNA solution (1 μg DNA per mg gold particles), vortexed and sonicated for a few seconds, and then added 2.5 M CaCl_2 and 0.05 M spermidine solution with vortex. This solution was kept on ice for 10 min and the DNA-coated gold particles were collected and washed by 100% ethanol three times. Finally, the particles were resuspended in 100% ethanol with appropriate concentration and used to make bullets. Control plasmid (no insert), E7, NCRT, NCRT/E7, PCRT/E7, CCRT/E7, or CRT/E7 DNA-coated gold particles were delivered to the shaved

abdominal region of mice using a low pressure-accelerated Gene Gun (BioWare Technologies Co. Ltd., Taipei, Taiwan) with a 50 psi discharge pressure of helium.

2.4. Intracellular cytokine staining and flow cytometry analysis

Mice were immunized with 2 µg of the various DNA vaccines and received a booster with the same regimen 1 week later. Splenocytes were harvested 1 week after the last vaccination. Before intracellular cytokine staining, 5×10^6 pooled splenocytes from each vaccination group were incubated for 16 h with either 1 µg/ml of E7 peptide (aa 49-57) containing an MHC class I epitope [29] for detecting E7-specific CD8⁺ T cell precursors or 10 µg/ml of E7 peptide (aa 30-67) containing an MHC class II epitope [30] for detecting E7-specific CD4⁺ T cell precursors. Cell surface marker staining for CD8 or CD4 and intracellular cytokine staining for IFN-γ, as well as flow cytometry analysis, were performed using conditions described previously [31].

2.5. Enzyme-linked immunoabsorbent assay (ELISA) for anti-E7 antibody

For the detection of HPV 16 E7-specific antibodies in the sera, a direct ELISA was used as described previously [5]. Mice were immunized with 2 µg of the various DNA vaccines and received a booster with the same regimen 1 week later. Sera were prepared from mice on day 14 after immunization. Briefly, a 96-microwell plate was coated with 100 µl of bacteria-derived HPV-16 E7 proteins (0.5 µg/ml) and incubated at 4 °C overnight. The wells were then blocked with phosphate-buffered saline (PBS) containing 20% fetal bovine serum. Sera were prepared from mice on day 14, post immunization, serially diluted in PBS, added to the ELISA wells, and incubated at 37 °C for 2 h. After washing with PBS containing 0.05% Tween 20, the plate was incubated with a 1:2000 dilution of a peroxidase-conjugated rabbit anti-mouse IgG antibody (Zymed, San Francisco, CA) at room temperature for 1 h. The plate was washed, developed with 1-Step Turbo TMB-ELISA (Pierce, Rockford, IL), and stopped with 1 M H₂SO₄. The ELISA plate was read with a standard ELISA reader at 450 nm.

2.6. In vivo tumor protection experiments

For the tumor protection experiment, C57BL/6 mice (five per group) either received no vaccination or were immunized with 2 µg/mouse of plasmid encoding no insert, NCRT, E7, NCRT/E7, PCRT/E7, CCRT/E7 or NCRT mixed with E7 using a gene gun. One week later, mice were boosted with the same regimen as the first vaccination. One week after the last vaccination, mice were subcutaneously challenged with 5×10^4 TC-1 cells/mouse in the right leg. Mice were monitored for evidence of tumor growth by palpation and inspection twice a week until they were sacrificed at day 60.

2.7. In vivo antibody depletion experiments

In vivo antibody depletions were performed as described previously [28]. Briefly, C57BL/6 mice (5 per group) were vaccinated with 2 mg/mouse of NCRT/E7 DNA via gene gun, boosted 1 week later, and challenged with 5×10^4 cells/mouse TC-1 tumor cells. Depletion was started one week prior to tumor challenge. MAb GK1.5 was used for CD4 depletion, MAb 2.43 was used for CD8 depletion, and MAb PK136 was used for NK1.1 depletion. Depletion was terminated on day 60 after tumor challenge.

2.8. In vivo tumor treatment experiments

In vivo tumor treatment experiments were performed using a previously described lung hematogenous spread model [32]. C57BL/6 mice were challenged with 5×10^4 TC-1 tumor cells/mouse via tail vein injection. Nude (BALB/c nu/nu) mice (five per group) were challenged with 1×10^5 cells/mouse TC-1 tumor cells via tail vein. Two days after tumor challenge, mice received 16 µg/mouse of DNA encoding no insert, NCRT DNA, E7 DNA, NCRT/E7 DNA, PCRT/E7 DNA, CCRT/E7 DNA, or CRT/E7 DNA by a gene gun, followed by two boosters with the same regimen at one-week intervals (a total of three shots, 48 µg DNA/mouse). Mice receiving no vaccination were used as a negative control. Mice were sacrificed and lungs were explanted on day 21 after tumor challenge. The pulmonary tumor nodules in each mouse were evaluated and counted by experimenters blinded to sample identity.

2.9. Immunohistochemical labeling for the quantitation of microvessel density

Labeling of intratumoral microvessels was performed with rat anti-mouse CD31 mAb (1:30 dilution, Bioscience), followed by VECTOR[®] M.O.M.[™]. Immunodetection Kit (VECTOR; Burlingame, CA). The method for quantitating microvessel density (MVD) has been described previously [33]. Briefly, slides were prepared and examined at 20× and 100×. In each section, the three most vascularized areas were chosen. Microvessel counts were obtained at 200× and the mean number in the three fields for each tumor was calculated and referred to as the MVD count. Large vessels with thick muscular walls and lumina greater than approximately eight blood cells were excluded from the count. We counted and compared MVD in tumors of similar size to minimize the influence of tumor size on the measurements. All measurements were performed by a single pathologist, blinded to sample identity.

2.10. In vivo angiogenesis assay using Matrigel

In vivo angiogenesis was assessed using the Matrigel plug assay with a protocol similar to that described previously [5,34]. Mice were immunized with 16 µg of plasmid without

insert, wild-type E7, NCRT, NCRT/E7, PCRT/E7, CCRT/E7 or CRT/E7 DNA on day 0 and received a booster with the same regimen on day 7. Matrigel (Becton Dickinson and Co., Franklin Lakes, New Jersey, USA) was mixed with heparin (final concentration of 50 U/ml), bFGF (final concentration of 20 ng/ml), and VEGF (final concentration of 200 ng/ml) at 4 °C. A total of 0.5 ml/mouse of this Matrigel mixture was injected subcutaneously into the abdominal midline of DNA-vaccinated mice on day 7. Naive mice injected with Matrigel mixed with heparin, bFGF and VEGF served as a positive control; naive mice injected with Matrigel alone were used as a negative control. Mice were euthanized on day 16. The Matrigel plugs were resected from surrounding connective tissues. Half of the Matrigel plugs were fixed in 10% formaldehyde, embedded in paraffin, sectioned, and stained with hematoxylin and eosin or Giemsa stains to calculate microvessel density. In each section, the five most vascular areas were chosen. Microvessel counts were obtained at 400 \times , and the mean number in the five fields for the Matrigel plugs was calculated and referred to as the MVD count. The remaining half of the Matrigel plugs was assayed for hemoglobin content according to manufacturer's instructions (Drabkin's reagent kit; Sigma Diagnostics Co., St. Louis, MO, USA).

2.11. Statistical analysis

All data expressed as means \pm S.D. are representative of at least two different experiments. Data for intracellular cytokine staining with flow cytometry analysis and tumor treatment experiments were evaluated by analysis of variance (ANOVA). Comparisons between individual data points were made using a Student's *t*-test. In the tumor protection experiment, the principal outcome of interest was time to development of tumor. The event time distributions for different mice were compared by Kaplan and Meier and by log-rank analyses.

3. Results

3.1. Vaccination with DNA encoding NCRT, PCRT, or CCRT linked to E7 significantly enhances the E7-specific CD8⁺ T cell response

A schematic diagram of the DNA constructs used in the study is shown in Fig. 1. To determine if the different domains of calreticulin when linked with the E7 DNA vaccines could enhance E7-specific T cell-mediated immune responses in mice, we performed intracellular cytokine staining with flow cytometry analysis to characterize E7-specific CD8⁺ and CD4⁺ T cell precursors. As shown in Fig. 2A, mice vaccinated with NCRT/E7, PCRT/E7, or CCRT/E7 DNA generated higher frequencies of E7-specific IFN- γ -secreting CD8⁺ T cell precursors when compared to mice vaccinated with E7 DNA ($P < 0.01$). DNA encoding no insert was used as a negative control. Our results also indicated that the phys-

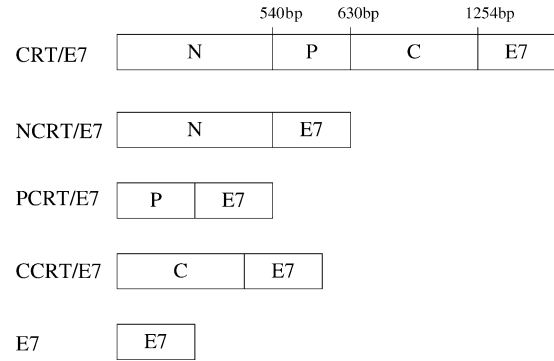


Fig. 1. Diagram depicting the composition of the various DNA constructs used in the study. CRT is composed of three identified domains: N (1–540 bp), P (541–807 bp), and C (808–1256 bp). DNA constructs were generated to encode each of these domains linked to HPV-16 E7.

ical linkage of NCRT to E7 was required for enhancement of CD8⁺ T cell activity, since DNA encoding the N domain of CRT mixed with E7 DNA did not generate enhancement of CD8⁺ T cell activity (data not shown). Vaccination with CRT/E7 DNA generated a slightly higher number of E7-specific CD8⁺ T cell precursors (220.5 ± 18.5) compared to NCRT/E7 (178.0 ± 18.5), PCRT/E7 (140.0 ± 16.0) and CCRT/E7 (128.0 ± 10.0) ($P < 0.01$). Thus, our data suggest that NCRT/E7, PCRT/E7, and CCRT/E7 DNA vaccines are capable of enhancing the E7-specific CD8⁺ T cell response in vaccinated mice, although not as strongly as CRT/E7.

We further evaluated whether CRT, NCRT, PCRT, or CCRT could enhance the E7-specific CD4⁺ T cell response when linked to E7 in a DNA vaccine. DNA encoding no insert was used as a negative control. Mick-2 cells were used as a positive control and generated IFN- γ -secreting CD4⁺ T cells in mice (data not shown). As shown in Fig. 2B, we observed no increase in the number of E7-specific IFN- γ -secreting CD4⁺ T cells in mice vaccinated with NCRT/E7, PCRT/E7, CCRT/E7, or CRT/E7 DNA compared to mice vaccinated with control plasmid, E7, or NCRT DNA (Fig. 2B).

3.2. Vaccination with NCRT/E7 DNA significantly enhances the E7-specific antibody response

We performed ELISA to determine if vaccination with NCRT/E7, PCRT/E7, or CCRT/E7 DNA could enhance E7-specific antibody responses in vaccinated mice compared to vaccination with wild-type E7 DNA. As shown in Fig. 2C, vaccination with NCRT/E7 or CRT/E7 DNA generated significantly higher titers of anti-E7 antibodies in the sera of mice compared with the other vaccinated groups ($P < 0.01$). There was no significant difference between the titers of E7 antibody generated by NCRT/E7 and CRT/E7. Our results indicated that the fusion of NCRT to E7 could enhance the E7-specific antibody response compared to wild-type E7 and that the titer of E7-specific antibody generated by the NCRT/E7 DNA vaccine is comparable to that generated by the CRT/E7 DNA vaccine.

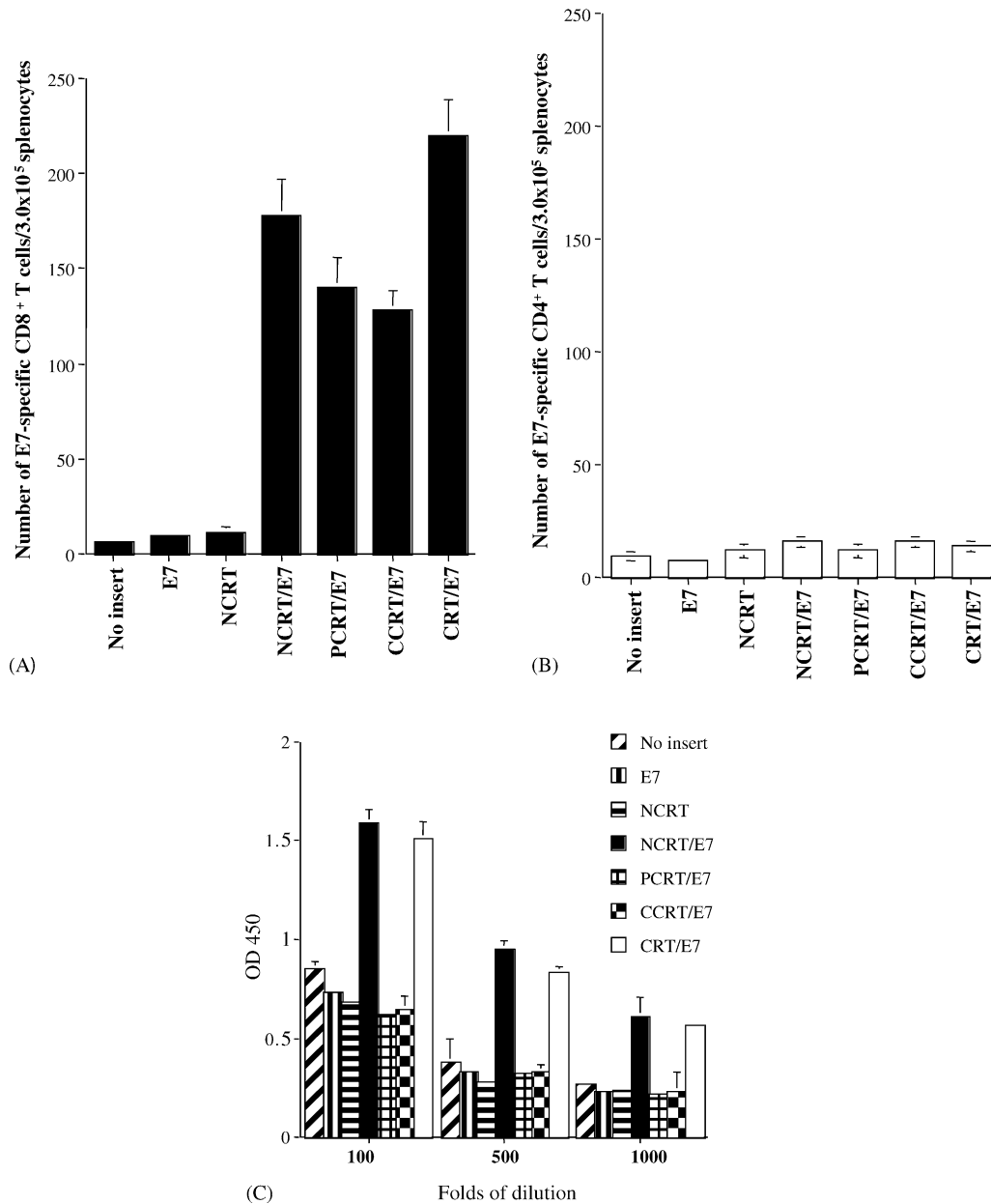


Fig. 2. Immunological profile of vaccinated mice using intracellular cytokine staining and flow cytometry analysis and ELISA. Mice were vaccinated with DNA encoding no insert, E7, NCRT, NCRT/E7, CCRT/E7, PCRT/E7, or CRT/E7. Splenocytes from vaccinated mice were harvested 7 days after vaccination, cultured *in vitro* with MHC class I-restricted (aa 49–57) or class II-restricted (aa 30–67) E7 peptide overnight, and stained for intracellular IFN- γ and CD4 or CD8. (A) Bar graph depicting the number of antigen specific IFN- γ -secreting CD8⁺ T cell precursors/ 3×10^5 splenocytes (mean \pm S.D.). (B) Bar graph depicting the number of antigen specific IFN- γ -secreting CD4⁺ T cell precursors/ 3×10^5 splenocytes (mean \pm S.D.). *Note:* Mice vaccinated with CRT/E7, NCRT/E7, PCRT/E7, or CCRT/E7 DNA generated higher numbers of E7-specific IFN- γ -secreting CD8⁺ T cell precursors than the other vaccination groups. (C) Bar graph demonstrating E7-specific antibodies in mice vaccinated with various DNA vaccines. The results from the 1:100, 1:500, and 1:1,000 dilution are presented, showing mean absorbance (OD450 nm) \pm S.D. All data above are from one representative experiment of two performed. *Note:* NCRT/E7 DNA and CRT/E7 vaccines generated significantly higher E7-specific antibody responses when compared with mice vaccinated with the other DNA vaccines ($P < 0.01$, one-way ANOVA).

3.3. Vaccination with NCRT/E7, PCRT/E7, or CCRT/E7 DNA enhances tumor protection in mice challenged with an E7-expressing tumor cell line

To determine if the observed enhancement of the E7-specific CD8⁺ T cell response translated into a significant E7-specific protective antitumor effect, we performed an *in*

vivo tumor protection experiment using a previously characterized E7-expressing tumor model, TC-1 [28]. As shown in Fig. 3, 100% of mice receiving PCRT/E7, CCRT/E7, or CRT/E7 DNA vaccination also remained tumor-free 60 days after TC-1 challenge. In comparison, all mice vaccinated with wild-type E7 DNA developed tumors within 14 days of challenge. This suggests that each of the three domains

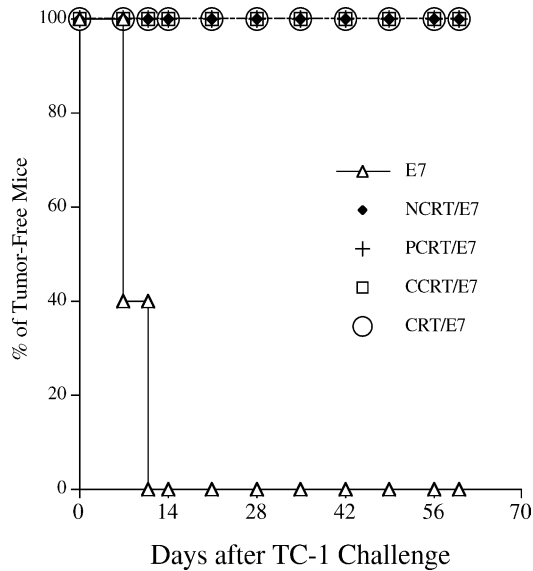


Fig. 3. In vivo tumor protection experiments in mice vaccinated with various DNA vaccines. Mice were immunized with DNA vaccines encoding E7, NCRT/E7, PCRT/E7, CCRT/E7 or CRT/E7 and then were challenged with TC-1 tumor cells. Note: 100% of mice receiving NCRT/E7, PCRT/E7, CCRT/E7, or CRT/E7 remained tumor-free 60 days after TC-1 challenge.

of calreticulin can protect vaccinated mice against a lethal challenge with E7-expressing tumor cells when linked to the E7 antigen in a DNA vaccine.

3.4. Treatment with NCRT/E7, PCRT/E7, or CCRT/E7 DNA leads to significant reduction of pulmonary tumor nodules in C57BL/6 wild-type mice

We further assessed the therapeutic potential of each vaccine by performing an in vivo tumor treatment experiment using a previously described lung hematogenous spread model [5]. As shown in Fig. 4, C57BL/6 mice treated with NCRT/E7 DNA (1.0 ± 0.4), PCRT/E7 (1.2 ± 0.8), or CCRT/E7 (1.4 ± 0.6) all exhibited significantly fewer pulmonary tumor nodules than mice treated with the other DNA vaccines (wild-type E7 (139.0 ± 11.0) or NCRT (34.0 ± 3.2) did (one-way ANOVA, $P < 0.001$). These data indicated that any of the three domains of calreticulin, when linked with E7 antigen, could generate more potent antitumor effects than wild-type E7 DNA constructs in a lung hematogenous spread model.

We also observed that treatment of mice with NCRT DNA also resulted in significantly fewer tumor nodules than treatment with wild-type E7 DNA or no treatment (one-way ANOVA, $P < 0.001$). This suggests that NCRT may generate an antitumor effect that is independent of antigen-specific T cell-mediated immunity.

3.5. Treatment with NCRT/E7 or NCRT DNA leads to significant reduction of pulmonary tumor nodules in immunocompromised mice

To confirm that treatment with NCRT, NCRT/E7, or CRT/E7 DNA could generate a T cell-independent antitu-

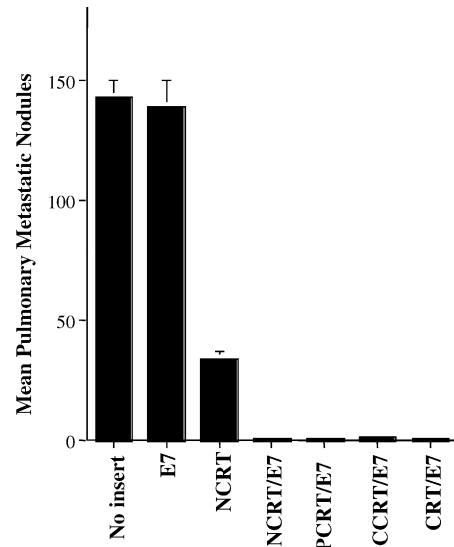


Fig. 4. In vivo tumor treatment experiments in C57BL/6 mice. Bar graph depicting mean pulmonary tumor nodules in each vaccinated group. Mice were challenged with TC-1 tumor cells and subsequently treated with DNA encoding no insert, E7, NCRT, NCRT/E7, PCRT/E7, CCRT/E7, or CRT/E7 at a high therapeutic dose. The data are expressed as mean number of pulmonary tumor nodules \pm S.D. Note: Mice treated with DNA encoding NCRT/E7, PCRT/E7, CCRT/E7, or CRT/E7 showed similar numbers of tumor nodules, all significantly lower than numbers in mice treated with DNA encoding E7, no insert, or NCRT.

mor effect, we performed an in vivo tumor treatment experiment using immunocompromised (BALB/c nu/nu) mice. As shown in Fig. 5A, nude mice treated with NCRT, NCRT/E7, or CRT/E7 DNA displayed a significantly lower mean number of pulmonary tumor nodules (18.0 ± 2.0 for NCRT, 25.0 ± 4.0 for NCRT/E7) compared with mice treated with wild-type E7 DNA (215.0 ± 10.0), plasmid without insert (217.5 ± 17.0), or naive group (230.0 ± 22.5) (one-way ANOVA, $P < 0.001$). Interestingly, no significant reduction in tumor nodules could be detected in mice treated with PCRT/E7 or CCRT/E7 compared to mice treated with wild-type E7. In addition, nude mice treated with NCRT/E7 DNA exhibited significantly fewer pulmonary tumor nodules than nude mice treated with CRT/E7 DNA (one-way ANOVA, $P < 0.05$). Our data suggest that treatment with NCRT, NCRT/E7, or CRT/E7 DNA are able to generate an antitumor effect even in the absence of T cell-mediated immune responses and that PCRT/E7 and CCRT/E7 DNA are not able to do this.

3.6. Tumors from BALB/c nude mice treated with NCRT, NCRT/E7, or CRT/E7 DNA show a reduction in microvessel density (MVD)

To determine whether the antitumor effect of NCRT, NCRT/E7, or CRT/E7 DNA in the absence of T cells might be mediated through antiangiogenesis, we measured MVD in the pulmonary tumors of nude mice treated with various DNA vaccines. As shown in Fig. 5B, treatment of nude mice with NCRT, NCRT/E7, or CRT/E7 DNA resulted in sig-

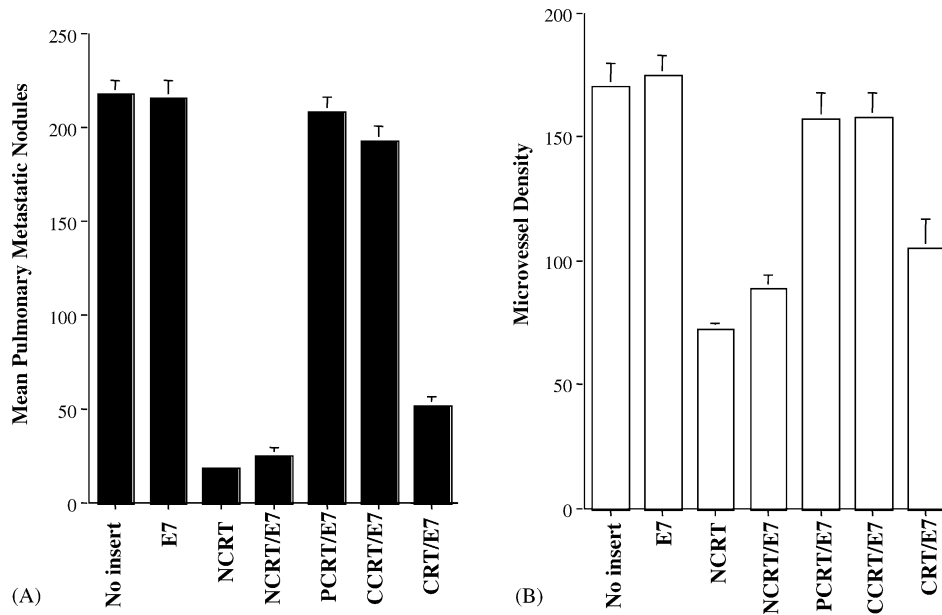


Fig. 5. In vivo tumor treatment experiments in nude mice and the microvessel density of pulmonary tumor nodules in DNA-treated nude mice. (A) Bar graph depicting mean numbers of pulmonary tumor nodules in treated BALB/c (*nu/nu*) mice. Mice were challenged with TC-1 tumor cells and were subsequently treated with the various DNA vaccines at a high therapeutic dose. Note: Nude mice treated with NCRT, NCRT/E7 or CRT/E7 DNA vaccines showed significantly lower numbers of pulmonary tumor nodules compared with the wild-type E7, PCRT/E7 or CCRT/E7 DNA groups. (B) Bar graph depicting mean microvessel density in pulmonary tumor nodules in mice treated with the various DNA constructs. Immunohistochemical labeling and microvessel counts were performed. Note: The MVDs of the pulmonary tumor nodules in the NCRT, NCRT/E7, and CRT/E7 groups were significantly lower than the wild-type E7, PCRT/E7 or CCRT/E7 groups.

nificantly lower MVD in pulmonary tumors than treatment with wild-type E7, PCRT/E7 or CCRT/E7 group (one-way ANOVA, $P < 0.001$). MVD in pulmonary tumors was significantly lower in nude mice treated with NCRT/E7 DNA than in nude mice treated with CRT/E7 DNA (one-way ANOVA, $P < 0.05$). Taken together, our data suggest that the T cell-independent antitumor effect elicited by vaccination with NCRT, NCRT/E7, or CRT/E7 DNA is antiangiogenic and that this angiogenic effect may be related to the N domain of CRT.

3.7. Matrigels from C57BL/6 mice challenged with TC-1 and treated with NCRT, NCRT/E7, or CRT/E7 DNA show reduced microvessel density and hemoglobin content

To provide a more quantitative assessment of antiangiogenesis in C57BL/6 mice treated with the various DNA constructs, we performed an in vivo angiogenesis assay using Matrigel [5]. As shown in Fig. 6A, the hemoglobin contents of Matrigel implants from NCRT, NCRT/E7, or CRT/E7-treated mice were significantly lower than those from mice treated with DNA encoding no insert, E7, PCRT/E7, or CCRT/E7 ($P < 0.01$, ANOVA). This assay revealed that NCRT or NCRT/E7 DNA could generate a similar degree of inhibition of bFGF- and VEGF-induced in vivo angiogenesis. Interestingly, the hemoglobin contents of Matrigel implants from NCRT/E7-treated mice were significantly lower than those from CRT/E7-treated mice ($P < 0.01$, ANOVA). We also examined the MVD of Matrigel samples to provide another measure of angiogenesis inhibition, since red blood

cells may extravasate from vessels and affect the hemoglobin count. As seen in Fig. 6B, the mean MVDs in Matrigel samples from NCRT (23.7 ± 10.4), NCRT/E7 (21.3 ± 4.7), and CRT/E7 (29.0 ± 9.2) DNA-treated mice were similar and significantly lower than the MVDs in Matrigel samples from no insert (98.3 ± 31.8), wild-type E7 (76.7 ± 12.0), CCRT/E7 (77.3 ± 9.6), or PCRT/E7 (76.3 ± 6.7) DNA-treated mice. Thus, our data confirm that the N domain of CRT is responsible for the antiangiogenic effect observed in mice treated with CRT/E7.

3.8. Linkage of NCRT to E7 is essential for generating the antitumor effect against TC-1 cells in vaccinated mice

To assess whether the linkage of NCRT to E7 is essential for the antitumor effect against E7-expressing tumors in vaccinated mice, we performed in vivo tumor protection experiments using TC-1 tumor cells. Mice were vaccinated with various DNA constructs, including E7 DNA, NCRT DNA, NCRT/E7, and NCRT DNA mixed with E7 DNA. One week after the last vaccination, mice were challenged with 5×10^4 /mouse of TC-1 cells. As shown in Fig. 7A, all mice vaccinated with the NCRT/E7 DNA vaccine remained tumor-free. In contrast, all mice vaccinated with the other DNA vaccines (including NCRT mixed with E7) developed tumors within 2 weeks after challenge with TC-1 cells. Our results indicate that the linkage of NCRT to E7 was essential for the observed antitumor effects in the vaccinated mice.

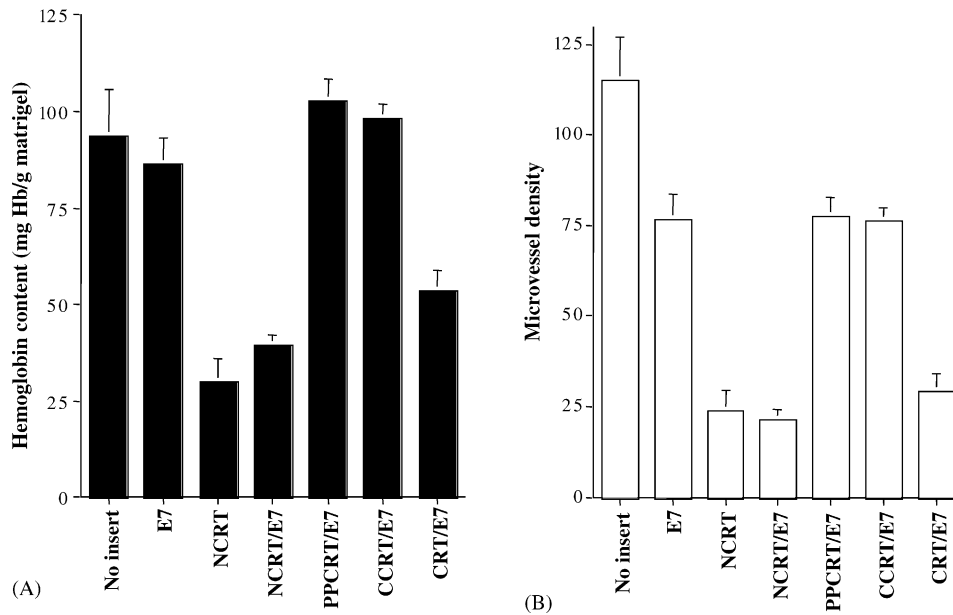


Fig. 6. In vivo angiogenesis assay using Matrigel to characterize the antiangiogenic effect resulting from treatment with the various DNA constructs. Mice were treated with various DNA constructs and injected with Matrigel. Nine days later, mice were euthanized, and Matrigel plugs were resected. (A) Bar graph depicting Matrigel hemoglobin content for mice treated with DNA vaccines. *Note:* The NCRT, NCRT/E7, and CRT/E7 groups had lower hemoglobin concentrations compared to the wild-type E7, PCRT/E7, and CCRT/E7 groups. (B) Bar graph displaying microvessel density of the Matrigel in mice treated with various DNA vaccines. The Matrigel plugs were fixed, embedded, sectioned, and stained to calculate microvessel density. *Note:* The mean numbers of MVD in Matrigel samples from NCRT, NCRT/E7 or CRT/E7 DNA-treated mice were similar and significantly lower than those of the MVD in Matrigel samples from pcDNA3 without insert, wild-type E7, CCRT/E7, or PCRT/E7 DNA-treated mice.

3.9. CD8⁺ T cells, but not CD4⁺ T cells or NK cells, are important for the antitumor effect generated by the NCRT/E7 DNA vaccine

To determine the subset of lymphocytes that is important for the antitumor effect generated by the NCRT/E7 DNA

vaccine, we performed in vivo antibody depletion experiments. As shown in Fig. 7B, all NCRT/E7 DNA-vaccinated mice depleted of CD8⁺ T cells and all unvaccinated naive mice grew tumors within 14 days after tumor challenge. In contrast, all NCRT/E7 DNA-vaccinated mice depleted of CD4⁺ T cells and NK cells remained tumor free 56 days

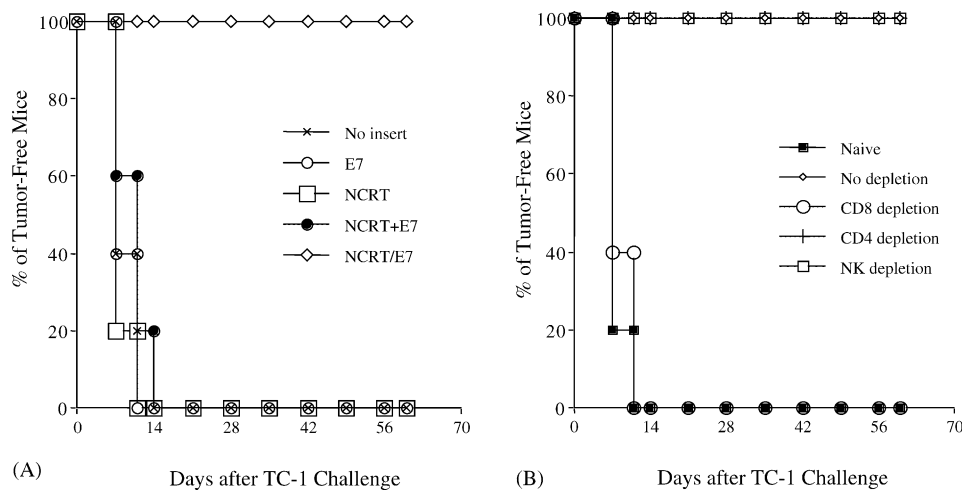


Fig. 7. In vivo tumor protection experiments in mice vaccinated with various DNA vaccines and in vivo antibody depletion experiments in mice vaccinated with NCRT/E7. (A) Mice were immunized with various DNA vaccines and challenged as described in the Section 2 to assess the antitumor effect generated by each DNA vaccine. (B) An in vivo antibody depletion experiment was performed to determine the effect of lymphocyte subsets on the potency of the NCRT/E7 DNA vaccine. Mice were vaccinated, challenged with TC-1, and depleted of the relevant subset of lymphocytes as described in Section 2. *Note:* that depletion of CD8⁺ T cells, but not of CD4⁺ T cells or NK cells, led to significant tumor growth in NCRT/E7 DNA-vaccinated mice. The data from the antibody depletion experiments shown here are from one representative experiment of two performed.

after tumor challenge. These results suggest that CD8⁺ T cells, but not CD4⁺ T cells or NK cells, were essential for the antitumor immunity generated by the NCRT/E7 DNA vaccine.

4. Discussion

In this study, we demonstrated that linkage of NCRT, PCRT, or CCRT to the HPV-16 E7 antigen can significantly enhance the potency of an E7-expressing DNA vaccine. All three domains of calreticulin linked with E7 DNA elicited strong E7-specific CD8⁺ T cell immune responses, generated significant CD8⁺ T cell-dependent protective effects against subcutaneous HPV-16 E7-expressing tumors, and could effectively treat lethal pulmonary tumor nodules. In comparison, vaccination with only NCRT/E7 or CRT/E7 DNA was able to significantly enhance the E7-specific antibody response when compared to the other DNA vaccine constructs. Furthermore, only DNA vaccines encoding the N domain of CRT generated a therapeutic effect due to inhibition of angiogenesis, which likely contributed to reduction of pulmonary tumor nodules. Thus, a DNA vaccine encoding NCRT chimerically linked to a tumor antigen represents another valid approach combining immunological and antiangiogenic approaches for the generation of a potent antitumor effect.

Our data demonstrated that all three domains of calreticulin could enhance the E7-specific CD8⁺ T cell immune response when linked with the HPV-16 E7 antigen. It has been previously shown that professional APCs, directly transfected via gene gun, play a primary role in eliciting an antigen-specific T cell response to DNA vaccination [35]. Full length CRT has been shown to be able to enhance MHC class I processing of antigen by targeting linked antigen to the ER [5]. One or more domains of CRT may also enhance MHC class I processing of the linked E7 antigen in transfected professional APCs. Another mechanism that may play a role in the enhancement of E7-specific CD8⁺ T cell immune responses *in vivo* is the so-called “cross-priming” effects, whereby secretion of chimeric protein or lysis of cells expressing chimeric antigen releases the chimeric protein exogenously to be taken up and processed by other APCs via the MHC class I restricted pathways. CD91, an $\alpha 2$ macroglobulin receptor, serves as a receptor for heat shock proteins, including calreticulin, gp96, HSP70 and HSP90 and facilitate the cross-priming effects [9]. It is still uncertain which of the three domains of CRT is capable of binding with CD91. These direct and cross-priming mechanisms may provide some explanation for the observed enhancement of E7-specific CD8⁺ T cell activity in mice vaccinated with NCRT/E7, PCRT/E7 or CCRT/E7 DNA.

Out of the three domains of CRT, we observed that E7-specific antibody titers were significantly enhanced by NCRT/E7 vaccination only. This may be due to the fact that NCRT encodes the signal sequence of CRT, allowing extra-

cellular secretion and stimulation of B cells by NCRT/E7. Vaccination with PCRT/E7 or CCRT/E7 DNA may not have been capable of eliciting an E7-specific Ab response because they lack this sequence. To address if T cells are required for the observed E7-specific antibody response, we have used immunocompromised mice (BALB/c *nu/nu*) for our studies. Our data indicate that nude mice vaccinated with CRT/E7 are capable of generating an E7-specific antibody response (data not shown), suggesting that the antibody response mediated by calreticulin may be contributed by T cell independent mechanisms. Even though antibody-mediated responses have not been shown to play an important role in controlling HPV-associated malignancies, antigen-specific Abs are significant in other tumor models, such as the breast cancer model with the HER-2/neu antigen. The chimeric NCRT or CRT vaccine strategy may be used to generate HER-2/neu-specific Ab's to induce growth arrest in cells expressing high levels of HER-2/neu on the cell surface [36].

We observed that treatment of immunocompromised mice (BALB/c *nu/nu*) with NCRT/E7 or NCRT DNA generated comparable T cell-independent antitumor effects. Meanwhile, tumor treatment experiments and examination of microvessel density in nude mice and Matrigel experiments in C57BL/6 mice revealed that NCRT/E7 DNA generated a stronger antiangiogenic effect than CRT/E7 DNA. NCRT, the N-terminal domain of calreticulin, has been demonstrated to inhibit endothelial cell proliferation in response to bFGF or VEGF and angiogenesis *in vivo* [10,11]. By inhibiting endothelial cell growth, NCRT would likely reduce tumor neovascularization to inhibit tumor growth. The NCRT and NCRT/E7 DNA vaccines both showed T-cell independent antitumor effects. Thus, it seems likely that NCRT/E7 and CRT/E7 are two chimeric molecules that can control established tumors through E7-specific CD8⁺ T cell-mediated immune responses and inhibit the growth of tumor vasculature through antiangiogenesis.

In order to generate an effective antiangiogenic antitumor effect, it is necessary to administer CRT or NCRT DNA repeatedly at high doses. Previous studies have indicated that single DNA vaccination results in peak serum CRT levels at 7 days post vaccination, tapering off to near-baseline levels within 14 days post vaccination [37]. In addition, the level of serum CRT depends on the dose of CRT DNA [37]. Typical DNA vaccine doses (2 μ g) did not show any detectable serum CRT. We have used repeated, high-dose, CRT DNA vaccination to generate detectable levels of serum CRT and antiangiogenic effects in vaccinated mice [5]. Thus, for an effective antiangiogenic antitumor response, a relatively high and repeated dose of CRT DNA is required.

The antiangiogenic property of a NCRT- or CRT-encoding DNA vaccine raises certain safety concerns. For example, wound healing requires neovascularization, which may be inhibited by angiogenesis inhibitors. However, prior studies have shown that CRT does not impair wound healing at tumor-inhibiting doses [38]. Furthermore, we have conducted experiments showing that vaccination with the CRT/E7 DNA

vaccine does not inhibit wound healing or result in pathologic changes in the major organs of mice (data not shown). Thus, concerns for inhibition of wound healing after therapeutic doses of DNA encoding CRT or NCRT are likely minimal and should not inhibit clinical translation of antiangiogenic DNA vaccines encoding CRT or NCRT.

In summary, our results indicate that fusion of NCRT, PCRT or CCRT to HPV-16 E7 can generate an impressive antitumor effect against HPV-16 E7-expressing murine tumors through enhancement of E7-specific CD8⁺ T cell-mediated immune responses. However, only NCRT/E7 can generate antitumor effect through both E7-specific CD8⁺ T cell-mediated immune responses and antiangiogenesis, as CRT/E7 does. Thus, the fusion of NCRT to an antigen gene is a promising approach to cancer therapy that potentially can be applied to other cancer systems with known tumor-specific antigens.

Acknowledgements

We would like to thank Ken-Yu Lin and Dr. Richard Roden for critical review of the manuscript. This study was supported by grants from the National Cancer Institute and American Cancer Society.

References

- [1] Boon T, Cerottini JC, Van den Eynde B, van der Bruggen P, Van Pel A. Tumor antigens recognized by T lymphocytes. *Ann Rev Immunol* 1994;12:337–65 [review].
- [2] Chen CH, Wu TC. Experimental vaccine strategies for cancer immunotherapy. *J Biomed Sci* 1998;5(4):231–52.
- [3] Folkman J. Angiogenesis: initiation and control. *Ann N Y Acad Sci* 1982;401:212–27.
- [4] Hanahan D, Folkman J. Patterns and emerging mechanisms of the angiogenic switch during tumorigenesis. *Cell* 1996;86(3):353–64.
- [5] Cheng WF, Hung CF, Chai CY, et al. Tumor-specific immunity and antiangiogenesis generated by a DNA vaccine encoding calreticulin linked to a tumor antigen. *J Clin Invest* 2001;108(5):669–78.
- [6] Nash PD, Opas M, Michalak M. Calreticulin: not just another calcium-binding protein. *Mol Cell Biochem* 1994;135(1):71–8.
- [7] Spee P, Neeftjes J. TAP-translocated peptides specifically bind proteins in the endoplasmic reticulum, including gp96, protein disulfide isomerase and calreticulin. *Eur J Immunol* 1997;27(9):2441–9.
- [8] Sadasivan B, Lehner PJ, Ortman B, Spies T, Cresswell P. Roles for calreticulin and a novel glycoprotein, tapasin, in the interaction of MHC class I molecules with TAP. *Immunity* 1996;5(2):103–14.
- [9] Basu S, Srivastava PK. Calreticulin, a peptide-binding chaperone of the endoplasmic reticulum, elicits tumor- and peptide-specific immunity. *J Exp Med* 1999;189(5):797–802.
- [10] Pike SE, Yao L, Jones KD, et al. Vasostatin, a calreticulin fragment, inhibits angiogenesis and suppresses tumor growth. *J Exp Med* 1998;188(12):2349–56.
- [11] Pike SE, Yao L, Setsuda J, et al. Calreticulin and calreticulin fragments are endothelial cell inhibitors that suppress tumor growth. *Blood* 1999;94(7):2461–8.
- [12] Yao L, Pike SE, Tosato G. Laminin binding to the calreticulin fragment vasostatin regulates endothelial cell function. *J Leukoc Biol* 2002;71(1):47–53.
- [13] Krause KH, Michalak M. Calreticulin. *Cell* 1997;88(4):439–43.
- [14] Burns K, Duggan B, Atkinson EA, et al. Modulation of gene expression by calreticulin binding to the glucocorticoid receptor. *Nature* 1994;367(6462):476–80.
- [15] Singh NK, Atreya CD, Nakhasi HL. Identification of calreticulin as a rubella virus RNA binding protein. *Proc Natl Acad Sci USA* 1994;91(26):12770–4.
- [16] Rojiani MV, Finlay BB, Gray V, Dedhar S. In vitro interaction of a polypeptide homologous to human Ro/SS-A antigen (calreticulin) with a highly conserved amino acid sequence in the cytoplasmic domain of integrin alpha subunits. *Biochemistry* 1991;30(41):9859–66.
- [17] Corbett EF, Oikawa K, Francois P, et al. Ca²⁺ regulation of interactions between endoplasmic reticulum chaperones. *J Biol Chem* 1999;274(10):6203–11.
- [18] Baksh S, Michalak M. Expression of calreticulin in *Escherichia coli* and identification of its Ca²⁺ binding domains. *J Biol Chem* 1991;266(32):21458–65.
- [19] Vassilakos A, Michalak M, Lehrman MA, Williams DB. Oligosaccharide binding characteristics of the molecular chaperones calnexin and calreticulin. *Biochemistry* 1998;37(10):3480–90.
- [20] Andrin C, Pinkoski MJ, Burns K, et al. Interaction between a Ca²⁺-binding protein calreticulin and perforin, a component of the cytotoxic T-cell granules. *Biochemistry* 1998;37(29):10386–94.
- [21] Fraser SA, Michalak M, Welch WH, Hudig D. Calreticulin, a component of the endoplasmic reticulum and of cytotoxic lymphocyte granules, regulates perforin-mediated lysis in the hemolytic model system. *Biochem Cell Biol* 1998;76(5):881–7.
- [22] Michalak M, Burns K, Andrin C, et al. Endoplasmic reticulum form of calreticulin modulates glucocorticoid-sensitive gene expression. *J Biol Chem* 1996;271(46):29436–45.
- [23] Kuwabara K, Pinsky DJ, Schmidt AM, et al. Calreticulin, an antithrombotic agent which binds to vitamin K-dependent coagulation factors, stimulates endothelial nitric oxide production, and limits thrombosis in canine coronary arteries. *J Biol Chem* 1995;270(14):8179–87.
- [24] Dai E, Stewart M, Ritchie B, et al. Calreticulin, a potential vascular regulatory protein, reduces intimal hyperplasia after arterial injury. *Arterioscler Thromb Vasc Biol* 1997;17(11):2359–68.
- [25] Hung C-F, Cheng W-F, Chai C-Y, et al. Improving vaccine potency through intercellular spreading and enhanced MHC class I presentation of antigen. *J Immunol* 2001;166:5733–40.
- [26] Michalak M, Corbett EF, Mesaali N, Nakamura K, Opas M. Calreticulin: one protein, one gene, many functions. *Biochem J* 1999;344(Pt 2):281–92.
- [27] Michalak M, Mariani P, Opas M. Calreticulin, a multifunctional Ca²⁺ binding chaperone of the endoplasmic reticulum. *Biochem Cell Biol* 1998;76(5):779–85.
- [28] Lin K-Y, Guarnieri FG, Staveley-O'Carroll KF, et al. Treatment of established tumors with a novel vaccine that enhances major histocompatibility class II presentation of tumor antigen. *Cancer Res* 1996;56:21–6.
- [29] Feltkamp MC, Smits HL, Vierboom MP, et al. Vaccination with cytotoxic T lymphocyte epitope-containing peptide protects against a tumor induced by human papillomavirus type 16-transformed cells. *Eur J Immunol* 1993;23(9):2242–9.
- [30] Tindle RW, Croft S, Herd K, et al. A vaccine conjugate of 'IS-CAR' immunocarrier and peptide epitopes of the E7 cervical cancer-associated protein of human papillomavirus type 16 elicits specific Th1- and Th2-type responses in immunized mice in the absence of oil-based adjuvants. *Clin Exp Immunol* 1995;101(2):265–71.
- [31] Cheng WF, Hung CF, Hsu KF, et al. Cancer immunotherapy using Sindbis virus replicon particles encoding a VP22-antigen fusion. *Hum Gene Ther* 2002;13(4):553–68.
- [32] Ji H, Wang T-L, Chen C-H, et al. Targeting HPV-16 E7 to the endosomal/lysosomal compartment enhances the antitumor immunity of

- DNA vaccines against murine HPV-16 E7-expressing tumors. *Hum Gene Ther* 1999;10(17):2727–40.
- [33] Cheng WF, Lee CN, Chu JS, et al. Vascularity index as a novel parameter for the in vivo assessment of angiogenesis in patients with cervical carcinoma. *Cancer* 1999;85(3):651–7.
- [34] Coughlin CM, Salhany KE, Wysocka M, et al. Interleukin-12 and interleukin-18 synergistically induce murine tumor regression which involves inhibition of angiogenesis. *J Clin Invest* 1998;101(6):1441–52.
- [35] Porgador A, Irvine KR, Iwasaki A, Barber BH, Restifo NP, Germain RN. Predominant role for directly transfected dendritic cells in antigen presentation to CD8+ T cells after gene gun immunization. *J Exp Med* 1998;188(6):1075–82.
- [36] Harwerth IM, Wels W, Schlegel J, Muller M, Hynes NE. Monoclonal antibodies directed to the erbB-2 receptor inhibit in vivo tumour cell growth. *Br J Cancer* 1993;68(6):1140–5.
- [37] Xiao F, Wei Y, Yang L, et al. A gene therapy for cancer based on the angiogenesis inhibitor, vasostatin. *Gene Ther* 2002;9(18):1207–13.
- [38] Lange-Asschenfeldt B, Velasco P, Streit M, et al. The angiogenesis inhibitor vasostatin does not impair wound healing at tumor-inhibiting doses. *J Invest Dermatol* 2001;117(5):1036–41.

Antigen-Specific CD8⁺ T Lymphocytes Generated from a DNA Vaccine Control Tumors through the Fas–FasL Pathway

Wen-Fang Cheng,¹ Chien-Nan Lee,¹ Ming-Cheng Chang,¹ Yi-Ning Su,²
Chi-An Chen,^{1,*} and Chang-Yao Hsieh¹

¹Department of Obstetrics and Gynecology and ²Medical Genetics, National Taiwan University Hospital, National Taiwan University, Taipei, Taiwan

*To whom correspondence and reprint requests should be addressed. Fax: +886 2 2395 9476. E-mail: cachen@ha.mc.ntu.edu.tw.

Available online 24 June 2005

Human papillomavirus, particularly type 16, and its oncogenic proteins, E6 and E7, are consistently expressed in most cervical cancers. One of the major issues facing cancer immunotherapy is that many human cancers evade the immune system by downregulating the expression of Fas molecules. An E7-expressing murine tumor model with a downregulated Fas expression—TC-1 P3(A15) tumors—was created. A DNA vaccine encoding calreticulin linked to E7 (CRT/E7) was able to generate protective and therapeutic antitumor effects against TC-1 P3(A15) tumors. *In vitro* Ab depletion and *in vivo* adoptive experiments showed that the antitumor effect of E7-specific CD8⁺ T lymphocytes against the TC-1 P3(A15) tumor cells was through the Fas–FasL-dependent CTL effector mechanism, and the TC-1 P3(A15) tumor cells needed higher numbers of antigen-specific CD8⁺ T lymphocytes for *in vivo* elimination. Our results demonstrated that chimeric CRT/E7 DNA vaccine resulted in control of tumors with downregulated Fas expression, highlighting the importance of the Fas–FasL pathway in the potent antitumor effect of antigen-specific CD8⁺ cytotoxic T lymphocytes and the role of Fas as part of *in vivo* tumor evasion.

Key Words: human papillomavirus, Fas, Fas ligand, DNA vaccine, tumor evasion

INTRODUCTION

Cervical cancer is the second leading cause of death from cancer in women and approximately 500,000 women worldwide develop cervical cancer yearly [1]. Genital human papillomavirus (HPV) types 16 and 18 and, less frequently, types 31, 33, 35, 45, 51, and 56 have been implicated in the etiology of cervical and other anogenital cancers [2]. More than 90% of cervical cancers have been associated with HPV infection, particularly type 16 infection. The type 16 oncogenic proteins E6 and E7 are consistently expressed in most cervical cancers [2]. Antigen-specific cancer vaccines have proved to be useful and a promising approach against tumors [3]. HPV16 E7 has been utilized as the target antigen for the development of antigen-specific immunotherapies or vaccines for HPV-associated cervical malignancies [4]. One concern about the efficacy of immunotherapy is that tumors can evade immune responses through various mechanisms, including MHC class I downregulation [5], Fas downregulation [6], and secretion of inhibitory factors such as VEGF [7], TGF- β [7], or IL-10 [8].

We have previously demonstrated that calreticulin linked with the HPV16 E7 antigen (CRT/E7), a naked DNA vaccine, enhances MHC class I presentation, improves CD8⁺ T cell activity, and generates an antitumor effect against MHC class I normal-expressing tumors that also express E7 (TC-1) [9]. Cervical cancer cells have been proven to evade the immunological surveillance through downregulation of MHC class I expression [10] or Fas expression [11]. Tumor cells with downregulated Fas expression show a hindered killing effect by cytotoxic CD8⁺ T cells and there then is a limited ability of the antigen-specific CD8⁺ T cells to control the tumors. Thus, it is important to utilize a suitable tumor model with downregulated Fas to evaluate the antitumor effect and mechanism of the CRT/E7 DNA vaccine. We have successfully generated a MHC class I-downregulated, E7-expressing tumor cell line, TC-1 P3(A15). Using this model, we found that vaccination with a DNA vaccine encoding E7 linked to mycobacterial heat shock protein 70 (HSP70) generated a significant antitumor effect against TC-1 P3(A15) [12].

In this study, we again used the TC-1 P3(A15) tumor cells to test whether the CRT/E7 DNA vaccine could also control the tumor growth induced by TC-1 P3(A15) tumor cells and to evaluate if there were further mechanisms by which TC-1 P3(A15) tumor cells are able to evade immunological surveillance and to elucidate further the mechanisms of action of the CRT/E7 DNA vaccine against TC-1 P3(A15) tumor cells. Our results demonstrated that vaccination with CRT/E7 DNA was still able to generate a potent antitumor effect against TC-1 P3(A15) tumors compared to the wild-type E7 DNA vaccine. The Fas expression of the TC-1 P3(A15) tumor cells was downregulated compared to TC-1 tumor cells and it could be upregulated by IFN- γ . TC-1 P3(A15) tumor cells, when pretreated with IFN- γ , could stimulate more tumor-specific IFN- γ -secreting CD8⁺ T cells. E7-specific CD8⁺ T cells also could generate a level of higher specific cytotoxic activity against IFN- γ -pretreated TC-1 P3(A15) tumor cells. In addition, most of the E7-specific CD8⁺ T lymphocytes expressed Fas ligand (FasL) by flow-cytometric analysis. The specific cytolytic activities of E7-specific CD8⁺ T lymphocytes against the tumor cells could be blocked by pretreating with anti-Fas antibody through *in vitro* Ab depletion experiments. Our results suggest that the antitumor effect of E7-specific CD8⁺ T lymphocytes might be through the Fas-FasL pathway. The adoptive transfer of E7-specific CD8⁺ T cells could control the growth of TC-1 P3(A15) tumor cells, although higher numbers of E7-specific CD8⁺ T cells were required for the clearance of TC-1 P3(A15) tumors compared to those needed for the

clearance of TC-1 tumors. The *in vivo* Fas expression of the TC-1 P3(A15) tumor cells was significantly lower when treated by the adoptive transfer of E7-specific CD8⁺ T cells compared to without treatment. Downregulated Fas expression is an important tumor evasion mechanism for E7-expressing tumors and the Fas-FasL pathway plays an important role in the antitumor effect of antigen-specific CD8⁺ T cells generated by a DNA vaccine.

RESULTS

Fas Expression of TC-1 P3(A15) Is Downregulated and Can Be Upregulated by IFN- γ

As shown in Fig. 1A, Fas expression of TC-1 P3(A15) tumor cells was lower than that of the TC-1 tumor cells (mean fluorescence intensity (MFI) 13.7 vs 41.1). IFN- γ could enhance the percentage of positive Fas expression of TC-1 tumor cells from 40% to more than 80% as early as 24 h after stimulation (Fig. 1B). Meanwhile, IFN- γ also enhanced the percentage of positive Fas expression of TC-1 P3(A15) tumor cells from 10% to more than 80%, which is comparable to that of TC-1 tumor cells. However, the MFIs of Fas expression for TC-1 were higher than those for TC-1 P3(A15) at every indicated time when stimulated with IFN- γ (Fig. 1C).

Our results showed that Fas expression of TC-1 P3(A15) tumor cells was downregulated. Although IFN- γ could upregulate the Fas expression of TC-1 P3(A15) tumor cells, the Fas expression of TC-1 P3(A15) tumor cells was still lower than that of TC-1.

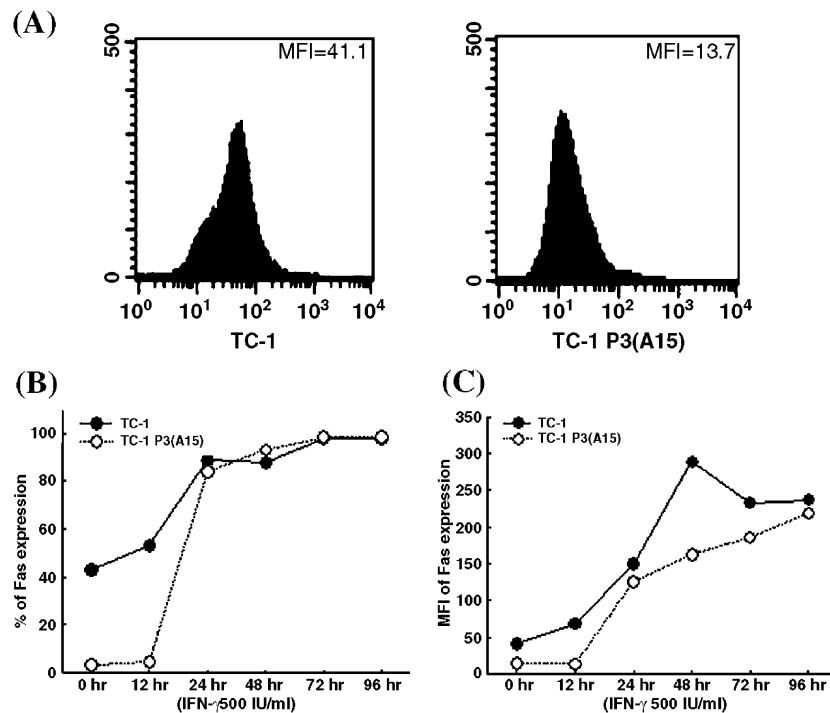


FIG. 1. Fas expression of TC-1 and TC-1 P3(A15) tumor cells and the effect of IFN- γ on the Fas expression of tumor cells. (A) Representative graphs of Fas expression of the TC-1 and TC-1 P3(A15) tumor cells. (B) Percentages of Fas expression in TC-1 and TC-1 P3(A15) with IFN- γ stimulation. (C) MFIs of Fas expression in TC-1 and TC-1 P3(A15) with IFN- γ stimulation.

Linkage of CRT to E7 in a DNA Vaccine Controls TC-1 P3(A15) Tumors

Mice vaccinated with CRT/E7 DNA generated 100% protection against the growth of TC-1 and TC-1 P3(A15) tumors up to 90 days after tumor challenge (Figs. 2A and 2B). All of the other vaccinated mice developed tumors within 20 days of TC-1 or TC-1 P3(A15) tumor challenge. Furthermore, vaccination with a mixture of E7 DNA and CRT DNA did not generate any appreciable antitumor effect against TC-1 P3(A15) (data not shown).

In the tumor treatment experiments, mice treated with CRT/E7 DNA exhibited significantly fewer pulmonary tumor nodules than mice treated with the other DNA vaccines when challenged with TC-1 tumor cells (Fig. 2C). Also, as shown in Fig. 2D, mice treated with CRT/E7 DNA exhibited significantly fewer pulmonary tumor nodules (1.3 ± 0.6) than mice treated with wild-type E7 (36.0 ± 2.5), CRT (8.0 ± 1.5), or empty plasmid DNA (42.5 ± 2.5) or mice without vaccination (40.5 ± 2.5) when challenged with TC-1 P3(A15) tumor cells.

Taken together, these results indicated that the linkage of CRT to E7 is capable of protecting and controlling both Fas normal-expressing and Fas-down-regulated tumors.

IFN- γ -Pretreated TC-1 P3(A15) Tumor Cells Induce Higher Numbers of Functional Tumor-Specific CD8⁺ T Cells Than the Original TC-1 P3(A15)

We further evaluated if the ability of tumor-specific CD8⁺ T lymphocytes to induce IFN- γ secretion was different between TC-1 and TC-1 P3(A15) tumor cells. The representative graphs of flow-cytometric analysis in different groups are shown in Fig. 3A. The numbers of IFN- γ -secreting tumor-specific CD8⁺ T lymphocytes were low in the naïve groups regardless of whether they were cocultured with original or IFN- γ -pretreated TC-1 or TC-1P3(A15) cells (Fig. 3B). The numbers of IFN- γ -secreting tumor-specific CD8⁺ T lymphocytes in the CRT/E7 DNA-vaccinated group were higher when cultured with the TC-1 tumor cells than with the TC-1 P3(A15) tumor cells (135.0 ± 5.4 for original TC-1, 20.0 ± 2.8 for original TC-

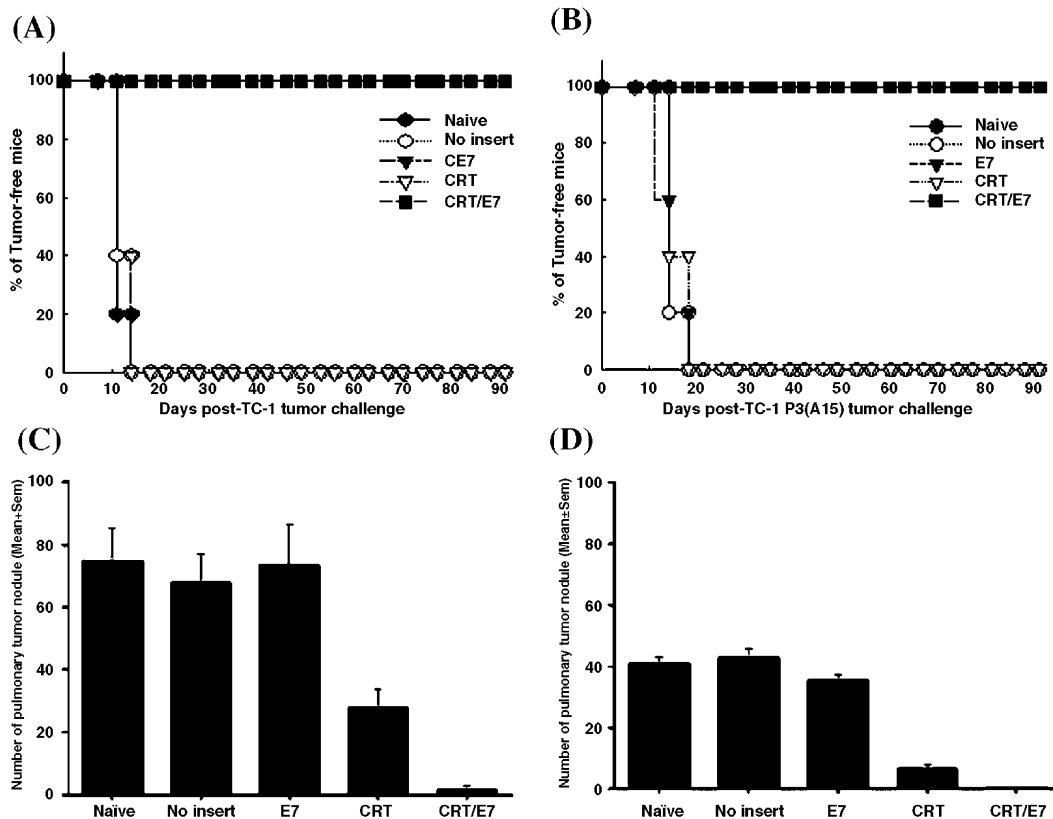


FIG. 2. *In vivo* tumor protection and treatment experiments against TC-1 or TC-1 P3(A15) tumor cells in mice vaccinated with various DNA vaccines. (A) Tumor protection experiments against TC-1. (B) Tumor protection experiments against TC-1 P3(A15). (C) Tumor treatment experiments against TC-1. (D) Tumor treatment experiments against TC-1 P3(A15).

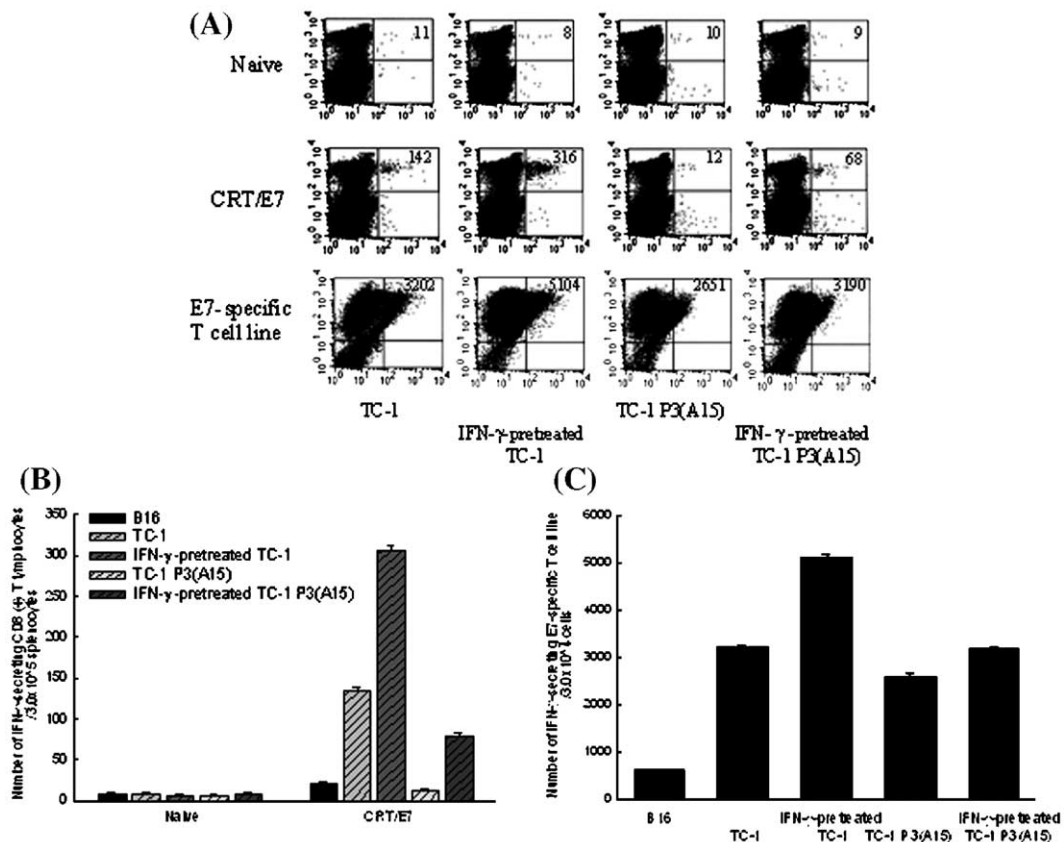


FIG. 3. Numbers of IFN- γ -secreting tumor-specific CD8⁺ T lymphocytes from splenocytes of naive or CRT/E7 DNA-vaccinated mice and the E7-specific CD8⁺ T cell line. (A) Representative graphs of flow-cytometric analysis. (B) Histogram demonstrating the number of IFN- γ -secreting tumor-specific CD8⁺ T lymphocytes from naive and CRT/E7 DNA-vaccinated mice. (C) Histogram demonstrating the numbers of IFN- γ -secreting tumor-specific CD8⁺ T cells in the E7-specific CD8⁺ T cell line.

1 P3(A15), $P < 0.01$, one-way ANOVA; 306.0 ± 20.0 for IFN- γ -pretreated TC-1, 79.0 ± 7.0 for IFN- γ -pretreated TC-1 P3(A15), $PP < 0.01$, one-way ANOVA). In addition, IFN- γ -pretreated TC-1 or TC-1 P3(A15) tumor cells induced more IFN- γ -secreting tumor-specific CD8⁺ T cells compared to the original TC-1 or TC-1 P3(A15) (Fig. 3B). Similar results were also noted when we changed the effector cells to the E7-specific CD8⁺ T cell line (Fig. 3C). The IFN- γ -pretreated TC-1 P3(A15) (3180.0 ± 72.1) cells could only stimulate similar numbers of IFN- γ -secreting tumor-specific CD8⁺ T cells compared to original TC-1 (3196.0 ± 49.2).

Our results revealed that the original TC-1 P3(A15) tumor cells could stimulate E7-specific CD8⁺ T lymphocytes to secrete IFN- γ , although they did this less effectively compared to the original TC-1 tumor cells. However, when we pretreated TC-1 P3(A15) tumor cells with IFN- γ , they were able to stimulate higher numbers of E7-specific CD8⁺ T lymphocytes to secrete IFN- γ than the original TC-1 P3(A15) tumor cells.

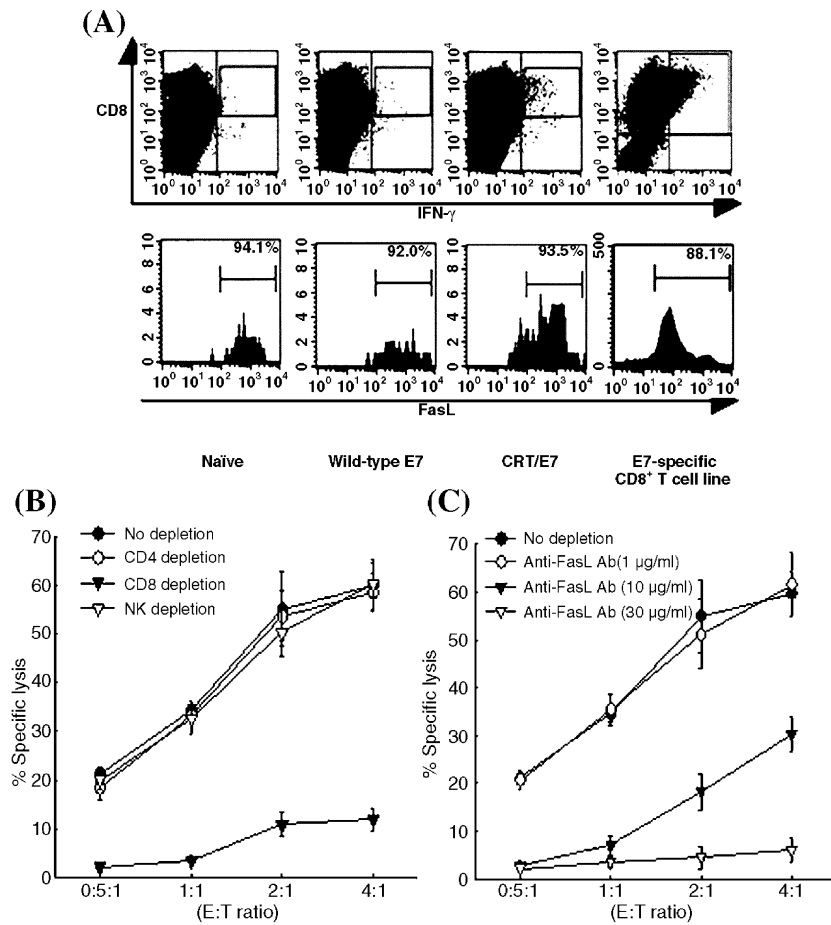
Having established this, it was necessary to identify whether IFN- γ pretreatment affected E7-specific lysis.

FasL Was Expressed in Functional E7-Specific CD8⁺ T Lymphocytes and Plays an Essential Role in the Cytolysis of E7-Expressing Tumors

We then checked the expression of FasL on the E7-specific CD8⁺ T lymphocytes from various DNA-vaccinated mice and the E7-specific CD8⁺ T cell line. Most of the E7-specific IFN- γ -secreting CD8⁺ T cells, regardless of whether they were from naive mice (94.1%), wild-type E7- (92.0%) or CRT/E7- (93.5%) vaccinated mice, or the E7-specific CD8⁺ T cell line (88.1%), did express FasL (Fig. 4A).

To evaluate the role of the Fas-FasL pathway in the antitumor effect of the E7-specific chimeric DNA vaccine, we then performed *in vitro* antibody depletion experiments. As shown in Fig. 4B, the percentages of specific lysis of the E7-specific CD8⁺ T cell line in the CD8-depleted group decreased significantly compared to

FIG. 4. FasL expression of E7-specific CD8⁺ T lymphocytes and *in vitro* Ab depletion assays for E7-expressing tumors. (A) Representative graphs of flow-cytometric analysis of FasL expression of E7-specific CD8⁺ T lymphocytes. (B) The percentages of specific lysis for TC-1 with *in vitro* depletion of CD4, CD8, or NK1.1 lymphocytes. (C) The percentages of specific lysis for TC-1 with *in vitro* depletion of FasL.



those without Ab depleted, in the CD4- or NK-depleted group. In addition, the percentages of specific lysis in the FasL Ab-depletion experiments showed that FasL blocking led to a significantly gradual loss of cytotoxic activity that correlated with the concentration of FasL antibody (Fig. 4C) (E:T ratio 4:1, $61.6 \pm 6.6\%$ for 1 μ g/ml FasL Ab, $30.4 \pm 3.6\%$ for 10 μ g/ml FasL Ab, $6.1 \pm 2.6\%$ for 30 μ g/ml FasL Ab, PP < 00.001, ANOVA). We also found a similar phenomenon when we changed the effector cells to the splenocytes from CRT/E7 DNA-vaccinated mice (data not shown).

Our data showed that E7 induced IFN- γ -secreting CD8⁺ T lymphocytes from a range of origins. And the Fas-FasL pathway plays an important role in the killing of E7-expressing tumor cells via E7-specific CD8⁺ T lymphocytes generated from chimeric E7-specific DNA vaccine.

Higher Numbers of E7-Specific CD8⁺ T Lymphocytes Are Needed to Eliminate Fas-Downregulated E7-Expressing Tumor Cells

We performed adoptive transfer of the E7-specific CD8⁺ T cells to evaluate if E7-specific CD8⁺ T lymphocytes could control the growth of Fas normal-expressing and down-

regulated E7-expressing tumor cells. As shown in Fig. 5, E7-specific CD8⁺ T cells could eliminate both TC-1 and TC-1 P3(A15) tumor cells in a dose-dependent manner. However, mice challenged with Fas-downregulated TC-1

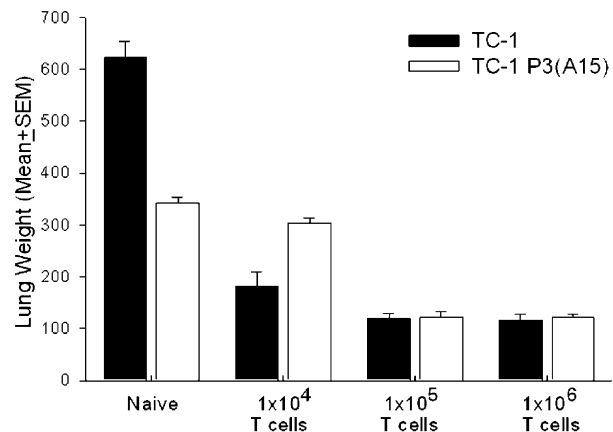


FIG. 5. Antitumor effects for TC-1 and TC-1 P3(A15) tumor cells with adoptive transfer of E7-specific CD8⁺ cytotoxic T lymphocytes.

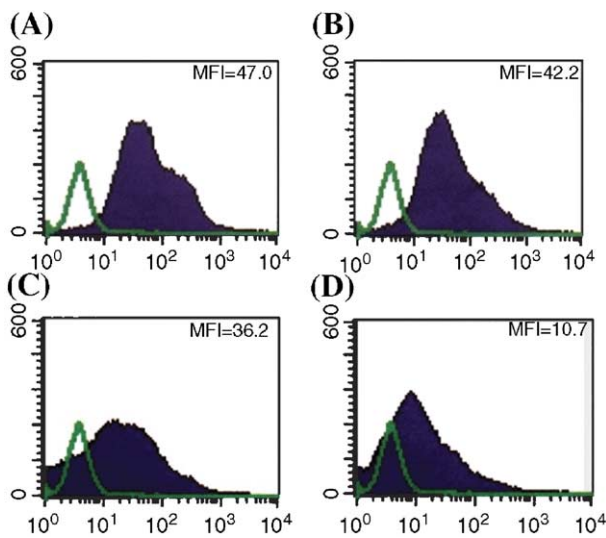


FIG. 6. *In vivo* Fas expression of the TC-1 and TC-1 P3(A15) tumor cells. (A) TC-1 from the naïve mice and (B) TC-1 from mice with the adoptive transfer of E7-specific CD8⁺ T cells. (C) TC-1 P3(A15) from the naïve mice and (D) TC-1 P3(A15) from mice with the adoptive transfer of E7-specific CD8⁺ T cells.

P3(A15) tumor cells needed higher numbers of E7-specific CD8⁺ T cells (around 10-fold) to eliminate the TC-1 P3(A15) tumor cells compared to those challenged with Fas normal-expressing TC-1.

Our data showed that higher numbers of antigen-specific CD8⁺ T cells are needed to eliminate Fas-downregulated tumor cells than to eliminate Fas normal-expressing tumor cells.

Fas Expression in the TC-1 P3(A15) Tumor Cells Was Lower in E7-Specific CD8⁺ T-Cell-Treated Mice

We finally evaluated whether the *in vivo* Fas expression of TC-1 and TC-1 P3(A15) tumor cells was different under various immune surveillance conditions. As shown in Figs. 6A and 6B, the *in vivo* Fas expression of the TC-1 cells decreased slightly in the E7-specific CD8⁺ T-cell-treated group compared with the naïve group (MFI 42.2 vs 47.0). However, the *in vivo* Fas expression of the TC-1 P3(A15) cells was significantly lower in the E7-specific CD8⁺ T-cell-treated group compared with the naïve group (MFI 10.7 vs 36.2) (Figs. 6C and 6D).

Our data revealed that antigen-specific tumor cells might downregulate their Fas expression to escape the surveillance of antigen-specific CD8⁺ T lymphocytes *in vivo*.

DISCUSSION

IFN- γ was required for the generation of a potent antitumor effect against TC-1 P3(A15) tumor cells. Our data showed that IFN- γ helps overcome Fas downregulation and restore Fas expression (Fig. 1). CRT/E7 has been

proven to enhance the number of IFN- γ -secreting E7-specific CD8⁺ T cells [9] and promote tumor protection and has therapeutic effects on the TC-1 P3(A15) tumor cells in our study (Fig. 2). IFN- γ -pretreated TC-1 and TC-1 P3(A15) tumor cells stimulated larger numbers of IFN- γ -secreting tumor-specific CD8⁺ T cells (Fig. 3). In addition, our previous work has shown that the potency of the E7/HSP70 DNA vaccine in normal C57BL/6 mice is lost in IFN- γ -KO C57BL/6 mice [12]. IFN- γ is a key cytokine in tumor immunity, and it is positively associated with tumor rejection. Tumor cells transfected to secrete IFN- γ are often rejected [20,21]. Blocking endogenous IFN- γ by neutralizing antibodies inhibits tumor rejection, and it has been reported that IFN- γ -KO or IFN- γ R-KO mice exhibit impaired tumor rejection [22–24]. Also, the efficacy of CD8⁺ T cells to mediate tumor rejection upon adoptive transfer has been shown to correlate with IFN- γ production [25,26].

Differences in cytokine production also provide an explanation for the antitumor effect mediated by vaccination with CRT/E7 DNA. Plasmid DNA might contain immunostimulatory elements known as CpG islands, which have been shown to contribute to the induction of certain Th1 cytokines such as IFN- γ and IL-12, thus enhancing antigen-specific immunity [27]. Oligodeoxynucleotides containing unmethylated CpG dinucleotides (CpG motif) were quite effective in inducing NK cell lytic activity [28]. CpG islands can also trigger maturation and activation of dendritic cells [29] and induce Th1 responses [30]. Further studies would help to elucidate the relative influence of these vaccine characteristics on the antitumor effect.

Fas downregulation represents one of the mechanisms by which the host defense can be evaded. Fas, a member of the TNF receptor family, is a death receptor that induces apoptosis upon ligation with anti-Fas Ab or the natural Fas ligand [31]. Fas-mediated apoptosis plays roles in the immune system, including the apoptotic selection process during T cell development, clonal deletion of autoreactive T cells in the periphery, and activation-induced suicide of T cells, and as an effector mechanism of CTL [31]. Fas is expressed on a variety of cell types, such as activated lymphocytes and some solid tumors, and the expression of Fas can be upregulated by exposure to either IFN- γ or TNF- α [32–34]. Our survey showed that the Fas expression of the original TC-1 P3(A15) tumor cells was downregulated and the expression of Fas on TC-1 P3(A15) cells was upregulated by IFN- γ (Fig. 1). Our results are consistent with previous studies in which it was found that IFN- γ can increase Fas expression on tumor cells and enhance antitumor effect in Fas-expressing tumor cells [35–37]. IFN- γ has been shown to upregulate the Fas expression in a variety of mouse solid tumor cell lines such as 3LL, B16, Colon 26, and M109 [38]. Despite the ubiquitous expression of Fas on various solid tumors, its role as a possible therapeutic target has

not been well characterized. Therefore, to evaluate further the potential role of this pathway in the endogenous host response against solid tumors and the potential therapeutic utility of manipulating Fas expression in tumor cells, there needs to be further research.

The progressive downregulation of Fas expression has been noted during tumor progression. Rosen *et al.* observed upregulated Fas expression on tumor cells *in vivo* and suggested that a Fas-based mechanism plays a role in tumor immunity at the early stages of tumor growth [39]. Our study first found that the *in vitro* Fas expression of the TC-1 P3(A15) cells was downregulated (Fig. 1). We then examined the *in vivo* levels of Fas expression of tumor cells in the lungs of mice after treatment by adoptive transfer of E7-specific CD8⁺ T cells. The *in vivo* Fas expression of the TC-1 P3(A15) tumor cells was lower in the E7-specific CD8⁺ T-cell-treated group than in the naïve group (Fig. 6). A difference between the levels of cell surface *in vivo* Fas expression of tumor cells treated with Ag-specific CTL and with saline has also been reported [19]. Our survey supports the idea that loss of Fas expression and function by different cancer types is associated with a more malignant phenotype and sustains the idea that the host Fas–FasL system is important for the regulation of local tumor growth [40–43].

Antigen-specific cytotoxic T cells kill target tumor cells via the Fas–FasL pathway. FasL is a type II membrane protein that, like TNF, can be processed to a soluble form by a metalloproteinase [44]. Expression of FasL is usually limited to activated T cells, NK cells, and cells in immunologically privileged sites such as testis and eye [45]. Although CD8⁺ cytotoxic lymphocytes play important roles in antitumor activity, it remains to be fully understood whether optimal tumor regression by MHC-restricted, Ag-specific CD8⁺ CTL requires functional Fas–FasL interactions and whether the disruption or disengagement of that interaction allows subpopulations of tumor cells to escape from death [46–49]. A FasL-dependent CTL effector mechanism is important for optimal tumor regression in adoptive immunotherapy. Our data showed that the E7-specific CD8⁺ T lymphocytes would express FasL (Fig. 4A). When we pretreated the E7-specific CD8⁺ T cells with anti-CD8 or anti-FasL antibody, the killing effects of these cells on tumor cells significantly decreased (Figs. 4B and 4C). In addition, IFN- γ increased Fas expression of TC-1 and TC-1 P3(A15) tumor cells (Fig. 1) and also improved the percentages of FasL-mediated cytotoxic lysis in our survey (Fig. 4C). We also demonstrated that adoptive transfer of the E7-specific CD8⁺ cytotoxic T cells cured most mice of established experimental pulmonary metastases (Fig. 5). Seki *et al.* also observed a similar phenomenon. Cytokines such as IFN- γ and TNF- α may increase the sensitivity of tumor cells to CTL lysis by the FasL-mediated death pathway and through this, the adoptive transfer of the tumor-specific cytotoxic T cells into tumor-bearing mice cured most

mice of established experimental pulmonary metastases [6]. Fas–FasL seems to be an important pathway for the antitumor effect of E7-specific CD8⁺ CTL generated by the E7-specific DNA vaccine in our system. It would be worth evaluating whether any other pathway is involved in the antitumor effect of the DNA vaccine-generated E7-specific CD8⁺ cytotoxic T lymphocytes.

In summary, our results indicated that CRT/E7 DNA generates an impressive antitumor effect against downregulated Fas, HPV16 E7-expressing murine tumors. We found that IFN- γ played an important role in mediating this antitumor effect by upregulating the Fas expression of the tumor cells. The E7-specific CD8⁺ T lymphocytes kill the target tumor cells via the Fas–FasL pathway. Thus, the E7-specific chimeric DNA vaccine is able to prevent and control lethal Fas normal-expressing and downregulated, E7-expressing tumor cells in our preclinical animal model. Therefore, an antigen-specific DNA vaccine may possibly have a significant potential role if clinically applied.

MATERIALS AND METHODS

Generation of TC-1 P3(A15) tumor cell line. The production and maintenance of TC-1 and TC-1 P3(A15) cells have been described previously [13]. On the day of TC-1 and TC-1 P3(A15) cell tumor challenge, tumor cells were harvested by trypsinization, washed twice with 1 \times Hanks buffered salt solution (HBSS), and finally resuspended in 1 \times HBSS to the designated concentration for injection.

Fas expression of TC-1 and TC-1 P3(A15) tumor cells. To detect the Fas expression of TC-1 or TC-1 P3(A15) tumor cells, biotin-conjugated anti-Fas monoclonal antibody and PE-conjugated streptavidin (PharMingen, San Diego, CA, USA) were added to tumor cells and incubated. Analysis was done on a Becton–Dickinson FACScan with CELLQuest software (Becton–Dickinson Immunocytometry System, Mountain View, CA, USA).

In a separate experiment, Fas expression of the TC-1 or TC-1 P3(A15) tumor cells was assessed at various time points with 1 μ g/ml IFN- γ stimulation (Research and Diagnostic Systems, Inc., Minneapolis, MN, USA). Fas expression was assessed as described above.

***In vitro* measurement of tumor cell proliferation.** The *in vitro* tumor cell proliferation was assessed using a reported method with some modifications [14]. TC-1 and TC-1 P3(A15) tumor cells (2×10^3) were seeded in triplicate in flat-bottom 96-well microtiter plates and incubated for various times. MTT solution (30 μ l; 5 mg/ml) was added and incubated for 4 h; then 100 μ l of DMSO was added to dissolve the formazan crystals and the absorptions at 570 and 630 nm were measured using an ELISA reader.

Mice. Six- to eight-week-old female C57BL/6J mice were bred in and purchased from the animal facility of National Taiwan University Hospital (Taipei, Taiwan). All animal procedures were performed according to approved protocols and in accordance with recommendations for the proper use and care of laboratory animals.

***In vivo* tumor growth kinetics.** TC-1 or TC-1 P3(A15) tumor cells (5×10^4) were injected into naïve mice subcutaneously. Mice were monitored regularly for evidence of tumor growth by palpation and inspection twice a week. Tumor size was measured and recorded serially until they were sacrificed.

Preparation of DNA constructs, generation of DNA bullets, and vaccination of mice. The generation of pcDNA3-E7, pcDNA3-CRT, and pcDNA3-CRT/E7 has been described previously [15]. Gene gun particle-

mediated DNA vaccinations were performed using a low pressure-accelerated gene gun (BioWare Technologies Co. Ltd., Taipei, Taiwan). The gold particles were weighted and suspended in 70% ethanol. This suspension was vortexed vigorously and then centrifuged to collect the particles. The collected particles were resuspended in DNA solution (1 μ g DNA/ μ g gold particles), vortexed, and sonicated for a few seconds and then added to 2.5 M CaCl₂ and 0.05 M spermidine solution with vortexing. This solution was kept on ice for 10 min and the DNA-coated gold particles were collected and washed with 100% ethanol three times. Finally, the particles were resuspended in 100% ethanol at the appropriate concentration and used to make bullets. Mice were immunized with 2 μ g of E7 DNA, CRT DNA, CRT/E7 DNA, or empty plasmid using the gene gun and then boosted with the same vaccination 1 week later.

In vivo tumor protection experiments. Mice were vaccinated with 2 μ g of various DNA vaccines using the gene gun and then boosted 1 week later. One week after the last vaccination, the mice were challenged with 5 \times 10⁴ TC-1 or TC-1 P3(A15) tumor cells by subcutaneous injection in the right leg. Tumor growth was monitored by visual inspection and palpation twice weekly until 90 days after tumor challenge.

In vivo tumor treatment experiments. Mice were first challenged with 1 \times 10⁴ TC-1 or TC-1 P3(A15) tumor cells/mouse intravenously through the tail vein using a previously described lung metastasis model [15]. Three days after tumor challenge, mice were vaccinated with 2 μ g of various naked DNA vaccines. Mice were boosted with the same vaccination 1 week later. Mice were then sacrificed and lungs were explanted on day 28 after tumor challenge. The weight of the lungs and number of pulmonary metastatic nodules in each mouse were evaluated and counted under a dissecting microscope.

IFN- γ cytokine and/or fasL staining and flow cytometry analysis. In the first experiment, splenocytes from various DNA-vaccinated mice were prepared as previously described [16]. The E7-specific CD8⁺ T cell line was kindly provided by Dr. T. C. Wu (Johns Hopkins Medical Institutes, Baltimore, MD, USA). TC-1 and TC-1 P3(A15) tumor cells were stimulated with 1 μ g/ml IFN- γ for 48 h. Splenocytes from the different vaccinated groups or the E7-specific CD8⁺ T cell line were cocultured with original or IFN- γ -pretreated TC-1 or TC-1 P3(A15) cells overnight. Cell surface marker staining for CD8 and intracellular cytokine staining for IFN- γ were performed as described previously.

In the second experiment, splenocytes from various vaccinated groups of mice were cultured with 1 μ g/ml E7 peptide (aa 49–57), and the E7-specific CD8⁺ T cell line was cultured with irradiated TC-1 cells overnight. The cells were stained with Cy-chrome-conjugated monoclonal rat anti-mouse CD8 antibody and phycoerythrin-conjugated anti-mouse FasL antibody (PharMingen) and subjected to FITC-conjugated anti-mouse IFN- γ antibody (PharMingen) as described earlier. Analysis was done on a Becton–Dickinson FACScan with CELLQuest software as described earlier.

In vitro Ab depletion experiments. For the *in vitro* antibody blocking experiments, the monoclonal antibody (MAb) GK1.5 was used for CD4 blocking, MAb 2.43 was used for CD8 blocking, PK136 was used for NK cell blocking, and anti-FasL antibody (MFL-3; PharMingen) was used for FasL blocking [17]. Antibodies or their respective control IgG preparations (hamster IgG, rat IgG) were added to the cultured E7-specific CD8⁺ T cell line 1 day before CTL assays and incubated overnight. CTL assays were performed the next day as described earlier.

Adoptive transfer of E7-specific CD8⁺ T cells for in vivo tumor treatment experiments. Adoptive transfer experiments were performed by a previously described method with modification [18]. Briefly, mice were challenged with 5 \times 10⁴ TC-1 or TC-1 P3(A15) tumor cells per mouse through the tail vein. Seven days after tumor challenge, mice received various numbers of E7-specific CD8⁺ T cells/mouse intravenously through the tail vein in 0.1 ml of HBSS and the same regimen every 7 days for 2 weeks (a total of three shots). The mice were sacrificed and lungs were explanted on day 28. The lung weight and number of pulmonary nodules in each mouse were evaluated and counted as described earlier.

In vivo Fas expression of tumor cells. Mice were challenged with 5 \times 10⁴ TC-1 or TC-1 P3(A15) tumor cells per mouse through the tail vein. Seven days after tumor challenge, 1 \times 10⁵ E7-specific CD8⁺ T cells were injected intravenously through the tail vein every 7 days as described earlier. The mice were sacrificed on day 28 and the lungs were removed and digested for 4–6 h at room temperature with an enzyme mixture containing hyaluronidase (0.1 mg/ml), collagenase (1 mg/ml), and DNase I (30 U/ml) (Sigma–Aldrich, St. Louis, MO, USA). *In vivo* Fas expression of the tumor cells was detected as described previously [19]. Lung cell preparations were stained with PE-conjugated anti-Fas mAb as well as FITC-conjugated anti-CD45 mAb (BD PharMingen) and consequently this excluded leukocytes from the analysis. Based on the light-scatter properties, the large cell population, which is consistent with TC-1 and TC-1 P3(A15) tumor cell morphology, was gated, and the frequency of Fas⁺CD45⁻ cells in that population was determined.

ACKNOWLEDGMENTS

Dr. Wen-Fang Cheng (RE88P005) is a recipient of the NHRI Physician Scientist Fellowship Award. This work was supported by grants from National Taiwan University Hospital (91-F002) and the National Science Committee of Taiwan (91-2314-B-002-369 and 92-2314-B-002-326).

RECEIVED FOR PUBLICATION SEPTEMBER 10, 2004; ACCEPTED APRIL 12, 2005.

REFERENCES

- Durst, M., Gissmann, L., Ikenberg, H., and zur Hausen, H. (1983). A papillomavirus DNA from a cervical carcinoma and its prevalence in cancer biopsy samples from different geographic regions. *Proc. Natl. Acad. Sci. USA* **80**: 3812–3815.
- Bosch, F. X., et al. (1995). Prevalence of human papillomavirus in cervical cancer: a worldwide perspective. International Biological Study on Cervical Cancer (IBSCC) Study Group. *J. Natl. Cancer. Inst.* **87**: 796–802.
- Pardoll, D. M. (1998). Cancer vaccines. *Nat. Med.* **4**: 525–531.
- Cheng, W. F., et al. (2001). Enhancement of Sindbis virus self-replicating RNA vaccine potency by linkage of Mycobacterium tuberculosis heat shock protein 70 gene to an antigen gene. *J. Immunol.* **166**: 6218–6226.
- Restifo, N. P., et al. (1993). Molecular mechanisms used by tumors to escape immune recognition: immunogenotherapy and the cell biology of major histocompatibility complex class I. *J. Immunother.* **14**: 182–190.
- Seki, N., et al. (2002). Tumor-specific CTL kill murine renal cancer cells using both perforin and Fas ligand-mediated lysis in vitro, but cause tumor regression in vivo in the absence of perforin. *J. Immunol.* **168**: 3484–3492.
- Beck, C., Schreiber, H., and Rowley, D. (2001). Role of TGF-beta in immune-evasion of cancer. *Microsc. Res. Tech.* **52**: 387–395.
- Urosevic, M., and Dummer, R. (2003). HLA-g and IL-10 expression in human cancer—Different stories with the same message. *Semin. Cancer. Biol.* **13**: 337–342.
- Cheng, W. F., et al. (2001). Tumor-specific immunity and antiangiogenesis generated by a DNA vaccine encoding calreticulin linked to a tumor antigen. *J. Clin. Invest.* **108**: 669–678.
- Serrano, A., et al. (2000). A mutation determining the loss of HLA-A2 antigen expression in a cervical carcinoma reveals novel splicing of human MHC class I classical transcripts in both tumoral and normal cells. *Immunogenetics* **51**: 1047–1052.
- Mikaelsdottir, E. K., et al. (2003). HPV subtypes and immunological parameters of cervical cancer in Iceland during two time periods, 1958–1960 and 1995–1996. *Gynecol. Oncol.* **89**: 22–30.
- Cheng, W. F., et al. (2003). CD8⁺ T cells, NK cells and IFN-gamma are important for control of tumor with downregulated MHC class I expression by DNA vaccination. *Gene Ther.* **10**: 1311–1320.
- Lin, K.-Y., et al. (1996). Treatment of established tumors with a novel vaccine that enhances major histocompatibility class II presentation of tumor antigen. *Cancer Res.* **56**: 21–26.
- Behrens, C. K., Igney, F. H., Arnold, B., Moller, P., and Krammer, P. H. (2001). CD95 ligand-expressing tumors are rejected in anti-tumor TCR transgenic perforin knockout mice. *J. Immunol.* **166**: 3240–3247.
- Hung, C. F., et al. (2001). Cancer immunotherapy using a DNA vaccine encoding the translocation domain of a bacterial toxin linked to a tumor antigen. *Cancer Res.* **61**: 3698–3703.
- Hung, C. F., et al. (2003). Enhancing major histocompatibility complex class I antigen presentation by targeting antigen to centrosomes. *Cancer Res.* **63**: 2393–2398.
- Simon, M. M., et al. (2000). Cytotoxic T cells specifically induce Fas on target cells, thereby facilitating exocytosis-independent induction of apoptosis. *J. Immunol.* **165**: 3663–3672.

18. Ryan, M. H., Bristol, J. A., McDuffie, E., and Abrams, S. I. (2001). Regression of extensive pulmonary metastases in mice by adoptive transfer of antigen-specific CD8(+) CTL reactive against tumor cells expressing a naturally occurring rejection epitope. *J. Immunol.* **167**: 4286–4292.
19. Caldwell, S. A., Ryan, M. H., McDuffie, E., and Abrams, S. I. (2003). The Fas/Fas ligand pathway is important for optimal tumor regression in a mouse model of CTL adoptive immunotherapy of experimental CMS4 lung metastases. *J. Immunol.* **171**: 2402–2412.
20. Gansbacher, B., Bannerji, R., Daniels, B., Zier, K., Cronin, K., and Gilboa, E. (1990). Retroviral vector-mediated gamma-interferon gene transfer into tumor cells generates potent and long lasting antitumor immunity. *Cancer Res.* **50**: 7820–7825.
21. Hock, H., Dorsch, M., Kunzendorf, U., Qin, Z., Diamantstein, T., and Blankenstein, T. (1993). Mechanisms of rejection induced by tumor cell-targeted gene transfer of interleukin 2, interleukin 4, interleukin 7, tumor necrosis factor, or interferon gamma. *Proc. Natl. Acad. Sci. USA* **90**: 2774–2778.
22. Hung, K., Hayashi, R., Lafond-Walker, A., Lowenstein, C., Pardoll, D., and Levitsky, H. (1998). The central role of CD4(+) T cells in the antitumor immune response. *J. Exp. Med.* **188**: 2357–2368.
23. Prevost-Blondel, A., Neuenhahn, M., Rawiel, M., and Pircher, H. (2000). Differential requirement of perforin and IFN-gamma in CD8 T cell-mediated immune responses against B16.F10 melanoma cells expressing a viral antigen. *Eur. J. Immunol.* **30**: 2507–2515.
24. Qin, Z., and Blankenstein, T. (2000). CD4+ T cell-mediated tumor rejection involves inhibition of angiogenesis that is dependent on IFN gamma receptor expression by nonhematopoietic cells. *Immunity* **12**: 677–686.
25. Barth, R. J., Jr., Mule, J. J., Spiess, P. J., and Rosenberg, S. A. (1991). Interferon gamma and tumor necrosis factor have a role in tumor regressions mediated by murine CD8+ tumor-infiltrating lymphocytes. *J. Exp. Med.* **173**: 647–658.
26. Becker, C., et al. (2001). Adoptive tumor therapy with T lymphocytes enriched through an IFN-gamma capture assay. *Nat. Med.* **7**: 1159–1162.
27. Klinman, D. M., Yamshchikov, G., and Ishigatsubo, Y. (1997). Contribution of CpG motifs to the immunogenicity of DNA vaccines. *J. Immunol.* **158**: 3635–3639.
28. Ballas, Z. K., Rasmussen, W. L., and Krieg, A. M. (1996). Induction of NK activity in murine and human cells by CpG motifs in oligodeoxynucleotides and bacterial DNA. *J. Immunol.* **157**: 1840–1845.
29. Sparwasser, T., et al. (1998). Bacterial DNA and immunostimulatory CpG oligonucleotides trigger maturation and activation of murine dendritic cells. *Eur. J. Immunol.* **28**: 2045–2054.
30. Jakob, T., Walker, P. S., Krieg, A. M., Udey, M. C., and Vogel, J. C. (1998). Activation of cutaneous dendritic cells by CpG-containing oligodeoxynucleotides: a role for dendritic cells in the augmentation of Th1 responses by immunostimulatory DNA. *J. Immunol.* **161**: 3042–3049.
31. Nagata, S., and Golstein, P. (1995). The Fas death factor. *Science* **267**: 1449–1456.
32. Fellenberg, J., Mau, H., Scheuerpflug, C., Ewerbeck, V., and Debatin, K. M. (1997). Modulation of resistance to anti-APO-1-induced apoptosis in osteosarcoma cells by cytokines. *Int. J. Cancer* **72**: 536–542.
33. Watanabe-Fukunaga, R. (1992). The cDNA structure, expression, and chromosomal assignment of the mouse Fas antigen. *J. Immunol.* **148**: 1274–1279.
34. Weller, M., Frei, K., Groscurth, P., Krammer, P. H., Yonekawa, Y., and Fontana, A. (1994). Anti-Fas/APO-1 antibody-mediated apoptosis of cultured human glioma cells: induction and modulation of sensitivity by cytokines. *J. Clin. Invest.* **94**: 954–964.
35. Shin, E. C., et al. (2001). IFN-gamma induces cell death in human hepatoma cells through a TRAIL/death receptor-mediated apoptotic pathway. *Int. J. Cancer* **93**: 262–268.
36. Xu, X., Fu, X. Y., Plate, J., and Chong, A. S. (1998). IFN-gamma induces cell growth inhibition by Fas-mediated apoptosis: requirement of STAT1 protein for up-regulation of Fas and FasL expression. *Cancer Res.* **58**: 2832–2837.
37. Ahn, E. Y., Pan, G., Vickers, S. M., and McDonald, J. M. (2002). IFN-gamma upregulates apoptosis-related molecules and enhances Fas-mediated apoptosis in human cholangiocarcinoma. *Int. J. Cancer* **100**: 445–451.
38. Lee, J. K., et al. (2000). IFN-gamma-dependent delay of in vivo tumor progression by Fas overexpression on murine renal cancer cells. *J. Immunol.* **164**: 231–239.
39. Rosen, D., Li, J. H., Keidar, S., Markon, I., Orda, R., and Berke, G. (2000). Tumor immunity in perforin-deficient mice: a role for CD95 (Fas/APO-1). *J. Immunol.* **164**: 3229–3235.
40. Bergmann-Leitner, E. S., and Abrams, S. I. (2000). Differential role of Fas/Fas ligand interactions in cytolysis of primary and metastatic colon carcinoma cell lines by human antigen-specific CD8+ CTL. *J. Immunol.* **164**: 4941–4954.
41. Keane, M. M., et al. (1996). Fas expression and function in normal and malignant breast cell lines. *Cancer Res.* **56**: 4791–4798.
42. Krammer, P. H., Galle, P. R., Moller, P., and Debatin, K. M. (1998). CD95(APO-1)/Fas-mediated apoptosis in normal and malignant liver, colon, and hematopoietic cells. *Adv. Cancer Res.* **75**: 251–273.
43. Owen-Schaub, L., Chan, H., Cusack, J. C., Roth, J., and Hill, L. L. (2000). Fas and Fas ligand interactions in malignant disease. *Int. J. Oncol.* **17**: 5–12.
44. Nagata, S. (1997). Apoptosis by death factor. *Cell* **88**: 355–365.
45. Suda, T., et al. (1995). Expression of the Fas ligand in cells of T cell lineage. *J. Immunol.* **154**: 3806–3813.
46. Dudley, M. E., et al. (2002). Cancer regression and autoimmunity in patients after clonal repopulation with antitumor lymphocytes. *Science* **298**: 850–854.
47. Pardoll, D. M. (2000). Therapeutic vaccination for cancer. *Clin. Immunol.* **95**: S44–S62.
48. Romero, P., et al. (1998). Ex vivo staining of metastatic lymph nodes by class I major histocompatibility complex tetramers reveals high numbers of antigen-experienced tumor-specific cytolytic T lymphocytes. *J. Exp. Med.* **188**: 1641–1650.
49. Greten, T. F., and Jaffee, E. M. (1999). Cancer vaccines. *J. Clin. Oncol.* **17**: 1047–1060.



The molecular regulation of GADD153 in apoptosis of cultured vascular smooth muscle cells by cyclic mechanical stretch

Wen-Pin Cheng¹, Huei-Fong Hung², Bao-Wei Wang², and Kou-Gi Shyu^{1,2*}

¹Graduate Institute of Medical Sciences, College of Medicine, Taipei Medical University, Taipei, Taiwan; and ²Division of Cardiology, Shin Kong Wu Ho-Su Memorial Hospital, 95 Wen-Chang Road, Taipei 111, Taiwan

Received 27 June 2007; revised 22 October 2007; accepted 24 October 2007

Time for primary review: 25 days

KEYWORDS

GADD153;
Stretch;
Smooth muscle cells;
Apoptosis

Aims The expression of GADD153 (growth arrest and DNA damage-inducible gene 153), an apoptosis-regulated gene, increases during endoplasmic reticulum (ER) stress. How mechanical stretch affects the regulation of GADD153 in vascular smooth muscle cells (VSMCs) during apoptosis is not fully understood. We aimed to test the hypothesis that mechanical stretch induces GADD153 expression in VSMCs undergoing apoptosis.

Methods and results Rat VSMCs grown on a flexible membrane base were stretched by vacuum to 20% of maximum elongation, at 60 cycles/min. An *in vivo* model of aorta-caval shunt in adult rats was used to investigate GADD153 expression. Cyclic stretch significantly increased GADD153 protein and mRNA expression after 18 h of stretch. Addition of c-jun N-terminal kinase (JNK) inhibitor SP600125, JNK siRNA, tumour necrosis factor- α (TNF- α) and TNF- α receptor antibody 30 min before stretch inhibited the induction of GADD153 protein. Gel shift assay showed that DNA-binding activity of activating factor 1 (AP-1) increased after stretch. SP600125, JNK siRNA and TNF- α antibody abolished the binding activity induced by stretch. Stretch increased while GADD153-Mut plasmid, SP600125, and c-jun antibody abolished the promoter activity. Both conditioned media from stretched VSMCs and exogenous administration of TNF- α recombinant protein to the non-stretched VSMCs increased GADD153 protein expression similar to that seen after stretch. An *in vivo* model of aorta-caval shunt in adult rats also demonstrated the increased GADD153 protein expression in the aorta.

Conclusion Cyclic stretch enhanced GADD153 expression in cultured rat VSMCs. The stretch-induced GADD153 is mediated by TNF- α , at least in part, through the JNK and AP-1 pathway. These findings suggest that GADD153 plays a role in stretch-induced VSMC apoptosis.

1. Introduction

In recent years, vascular smooth muscle cells (VSMCs) apoptosis has been increasingly implicated in both development and outcome of atherosclerotic disease.¹ Apoptosis of VSMCs is sufficient to induce features of plaque vulnerability in atherosclerosis.² Apoptosis pathways include death initiated by ligation of membrane-bound death receptor, release of proapoptotic factors from mitochondria or stress at the endoplasmic reticulum (ER). Protein folding in the ER is impaired under various physical and pathological conditions, called ER stress.³ In order to overcome ER stress, the organelle has a specific signalling pathway termed the unfolded protein response (UPR).⁴ When the accumulation of protein aggregates is overwhelming or their clean-up somehow hampered, the stress cannot be resolved and

the cell dies by apoptosis.⁵ One of the components of the ER stress-mediated apoptosis pathway is C/EBP homologous protein (CHOP), also known as GADD153.⁶

GADD153 plays a critical role in cell survival or cell death as part of the UPR. Previously, JNK/AP-1 was reported to contribute significantly to GADD153 gene transcriptional activity by oxidative stress.^{6,7} Moreover, GADD153 gene promoter activity is negatively regulated by nuclear factor-1 in VSMCs.⁸ GADD153 is expressed at undetectable levels in growing mammalian cells but is markedly increased by treatment with genotoxic agents, calcium ionophore, lipopolysaccharide, and nutrient deprivation.^{9,10} Microinjection of GADD153 protein into NIH3T3 cells induces G1/S arrest of the cell cycle.¹¹

The application of cyclic stretch to cultured VSMCs has been used as an *in vitro* experimental approach to study molecular events in response to mechanical overload. Cells in the cardiovascular system are continually subjected to mechanical forces due to changes in pressure and volume.

* Corresponding author. Tel: +886 2 2833 2211; fax: +886 2 2836 5775.
E-mail address: shyukg@ms12.hinet.net

VSMCs are the major cellular components of the blood vessel wall and are subjected to a dynamic mechanical environment modulated by pulsatile pressure and oscillatory shear forces. The cyclic strain model system subjects cultured cells to repetitive stretch-relaxation at rates comparable to dynamic stretch overload *in vivo*. It has been reported that cyclic mechanical stretch-induced apoptosis in VSMCs.^{12–14} However, there is still much debate and controversy concerning the role of apoptosis in heart failure.¹⁵ There is a good evidence to show that GADD153 plays an important role in VSMCs apoptosis.¹⁶ However, there is no conclusive proof on how cyclic mechanical stretch affects the GADD153 on the apoptosis in VSMCs. Thus, in this study, we first investigated the mechanism and signal pathways of GADD153 by cyclic mechanical stretch and secondly, investigated the effect of GADD153 induced by cyclic stretch on the apoptosis in VSMCs.

2. Methods

2.1 Vascular smooth muscle cells culture

Primary cultures of vascular smooth muscle cells (VSMCs) were grown by the explant technique from the thoracic aorta of 200–250 g male Sprague–Dawley rats, as described previously.^{17,18} Cells were cultured in medium 199 containing 20% foetal calf serum, 0.1 mmol/L non-essential amino acids, 1 mmol/L sodium pyruvate, 4 mmol/L L-glutamine, 100 U/mL penicillin, and 100 µg/mL streptomycin at 37°C under 5%CO₂/95% air in a humidified incubator. When confluent, VSMC monolayers were passaged every 6–7 days after trypsinization and were used for experiment from the third to sixth passages. These third to sixth passage cells were then cultured in Flexcell I flexible membrane dish in medium 199 containing 0.5% foetal calf serum, and the cells were incubated for a further 2 days to render them quiescent before the initiation of each experiment. The study conforms to Guide for the Care and Use of Laboratory Animals published by the US National Institutes of Health (NIH Publication No. 85-23, revised 1996). The study was reviewed and approved by the Institutional Animal Care and Use Committee of the Shin Kong Wu Ho-Su Memorial Hospital.

2.2 *In vitro* cyclic stretch on cultured vascular smooth muscle cells

The strain unit Flexcell FX-2000 (Flexcell International Co., NC, USA) consists of a vacuum unit linked to a valve controlled by a computer program. VSMCs cultured on the flexible membrane base were subjected to cyclic stretch produced by this computer-controlled application of sinusoidal negative pressure as characterized and described in detail previously.^{19,20} A frequency of 1 Hz (60 cycles/min) was used for cyclic stretch.

2.3 Western blot analysis

Western blot was performed as previously described.²¹ Mouse monoclonal anti-GADD153 antibody (Santa Cruz Biotechnology, CA, USA) was used.

2.4 Reverse transcription polymerase chain reaction and northern blot analysis

Total RNA was isolated from VSMCs using the single-step acid guanidinium thiocyanate/phenol/chloroform extraction method. The cDNA produced by reverse transcription (RT) was used to generate GADD153 probes by polymerase chain reaction (PCR) as described previously.²² The primers for GADD153 were 5'-CTCCCCACCAC-CATCG-3' and 5'-GCCACTCAGGAGTCCC-3'. The PCR products were run on 2% agarose gel for DNA fragment size verification, then

eluted and served as a probe in the northern blot analysis. The northern blot was performed as described previously.²³

2.5 Electrophoretic mobility shift assay

Nuclear protein concentrations from cultured VSMCs were determined by Biorad protein assay. Consensus and control oligonucleotides (Santa Cruz Biotechnology) were labelled by polynucleotides kinase incorporation of [γ ³²-p]dATP. Oligonucleotides sequences included the activating factor 1 (AP-1) consensus 5'-CGCTTGAT-GACTCAGCCGGAA-3'. The AP-1 mutant oligonucleotides sequences were 5'-CGCTTGATGACTTGGCCGGAA-3'. Electrophoretic mobility shift assay was performed as described previously.²⁰ Controls were performed in each case with mutant oligonucleotides or cold oligonucleotides to compete with labelled sequence.

2.6 Chromatin immunoprecipitation assay

Chromatin immunoprecipitation (CHIP) assays were carried out with the CHIP kit (Upstate Biotech, Temecula, CA, USA). The assay was performed as the manufacturer's instruction. One-third of the cell lysate from stretched VSMCs was immunoprecipitated by anti-c-jun monoclonal antibody (Cell Signalling, Beverly, MA, USA) and then was analysed by PCR of the GADD153 promoter and the remaining two-thirds cell lysate were added with anti-acetylated histone H3 antibody and analysed by PCR of GADD153 promoter. The primers for the GADD153 promoter were 5'-CCTCCCACCACCATCG-3' and 5'-GCCA-CTCAGGAGTCCC-3'. The primers for the GAPDH were 5'-CAT-CACCATCTCCAGGAGC-3' and 5'-GGATGATGTTCTGGGCTGCC-3'.

2.7 RNA interference

VSMCs were transfected with 800 ng GADD153 annealed siRNA oligonucleotide or siRNA of JNK1 (Dharmacon, Lafayette, CO, USA). GADD153 siRNA is a target-specific 21 nt siRNA according to a computer program provided by Dharmacon. The GADD153 targeted base sequences were sense: 5'-GGU AUGAGG AU-CUGCAGGAUU; antisense: 5'-P.UCCUGCAGAUCCUCAUACUUU. The sequences of the scramble siRNA for GADD153 were 5'-GGU AUGAGCUAGAGCAGGAUU; antisense: 5'-P.UCCUGCUCUAGCUAUACUUU. The sequence of JNK1 siRNA and negative control, a non-targeting siRNA (control siRNA) were used as described previously.²³

2.8 Promoter activity assay

A -845 to +85 bp rat GADD153 promoter construct was generated as follows. Rat genomic DNA was amplified with forward primer, CTCGAGGAAGGGCA TAAGAGCATCA and reverse primer, CCGTTCTCCTCAGGTTCCGGCTGT. The amplified product was digested with M1ul and Bg1II restriction enzymes and ligated into pGL3-basic luciferase plasmid vector (Promega, Madison, WI, USA) digested with the same enzymes. The GADD153 promoter contains AP-1 conserved sites (TGACTCA) at -246 to -240 bp. For the mutant, the AP-1 binding sites were mutated using the mutagenesis kit (Stratagene, La Jolla, CA, USA). Site-specific mutations were confirmed by DNA sequencing. Plasmids were transfected into VSMCs using a low pressure-accelerated gene gun (Bioware Technologies, Taipei, Taiwan) essentially following the protocol from the manufacturer. In brief, 2 µg of plasmid DNA was suspended in 5 µL of PBS and was delivered to the cultured VSMCs at a helium pressure of 15 psi. The transfection efficiency using this method is 30%. Following 12 h of cyclic stretching, cell extracts were prepared using Dual-Luciferase Reporter Assay System (Promega) and measured for dual luciferase activity by luminometer (Turner Designs, Sunnyvale, CA, USA).

2.9 Measurement of TNF- α concentration by enzyme-linked immunosorbent assay

Conditioned medium from VSMCs subjected to cyclic stretch and those from control (unstretched) cells were collected for TNF- α measurement. The level of TNF- α was measured by a quantitative sandwich enzyme immunoassay technique (R&D Systems, Minneapolis, MN, USA). The lowest limit of TNF- α ELISA kit was 52 pg/mL.

2.10 Real-time PCR

The real-time PCR was performed as described previously.²² The primers used were as follows: TNF- α , 5'-d(CCCACGTCGTAGCAAC)-3' (forward) and 5'-d(CGGACTCCGTGATGTC)-3' (reverse); GAPDH, 5'-d(CATCACCATCTTCCA GGAGC) (forward) and 5'-d(GGATGATGTCTGGGCTGCC)-3' (reverse).

2.11 Cytotoxicity study

Cytotoxicity study was performed as described previously.²⁰ For detection of cell injury induced by stretch, cell viability after application of cyclic stretch was monitored by trypan blue staining.

2.12 Flow cytometric analysis for apoptotic quantitation

Apoptotic cells were quantified as the percentage of cells with hypodiploid DNA (sub-G1). VSMCs were fixed with 70% ethanol and treated with RNase. Then nuclei were stained with propidium iodide. The DNA content was measured by using a FACSCalibur flow cytometer and Cell Quest software (Becton-Dickinson, Franklin Lakes, NJ, USA). For all assays, 10 000 cells were counted.

2.13 Terminal deoxynucleotidyl transferase-mediated dUTP nick-end labelling assay

DNA fragmentation was determined by terminal deoxynucleotidyl transferase-mediated dUTP nick-end labelling (TUNEL) using the ApopTag peroxidase *in situ* apoptosis detection kit (Chemicon International, Temecula, CA, USA). At the end of cyclic stretch, VSMCs were fixed in 4% paraformaldehyde for 10 min followed by a staining procedure according to the manufacturer's protocol.

2.14 Rat model of aorta-caval shunt

The aorta-caval shunt was produced as previously described.²⁴ In brief, the aorta was punctured at the union of the segment two-thirds caudal to the left renal artery and one-third cephalic to the aortic bifurcation, with an 18-gauge disposable needle held with a plastic syringe. The induced aorta-caval shunt caused a ratio of 1.7 of pulmonary flow to systemic flow. Sham-operated control animals were prepared in a similar manner, except that the aorta was not punctured.

2.15 Statistical analysis

All results were expressed as means \pm SEM. Statistical significance was evaluated using of variance (GraphPad Software Inc., San Diego, CA, USA). The Dunnett's test was used to compare multiple groups to a single control group. Tukey-Kramer comparison was used for pairwise comparisons between multiple groups after the ANOVA $P < 0.05$ was considered as significant. A value of $P < 0.05$ was considered to denote statistical significance.

3. Results

3.1 Cyclic stretch enhances GADD153 protein and mRNA expression in vascular smooth muscle cells

The level of GADD153 protein began to increase as early as 6 h after stretch to 20% elongation was applied, reached a maximum of 4.5-fold over the control by 18 h, remained elevated up to 24 h and tended to decline at 48 h. When VSMCs were stretched at 10% elongation, the level of GADD153 protein was similar to that of control without stretch (Figure 1A and B). The northern blots showed that GADD153 messages increased maximally after 18 h of stretch at 20% elongation (Figure 1C and D). These results indicated that cyclic stretch-induced GADD153 expression in VSMCs.

3.2 Stretch-induced GADD153 protein expression in vascular smooth muscle cells is mediated by JNK

To investigate the possible signal pathway mediating the stretch-induced GADD153 in VSMCs, the VSMCs were stretched 20% for 18 h in the presence and absence of inhibitors or siRNA. As shown in Figure 2, the stretch-induced increases of GADD153 proteins were significantly blocked

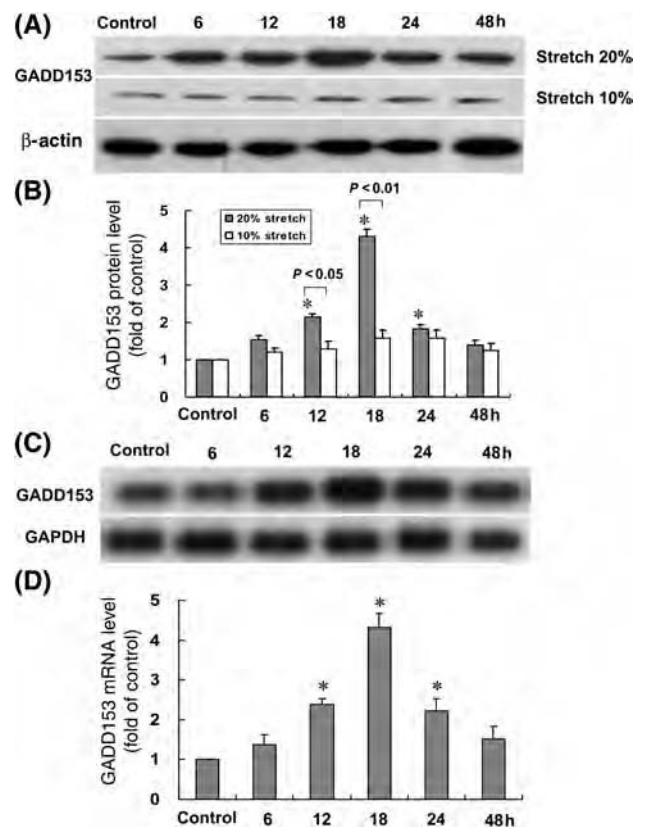


Figure 1 Effects of cyclic stretch on GADD153 protein and mRNA expression in vascular smooth muscle cells (VSMCs). (A) Representative western blots for GADD153 in VSMCs subjected to cyclic stretch by 20 or 10% for various periods of time. (B) Quantitative analysis of GADD153 protein levels. The values from stretched VSMCs have been normalized to values in control cells ($n = 5$ per group). (C) Representative northern blots for GADD153 mRNA levels in VSMCs subjected to cyclic stretch by 20% for various periods of time. (D) Quantitative analysis of GADD153 mRNA levels. The values from stretched VSMCs have been normalized to matched GAPDH measurement and then expressed as a ratio of normalized values to mRNA in control cells ($n = 5$ per group). * $P < 0.01$ vs. control.

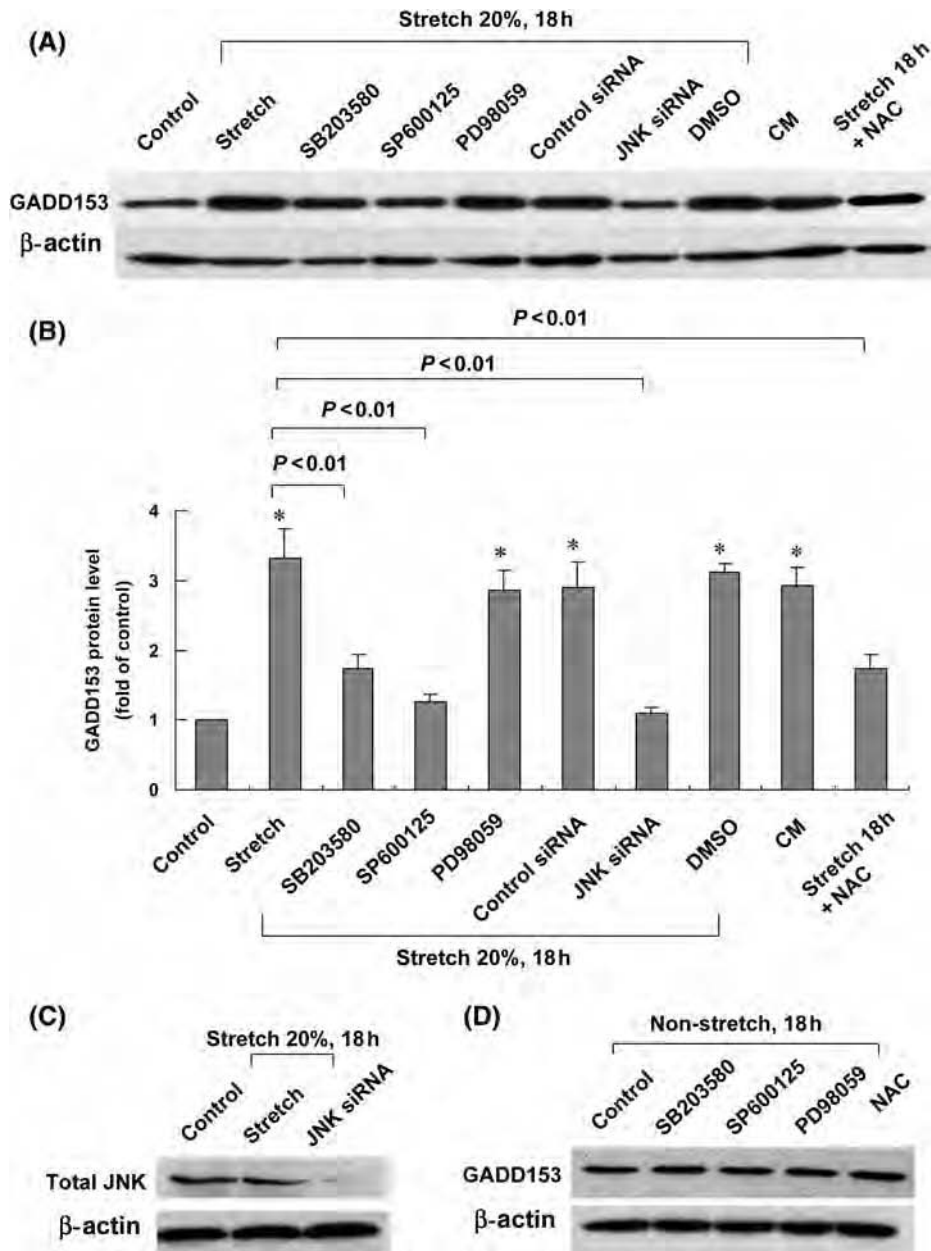


Figure 2 Effects of MAPK inhibitors on GADD153 protein expression induced by cyclic stretch in vascular smooth muscle cells (VSMCs). (A) Representative western blots for GADD153 protein levels in VSMCs subjected to cyclic stretch in the absence or presence of inhibitors, siRNA, and vehicle (DMSO 0.1%). CM, conditioned medium; NAC, *N*-acetylcysteine. (B) Quantitative analysis of GADD153 protein levels. The values from stretched VSMCs have been normalized to values in control cells ($n = 5$ per group). * $P < 0.01$ vs. control. (C) JNK siRNA knocked down total JNK protein expression ($n = 3$). (D) GADD153 protein expression in non-stretched cells treated with different inhibitors ($n = 3$).

after the addition of SP600125 (20 μ M) 30 min before stretch. The GADD153 proteins induced by stretch were not affected by the addition of PD98059 (50 μ M), but partially blocked by the addition of SB203580 (3 μ M) and *N*-acetylcysteine (500 μ M). SP600125 is a potent, cell-permeable, selective, and reversible inhibitor of JNK. PD98059 is a specific and potent inhibitor of ERK kinase. SB203580 is a highly specific, cell permeable inhibitor of p38 kinase. *N*-Acetylcysteine is a free radical scavenger.

To test the specific effect of JNK MAP kinase pathway mediating the expression of GADD153, JNK siRNA was transfected to VSMCs before cyclic stretch. Moreover, JNK siRNA also completely blocked the GADD153 expression induced

by stretch. JNK siRNA knocked down the expression of total JNK protein (Figure 2C). The DMSO alone as a vehicle control and control siRNA did not affect the GADD153 expression induced by cyclic stretch. All the inhibitors used on non-stretched cells did not change the GADD153 protein expression (Figure 2D). These findings implicated that JNK pathway, but not p42/p44 MAP kinases, mediated the induction of GADD153 proteins by stretch in VSMCs. The conditioned medium from stretched VSMCs could induce the same increase in GADD153 protein expression in non-stretched VSMCs. These findings suggested that cyclic stretch regulated GADD153 protein in VSMCs possibly via autocrine or paracrine mechanisms.

3.3 Cyclic stretch increases AP-1 binding activity

Cyclic stretch of VSMCs for 6–18 h significantly increased the DNA-protein binding activity of AP-1 (Figure 3A). An excess of unlabelled AP-1 oligonucleotide competed with the probe for binding AP-1 protein, whereas an oligonucleotide containing a 2 bp substitution in the AP-1 binding site did not compete for binding. Addition of SP600125 and TNF- α antibody (5 μ g/mL, purchased from R&D Systems) 30 min before stretch abolished the DNA-protein binding activity induced by cyclic stretch. JNK siRNA, similar to SP600125, also abolished the DNA-protein binding activity induced by stretch (Figure 3B). Exogenous administration of TNF- α to the VSMCs without stretch increased the AP-1-DNA binding activity. Addition of c-jun antibody shifted the DNA-protein binding site. Moreover, CHIP assay confirmed that stretch enhanced AP-1 binding activity in VSMCs (Figure 3C). These results demonstrated that stretch enhanced AP-1 binding activity in VSMCs.

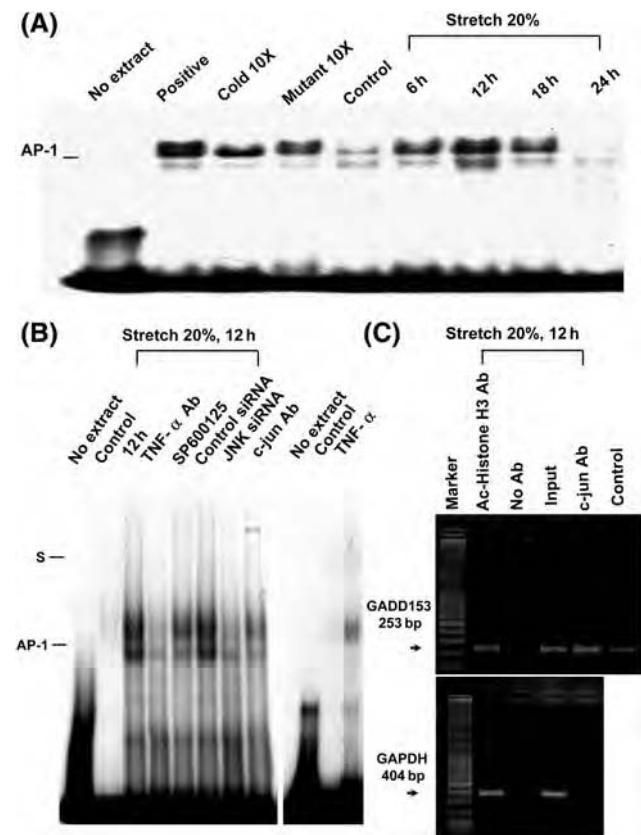


Figure 3 Effects of cyclic stretch on GADD153 binding activity in vascular smooth muscle cells (VSMCs). (A) Representative EMSA showing protein binding to AP-1 oligonucleotide in nuclear extracts of VSMCs after cyclic stretch during various times. (B) Representative EMSA showing protein binding to AP-1 oligonucleotide in nuclear extracts of VSMCs after cyclic stretch in the absence or presence of JNK inhibitors. Arrow indicates the mobility of the complex. Similar results were found in another independent experiment. Cold oligo means unlabeled AP-1 oligonucleotide. A significant supershifted complex after incubation with c-jun antibody was observed. (C) AP-1 binding activity enhanced by stretch was analysed in VSMCs by CHIP assay with anti-acetylated histone H3 and c-jun antibody. Similar results were found in another independent experiment. Control indicates control cells without stretch.

3.4 Cyclic stretch increases GADD153 promoter activity through AP-1

To study whether the GADD153 expression induced by stretch is regulated at the transcriptional level, we cloned the promoter region of rat GADD153 (–845 to +85) and constructed a luciferase reporter plasmid (pGL3-Luc). The GADD153 promoter construct contains SP-1, NF-IL6, NF1 and AP-1 binding sites. As shown in Figure 4, transient transfection experiment in VSMC using this reporter gene revealed that stretch for 12 h significantly caused GADD153 promoter activation. This result indicated that GADD153 expression is induced at transcriptional level during cyclic stretch in VSMCs.

When the AP-1 binding sites were mutated, the increased promoter activity induced by stretch was abolished. Moreover, addition of c-jun antibody and SP600125 caused an inhibition of transcription. These results suggested that AP-1 binding site in the GADD153 promoter is essential for the transcriptional regulation by cyclic stretch.

3.5 Cyclic stretch stimulates secretion of TNF- α from vascular smooth muscle cells

As shown in Figure 5A, cyclic stretch significantly began to increase the TNF- α secretion from VSMCs at 6 h after stretch and reached a maximum at 12 h and remained elevated for 24 h. Cyclic stretch also significantly enhanced the expression of TNF- α mRNA (Figure 5B). These results indicated that stretch causes secretion of TNF- α for VSMCs.

3.6 Exogenous TNF- α increases GADD153 protein expression

To investigate the direct effect of TNF- α on GADD153 expression in VSMCs, TNF- α at different concentrations was administrated to the cultured medium for 18 h. As shown in Figure 6, the effect of TNF- α on GADD153

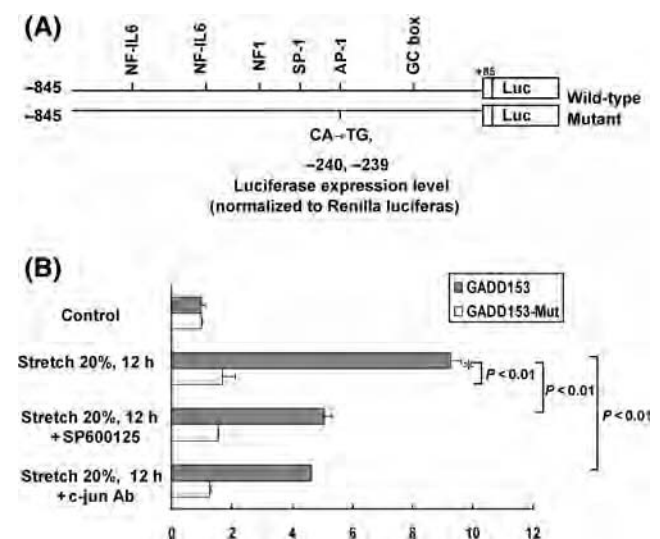


Figure 4 Effect of cyclic stretch on GADD153 promoter activity in vascular smooth muscle cells (VSMCs). (A) Constructs of GADD153 promoter gene. Positive +1 demonstrates the initiation site for the GADD153 transcription. (B) Quantitative analysis of GADD153 promoter activity. VSMCs were transiently transfected with pGADD153-Luc by gene gun. The luciferase activity in cell lysates was measured and was normalized with Renilla activity ($n = 3$ per group). * $P < 0.01$ vs. control.

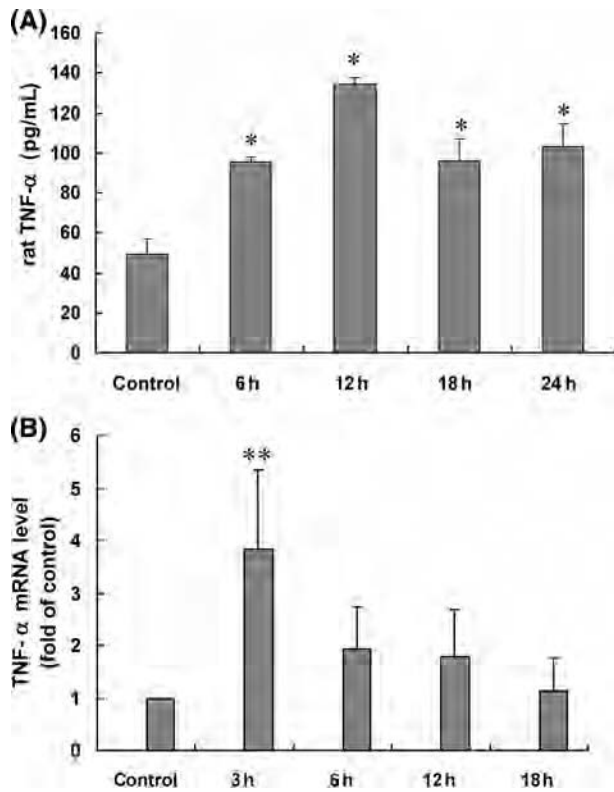


Figure 5 Effects of cyclic stretch on TNF- α secretion for vascular smooth muscle cells (VSMCs). (A) Cyclic stretch increased release of TNF- α from VSMCs subjected to cyclic stretch by 20% for various periods of time ($n = 3$). * $P < 0.01$ vs. control. (B) Cyclic stretch increased TNF- α mRNA expression in VSMCs ($n = 4$). ** $P < 0.02$ vs. control.

protein expression was dose-dependent. Addition of TNF- α and TNF- α receptor monoclonal antibody 30 min before stretch significantly blocked the expression of GADD153 induced by cyclic stretch. These findings suggested that TNF- α enhances GADD153 expression by cyclic stretch.

3.7 Cyclic stretch-induced apoptosis is mediated by GADD153 in vascular smooth muscle cells

As shown in *Figure 7A* and *B*, cyclic stretch not only enhanced the death rate but also decreased the viability of VSMCs measured by a cell counter and MTT assay. This result suggested that cyclic stretch-induced cell death of VSMCs.

As shown in *Figure 7C*, apoptosis was assessed by PI staining and FACS analysis. The percentage of cells in the sub-G1 fraction stained with PI was elevated after stretch for 18 h and addition of TNF- α . The TUNEL assay was used to confirm the presence of apoptotic nuclei after cyclic stretch (*Figure 7D*). A significant increase in TUNEL-positive nuclei was present after stretch for 18 h and addition of TNF- α . These increases of apoptosis in VSMCs induced by stretch were significantly reversed by GADD153 siRNA and transient transfection of GADD153-Mut plasmid. These findings demonstrated that GADD153 mediates stretch-induced apoptosis of VSMCs. To further investigate the mechanism of GADD153-induced cell death in stretched VSMCs, caspase activity was measured by colorimetric activity assay kit (Chemicon International). As shown in Supplementary

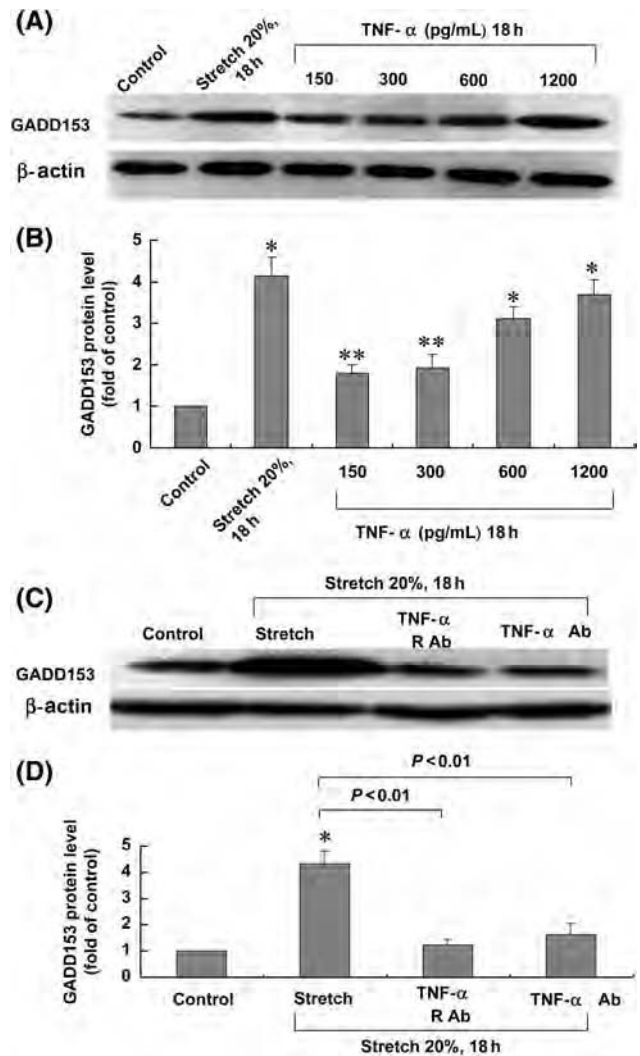


Figure 6 Exogenous administration of TNF- α increases GADD153 protein expression. (A and C) Representative western blots for GADD153 in VSMCs after exogenous administration of TNF- α , TNF- α , and TNF- α monoclonal antibody. (B and D) Quantitative analysis of GADD153 protein levels. The values from treated VSMCs have been normalized to matched β -actin measurement and then expressed as a ratio of normalized values to control cells ($n = 3$ per group). * $P < 0.01$ vs. control; ** $P < 0.05$ vs. control.

material online, *Figure S1*, mechanical stretch increased caspases 3 and 8 activity. GADD153 siRNA and mutant GADD153 abolished the increase of caspase 3 induced by stretch but not caspase 8. TNF- α alone also induced caspases 3 and 8. These findings indicate that caspase 3 is involved in the GADD153-induced apoptosis of VSMCs under mechanical stretch.

3.8 *In vivo* aorta-caval shunt increases aortic GADD153 protein expression

Aorta-caval shunt was performed to explore whether GADD153 expression was increased under volume-overload *in vivo*. As shown in *Figure 8*, the GADD153 protein expression in rat aorta significantly increased at 5 day after induction of aorta-caval shunt. It reached a maximum of 4.3-fold over the sham and remained elevated up to 7 days. The *in vivo* aorta-caval shunt also induced caspase 3 activity and increased apoptosis by TUNEL

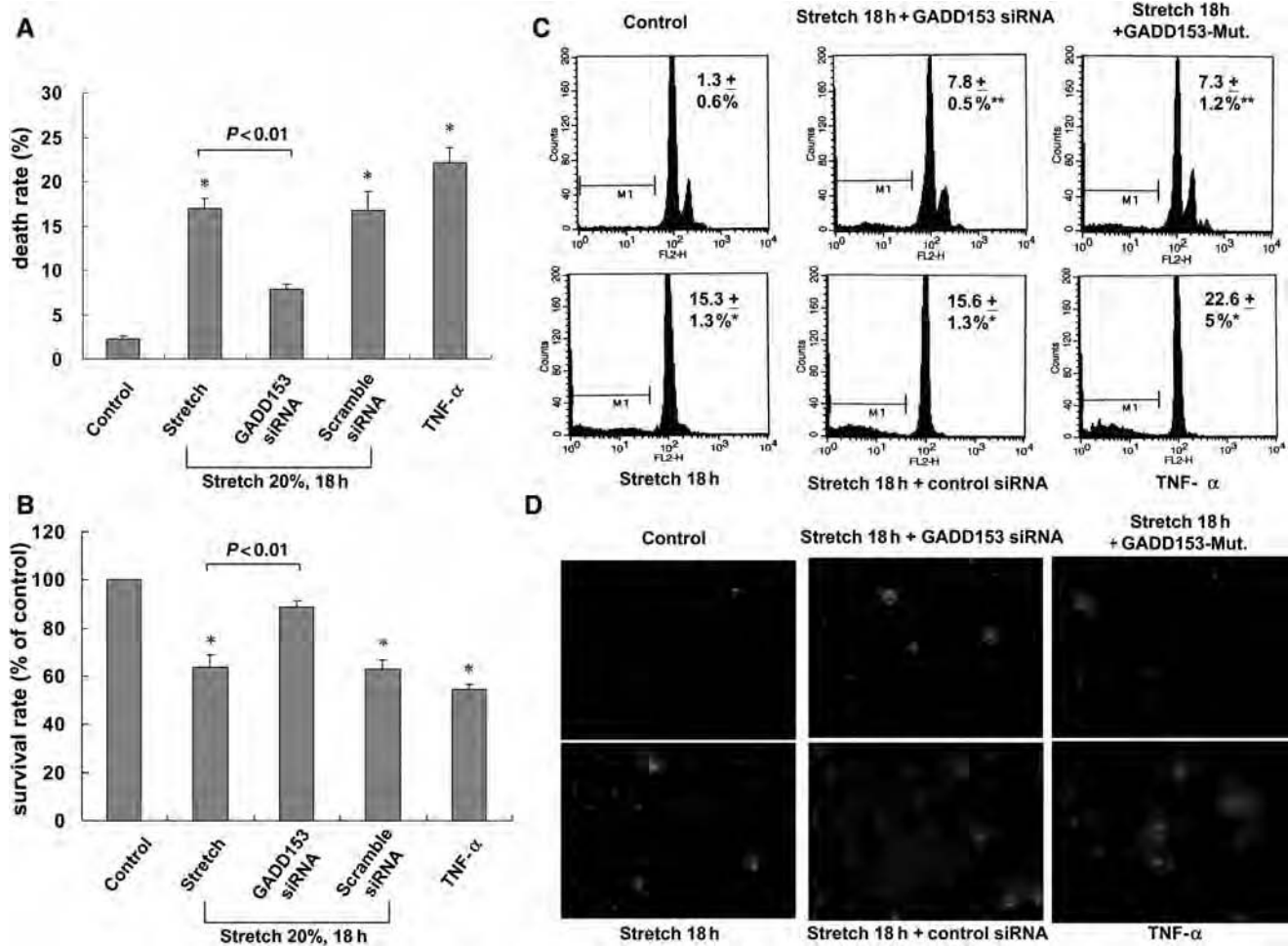


Figure 7 Effect of GADD153 on stretch-induced apoptosis in vascular smooth muscle cells (VSMCs). Quantitative analysis of trypan blue exclusion (A) and MTT assay (B) for VSMCs viability after stretch and addition of GADD153 siRNA or 500 pg/mL TNF- α . ($n = 6$). * $P < 0.01$ vs. control. (C) VSMCs were subjected to cyclic stretch, addition of 500 ng/mL TNF- α , or siRNA and transient transfection of GADD153-Mut plasmid before stretch. Quantification of the apoptotic fractions was performed using FACSscan. ($n = 3$). * $P < 0.01$ vs. control; ** $P < 0.05$ vs. stretch 18 h. (D) Representative microscopy images of VSMCs after cyclic stretch 18 h, addition of 500 pg/mL TNF- α , or siRNA and transient transfection of GADD153-Mut plasmid before stretch then stained with a TUNEL kit. Similar results were observed in another two independent experiments.

assay (see Supplementary material online, *Figure S2*) in the aorta. Treatment with SP600125 abolished the induction of caspase 3 and apoptosis.

4. Discussion

In this study, we demonstrated several significant findings. First, cyclic stretch upregulates GADD153 expression in rat VSMCs; secondly, cyclic stretch induces TNF- α expression in VSMCs; thirdly, TNF- α acts as an autocrine factor to mediate the increased GADD153 expression induced by cyclic stretch; fourthly, JNK MAP kinase and AP-1 transcription factor are involved in the signalling pathway of GADD153 induction; fifthly, cyclic stretch induces VSMCs apoptosis via GADD153; and sixthly, *in vivo* acute haemodynamic overload increases aortic GADD153 expression. GADD153 was upregulated in both a time- and load-dependent manner by cyclic stretch. Cyclic stretch of VSMCs increased both GADD153 protein and mRNA expression.

In our study, exogenous addition of TNF- α to non-stretched VSMCs is sufficient to induce a similar GADD153

protein expression as observed in stretched VSMCs. These results provide the first evidence that TNF- α mediates cyclic stretch-induced expression of GADD153 in VSMCs. Our study revealed that TNF- α acts as an autocrine mediator in response to cyclic stretch in VSMCs. Previously, we have demonstrated that cyclic stretch-induced TNF- α secretion and mRNA expression in HUVECs.²⁵ In this study, we found that cyclic stretch also enhanced TNF- α expression in VSMCs. However, another study showed no increased concentration of TNF- α in the medium collected from pulmonary VSMCs at 24 and 48 h after 25% stretch.¹⁴ Sotoudeh *et al.* used pulmonary VSMCs, whereas our study used rat aortic VSMCs. Different species, stretch intension and stretch time may explain the discrepancy.

Our results suggested that TNF- α is responsible for AP-1-DNA binding in VSMCs. In this study, we demonstrated that cyclic stretch stimulation of AP-1-DNA binding activity required at least phosphorylation of JNK since JNK inhibitor and JNK siRNA abolished the AP-1 binding activity. SP600125, a potent and specific inhibitor of JNK MAP kinase, inhibited the GADD153 expression induced by stretch. SB203580, a potent and specific inhibitor of p38,

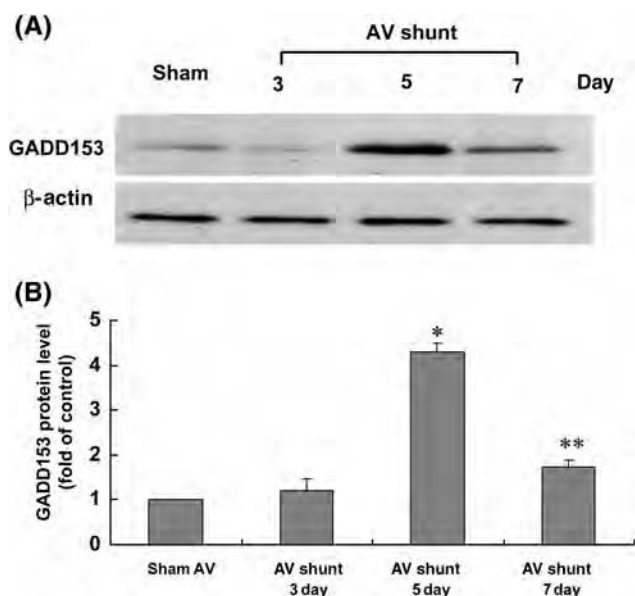


Figure 8 Effect of *in vivo* model of aorta-caval shunt (AV shunt) on aortic GADD153 protein levels. (A) Representative western blots for GADD153 in rat aorta after short-term induction of AV shunt. (B) Quantitative analysis of GADD153 protein levels. The values have been normalized to β -actin measurement and then expressed as a ratio of normalized values to GADD153 protein in sham. ($n = 5$ per group). * $P < 0.01$ vs. control; ** $P < 0.05$ vs. control.

had partial inhibitory effect, whereas inhibitors of p42/p44 MAP kinase did not have the inhibitory effect. JNK and MAP kinases are important intracellular signalling pathways that regulate GADD153.^{26,27} We also demonstrated that the JNK1 siRNA significantly inhibited GADD153 expression induced by stretch. AP-1, a well-characterized downstream target of JNK is needed for GADD153 promoter activity in rat VSMCs.²⁸ Oxidative stress resulting in the induction of GADD153 expression is mediated by an AP-1 site in GADD153 promoter.^{28,29} *N*-Acetylcysteine had partial inhibitory effect on the stretch-induced GADD153 expression. Since *N*-acetylcysteine is a free radical scavenger and mechanical stretch is known to affect the production of reactive oxygen species, the findings in our study may indicate a potential role of reactive oxygen species in the induction of GADD153 by mechanical stretch. In this study, we demonstrated that increased transcriptional activity of GADD153 promoter by cyclic stretch was AP-1 dependent via reporter gene assay. These data implicated that the JNK MAP kinase pathway, but not the p42/p44 MAP kinase pathway, is the major pathway involved in the induction of GADD153 by stretch and mediates the increased binding activity of AP-1.

Our results revealed that cyclic stretch-induced apoptosis of VSMCs is regulated by GADD153. Cyclic mechanical stretch-induced apoptosis in VSMCs has been reported to be mediated by endothelin B receptor and β_1 -integrin.^{12,13} Death receptors such as TNF receptor-1 are a critical factor in mechanical stretch-induced apoptosis in VSMCs.¹⁴ Morrow *et al.*³⁰ showed that cyclic strain inhibits SMC growth while enhances SMC apoptosis, at least in part, through regulation of Notch receptor and downstream target gene expression. In this study, our findings suggested that the ER stress related protein GADD153 may be involved in the apoptosis of VSMCs induced by mechanical stretch.

Although GADD153 has been considered to be an apoptosis-related gene, the downstream of CHOP does not sufficiently account for the cell death. Overexpression of GADD153 leads to decrease anti-apoptotic protein Bcl-2 which promotes cell viability.³¹ GADD153 overexpression and the concomitant down-regulation of cardiac ankyrin repeat protein might have an important role in apoptosis of H9c2 cells during hypoxia.³² Tribbles-related protein 3 is involved in GADD153-dependent cell death during ER stress.³³ But, the correlation of GADD153 between apoptosis is still unknown. We have demonstrated that mechanical stretch and TNF- α induced caspase 3 and GADD153 siRNA and mutant GADD153 abolished the induction of caspase 3 by stretch. Our result suggests that caspase 3 is involved in the GADD153-induced apoptosis of VSMCs under mechanical stretch.

In our study, we further confirmed the increased aortic GADD153 expression and caspase 3 in acute haemodynamic overload as in aorta-caval shunt. It has been reported that GADD153 protein expression increased in the carotid artery balloon injury model in rats.³⁴ It suggested that GADD153 may be enhanced during acute haemodynamic overload *in vivo*. The increased GADD153 protein expression after acute haemodynamic overload may contribute to the regulation of vascular repair and remodelling, which involves VSMC proliferation and apoptosis.

In summary, our study reports for the first time that cyclic mechanical stretch enhances GADD153 expression in cultured rat VSMCs. The stretch-induced GADD153 is mediated by TNF- α , at least in part, through JNK MAP kinase and AP-1 pathway.

Supplementary material

Supplementary material is available at *Cardiovascular Research* online.

Funding

This study was sponsored in part by Shin Kong Wu H0-Su Memorial Hospital, Taipei, Taiwan.

Conflict of interest: none declared.

References

1. Isner JM, Kearney M, Bortman S, Passeri J. Apoptosis is human atherosclerosis and restenosis. *Circulation* 1995;**91**:2703–2711.
2. Clarke MC, Figg N, Maguire JJ, Davenport AP, Goddard M, Littlewood TD *et al.* Apoptosis of vascular smooth muscle cells induces features of plaque vulnerability in atherosclerosis. *Nat Med* 2006;**12**:1075–1080.
3. Kaufman RJ. Stress signaling from the lumen of the endoplasmic reticulum: coordination of gene transcriptional and translational controls. *Genes Dev* 1999;**13**:1211–1233.
4. Ron D. Translational control in the endoplasmic reticulum stress response. *J Clin Invest* 2002;**110**:1383–1388.
5. Di Sano F, Ferraro E, Tufi R, Achsel T, Piacentini M, Cecconi F. ER stress induces apoptosis by an apoptosome-dependent but caspase-12 independent mechanism. *J Biol Chem* 2006;**281**:2693–2700.
6. Oyadomar S, Mori M. Roles of CHOP/GADD153 in endoplasmic reticulum stress. *Cell Death Differ* 2004;**11**:381–389.
7. Kim R, Emi M, Tanabe K, Murakami S. Role of unfolded protein response in cell death. *Apoptosis* 2006;**11**:5–13.
8. Nakamura M, Okura T, Kitami Y, Hiwada K. Nuclear factor 1 is a negative regulator of gadd153 gene expression in vascular smooth muscle cells. *Hypertension* 2001;**37**:419–424.

9. Matsumoto M, Minami M, Takeda K, Sakao Y, Akira S. Ectopic expression of CHOP (GADD153) induces apoptosis in M1 myeloblastic leukemia cells. *FEBS Lett* 1996;**395**:143–147.
10. Kastan MB, Zhan Q, El-Deiry WS, Carrier F, Jacks T, Walsh WV *et al.* A mammalian cell cycle checkpoint pathway utilizing p53 and GADD45 is defective in ataxia-telangiectasia. *Cell* 1992;**71**:587–597.
11. Barone MV, Crozat A, Tabaee A, Philipson L, Ron D. CHOP (GADD153) and its oncogenic variant, TLS-CHOP, have opposing effects on the induction of G1/S arrest. *Genes Dev* 1994;**8**:453–464.
12. Cattaruzza M, Dimigen C, Ehrenreich H, Hecker M. Stretch-induced endothelial B receptor-mediated apoptosis in vascular smooth muscle cells. *FASEB J* 2000;**14**:991–998.
13. Wernig F, Mayr M, Xu Q. Mechanism stretch-induces apoptosis in smooth muscle cells is mediated by β 1-integrin signaling pathway. *Hypertension* 2003;**41**:903–911.
14. Sotoudeh M, Li YS, Yajima N, Chang CC, Tsou TC, Wang Y *et al.* Induction of apoptosis in vascular smooth muscle cells by mechanical stretch. *Am J Physiol Heart Circ Physiol* 2002;**282**:H1709–H1716.
15. Kang PM, Izumo S. Apoptosis and heart failure: a critical review of the literature. *Circ Res* 2000;**86**:1107–1113.
16. Igase M, Okura T, Nakamura M, Takata Y, Kitami Y, Hiwada K. Role of GADD153 (growth arrest and DNA damage-inducible gene 153) in vascular smooth muscle cell apoptosis. *Clin Sci* 2001;**100**:275–281.
17. Stavri GT, Zachary IC, Baskerville PA, Martin JF, Erusalimsky JD. Basic fibroblast growth factor upregulates the expression of vascular endothelial growth factor in vascular smooth muscle cells: synergistic interaction with hypoxia. *Circulation* 1995;**92**:1–14.
18. Shyu KG, Chao YM, Wang BW, Kuan P. Regulation of discoidin domain receptor 2 by cyclic mechanical stretch in cultured rat vascular smooth muscle cells. *Hypertension* 2005;**46**:614–621.
19. Cheng JJ, Wung BS, Chao YJ, Wang DL. Cyclical strain enhances adhesion of monocytes to endothelial cells by increasing intercellular adhesion molecular-1 expression. *Hypertension* 1996;**28**:386–391.
20. Shyu KG, Ko WH, Yang WS, Wang BW, Kuan P. Insulin-like growth factor-1 mediates stretch-induced upregulation of myostatin expression in neonatal rat cardiomyocytes. *Cardiovasc Res* 2005;**68**:405–414.
21. Liang YJ, Lai LP, Wang BW, Juang SJ, Chang CM, Leu JG *et al.* Mechanical stress enhances serotonin 2B receptor modulating brain natriuretic peptide through nuclear factor-kappaB in cardiomyocytes. *Cardiovasc Res* 2006;**72**:303–312.
22. Chang H, Shyu KG, Wang BW, Kuan P. Regulation of hypoxia-inducible factor-1 α by cyclical mechanical stretch in rat vascular smooth muscle cells. *Clin Sci* 2003;**105**:447–456.
23. Shyu KG, Wang BW, Yang YH, Tsai SC, Lin S, Lee CC. Amphetamine activates connexin43 gene expression in cultured neonatal rat cardiomyocytes through JNK and AP-1 pathway. *Cardiovasc Res* 2004;**63**:98–108.
24. Shyu KG, Lu MJ, Chang H, Sun HY, Wang BW, Kuan P. Carvedilol modulates the expression of hypoxia-inducible factor-1 α and vascular endothelial growth factor in a rat model of volume-overload heart failure. *J Card Fail* 2005;**11**:156–165.
25. Wang BW, Chang H, Lin SK, Kuan P, Shyu KG. Induction of matrix metalloproteinase-14 and -2 by cyclic mechanical stretch is mediated by tumor necrosis factor- α in cultured human umbilical vein endothelial cells. *Cardiovasc Res* 2003;**59**:460–469.
26. Wang XZ, Ron D. Stress-induced phosphorylation and activation of the transcription factor CHOP (GADD153) by p38 MAP Kinase. *Science* 1996;**272**:1347–1349.
27. Xu C, Bailly-Maitre B, Reed JC. Endoplasmic reticulum stress: cell life and death decisions. *J Clin Invest* 2005;**115**:2656–2664.
28. Guyton KZ, Xu Q, Holbrook NJ. Induction of mammalian stress response GADD153 by oxidative stress: role of AP-1 element. *Biochem J* 1996;**314**:547–554.
29. Tang JR, Nakamura M, Okura T, Takata Y, Watanabe S, Yang ZH *et al.* Mechanism of oxidative stress-induced GADD153 gene expression in vascular smooth muscle cells. *Biochem Biophys Res Commun* 2002;**290**:1255–1259.
30. Morrow D, Sweeney C, Birney YA, Cummins PM, Walls D, Redmond EM *et al.* Cyclic strain inhibits notch receptor signaling in vascular smooth muscle cells in vitro. *Circ Res* 2005;**96**:567–575.
31. McCullough KD, Martindale JL, Klotz LO, Aw TY, Holbrook NJ. Gadd153 sensitizes cells to endoplasmic reticulum stress by down-regulating Bcl2 and perturbing the cellular redox state. *Mol Cell Biol* 2001;**21**:1249–1259.
32. Han XJ, Chae JK, Lee MJ, You KR, Lee BH, Kim DG. Involvement of GADD153 and cardiac ankyrin repeat protein in hypoxia-induced apoptosis of H9c2 cells. *J Biol Chem* 2005;**280**:23122–23129.
33. Ohoka N, Yoshii S, Hattori T, Onozaki K, Hayashi H. TRB3, a novel ER stress-inducible gene, is induced via ATF4-CHOP pathway and is involved in cell death. *EMBO J* 2005;**24**:1243–1255.
34. Amundson SA, Zhan Q, Penn LZ, Fornace AJ. Myc suppresses induction of the growth arrest gene gadd34, gadd45 and gadd153 by DNA-damaging agents. *Oncogene* 1998;**17**:2149–2154.



Hypoxia induces discoidin domain receptor-2 expression via the p38 pathway in vascular smooth muscle cells to increase their migration

Shih-Chung Chen ^{a,b}, Bao-Wei Wang ^c, Danny Ling Wang ^d, Kou-Gi Shyu ^{a,c,*}

^a Graduate Institute of Clinical Medicine, College of Medicine, Taipei Medical University, 250 Wu-Xin Street, Taipei 110, Taiwan

^b Division of Cardiology, Taipei Medical University-Wan Fang Hospital, Taipei 116, Taiwan

^c Department of Education and Research, Shin Kong Wu Ho-Su Memorial Hospital, Taipei 111, Taiwan

^d Institute of Biomedical Science, Academia Sinica, Taipei 11529, Taiwan

ARTICLE INFO

Article history:

Received 9 July 2008

Available online 26 July 2008

Keywords:

Discoidin domain receptor

Hypoxia

Mitogen-activated protein kinase

Smooth muscle cells

ABSTRACT

Discoidin domain receptor-2 (DDR2) is a receptor tyrosine kinase that binds to the extracellular matrix. We investigated the role of hypoxia in DDR2 expression in vascular smooth muscle cells (VSMCs) and the underlying mechanism. Subjecting VSMCs to hypoxia (2.5% O₂) induced DDR2 expression; treatments with a specific inhibitor (SB203580) of p38 mitogen-activated protein kinase (MAPK) or p38-specific small interference RNA (siRNA) abolished this hypoxia-induced DDR2 expression. Gel shifting assays showed that hypoxia increased the Myc–Max–DNA binding activity in the promoter region of DDR2; inhibition of p38 MAPK activation by SB203580 and p38-specific siRNA blocked hypoxia-induced DDR2 promoter activity. Hypoxia also induced matrix metalloproteinase-2 (MMP-2) activity in VSMCs and increased their migration. These VSMC responses to hypoxia were inhibited by DDR2- and p38-specific siRNAs. Our results suggested that hypoxia induces DDR2 expression in VSMCs at the transcriptional level, which is mediated by the p38 MAPK pathway and contributes to VSMC migration.

© 2008 Elsevier Inc. All rights reserved.

Communication between cells and their environment is mediated by specific cell surface receptors that transduce external signals to the inside of cells. An important class of signaling receptors are receptor tyrosine kinases (RTKs), which play crucial roles in many fundamental cellular processes [1]. Two members of this family, discoidin domain receptors 1 and 2 (DDR1 and 2) are unusual RTKs in that their ligands are extracellular matrix (ECM) rather than growth factor-like peptides [2,3]. DDRs bind to several collagens and stimulate production of matrix metalloproteinase (MMP) [3,4], which can digest the ECM proteins and promote cell migration. DDR1 is mainly expressed in epithelial cells bound to collagen types I through V and VIII, whereas DDR2 is found in vascular and mesenchymal cells and responds to the fibrillar collagen types I and III [5]. It has been shown that DDR2 interacts with Src following its activation by collagen type I [6]. Thus, DDR2 requires Src activity to exhibit maximal levels of tyrosine-phosphorylation [6].

The ECM is a dynamic structure that not only provides a scaffold for mechanical support and organization of tissues, but also regulates critical events in normal development and pathological conditions. The neointimal is composed of vascular smooth muscle cells

(VSMCs), which synthesize abundant ECM. Obstructive vascular diseases are characterized by degradation and synthesis of new ECM components; for example, interactions between VSMCs and ECM proteins are important in cell migration during atherosclerosis and restenosis. Evidence from *in vitro* and *in vivo* studies using DDR1 and DDR2-null mice suggests that DDR can regulate cell proliferation and matrix metalloproteinase (MMP)-mediated ECM remodeling [4,7–9]. DDR1 is expressed on migrating VSMCs after balloon catheter injury of the rat carotid artery, and intimal thickening after arterial injury is reduced in DDR1-knockout mice [4]. The activation of DDR2 by collagen results in increased production of MMP-1 [2] and MMP-2 [8]. Prolonged stimulation of DDR2 is also associated with the up-regulation of MMP-1 expression [3]. Previous studies have shown that DDR2 associated with the MMP-2-dependent mechanism plays an important role in migration and proliferation of hepatic stellate cells [8] and fibroblasts [9]. Recent studies have shown that DDR1 and DDR2 play potential roles in regulating VSMC-mediated collagen turnover in obstructive vascular diseases [10]. These findings suggest an important role for DDRs in regulating collagen matrix degradation and cellular reorganization in the vascular system.

Hypoxia elicits a variety of functional responses in VSMCs, including cell migration. In order to maintain vascular homeostasis, VSMCs cope with hypoxia by regulating the expression of a number of genes that are mediated by a variety of signaling cascades [11]. Hypoxia enhances endothelial cell migration in an

* Corresponding author. Address: Graduate Institute of Clinical Medicine, College of Medicine, Taipei Medical University, 250 Wu-Xin Street, Taipei 110, Taiwan. Fax: +886 2 28365775.

E-mail address: shyukg@ms12.hinet.net (K.-G. Shyu), T005651@ms.skhn.org.tw (K.-G. Shyu).

MMP-2-dependent manner [12]. However, the mechanisms by which hypoxia regulates VSMC migration remain unclear. Moreover, little is known about the role of DDR2 in modulating hypoxia-induced VSMC migration. The aim of this study is to elucidate the role of DDR2 in hypoxia-induced VSMC migration and isolate the mechanism by which hypoxia induces DDR2 expression. Understanding the oxygen-sensitive adaptive pathways in VSMCs may help develop therapeutic strategies to treat various hypoxia-related vascular diseases.

Materials and methods

VSMC cultures. VSMCs were grown by explanting the thoracic aorta of 200–250-g male Sprague–Dawley rats, as described [13]. Cells were cultured in medium 199 containing 20% FCS, 0.1 mmol/L nonessential amino acids, 1 mmol/L sodium pyruvate, 4 mmol/L L-glutamine, 100 U/mL penicillin, and 100 µg/mL streptomycin at 37 °C under 5% CO₂/95% air in a humidified incubator. When confluent, VSMCs were passaged after trypsinization and cultured in a Flexcell I flexible membrane dish, in medium 199 containing 0.5% FCS. The cells were incubated for another 2 days to render them quiescent before the hypoxia experiment. VSMCs between passages 3–6 were used.

Hypoxia apparatus. Hypoxic conditions (2.5% O₂) were achieved by adding medium pre-equilibrated with nitrogen gas to cells prior to incubating them in a Plexiglas chamber purged with water-saturated nitrogen gas to a pO₂=20 mmHg by an oxygen controller (PROOX model 110, Biospherix, Ltd., Redfield, NY) as previously described [14].

Western blot analysis. Western blot was performed as previously described [13]. Goat monoclonal anti-DDR2 antibody (Santa Cruz Biotechnology) was used.

Real-time RT-PCR. Total RNA was isolated from VSMCs using the single-step acid guanidinium thiocyanate/phenol/chloroform extraction method. Real-time RT-PCR was performed as described [13]. The DDR2 primers used were as follows: sense, 5'-GGCGGAACGAAAGTGCT-3'; antisense, 5'-ACCGTGACAAA CCGGG-3'.

Electrophoretic mobility shift assay (EMSA). Nuclear proteins from VSMCs were collected, and the EMSA was performed as described [13]. Consensus and control oligonucleotides (Santa Cruz Biotechnology) were labeled by polynucleotide kinase incorporation of [³²P]-dATP. Consensus oligonucleotide sequences for Myc–Max, the responsive element in the promoter region of DDR2, were 5'-GGAAGCAGACCACGTGGTCTGCTCC-3'. The Myc–Max mutant oligonucleotide sequences were 5'-GGAAGCAGACCACGGAGTCTGCTCC-3'. In parallel experiments, controls were performed in each case with either mutant oligonucleotides or unlabeled oligonucleotides to compete with the labeled sequences.

siRNA transfection. VSMCs were transfected with DDR2- or p38-specific siRNA (800 ng each) (Dharmacon) for 48 h before the hypoxia experiment. DDR2-specific siRNA is a target-specific 21 nt siRNA as designed by a computer program provided by Dharmacon. The sequences of sense and antisense DDR2-specific siRNA were 5'-GAUGAUAGCAACACUCGGAUU-3' and 5'-PUCCGAGUGUUGCUAUCUUCU-3', respectively. The p38-specific and control siRNA sequences were used as previously described [13].

Promoter activity assay. A –490 to +66 bp rat DDR2 promoter construct was generated. In brief, rat genomic DNA was amplified with sense (5'-GACAGAAGGGAAGTGCATCTTTAAG-3') and antisense (5'-GATTCAAAGTCTCCGCCGCTT-3') primers. The amplified product was digested with M1uI and BglII restriction enzymes and ligated into a pGL3-basic luciferase plasmid vector (Promega, Madison, WI) that was digested with the same enzymes. The DDR2 promoter contains Myc–Max conserved sites (ACGTG) at –258 to –254 bp. To construct a DDR2 mutant,

the Myc–Max binding sites were mutated using the mutagenesis kit (Stratagene, La Jolla, CA). Plasmids were transfected into VSMCs using a low pressure-accelerated gene gun (Bioware Technologies, Taipei, Taiwan). Two micrograms of plasmid DNA was suspended in 5 µl of PBS and delivered to the VSMCs. The transfection efficiency using this method is 25%. Cell extracts were prepared using the Dual-Luciferase Reporter Assay System (Promega) and measured by luminometer (Turner Designs, Sunnyvale, CA).

Zymography. ECM-degrading activity was detected by zymography. Proteins were extracted from cultured VSMCs, and equal amounts of sample protein were subjected to SDS–PAGE on gelatin-containing acrylamide gels (7.5% polyacrylamide and 2 mg/mL gelatin) under nonreducing conditions. Zymogram was performed as described [15].

Migration assay. The migration activity of VSMCs was determined using the growth factor-reduced Matrigel invasion system (Becton Dickinson) following the manufacturer's protocol. The migration assay was performed as previously described [13].

Statistical analysis. Results were expressed as mean ± SEM. Statistical significance was evaluated using analysis of variance (GraphPad Software Inc., San Diego, CA, USA). The Dunnett's test was used to compare multiple groups to a single control group. Turkey–Kramer comparison was used for pairwise comparisons between multiple groups after the ANOVA. A value of *P* < 0.05 was considered significant.

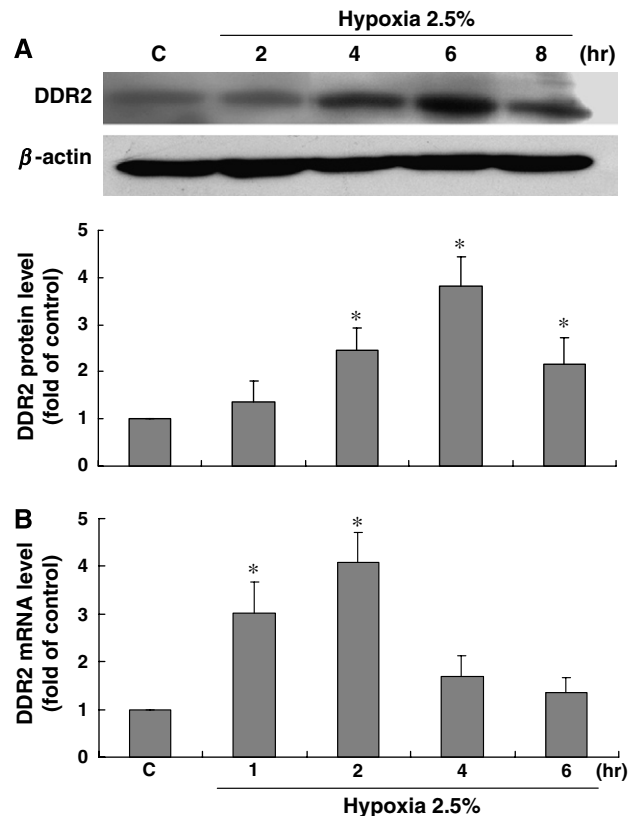


Fig. 1. Hypoxia induces DDR2 mRNA and protein expressions in VSMCs. VSMCs were kept as controls (C) or subjected to hypoxia (2.5% O₂) for the indicated times, and their protein (A) and mRNA (B) expressions were determined by western blot and quantitative RT-PCR analyses, respectively, as described in Materials and methods. Data are shown as mean ± SEM from 3 independent experiments. **P* < 0.05 vs. controls.

Results

Hypoxia induces DDR2 expression in VSMCs

VSMCs were incubated in the hypoxic chamber (2.5% O₂) for different periods of time, and DDR2 protein expression was examined by Western blot analysis. DDR2 protein expression in VSMCs was induced by hypoxia within 4 h, reached a maximal level at 6 h, and then declined but remained elevated after exposure to hypoxia for 8 h (Fig. 1A). RT-PCR analysis showed that hypoxia-induced mRNA expression of DDR2 in VSMCs as early as 1 h after exposure (Fig. 1B). This increase in DDR2 mRNA expression reached a maximal level after exposure to hypoxia for 2 h and then decreased to the basal level within 6 h. These results suggest that hypoxia induces transient increases in DDR2 expression in VSMCs.

Hypoxia-induced DDR2 expression in VSMCs is predominantly mediated by the p38 mitogen-activated protein kinase (MAPK) pathway

MAPK signaling pathways regulate gene expression and cellular function in response to hypoxia. To determine whether MAPK signaling pathways are involved in the hypoxia-induced DDR2 expression in VSMCs, VSMCs were pre-treated with specific inhibitors of ERK (PD98059), p38 MAPK (SB203580), and JNK (SP600125) and then subjected to hypoxia at 2.5% O₂ for 6 h. Treatment with PD98059 and SP600125 resulted in partial inhibition of hypoxia-induced DDR2 expression in VSMCs (Fig. 2). In contrast, treatment with SB203580, a specific inhibitor of p38 MAPK, abolished the hypoxia-induced DDR2 expression in VSMCs. Involvement of the p38 MAPK signaling pathway in hypoxia-induced DDR2 expression was substantiated by treating VSMCs with p38-specific siRNA, which also abolished the hypoxia-induced DDR2 expression (compared to control siRNA). These results suggest that the p38 MAPK signaling path-

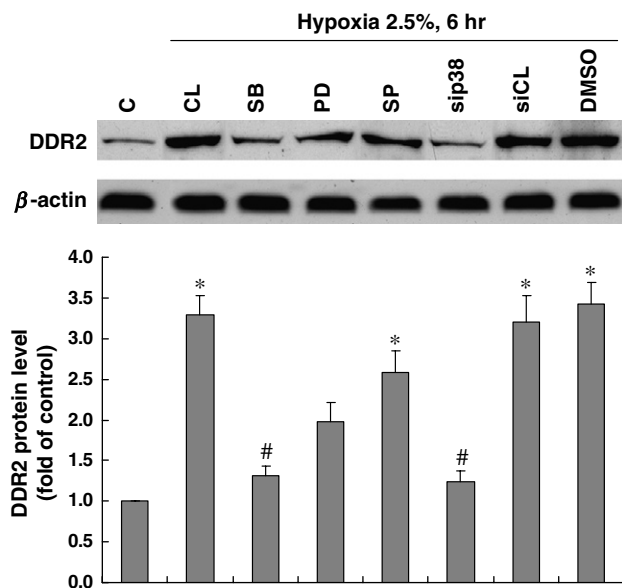


Fig. 2. Hypoxia-induced DDR2 expression is mediated by the p38 MAPK pathway. VSMCs were kept as controls (C) or subjected to hypoxia for 6 h (CL). In parallel experiments, the cells were either pre-treated with SB203580 (SB; 3 μ M), PD98058 (PD; 50 μ M), or SP600125 (SP; 20 μ M) for 30 min or transfected with control (siCL) or p38-specific siRNA (sip38; 40 nM) for 24 h. Data are shown as mean \pm SEM from 3 independent experiments. * P < 0.05 vs. controls. # P < 0.05 vs. hypoxic cells without pre-treatment.

way plays a predominant role in modulating DDR2 expression in VSMCs in response to hypoxic conditions.

Hypoxia induces increases in Myc–Max–DNA binding activity in the nucleus of VSMCs

Because the promoter regions of the DDR2 gene contain the Myc–Max binding domain that is responsible for expression in response to various stimuli, we investigated whether Myc–Max–DNA binding activity in the VSMC nuclei was influenced by hypoxia. Nuclear protein extracts from VSMCs subjected to hypoxia for 0.5–4 h were prepared for EMSA. The EMSA results obtained from incubating VSMC nuclear protein extracts with oligonucleotides corresponding to the Myc–Max binding sequences showed that treatment with hypoxia for 0.5 and 1 h caused an increase in binding activity (Fig. 3A). Pre-treatment of VSMCs with p38-specific siRNA (compared to control siRNA) or SB203580 significantly inhibited this hypoxia-induced promoter activity. The formation of the Myc–Max–DNA complex required the presence of a wild-type Myc–Max binding site, as demonstrated by a lack of competition by providing 10-fold excess of mutant oligonucleotide, whereas a

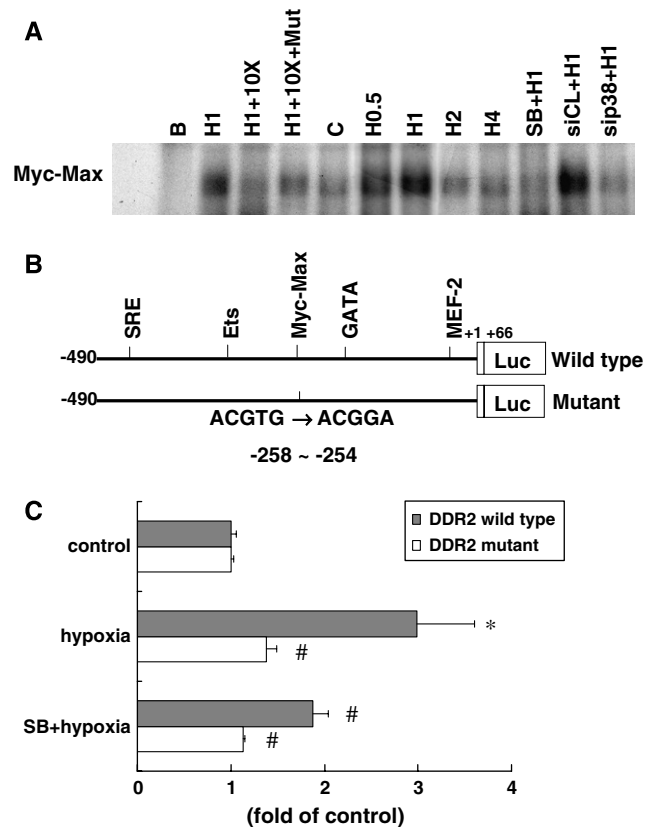


Fig. 3. Hypoxia-induced DDR2 expression in VSMCs is a transcriptional event. (A) VSMCs were kept as controls (C) or exposed to hypoxia for 0.5 h (H0.5), 1 h (H1), 2 h (H2), or 4 h (H4). EMSA was performed using total nuclear extracts and ³²P-labeled oligonucleotides containing wild-type or mutant (Mut) DDR2 Myc–Max binding sites. The specificity of the retarded complexes (Myc–Max) was assessed by pre-incubating the nuclear extracts with 10-fold excess unlabeled oligonucleotides (wild-type or mutant) as a competitor. In parallel experiments, the cells were either pre-treated with SB203580 (SB; 3 μ M) for 0.5 h or transfected with control (siCL) or p38-specific siRNA (sip38; 40 nM) for 24 h. (B) Blank (B and C) VSMCs were transfected with plasmids containing wild-type or mutant (Mut) DDR2 Myc–Max binding sites. The specificity of the retarded complexes (Myc–Max) was assessed by pre-incubating the nuclear extracts with 10-fold excess unlabeled oligonucleotides (wild-type or mutant) as a competitor. In parallel experiments, the cells were either pre-treated with SB203580 (SB; 3 μ M) for 30 min or transfected with control (siCL) or p38-specific siRNA (sip38; 40 nM) for 24 h. Their promoter activities were determined using the luciferase assay (C). In some experiments, the cells were pre-treated with SB203580 (SB; 3 μ M) for 30 min. Data are shown as mean \pm SEM from 3 independent experiments. * P < 0.05 vs. controls. # P < 0.05 vs. hypoxic cells transfected with wild-type constructs without pre-treatment.

10-fold concentration of unlabeled wild-type oligonucleotide effectively competed with ^{32}P -labeled oligonucleotide for Myc–Max binding. These results suggest that hypoxia plays a role in modulating DDR2 expression via the modulation of Myc–Max binding activity at the transcriptional level.

Hypoxia induces DDR2 promoter activity in VSMCs

To further determine whether the hypoxic modulation of DDR2 expression is a transcriptional event, VSMCs were transfected with promoter constructs containing the promoter regions of DDR2 (–490 bp) and the reporter gene luciferase (Fig. 3B) and then exposed to hypoxic condition for 1 h. VSMCs subjected to hypoxia at 2.5% O_2 for 1 h significantly increased DDR2 promoter activities by approximately 3-fold compared with control cells in normoxia (Fig. 3C). In contrast, hypoxic exposure of VSMCs transfected with promoter constructs containing DDR2 promoter regions in which the Myc–Max binding sites (between –258 and –254 bp) were mutated did not induce promoter activity.

These results suggest that the Myc–Max binding elements are responsible for the hypoxic induction of DDR2 promoter activity. The addition of SB203580 inhibited hypoxia-induced DDR2 promoter activity, suggesting that the p38 MAPK pathway is involved in hypoxia-induced DDR2 promoter activity in VSMCs.

DDR2 is involved in hypoxia-induced migration of VSMCs

To investigate whether DDR2 modulates VSMC migration in response to hypoxia, we further investigated the effect of hypoxia on MMP-2 activity in VSMCs and the involvement of DDR2 in VSMC migration. Zymographic assays demonstrated that MMP-2 activity was induced in VSMCs subjected to hypoxia at 2.5% O_2 for 12 h (Fig. 4A). Pre-treatment of VSMCs with DDR2- and p38-specific siRNAs (compared to control siRNA) and SB203580 abolished hypoxia-induced MMP-2 activity. These results suggest that DDR2 and p38 MAPK are involved in MMP-2 activation in VSMCs in response to hypoxia. We further explored the role of DDR2 in VSMC migration in response to hypoxia. Matrigel

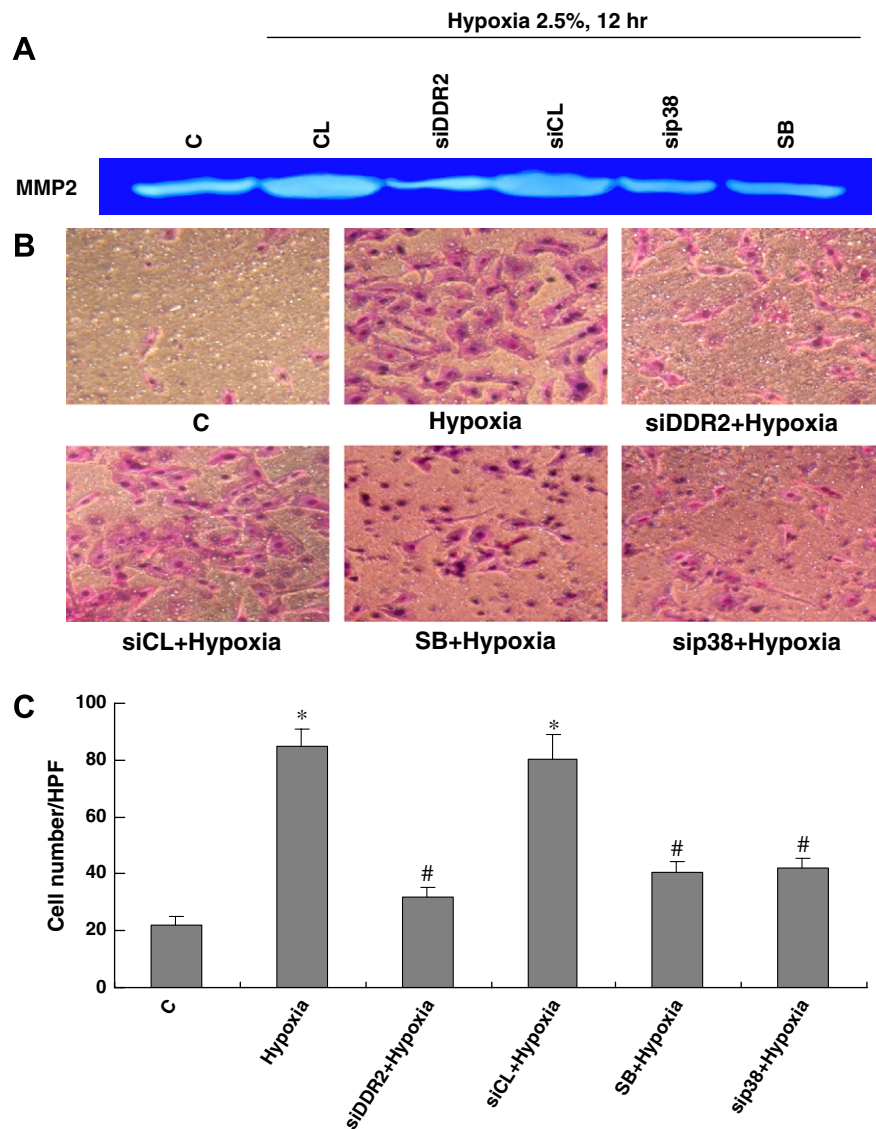


Fig. 4. Hypoxia induces MMP-2 activity in VSMCs and increases their migration through the p38/DDR2 signaling pathway. VSMCs were kept as controls (C) and exposed to hypoxia (CL) for 12 h, and their MMP-2 activity and migratory ability were determined by zymography (A) and Matrigel migration assays (B), respectively, as described in Materials and methods. In parallel experiments, the cells were either pre-treated with SB203580 (SB; 3 μM) for 30 min or transfected with control (siCL), p38- (sip38) or DDR2-specific siRNA (siDDR2; 40 nM) for 48 h. Data in (B) are shown as mean \pm SEM from 3 independent experiments. The stained migrated VSMCs were counted in 4 fields under a 400 \times high-power field (HPF). * P <0.05 vs. control. # P <0.05 vs. hypoxic cells without pre-treatment.

assays showed that VSMCs migrated significantly through the filter membrane under hypoxic conditions for 12 h (Fig. 4B). This hypoxia-induced increase in SMC migration was inhibited by transfecting the VSMCs with DDR2- and p38-specific siRNAs (compared to control siRNA), as well as pre-treating with SB203580. These results suggest that hypoxia increases VSMC migration, and this migration is mediated by the DDR2 and p38 MAPK signaling pathways.

Discussion

The main findings of our present study are summarized as follows. First, hypoxia induces DDR2 mRNA and protein expression in VSMCs. Second, the hypoxia-induced DDR2 expression in VSMCs is predominantly mediated by the p38 MAPK pathway. Third, hypoxia induces increased binding activity of Myc–Max–DNA, an important responsive element in the promoter region of DDR2, in the VSMC nuclei. In addition, mutation of the Myc–Max binding sequences in the promoter regions of the DDR2 gene significantly attenuated hypoxia-induced DDR2 promoter activity. These results suggest that Myc–Max transcription activity is responsible for the expression of DDR2 in response to hypoxia. Fourth, hypoxia induces MMP-2 activity in VSMCs. This hypoxia-induced MMP-2 activity is mediated by the DDR2 signaling pathway. Finally, VSMCs subjected to hypoxic conditions exhibit increased migratory ability that is mediated by the DDR2 and p38 MAPK signaling pathways. Because ECM is abundant in the atherosclerotic plaque, our present results suggest that acute hypoxia plays a pivotal role in regulating MMP-2 activity via DDR2 in VSMCs and, hence, modulates their migration, which may contribute to atherosclerosis.

DDR2 is associated with increased MMP-2 activity in hepatic stellate cells [8] and skin fibroblasts [9]. Overexpression of DDR2 in SMCs has been shown to lead to a down-regulation of collagen production and an up-regulation of MMP activity [10]. Recent studies have also demonstrated that hypoxia can up-regulate MMP-2 activity [16,17]. However, it is not clear whether hypoxia can regulate MMP-2 activity in VSMCs via a DDR2-dependent pathway. In the present study, we explored the role of DDR2 in regulating MMP-2 activity in hypoxic VSMCs. Our results showed for the first time that hypoxia increases DDR2 expression in VSMCs, with concurrent up-regulation of MMP-2 activity. Pre-treatment of VSMCs with DDR2-specific siRNA significantly inhibited the hypoxia-induced MMP-2 activity. Our results suggest that MMP-2 is a downstream target of the DDR2 signaling pathway in hypoxic VSMCs.

MAPKs comprise a family of serine/threonine kinases that function as pivotal mediators of signal transduction pathways. Three isoforms, p38, ERK, and JNK, play major roles in the regulation of cellular responses to hypoxia [14,18,19]. In the present study, pre-treatment of VSMCs with either a specific inhibitor of p38 MAPK (SB203580) or p38-specific siRNA abolished the hypoxia-induced DDR2 expression in VSMCs. In contrast, a specific inhibitor of ERK (PD98059) and JNK (SP600125) had only partially inhibitory effects on hypoxia-induced DDR2 expression. Our findings suggest that p38 MAPK plays a predominant role in the hypoxia-induced DDR2 expression in VSMCs.

The c-Myc transcription factor is a member of the “max network,” which consists of a family of basic helix–loop–helix leucine zipper (B-HLH-LZ) proteins that heterodimerize with Max [20]. As a regulator of gene transcription, Myc has multiple mechanisms through which it activates and represses target genes [21]. The promoter region of the DDR2 gene contains the Myc–Max binding elements that are responsible for DDR2 expression in cells in response to various stimuli. We found that hypoxia can increase Myc–Max–DNA binding. This hypoxia-induced Myc–Max binding activity is mediated by the p38 MAPK pathway, inasmuch as treatment of VSMCs with p38-specific siRNA and SB203580 significantly inhibited hypoxia-induced Myc–Max binding activity.

When VSMCs were transfected with the constructs that contain the DDR2 promoter region with mutated Myc–Max binding elements, hypoxia-induced DDR2 promoter activity was inhibited. These findings suggest that the Myc–Max binding elements in the DDR2 promoter regions are responsible for its expression in VSMCs in response to hypoxia.

Our present study has elucidated the role of DDR2 in VSMC migration under hypoxic conditions. Pre-treating VSMCs with DDR2-specific siRNA inhibited hypoxia-induced VSMC migration. In addition, the p38 MAPK specific inhibitor SB203580 and p38-specific siRNA also had inhibitory effects on hypoxia-induced VSMC migration. DDR2-specific siRNA attenuates neointimal formation after carotid injury [22]. DDR2 also plays pivotal roles in regulating VSMC-mediated collagen turnover in atherosclerosis. Our results confirm the role of DDR2 in hypoxia-induced VSMC migration.

In summary, our data have elucidated both the role of hypoxia in DDR2 expression and VSMCs and the contributions of DDR2 to VSMC migration in response to hypoxic conditions. Hypoxia-induced VSMC migration may contribute to the pathophysiological effects of hypoxia on the vasculature and, thus, may play a role in the development of atherosclerosis. Our findings suggest that DDR2 may be an important therapeutic target in the treatment of atherosclerosis.

Acknowledgment

This study was supported in part by a grant from Taipei Medical University-Wan Fang Hospital (97-WF-PHD-04), Taiwan.

References

- [1] J. Schlessinger, Cell signaling by receptor tyrosine kinases, *Cell* 103 (2000) 211–225.
- [2] W. Vogel, G.D. Gish, F. Alves, T. Pawson, The discoidin domain receptor tyrosine kinases are activated by collagen, *Mol. Cell* 1 (1997) 13–23.
- [3] A. Shrivastava, C. Radziejewski, E. Campbell, L. Kovac, M. McGlynn, T.E. Ryan, S. Davis, M.P. Goldfarb, D.J. Glass, G. Lemke, G.D. Yancopoulos, An orphan receptor tyrosine kinase family whose members serve as nonintegrin collagen receptors, *Mol. Cell* 1 (1997) 25–34.
- [4] G. Hou, W. Vogel, M.P. Bendeck, The discoidin domain receptor tyrosine kinase DDR1 in arterial wound repair, *J. Clin. Invest.* 107 (2001) 727–735.
- [5] F. Alves, W. Vogel, K. Mossie, B. Millauer, H. Hoffer, A. Ullrich, Distinct structural characteristics of discoidin I subfamily receptor tyrosine kinases and complementary expression in human cancer, *Oncogene* 10 (1995) 609–618.
- [6] K. Ikeda, L.H. Wang, R. Torres, H. Zhao, E. Olaso, F.J. Eng, P. Labrador, R. Klein, D. Lovett, G.D. Yancopoulos, S.L. Friedman, H.C. Lin, Discoidin domain receptor 2 interacts with Src and Shc following its activation by type I collagen, *J. Biol. Chem.* 277 (2002) 19206–19212.
- [7] G. Hou, W.F. Vogel, M.P. Bendeck, Tyrosine kinase activity of discoidin domain receptor 1 is necessary for smooth muscle cell migration and matrix metalloproteinase expression, *Circ. Res.* 90 (2002) 1147–1149.
- [8] E. Olaso, K. Ikeda, F.J. Eng, L. Xu, L.H. Wang, H.C. Lin, S.L. Friedman, DDR2 receptor promotes MMP-2-mediated proliferation and invasion by hepatic stellate cells, *J. Clin. Invest.* 108 (2001) 1369–1378.
- [9] E. Olaso, J.P. Labrador, L. Wang, K. Ikeda, F.J. Eng, R. Klein, D.H. Lovett, H.C. Lin, S.L. Friedman, Discoidin domain receptor 2 regulates fibroblast proliferation and migration through the extracellular matrix in association with transcriptional activation of matrix metalloproteinase-2, *J. Biol. Chem.* 277 (2002) 3606–3613.
- [10] N. Ferri, N.O. Carragher, E.W. Raines, Role of discoidin domain receptors 1 and 2 in human smooth muscle cell-mediated collagen remodeling: potential implications in atherosclerosis and lymphangiogenesis, *Am. J. Pathol.* 164 (2004) 1575–1585.
- [11] Y. Hou, C. Okamoto, K. Okada, N. Kawao, S. Kawata, S. Ueshima, O. Matsuo, c-Myc is essential for urokinase plasminogen activator expression on hypoxia-induced vascular smooth muscle cells, *Cardiovasc. Res.* 75 (2007) 186–194.
- [12] Y. Ben-Yosef, A. Miller, S. Shapiro, N. Lahat, Hypoxia of endothelial cells leads to MMP-2-dependent survival and death, *Am. J. Physiol. Cell Physiol.* 289 (2005) C1321–C1331.
- [13] K.G. Shyu, Y.M. Chao, B.W. Wang, P. Kuan, Regulation of discoidin domain receptor 2 by cyclic mechanical stretch in cultured rat vascular smooth muscle cells, *Hypertension* 46 (2005) 614–621.
- [14] S.C. Chen, Y.C. Liu, K.G. Shyu, D.L. Wang, Acute hypoxia to endothelial cells induces activating transcription factor 3 (ATF3) expression that is mediated via nitric oxide, *Atherosclerosis* [10 March 2008, Epub ahead of print].
- [15] B.W. Wang, H. Chang, S. Lin, P. Kuan, K.G. Shyu, Induction of matrix metalloproteinases-14 and -2 by cyclical mechanical stretch is mediated by tumor

- necrosis factor- α in cultured human umbilical vein endothelial cells, *Cardiovasc. Res.* 59 (2003) 460–469.
- [16] A. Mobasher, N. Platt, C. Thorpe, M. Shakibaei, Regulation of 2-deoxy-D-glucose transport, lactate metabolism, and MMP-2 secretion by the hypoxia mimetic cobalt chloride in articular chondrocytes, *Ann. NY Acad. Sci.* 1091 (2006) 83–93.
- [17] U.M. Munoz-Najar, K.M. Neurath, F. Vumbaca, K.P. Claffey, Hypoxia stimulates breast carcinoma cell invasion through MT1-MMP and MMP-2 activation, *Oncogene* 25 (2006) 2379–2392.
- [18] A.R. Nebreda, A. Porras, p38 MAP kinases: beyond the stress response, *Trends Biochem. Sci.* 25 (2000) 257–260.
- [19] L.W. Lo, J.J. Cheng, J.J. Chiu, B.S. Wung, Y.C. Liu, D.L. Wang, Endothelial exposure to hypoxia induces Egr-1 expression involving PKC α -mediated Ras/Raf-1/ERK1/2 pathway, *J. Cell. Physiol.* 188 (2001) 304–312.
- [20] S. Adhikary, M. Eilers, Transcriptional regulation and transformation by Myc proteins, *Nat. Rev. Mol. Cell. Biol.* 6 (2005) 635–645.
- [21] M. Wanzel, S. Herold, M. Eilers, Transcriptional repression by Myc, *Trends Cell Biol.* 13 (2003) 146–150.
- [22] K.G. Shyu, B.W. Wang, P. Kuan, H. Chang, RNA interference for discoidin domain receptor 2 attenuates neointimal formation in balloon injured rat carotid artery, *Arterioscler. Thromb. Vasc. Biol.* 28 (2008) 1447–1453.

IL-6-Encoding Tumor Antigen Generates Potent Cancer Immunotherapy Through Antigen Processing and Anti-apoptotic Pathways

Chang-Yao Hsieh¹, Chi-An Chen¹, Chia-Yen Huang¹, Ming-Cheng Chang¹, Chien-Nan Lee¹, Yi-Ning Su² and Wen-Fang Cheng^{1,2}

¹Department of Obstetrics and Gynecology, College of Medicine, National Taiwan University, Taipei, Taiwan; ²Graduate Institute of Clinical Medicine, College of Medicine, National Taiwan University, Taipei, Taiwan

A naked DNA vaccine delivered by gene gun into antigen-presenting cells (APCs) has emerged as an attractive strategy for antigen-specific cancer immunotherapy. However, APCs have a limited lifespan, hindering their long-term ability to prime antigen-specific T cells. Furthermore, the potency of DNA vaccines is limited by their inability to process and present antigens. Interleukin-6 (IL-6) could play a role in immunity and cell apoptosis. We explored how the DNA vaccine encodes IL-6 to a model tumor antigen, human papilloma virus type-16 (HPV-16) E7. Mice vaccinated with IL-6/E7 DNA exhibited dramatic increases in E7-specific T-cell immunities, anti-E7 antibody responses, and impressive anti-tumor effects against E7-expressing tumors. The *in vitro* results revealed that IL-6 enhances DNA vaccine potency through the major histocompatibility complex class I pathway via direct and cross-priming effects. In addition, the delivery of IL-6/E7 DNA prolonged the survival of transduced dendritic cells (DCs) *in vivo*. Our results indicated that the IL-6/E7 DNA vaccine combined the mechanisms of enhancing antigen processing and presentation with prolonging the survival of DCs. Using IL-6 represents an innovative approach to enhancing DNA vaccine potency and holds promise for cancer prevention and immunotherapy.

Received 9 October 2006; accepted 29 May 2007; advance online publication 3 July 2007. doi:10.1038/sj.mt.6300243

INTRODUCTION

The ideal cancer treatment should be able to eradicate systemic tumors at multiple sites in the body and have the specificity to discriminate between neoplastic and non-neoplastic cells. In this regard, antigen-specific cancer immunotherapy represents an attractive approach for treatment. Activating antigen-specific T-cell-mediated immune responses allows the killing of tumors associated with a specific antigen.¹ Intradermal administration of DNA vaccines using a gene gun can efficiently deliver specific genes into professional antigen-presenting cells (APCs) *in vivo*.²

Among the concerns about DNA vaccines is their limited potency. Several strategies have been applied to increase the potency of DNA vaccines, such as targeting an antigen by fusing molecules to enhance antigen processing,^{3,4} targeting antigens for rapid intracellular degradation,⁵ directing antigens to APCs by fusion to ligands for APC receptors⁶ or to a pathogen sequence such as fragment C of tetanus toxin,⁷ co-injecting cytokines,⁸ and administration with CpG oligonucleotides.⁹ In our previous studies, we used the gene gun approach to test several strategies that are able to route human papilloma virus type-16 (HPV-16) E7 model antigen and result in enhanced E7-specific CD8⁺ T-cell-mediated immune responses and anti-tumor effects.^{3,10,11} Another potential strategy to enhance DNA vaccine potency is to prolong dendritic cell (DC) survival by administering the DNA encoding the antigen with DNA encoding inhibitors of apoptosis to DCs.¹² Recently, combined strategies for enhancing the effects of DNA vaccine have been introduced in the development of cancer vaccines and immunotherapy.

Interleukin-6 (IL-6), a secreting cytokine, plays an important role in the expansion and activation of T cells and differentiation of B cells.^{13,14} IL-6 can inhibit T-cell apoptosis via the IL-6/soluble IL-6 receptor.¹⁵ IL-6 has also been shown to protect cells from apoptosis via the myeloid cell leukemia-1 (Mcl-1) pathway.¹⁶ It seems that IL-6 might be able to enhance anti-tumor immunity through its various functions in a variety of cells.

In this study, we tested IL-6 for its ability to enhance antigen processing and presentation and to prolong DC survival for E7-specific T-cell immune responses when it was linked with E7 in the DNA vaccine strategy. We chose HPV-16 E7 as a model antigen because HPVs, particularly HPV-16, are associated with a majority of cervical cancers, and E7 is essential for the induction and maintenance of cellular transformation. Effective vaccines against E7 can potentially control HPV infections and HPV-associated lesions.

RESULTS

DNA encoding IL-6 linked to E7 significantly enhances the E7-specific T-cell responses

Representative figures from flow cytometry analysis for E7-specific interferon- γ (IFN- γ)-secreting CD4⁺ T-cell precursors

The first two authors contributed equally to this work.

Correspondence: Wen-Fang Cheng, Graduate Institute of Clinical Medicine, College of Medicine, National Taiwan University, Taipei, Taiwan 100. E-mail: wenfangcheng@yahoo.com

are shown in **Figure 1a**. As shown in **Figure 1b**, mice vaccinated with IL-6/E7 DNA generated higher numbers of E7-specific IFN- γ -secreting CD4⁺ T-cell precursors than mice in the other DNA-vaccinated groups [8.0 ± 2.1 for naïve group, 12.5 ± 2.1 for no insert group, 11.0 ± 2.1 for E7 group, 5.5 ± 1.4 for IL-6 group, 6.5 ± 1.4 for E7 mixed with IL-6 group, 8.5 ± 1.4 for Mcl-1/E7 group, 77.0 ± 12.0 for IL-6/E7 group, $P < 0.05$ one-way analysis of variance (ANOVA)]. Mice immunized with IL-6/E7 DNA also generated higher numbers of E7-specific IL-4-secreting CD4⁺ T-cell precursors than the other groups (16.0 ± 2.8 for naïve group, 22.5 ± 2.1 for no insert group, 22.0 ± 3.5 for E7 group, 21.5 ± 2.1 for IL-6 group, 26.5 ± 2.8 for E7 mixed with IL-6 group, 18.5 ± 2.8 for Mcl-1/E7 group, 292.0 ± 16.5 for IL-6/E7 group, $P < 0.01$ one-way ANOVA) (**Figure 1c**).

Representative figures from flow cytometry analysis for E7-specific IFN- γ -secreting CD8⁺ T-cell precursors are shown in **Figure 1d**. Mice vaccinated with IL-6/E7 DNA generated higher numbers of E7-specific IFN- γ -secreting CD8⁺ T-cell precursors than mice vaccinated with the other DNA vaccines (4.0 ± 2.1 for naïve group, 6.0 ± 2.1 for no insert group, 6.5 ± 1.4 for E7 group,

4.0 ± 1.4 for IL-6 group, 9.0 ± 2.8 for E7 mixed with IL-6 group, 124.0 ± 6.3 for Mcl-1/E7 group, 432.5 ± 15.4 for IL-6/E7 group, $P < 0.01$ one-way ANOVA) (**Figure 1e**).

IL-6/E7 DNA enhances the E7-specific antibody responses

As shown in **Figure 1f**, the titers of anti-E7 antibody generated by the IL-6/E7 DNA vaccine were significantly higher than those generated by other DNA vaccines (for 1:100 dilution, naïve 0.434 ± 0.027 , no insert 0.418 ± 0.021 , E7 0.454 ± 0.037 , IL-6 0.403 ± 0.025 , E7 mixed with IL-6 0.415 ± 0.016 , Mcl-1/E7 0.425 ± 0.028 , IL-6/E7 1.063 ± 0.050 , $P < 0.01$ one-way ANOVA).

Enhanced E7 antigen through the MHC I pathway in cells transfected with IL-6/E7 DNA or in dendritic cells pulsed with IL-6/E7 protein

At an effector-to-target ratio of 45:1, 293 D^bK^b cells transfected with IL-6/E7 DNA generated significantly higher percentages of specific lyses ($57.2 \pm 6.5\%$ versus $9.4 \pm 1.3\%$, $P < 0.01$ one-way ANOVA) than cells transfected with wild-type E7 DNA

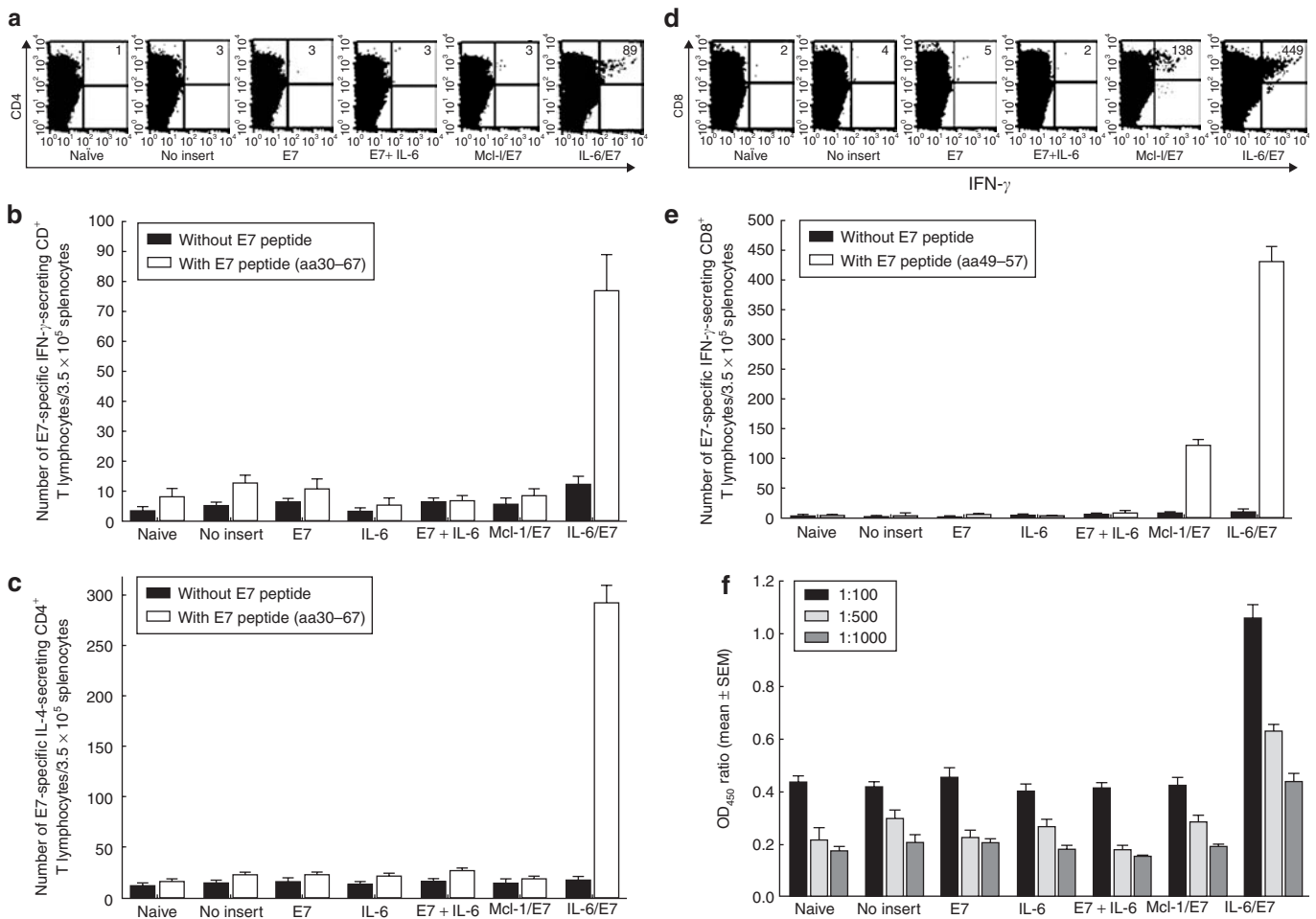


Figure 1 E7-specific immunological profiles of vaccinated mice. **(a)** Representative figures from flow cytometry analysis of E7-specific interferon- γ (IFN- γ)-secreting CD4⁺ T-cell precursors in each group. **(b)** Bar graph depicting the number of E7-specific IFN- γ -secreting CD4⁺ T-cell precursors per 3.5×10^5 splenocytes (mean \pm SEM). **(c)** Bar graph depicting the number of E7-specific interleukin-4 (IL-4)-secreting CD4⁺ T-cell precursors per 3.5×10^5 splenocytes (mean \pm SEM). **(d)** Representative figures from flow cytometry analysis of E7-specific IFN- γ -secreting CD8⁺ T-cell precursors in each group. **(e)** Bar graph depicting the number of antigen-specific IFN- γ -secreting CD8⁺ T-cell precursors per 3.5×10^5 splenocytes (mean \pm SEM). **(f)** Bar graph showing E7-specific antibodies in mice vaccinated with various DNA vaccines.

(Figure 2a). In addition, DCs pulsed with lysates of 293 D^bK^b cells transfected with IL-6/E7 DNA also generated a significantly higher percentage of specific lyses than DCs pulsed with 50 µg/ml of lysates of 293 D^bK^b cells transfected with wild-type E7 DNA construct (45.5 ± 2.0% versus 8.8 ± 0.3%, $P < 0.01$ one-way ANOVA) (Figure 2b).

IL-6/E7 DNA enhances tumor protection against TC-1 tumor cells

To determine whether the observed enhancement of E7-specific T-cell immunity could translate into a significant E7-specific protective anti-tumor effect, we performed an *in vivo* tumor protection experiment. As shown in Figure 3a, 100% of mice receiving IL-6/E7 DNA vaccination, when challenged with TC-1 tumor cells, remained tumor-free for 60 days afterward. Only 40% of the mice receiving Mcl-1/E7 remained tumor-free 60 days after the TC-1 challenge. All mice in the other groups, including the wild-type E7 group, developed tumors within 14 days of TC-1 tumor challenge.

CD8⁺ T cells, CD4⁺ T cells, and natural killer cells are essential for the anti-tumor effects by IL-6/E7 DNA

To determine the subset of lymphocytes important for the anti-tumor effects, we performed *in vivo* antibody (Ab) depletion

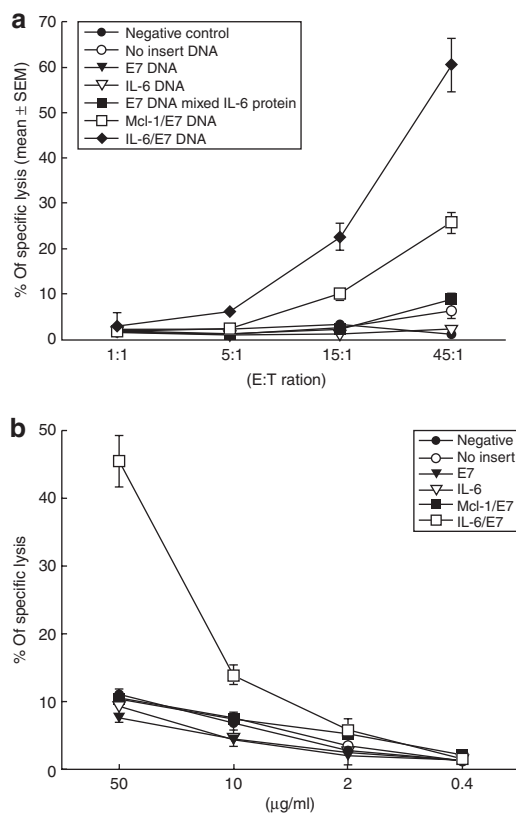


Figure 2 *In vitro* direct and cross-priming effects of various DNA constructs. **(a)** Cytotoxic T-lymphocyte (CTL) assays to demonstrate enhanced presentation of E7 directly by 293 D^bK^b cells transfected with the interleukin-6 (IL-6)/E7 DNA construct. **(b)** Bone marrow–derived dendritic cells pulsed with cell lysates containing IL-6/E7 DNA construct enhance presentation of E7, as demonstrated by CTL assays. E:T ratio, effector-to-target ratio.

experiments.³ As shown in Figure 3b, all naïve mice and all mice depleted of CD8⁺ T cells grew tumors within 14 days after the tumor challenge. In addition, 20% of mice depleted of CD4⁺ T cells and 40% of mice depleted of natural killer 1.1⁺ cells developed tumors within 60 days of tumor challenge.

IL-6/E7 DNA vaccine leads to significant reduction of pulmonary tumor nodules

We further assessed the therapeutic potential of IL-6/E7 DNA vaccine by using a previously described lung hematogenous spread model.¹⁷ The representative pulmonary tumor nodules in each group are shown in Figure 4a. As shown in Figure 4b, mice treated with IL-6/E7 (153.6 ± 18.2 mg) showed significantly lower lung weights than mice treated with the other DNA vaccines (wild-type E7 630.5 ± 19.5 mg, Mcl-1/E7 395.0 ± 20.5 mg, $P < 0.001$, one-way ANOVA). Mice treated with IL-6/E7 (1.5 ± 1.2) also exhibited significantly fewer pulmonary tumor nodules than mice treated with the other DNA vaccines (wild-type E7 87.6 ± 7.4, Mcl-1/E7 54.0 ± 5.0, $P < 0.001$, one-way ANOVA) (Figure 4c). In addition, the mice vaccinated with Mcl-1/E7 revealed lower numbers of pulmonary tumor nodules than the group vaccinated with wild-type E7 ($P < 0.05$, one-way ANOVA).

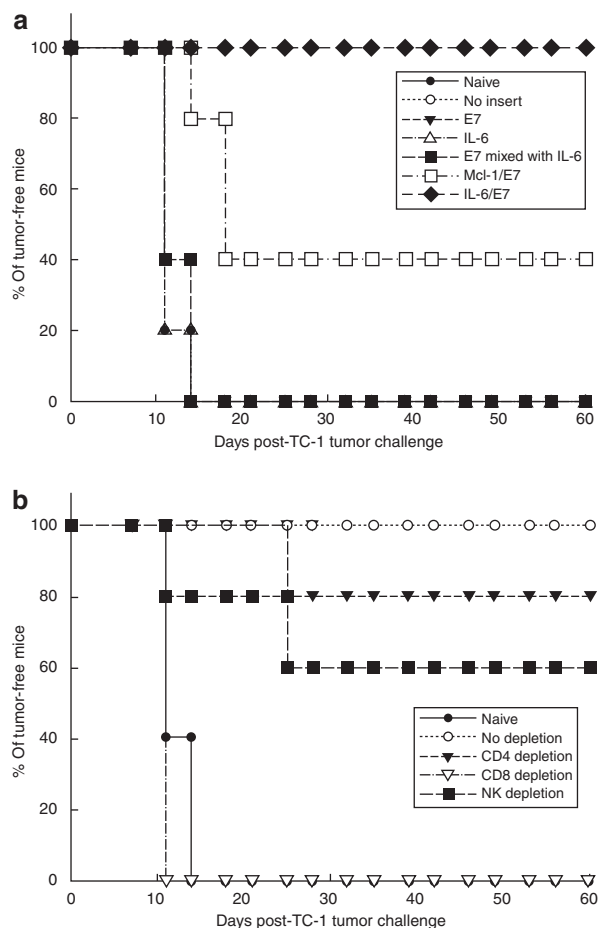


Figure 3 *In vivo* tumor protection experiments and *in vivo* Ab depletion experiments in mice. **(a)** *In vivo* tumor protection experiments on mice vaccinated with various DNA vaccines. **(b)** *In vivo* Ab depletion experiments on mice vaccinated with interleukin-6 (IL-6)/E7 DNA vaccine.

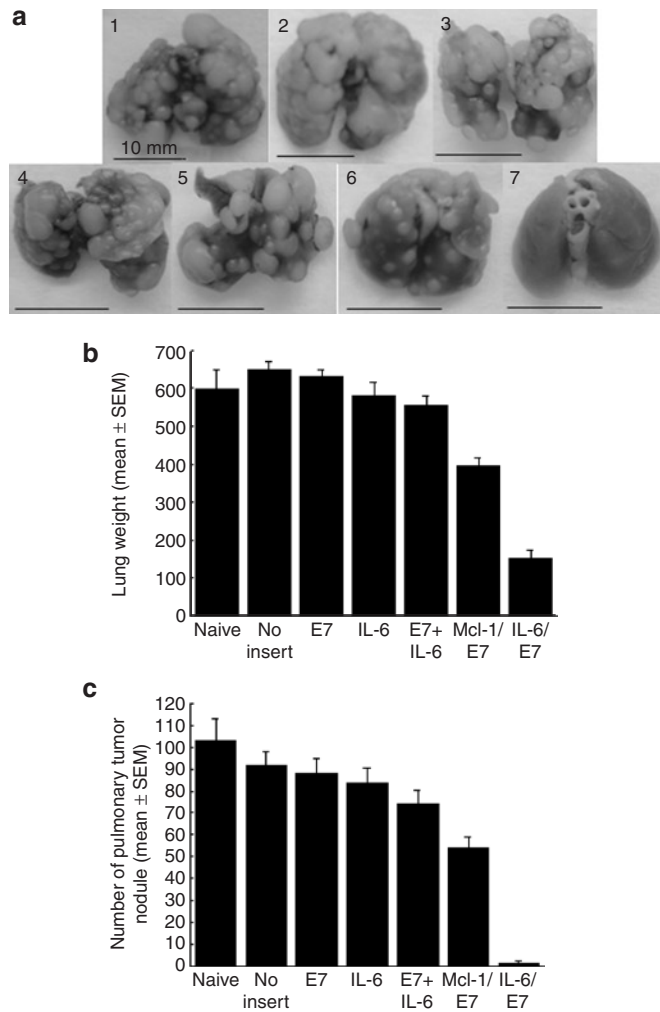


Figure 4 *In vivo* tumor treatment experiments in mice at a high therapeutic dose. (a) Representative figures of pulmonary tumor nodules in each group. 1: naive, 2: no insert, 3: E7, 4: interleukin-6 (IL-6), 5: E7 + IL-6, 6: Mcl-1/E7, 7: IL-6/E7. (b) Mean lung weights in each vaccinated group (\pm SEM). (c) Mean pulmonary tumor nodules in each vaccinated group (\pm SEM).

Improved survival of DNA-transfected DCs in mice vaccinated with IL-6/E7/GFP or Mcl-1/E7/GFP DNA

Representative figures from flow cytometry analysis are shown in **Figure 5a**. As shown in **Figure 5b**, there is no significant difference in the numbers of CD11c and GFP⁺ cells in the inguinal lymph nodes at day 1 after vaccination. However, 5 days after gene gun vaccination, we found greater percentages of GFP⁺CD11c⁺ cells in lymph nodes harvested from mice vaccinated with the Mcl-1/E7/GFP DNA and IL-6/E7/GFP than in lymph nodes harvested from mice vaccinated with E7/GFP and GFP-only DNA ($P < 0.01$, one-way ANOVA).

We further assayed for the apoptotic cells in CD11c⁺GFP⁺ cells derived from the draining lymph nodes of various vaccinated mice. Mice vaccinated with DNA encoding IL-6/E7/GFP or Mcl-1/E7/GFP demonstrated significantly lower percentages of apoptotic cells than mice vaccinated with GFP or E7/GFP DNA ($P < 0.01$, one-way ANOVA) (**Figure 5c**).

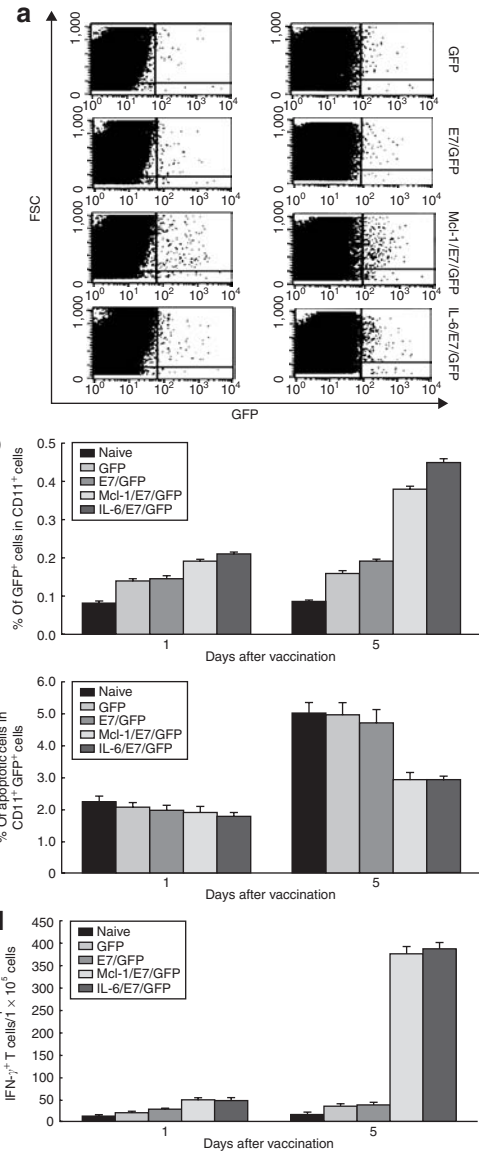


Figure 5 Characterization of DNA-transfected dendritic cells in the inguinal lymph nodes of vaccinated mice and activation of E7-specific CD8⁺ T cells by CD11c-enriched cells isolated from the inguinal lymph nodes of vaccinated mice. (a) Representative flow cytometry data for the percentage of green fluorescent protein (GFP)-transfected CD11c⁺ cells among the gated monocytes. (b) Bar graph depicting the percentage of CD11c⁺GFP⁺ monocytes among the gated monocytes (mean \pm SEM). (c) Bar graph depicting the percentage of apoptotic cells in CD11c⁺GFP⁺ cells (mean \pm SEM). (d) Bar graph depicting the number of E7-specific interferon- γ (IFN- γ)-secreting CD8⁺ T cells per 1×10^5 cells (mean \pm SEM). IL-6, interleukin-6.

CD11c-enriched cells from IL-6/E7/GFP and Mcl-1/E7/GFP DNA-vaccinated mice could activate an E7-specific CD8⁺ T-cell line

Using various DNA-vaccinated mice, we evaluated the ability of CD11c-enriched cells to stimulate INF- γ secretion from an E7-specific CD8⁺ T-cell line. As shown in **Figure 5d**, we compared CD11c-enriched cells 5 days after gun vaccination. Those isolated from mice vaccinated with IL-6/E7/GFP and Mcl-1/E7/GFP DNA were more effective in activating the E7-specific

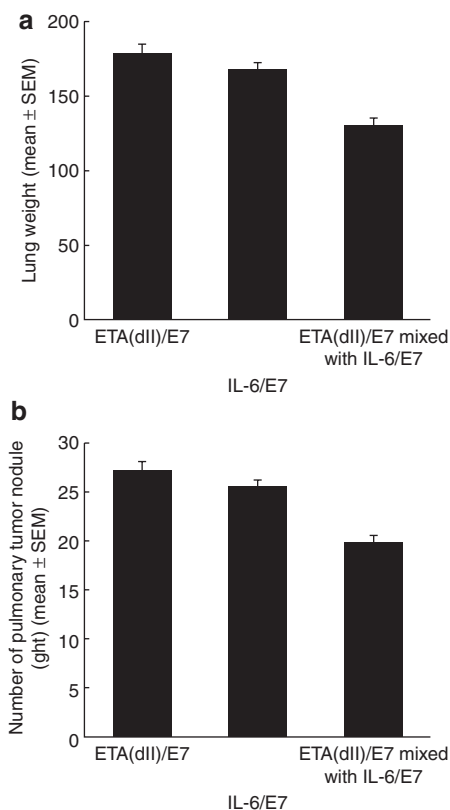


Figure 6 *In vivo* tumor treatment experiment to compare the anti-tumor effect in mice treated with different chimeric DNA vaccines. **(a)** Mean lung weights in each vaccinated group (\pm SEM). **(b)** Mean pulmonary tumor nodules in each vaccinated group (\pm SEM). IL-6, interleukin-6.

CD8⁺ T-cell line to secrete IFN- γ than those isolated from mice vaccinated with GFP and E7/GFP DNA ($P < 0.001$, one-way ANOVA).

IL-6/E7 combined with ETA(dII)/E7 DNA generated better anti-tumor effects than IL-6/E7 DNA only and ETA(dII)/E7 DNA only

We finally compared the chimeric E7 DNA vaccines in tumor treatment experiments. As shown in **Figure 6a**, mice vaccinated with IL-6/E7 mixed with exotoxin A (ETA)(dII)/E7 DNA (129.6 ± 4.9 mg) had the lowest lung weights. Those vaccinated with IL-6/E7 DNA had lung weights of 167.9 ± 4.1 mg, and those vaccinated with ETA(dII)/E7 DNA had lung weights of 177.9 ± 6.4 mg ($P < 0.001$). In addition, mice vaccinated with IL-6/E7 mixed with ETA(dII)/E7 DNA (6.2 ± 0.8) had the fewest pulmonary tumor nodules (**Figure 6b**).

IL-6/E7 generates higher killing effects on cervical cancer cells than E7 in cytotoxic T-lymphocyte assays

We finally performed cytotoxic T-lymphocyte (CTL) assays using various protein-pulsed cytotoxic T cells as effector cells and CaSki cells as target cells. As shown in **Figure 7**, the percentages of specific lyses of IL-6/E7 protein-pulsed cytotoxic cells on CaSki cells were significantly higher than those of E7 protein-pulsed E7-specific cytotoxic cells.

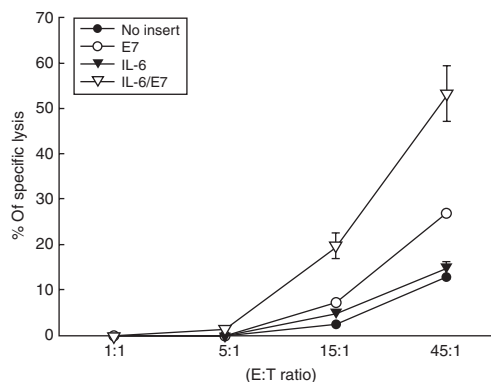


Figure 7 Cytotoxic T-lymphocyte assays of various protein-pulsed E7-specific CD8⁺ T cells used as effector cells and the CaSki tumor cell line used as a source of target cells. E:T ratio, effector-to-target ratio; IL-6, interleukin-6.

DISCUSSION

Our results support our hypothesis that an IL-6/E7 DNA vaccination strategy is an effective means of combating tumors. It combines strategies for enhancing antigen processing and presentation and prolonging DC life. The treatment is capable of enhancing antigen-specific immune responses and anti-tumor effects to a greater degree than a wild-type E7 DNA vaccination only. IL-6 linked with E7 generates strong E7-specific CD4⁺ and CD8⁺ T-cell immunities. Enhanced processing of the E7 antigen may be attributed to IL-6, resulting in increased major histocompatibility complex:peptide presentation to T lymphocytes (**Figure 2**). DC life is also prolonged via inhibition of apoptosis by IL-6, resulting in an increased quantity of longer-lived DCs in the draining lymph nodes (**Figure 5**). Thus, our data indicate that IL-6 linked with E7 works via two different mechanisms to enhance DNA vaccine potency.

IL-6 could enhance E7-specific CD8⁺ T-cell immunity and anti-tumor effects through enhancing antigen processing and presentation. IL-6 is a secreting cytokine that, when linked to E7, could enhance the antigen processing and presentation of E7 in our murine model (**Figure 2**). We also observed that the specific lyses of CTL assays in human peripheral mononuclear cells pulsed with the IL-6/E7 recombinant protein were higher than those after pulsing with wild-type E7 protein on natural human tumor cells (CaSki cells) (**Figure 7**). Other studies have demonstrated the advantages of linking IL-6 to E7 in terms of enhancing antigen processing and presentation. This linking has been done with other molecules, including HSP70, domains of exotoxin in *Pseudomonas aeruginosa*,¹⁸ VP22 of herpes simplex,¹⁹ calreticulin,³ and vasostatin.¹⁷

IL-6 could enhance E7-specific CD4⁺ T-cell immunity and anti-E7 antibody responses. IL-6 confers supportive but significant effects on type-1 helper T-cell (Th1)/Th2 responses in T cells. When T cells are stimulated with anti-CD3 and IL-6, their proliferation is significantly enhanced compared with anti-CD3 stimulation alone. IL-6 also affects the Th1/Th2 balance. Rincon *et al.* showed that IL-6 could induce more Th2 cytokine (such as IL-4) when it is added to a culture of inducing Th differentiation.²⁰ Thus, IL-6, probably produced by antigen-presenting cells, is a key modulator of Th1/Th2 differentiation.

The anti-apoptotic strategy could enhance the potency of antigen-specific DNA vaccines. Other researches have demonstrated that utilizing inhibitors of apoptosis such as Bcl-xL, Bcl-2, XIAP, dominant negative caspase-9, or dominant negative caspase-8 with tumor antigens enhances the antigen-specific immunities and anti-tumor effects.^{12,21,22} The Bcl-2 protein family comprises key regulators of cell survival that can suppress (e.g., Bcl-2, Bcl-xL, Mcl-1²³) or promote (e.g., Bad, Bax) apoptosis.²⁴ IL-6 has been shown to prolong cell survival via the Mcl-1 pathway.²⁵ Thus, DC-based vaccination could be enhanced by an approach that inhibits apoptosis and prolongs the survival of antigen-expressing DCs *in vivo*.¹² Proteins of the Bcl-2 family are known to be over-expressed in some cancers and therefore have been implicated as contributors to cellular immortalization.²⁶ In an effort to resolve these safety issues, we investigated the capacity of IL-6 to prevent CTL-induced DC death. Because IL-6 is naturally expressed in normal cells, it potentially represents a safe and effective method for enhancing DNA vaccine potency by offering a means of prolonging DC life without risking DC immortalization.²⁷

Combined strategies of cancer immunotherapy may generate better therapeutic effects than individual strategies. A DNA vaccine with IL-6 encoded with tumor antigens provides combinational strategies of antigen processing and presentation and anti-apoptotic mechanisms. Our results show that both IL-6/E7 and Mcl-1/E7 could provide anti-apoptotic functions for antigen-presenting cells (Figure 5). However, IL-6/E7 generates higher numbers of E7-specific CD8⁺ T-cell precursors and therefore may provide better tumor protection and therapeutic effects (Figures 1, 2, and 4). Our explanation is that IL-6/E7 may work through different strategies such as antigen processing and presentation and anti-apoptosis to generate better immunologic responses and anti-tumor effects than Mcl-1/E7, which is only anti-apoptotic. In addition, our results reveal that the chimeric DNA vaccines IL-6/E7 and ETA(dII)/E7, when mixed together, could generate more potent therapeutic effects than each on its own (Figure 7).

The IL-6/E7 DNA vaccine, generating humoral and cell-mediated immunities, aids both cancer prevention and treatment. Virus-like particles that generate anti-L1 Abs for the prevention of cervical cancer have been developed. The virus-like particles vaccine has been shown to prevent the HPV-16 infection and HPV-16-related cervical intraepithelial neoplasia.^{28,29} However, the virus-like particles vaccine does not provide therapeutic effects against HPV infection or HPV-related lesions. Our IL-6/E7 chimeric DNA vaccine could be utilized for both the prevention of HPV infection and the treatment of HPV-related lesions.

Although the vaccine may hold promise for cancer immunotherapy, some safety issues need to be resolved. DNA may integrate into the host genome, although it is estimated that the frequency of such integration is much lower than the frequency of spontaneous mutation and should not pose a significant risk.³⁰ Another issue is DNA vaccine-induced autoimmunity. Our results revealed that the titers of anti-IL-6 antibody by IL-6 DNA only (2.236 ± 0.27) were higher than those by wild-type E7 DNA (0.513 ± 0.031) and IL-6/E7 DNA (1.008 ± 0.041) ($P < 0.01$ one-way ANOVA), so

we performed a pathological examination of the vital organs in vaccinated mice. We did not observe abnormal inflammation or pathology (data not shown), indicating that IL-6/E7 is a potent vaccine with minimal side effects.

MATERIALS AND METHODS

Plasmid DNA constructs and preparation. IL-6 was amplified by polymerase chain reaction using human placenta complementary DNA as the template and a set of primers, namely, 5'-CCGCTCGAGAGGAGCCAGCTATGAACTC-3' and 5'-CCGGAATTCGACCAGAAGAAGGAATGC CC-3'. The amplified product was then cloned into the *XhoI/EcoRI* sites of pcDNA3 vector (Invitrogen, Carlsbad, CA). E7 was amplified by polymerase chain reaction using the DNA of the CaSki cell line as the template and with a set of primers, 5'-CCGGAAGCTTATGCATGGAGATACACC TAC-3' and 5'-CCCAAGCTTTTGAGAACAGATGG-3'. The product was cloned into the *HindIII* sites of pcDNA3-IL-6 to generate pcDNA3-IL-6/E7. To generate pcDNA3-Mcl-1/E7, an E7 DNA fragment was also cloned into the *HindIII* sites of pcDNA3-Mcl-1. To generate pcDNA3-IL-6/E7/GFP and pcDNA3-Mcl-1/E7/GFP, pcDNA3-IL-6/E7 or pcDNA3-Mcl-1/E7 was first digested by *HindIII*. The GFP fragment was obtained from plasmid pcDNA3-E7/GFP by *EcoRI/NotI* digestion. The DNA fragment was then filled in and ligated into IL-6/E7 or Mcl-1/E7 to generate the desired plasmids. Plasmid constructs were confirmed by sequencing.

Immunoblotting. 293 D^bK^b cells transfected with various DNA constructs were lysed,³¹ resolved on a sodium dodecyl sulfate-containing 12% polyacrylamide gel, and transferred to polyvinylidene difluoride nylon membranes (Millipore, Bedford, MA). They were probed with an antibody specific to E7 (Zymed, San Francisco, CA) or β -actin (Chemicon International, Temecula, CA), and then probed once more with either horseradish peroxidase-conjugated goat anti-mouse or anti-rabbit antibody. The specific bands were visualized using an enhanced chemiluminescence western blot system (Amersham, Buckinghamshire, UK). Our data revealed that the E7 and IL-6/E7 chimeric protein expression levels did not show significant alteration (Figure 8).

CTL assay using transfected 293 D^bK^b cells as target cells. CTL assays were performed by quantitative measurements of lactate dehydrogenase using the CytoTox96 non-radioactive cytotoxicity assay kit (Promega, Madison, WI) as described by Cheng *et al.*³ Various DNA-transfected 293 D^bK^b cells served as target cells, and a D^b-restricted E7-specific CD8⁺ T-cell line was used for effector cells.

CTL assay using dendritic cells pulsed with lysates of transfected 293 D^bK^b cells as target cells. CTL assays were performed using bone marrow-derived dendritic cells¹⁸ pulsed with various DNA-transfected

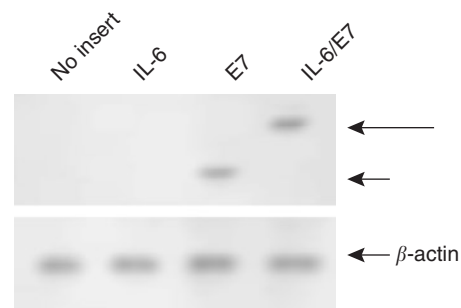


Figure 8 Immunoblotting of 293 D^bK^b cells transfected with pcDNA3-E7 or interleukin-6 (IL-6)/E7. Lysates from E7 or IL-6/E7 DNA-transfected 293 D^bK^b cells revealed a protein band with a size of approximately Mw 18,000 or 40,000 corresponding to E7 protein (short arrow) or IL-6/E7 protein (long arrow).

293 D^bK^b cell lysates as target cells. D^b-restricted E7-specific CD8⁺ T cells were used as effector cells as described by Hung *et al.*³²

Mice. Six- to eight-week-old female C57BL/6J mice were purchased and kept in the animal facility of the College of Medicine, National Taiwan University. There were five mice per group in every experiment. All of the animal procedures were performed according to approved protocols and in accordance with recommendations for the proper use and care of laboratory animals.

DNA vaccination. Preparation of DNA-coated gold particles and particle-mediated DNA vaccination using a helium-driven gene gun were performed as described previously.¹⁷

Intracellular cytokine staining and flow cytometry analysis. Each group of mice was immunized with 2 µg of various DNA vaccines and received a booster 1 week later. Splenocytes were harvested 1 week later and incubated with either 1 µg/ml of E7 peptide (aa 49–57)³³ or 10 µg/ml of E7 peptide (aa 30–67). Cell surface marker staining for CD8 or CD4 and intracellular cytokine staining for IFN-γ or IL-4, as well as flow cytometry analysis, were performed under conditions described earlier.^{17,18}

Enzyme-linked immunosorbent assay for anti-E7 antibody. The sera of the mice vaccinated with different DNAs were extracted 14 days after the last immunization. These were used to detect HPV-16 E7-specific Abs by a direct enzyme-linked immunosorbent assay as described by Cheng *et al.*³⁵

In vivo tumor protection experiments. Each group of mice was immunized with 2 µg of various DNA vaccines and boosted 1 week later. Mice were challenged with 5 × 10⁴ cells/mouse TC-1 cells subcutaneously 1 week after their last vaccination.³⁶ They were then monitored until 60 days after TC-1 tumor challenge.

In vivo antibody depletion experiments. *In vivo* Ab depletions were performed as described in our previous study.³⁷ The mice were vaccinated with IL-6/E7 DNA using a gene gun, boosted 1 week later, and challenged with 5 × 10⁴ cells/mouse TC-1 tumor cells. Depletion was started 1 week before tumor challenge. Following examples from prior research, we used monoclonal Ab GK1.5 for CD4 depletion,³⁸ monoclonal Ab 2.43 for CD8 depletion,³⁹ and monoclonal Ab PK136 for natural killer 1.1 depletion.⁴⁰

In vivo tumor treatment experiments. Mice were injected with 5 × 10⁴ TC-1 cells via their tail veins. Two days later, they received various DNA vaccines (16 µg/mouse). This was followed by a booster every 7 days. The mice were killed and their lungs were removed 28 days after TC-1 cells were injected. The pulmonary tumor nodules in each mouse were evaluated and counted by experimenters who were blind to their sample identity.

For a head-to-head comparison of chimeric DNA vaccines, the different vaccines we used were IL-6/E7 DNA only, ETA(dII)/E7 DNA only,³² IL-6/E7 mixed with ETA(dII)/E7 DNA, followed by a DNA vaccine booster every 7 days. Mice were killed 28 days after TC-1 cell injection to evaluate pulmonary tumor nodules as described above.

Preparation of CD11c⁺ cells in the inguinal lymph nodes from vaccinated mice. Each mouse received an intradermal injection of DNA administered with a gene gun in the abdominal region. Inguinal lymph nodes were harvested 1 or 5 days after vaccination. CD11c⁺ cells were enriched from lymph nodes using CD11c (N418) microbeads (Miltenyi Biotec, Auburn, CA).¹² Detection of apoptotic cells in the CD11c⁺ GFP⁺ cells was performed using annexin V-PE apoptosis detection Kit-I (BD Bioscience, San Diego, CA) to count the percentage of apoptotic cells, as described previously by Kim *et al.*¹²

Activation of an E7-specific CD8⁺ T-cell line by CD11c-enriched cells from vaccinated mice. CD11c-enriched cells (2 × 10⁴) were incubated with

2 × 10⁶ of the E7-specific CD8⁺ T-cell line,¹² and the cells were then stained for both surface CD8 and intracellular IFN-γ. They were analyzed by flow cytometry as described above.

CTL assays using CaSki cells as target cells. Monocyte-derived DCs of HLA-A2-positive volunteers were isolated and generated from peripheral blood mononuclear cells with granulocyte macrophage colony-stimulating factor (800 U/ml) and IL-4 (500 U/ml) for 6 days as described in our previous work.⁴¹ Fresh peripheral blood mononuclear cells from the same volunteer were collected and cultured with protein-pulsed mature DCs that were first pulsed with 50 mmol/l of cell lysates of no insert, E7-, IL-6-, or IL-6/E7-transfected 293 D^bK^b cells overnight and incubated with peripheral blood mononuclear cells to generate the E7-specific CD8⁺ T cells. CTL assays were performed with effector cells (E7-specific CD8⁺ T cells) and target cells (CaSki cells) mixed together at various ratios (1:1, 5:1, 15:1 and 45:1) to assess the quantity of lactate dehydrogenase as described above.

Statistical analysis. All data expressed as mean ± SEM are representative of at least two different experiments. Data for intracellular cytokine staining with flow cytometry analysis and tumor treatment experiments were evaluated by ANOVA.

ACKNOWLEDGMENTS

This study was supported by grant from the National Taiwan University Hospital (NTUH95-000-385). We would like to thank Hsin-Fang Yen-Yang (Academia Sinica, Taiwan) for the kind gift of pcDNA3-Mcl-1 and Tzzy-Chouu Wu (Johns Hopkins Medical Institutes, Baltimore, MD) for the 293 D^bK^b cells.

REFERENCES

- Boon, T, Cerottini, JC, Van den Eynde, B, van der Bruggen, P and Van Pel, A (1994). Tumor antigens recognized by T lymphocytes. *Annu Rev Immunol* **12**: 337–365.
- Condon, C, Watkins, SC, Celluzzi, CM, Thompson, K and Falow, LD Jr. (1996). DNA-based immunization by *in vivo* transfection of dendritic cells. *Nat Med* **2**: 1122–1128.
- Cheng, WF, Hung, CF, Chai, CY, Hsu, KF, He, L, Ling, M *et al.* (2001). Tumor-specific immunity and antiangiogenesis generated by a DNA vaccine encoding calreticulin linked to a tumor antigen. *J Clin Invest* **108**: 669–678.
- Chen, CH, Wang, TL, Hung, CF, Yang, Y, Young, RA, Pardoll, DM *et al.* (2000). Enhancement of DNA vaccine potency by linkage of antigen gene to an HSP70 gene. *Cancer Res* **60**: 1035–1042.
- Rodriguez, F, Zhang, J and Whitton, JL (1997). DNA immunization: ubiquitination of a viral protein enhances cytotoxic T-lymphocyte induction and antiviral protection but abrogates antibody induction. *J Virol* **71**: 8497–8503.
- Boyle, JS, Brady, JL and Lew, AM (1998). Enhanced responses to a DNA vaccine encoding a fusion antigen that is directed to sites of immune induction. *Nature* **392**: 408–411.
- King, CA, Spellerberg, MB, Zhu, D, Rice, J, Sahota, SS, Thompson, AR *et al.* (1998). DNA vaccines with single-chain Fv fused to fragment C of tetanus toxin induce protective immunity against lymphoma and myeloma. *Nat Med* **4**: 1281–1286.
- Weiss, WR, Ishii, KJ, Hedstrom, RC, Sedegah, M, Ichino, M, Barnhart, K *et al.* (1998). A plasmid encoding murine granulocyte-macrophage colony-stimulating factor increases protection conferred by a malaria DNA vaccine. *J Immunol* **161**: 2325–2332.
- Klinman, DM, Yamshchikov, G and Ishigatsubo, Y (1997). Contribution of CpG motifs to the immunogenicity of DNA vaccines. *J Immunol* **158**: 3635–3639.
- Cheng, WF, Lee, CN, Chang, MC, Su, YN, Chen, CA and Hsieh, CY (2005). Antigen-specific CD8⁽⁺⁾ T lymphocytes generated from a DNA vaccine control tumor through the Fas-FasL pathway. *Mol Ther* **12**: 960–968.
- Cheng, WF, Chen, LK, Chen, CA, Chang, MC, Hsiao, PN, Su, YN *et al.* (2006). Chimeric DNA vaccine reverses morphine-induced immunosuppression and tumorigenesis. *Mol Ther* **13**: 203–210.
- Kim, TW, Hung, CF, Ling, M, Juang, J, He, L, Hardwick, JM *et al.* (2003). Enhancing DNA vaccine potency by coadministration of DNA encoding antiapoptotic proteins. *J Clin Invest* **112**: 109–117.
- Hirano, T (1992). Interleukin-6 and its relation to inflammation and disease. *Clin Immunol Immunopathol* **62**: S60–S65.
- Tosato, G and Pike, SE (1988). Interferon-beta 2/interleukin 6 is a co-stimulant for human T lymphocytes. *J Immunol* **141**: 1556–1562.
- Curnow, SJ, Scheel-Toellner, D, Jenkinson, W, Raza, K, Durrani, OM, Faint, JM *et al.* (2004). Inhibition of T cell apoptosis in the aqueous humor of patients with uveitis by IL-6/soluble IL-6 receptor trans-signaling. *J Immunol* **173**: 5290–5297.
- Leu, CM, Wong, FH, Chang, C, Huang, SF and Hu, CP (2003). Interleukin-6 acts as an antiapoptotic factor in human esophageal carcinoma cells through the activation of both STAT3 and mitogen-activated protein kinase pathways. *Oncogene* **22**: 7809–7818.
- Cheng, WF, Hung, CF, Chen, CA, Lee, CN, Su, YN, Chai, CY *et al.* (2005). Characterization of DNA vaccines encoding the domains of calreticulin for

- their ability to elicit tumor-specific immunity and antiangiogenesis. *Vaccine* **23**: 3864–3874.
18. Liao, CW, Chen, CA, Lee, CN, Su, YN, Chang, MC, Syu, MH *et al.* (2005). Fusion protein vaccine by domains of bacterial exotoxin linked with a tumor antigen generates potent immunologic responses and antitumor effects. *Cancer Res* **65**: 9089–9098.
 19. Hung, CF, Cheng, WF, Hsu, KF, Chai, CY, He, L, Ling, M *et al.* (2001). Cancer immunotherapy using a DNA vaccine encoding the translocation domain of a bacterial toxin linked to a tumor antigen. *Cancer Res* **61**: 3698–3703.
 20. Rincon, M, Anguita, J, Nakamura, T, Fikrig, E and Flavell, RA (1997). Interleukin (IL)-6 directs the differentiation of IL-4-producing CD4⁺ T cells. *J Exp Med* **185**: 461–469.
 21. Kim, TW, Hung, CF, Boyd, DA, He, L, Lin, CT, Kaiserman, D *et al.* (2004). Enhancement of DNA vaccine potency by coadministration of a tumor antigen gene and DNA encoding serine protease inhibitor-6. *Cancer Res* **64**: 400–405.
 22. Kim, TW, Lee, JH, He, L, Boyd, DA, Hardwick, JM, Hung, CF *et al.* Modification of professional antigen-presenting cells with small interfering RNA *in vivo* to enhance cancer vaccine potency. *Cancer Res* **65**: 309–316.
 23. Reynolds, JE, Yang, T, Qian, L, Jenkinson, JD, Zhou, P, Eastman, A *et al.* (1994). Mcl-1, a member of the Bcl-2 family, delays apoptosis induced by c-Myc overexpression in Chinese hamster ovary cells. *Cancer Res* **54**: 6348–6352.
 24. Gross, A, McDonnell, JM and Korsmeyer, SJ (1999). BCL-2 family members and the mitochondria in apoptosis. *Genes Dev* **13**: 1899–1911.
 25. Jourdan, M, Veyrune, JL, De Vos, J, Redal, N, Couderc, G and Klein, B (2003). A major role for Mcl-1 antiapoptotic protein in the IL-6-induced survival of human myeloma cells. *Oncogene* **22**: 2950–2959.
 26. Brunda, MJ, Luistro, L, Warrior, RR, Wright, RB, Hubbard, BR, Murphy, M *et al.* (1993). Antitumor and antimetastatic activity of interleukin 12 against murine tumors. *J Exp Med* **178**: 1223–1230.
 27. Medema, JP, Schuurhuis, DH, Rea, D, van Tongeren, J, de Jong, J, Bres, SA *et al.* (2001). Expression of the serpin serine protease inhibitor 6 protects dendritic cells from cytotoxic T lymphocyte-induced apoptosis: differential modulation by T helper type 1 and type 2 cells. *J Exp Med* **194**: 657–667.
 28. Harper, DM, Franco, EL, Wheeler, CM, Moscicki, AB, Romanowski, B, Roteli-Martins, CM *et al.* (2006). Sustained efficacy up to 4.5 years of a bivalent L1 virus-like particle vaccine against human papillomavirus types 16 and 18: follow-up from a randomised control trial. *Lancet* **367**: 1247–1255.
 29. Koutsky, LA, Ault, KA, Wheeler, CM, Brown, DR, Barr, E, Alvarez, FB *et al.* (2002). A controlled trial of a human papillomavirus type 16 vaccine. *N Engl J Med* **347**: 1645–1651.
 30. Nichols, WW, Ledwith, BJ, Manam, SV and Troilo, PJ (1995). Potential DNA vaccine integration into host cell genome. *Ann NY Acad Sci* **772**: 30–39.
 31. Chen, CH, Ji, H, Suh, KW, Choti, MA, Pardoll, DM and Wu, TC (1999). Gene gun-mediated DNA vaccination induces antitumor immunity against human papillomavirus type 16 E7-expressing murine tumor metastases in the liver and lungs. *Gene Ther* **6**: 1972–1981.
 32. Hung, CF, Cheng, WF, Hsu, KF, Chai, CY, He, L, Ling, M *et al.* (2001). Cancer immunotherapy using a DNA vaccine encoding the translocation domain of a bacterial toxin linked to a tumor antigen. *Cancer Res* **61**: 3698–3703.
 33. Feltkamp, MC, Smits, HL, Vierboom, MP, Minnaar, RP, de Jongh, BM, Drijfhout, JW *et al.* (1993). Vaccination with cytotoxic T lymphocyte epitope-containing peptide protects against a tumor induced by human papillomavirus type 16-transformed cells. *Eur J Immunol* **23**: 2242–2249.
 34. Tindle, RW, Fernando, GJ, Sterling, JC and Frazer, IH (1991). A “public” T-helper epitope of the E7 transforming protein of human papillomavirus 16 provides cognate help for several E7 B-cell epitopes from cervical cancer-associated human papillomavirus genotypes. *Proc Natl Acad Sci USA* **88**: 5887–5891.
 35. Cheng, WF, Hung, CF, Hsu, KF, Chai, CY, He, L, Ling, M *et al.* (2001). Enhancement of sindbis virus self-replicating RNA vaccine potency by targeting antigen to endosomal/lysosomal compartments. *Hum Gene Ther* **12**: 235–252.
 36. Lin, KY, Guarnieri, FG, Staveley-O’Carroll, KF, Levitsky, HI, August, JT, Pardoll, DM *et al.* (1996). Treatment of established tumors with a novel vaccine that enhances major histocompatibility class II presentation of tumor antigen. *Cancer Res* **56**: 21–26.
 37. Cheng, WF, Hung, CH, Chai, CY, Hsu, KF, He, L, Ling, M *et al.* (2001). Enhancement of sindbis virus self-replicating RNA vaccine potency by linkage of herpes simplex virus type 1 VP22 protein to antigen. *J Virol* **75**: 2368–2376.
 38. Dialynas, DP, Quan, ZS, Wall, KA, Pierres, A, Quintans, J, Loken, MR *et al.* (1983). Characterization of the murine T cell surface molecule, designated L3T4, identified by monoclonal antibody GK1.5: similarity of L3T4 to the human Leu-3/T4 molecule. *J Immunol* **131**: 2445–2451.
 39. Sarmiento, M, Glasebrook, AL and Fitch, FW (1980). IgG or IgM monoclonal antibodies reactive with different determinants on the molecular complex bearing Lyt 2 antigen block T cell-mediated cytotoxicity in the absence of complement. *J Immunol* **125**: 2665–2772.
 40. Koo, GC, Dumont, FJ, Tutt, M, Hackett, J Jr. and Kumar, V (1986). The NK-1.1(-) mouse: a model to study differentiation of murine NK cells. *J Immunol* **137**: 3742–3747.
 41. Cheng, WF, Lee, CN, Su, YN, Chang, MC, Hsiao, WC, Chen, CA *et al.* (2005). Induction of human papillomavirus type 16-specific immunologic responses in a normal and an human papillomavirus-infected populations. *Immunology* **115**: 136–149.



Autologous neu DNA vaccine can be as effective as xenogenic neu DNA vaccine by altering administration route

Cheng-Fen Tu^{a,1}, Chi-Chen Lin^{a,b,c,1}, Ming-Chuan Chen^a, Tai-Ming Ko^a,
Chiu-Mei Lin^d, Ying-Chang Wang^{e,2}, Ming-Derg Lai^{a,b,c,*}

^a Department of Biochemistry and Molecular Biology, College of Medicine, National Cheng Kung University, Tainan, Taiwan, ROC

^b Institute of Basic Medicine, College of Medicine, National Cheng Kung University, Tainan, Taiwan, ROC

^c Center for Gene Regulation and Signal Transduction Research, National Cheng Kung University, Tainan, Taiwan, ROC

^d Department of Emergency Medicine, Shin Kong Wu Ho-Su Memorial Hospital, Taiwan, ROC

^e BioWare Technologies Co. Ltd, Taipei, Taiwan, ROC

Received 4 April 2006; received in revised form 25 July 2006; accepted 10 August 2006

Abstract

We examined the therapeutic efficacy of xenogenic human N'-terminal neu DNA vaccine and autologous mouse N'-terminal neu DNA vaccine on MBT-2 tumor cells in C3H mice. Intramuscular injection of xenogenic and autologous neu DNA vaccines produced comparable therapeutic efficacies. Mouse and human N'-neu DNA vaccine induced tumor infiltration of CD8⁺ T cells, while the human vaccine was less effective at stimulating natural killer cells. Depletion of CD8⁺ T cells abolished the therapeutic efficacy of both types of DNA vaccines. On the other hand, xenogenic neu DNA vaccine showed significantly better therapeutic efficacy than autologous DNA vaccine with gene gun immunization. Increased infiltration of CD8⁺ T cells was correlated with enhanced therapeutic efficacy in the human N'-neu group of mice. Therefore, intramuscular injection can enhance the therapeutic efficacy of autologous neu DNA vaccine.

© 2006 Published by Elsevier Ltd.

Keywords: Neu; DNA vaccine; Autologous; Xenogenic; Cancer; Intramuscular delivery

1. Introduction

The HER-2/ErbB-2/neu proto-oncogene encodes a 185 kDa protein (p185^{neu}) belonging to the epidermal growth factor receptor (EGFR) family. The protein is overexpressed in several types of cancer including breast, gastric, and bladder carcinomas. This involvement in cancer progression and worsening prognosis makes p185^{neu} an attractive target for cancer therapy [1]. Small interfering RNA (siRNA) inhibits the expression of the HER2/neu gene and induces apoptosis of HER-2 positive cancer cells [2].

Passive immunological treatment with Herceptin, a humanized anti-neu antibody, has shown anti-tumor activity in xenograft models and clinical trials [3,4]. The combinational use of chemotherapy and Herceptin can be beneficial [5], although combination therapy involving anthracyclines and Herceptin is associated with cardiac side effects [6,7], which may cause mitochondrial dysfunction in cardiomyocytes [8]. Prolonged administration of HER-2/neu-specific monoclonal antibody has generated neu antigen-negative tumor variants in a transgenic animal model [9].

Active vaccination with either DNA or proteins targeting p185^{neu} provides an alternative therapeutic approach. Vaccination against peptides and domains of p185^{neu} has prevented tumor formation in several animal models [10,11]. Recently, a Phase I clinical trial indicated that a HER-2/neu intracellular domain (ICD) protein vaccine incorporating granulocyte-macrophage colony-stimulating factor as an adjuvant was

* Corresponding author. Tel.: +886 6 2353535/5549; fax: +886 6 2741694.

E-mail address: a1211207@mail.ncku.edu.tw (M.-D. Lai).

¹ Both authors contribute equally to this work.

² Y.-C. Wang is an employee of BioWare Technologies Co. Ltd.

well tolerated and effective in eliciting neu-specific T-cell and antibody immunity [12]. Moreover, HER-2/neu peptide based vaccines induce anti-neu humoral response and cause humoral epitope-spreading in cancer patients [13]. DNA encoding full-length or truncated neu induces protective immunity against neu-expressing mammary tumors [14–19]. The efficacy of HER2/neu DNA as a therapeutic cancer vaccine for established tumors has also been demonstrated *in vivo* [20–23]. Most of these latter studies were performed on tumor cells artificially expressing exogenous p185^{neu} generated either by transgenic injection or by cell transfection [14–23]. Extending these observations, we have demonstrated the therapeutic efficacy of HER2/neu DNA vaccine on mouse tumors that naturally over-express mouse neu [24].

Xenogenic DNA may be required for effective induction of immunity with DNA vaccine against EGFR [25]. However, whether xenogenic DNA is required for DNA vaccines against other antigens including HER2/neu is presently unclear. Several lines of evidence suggest that immunological responses toward ErbB-2/neu may be different from those directed towards ErbB-1/EGFR. Neu-derived peptide epitopes are recognized by cancer-specific cytotoxic T lymphocytes and p185^{neu} antibody in cancer patients [26–29]. Furthermore, autologous human HER2/neu protein and peptide may induce appropriate cellular and humoral immunity in human patients [12].

In this report, we directly compare the therapeutic efficacy of DNA vaccines encoding the extracellular domain of either autologous mouse or xenogenic human p185^{neu} in a mouse tumor naturally overexpressing endogenous p185^{neu}. Our results indicate that autologous mouse neu DNA vaccine is comparably effective as the xenogenic human neu DNA vaccine following intramuscular injection. In contrast, xenogenic neu DNA vaccine is more effective than autologous neu DNA vaccine following gene gun administration.

2. Results

2.1. Construction and characterization of N-terminal extracellular domains of mN'-neu and hN'-neu DNA plasmids

The N-terminal of mouse p185^{neu} was cloned from mRNA of MBT-2 bladder cancer cells with RT-PCR and verified by DNA sequencing. The N-terminal of human p185^{neu} was subcloned from a full-length human p185^{neu} plasmid. Both mouse N'-neu and human N'-neu cDNA was expressed under the control of CMV promoter as described before [24], and named as mN'-neu and hN'-neu, respectively (Fig. 1A). COS-1 cells were transiently transfected with the plasmid and the expression of the extracellular domain of p185^{neu} was demonstrated by immunohistochemical analysis with mon-

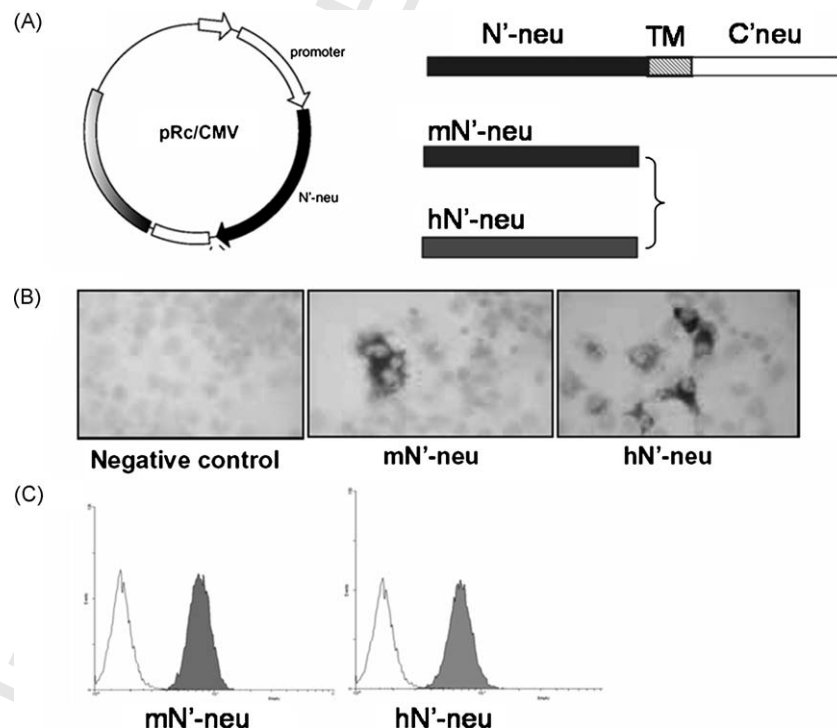


Fig. 1. Characterization of DNA vaccines: (A) schematic diagram of the human N'-neu (hN'-neu) and mouse N'-neu (mN'-neu) expressing vectors; (B) expression of N'-neu *in vitro* evaluated via immunocytochemistry; (C) expression of N'-neu *in vitro* evaluated with flow cytometry. Plasmid-transfected COS-1 cells were stained with mAb against the extracellular domain of mouse and human p185^{neu} followed by FITC-conjugated goat anti-mouse secondary antibody (grey or dark histogram for mouse and human N'-neu, white histogram for vector negative control).

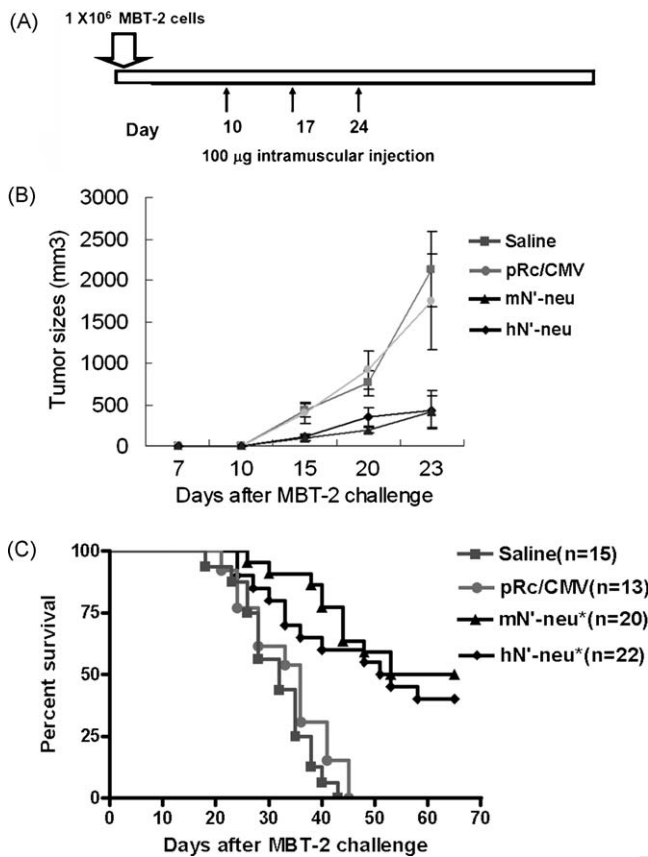


Fig. 2. Therapeutic effects of neu DNA vaccines on established tumor in C3H mice: (A) protocol for DNA vaccination. Ten days after subcutaneous tumor implantation, mice were inoculated with DNA vaccine intramuscularly three times at weekly intervals; (B) tumor volume was measured every third day. Data are means of the animals per group; bars, \pm S.D.; (C) lifespan of C3H mice after subcutaneous challenge with MBT-2 cells. The survival data were subjected to Kaplan-Meier analysis. The digit in the parenthesis is the number of mice in the experiment. The symbol (*) indicates a statistically significant difference when compared with the control saline mice ($P < 0.01$).

oclonal antibody against p185^{neu} (Fig. 1B). The expression of mN'-neu and hN'-neu plasmid was further confirmed by flow cytometry analysis (Fig. 1C).

2.2. Efficacy of mN'-neu and hN'-neu DNA vaccines in mice with established tumors

The protocol for inoculation of DNA vaccine is shown in Fig. 2A. We found that vaccination of mN'-neu or hN'-neu slowed the rate of growth of MBT-2 tumors compared with saline-treated mice. However, there was no difference between mN'-neu and hN'-neu vaccinated groups (Fig. 2B). In addition, the survival rate of vaccinated mice results also indicated that mN'-neu DNA vaccine showed similar efficacy as hN'-neu DNA vaccine (Fig. 2C). Xenogenic neu DNA vaccine did not show better efficacy than autologous mouse N'-neu DNA vaccine, as reported for EGFR DNA vaccine [25].

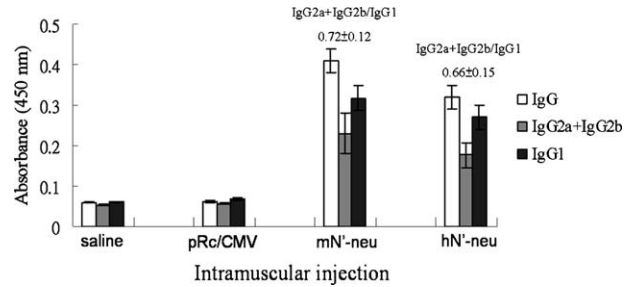


Fig. 3. Neu-specific IgG and IgG subclass titers from mice immunized using the intramuscular vaccination. The titers of anti-mouse p185^{neu} IgG and IgG subclass in sera of mice were determined with ELISA on dishes coated with the extracellular domain of mouse p185^{neu}. The overall IgG2a + IgG2b/IgG1 ratios (mean \pm standard derivations) for extracellular domain of mouse p185^{neu} antigen are shown above the bars.

2.3. Cellular and humoral immunity

To examine the immunological responses induced by N'-neu DNA vaccine, we measured the titer of total IgG anti-p185^{neu} antibody in mouse serum. mN'-neu DNA vaccine induced higher anti-p185^{neu} antibody response compared to the hN'-neu DNA vaccine, although the difference is statistical insignificant ($P = 0.12$) (Fig. 3). We further examined the IgG subtype of anti-neu antibody induced by DNA vaccine, the ratio of IgG2a + IgG2b/IgG1 was not significantly different between the mN'-neu and hN'-neu groups (Fig. 3). For the cellular immunity, we examined the infiltration of lymphocytes at tumor sites (Table 2). No macrophages were detected by immunostaining (data not shown). Massive infiltration of natural killer cells was observed in the mice vaccinated with mN'-neu DNA vaccine. Infiltration of CD4⁺ T cells and CD8⁺ T cells were observed in both mN'-neu and hN'-neu groups of mice. We observed considerably more increased infiltration of CD8⁺ T cells in the hN'-neu group of mice, although the increases did not reach statistical significance compare to the mN'-neu groups ($P = 0.09$) (Table 1). We further evaluated the cellular immunity with cytotoxic response to MBT-2 cells using splenocytes isolated vaccinated mice (Fig. 4). The splenocytes isolated from both mN'-neu and hN'-neu groups of mice lysed MBT-2 cells with equal potency.

Table 1
Infiltrated lymphocytes at tumor sites within cryosectioned samples

Vaccine group	CD4 ⁺ T cells	CD8 ⁺ T cells	NK cells
Saline (IM)	2 \pm 1	1 \pm 0	1 \pm 1
Vector (IM)	2 \pm 2	2 \pm 1	1 \pm 1
Mouse N'-neu (IM)	40 \pm 8	31 \pm 4	27 \pm 6*
Human N'-neu (IM)	32 \pm 7	41 \pm 7	7 \pm 2

Note: Cell count was performed at 400 \times magnification. Three samples and five randomly chosen fields/sample were evaluated. Results are expressed as mean \pm standard deviation of immunohistochemical positive cells in the cryosection. IM: intramuscular injection. The symbol (*) indicates a statistically significant difference when compared with the human N'-neu group ($P < 0.01$).

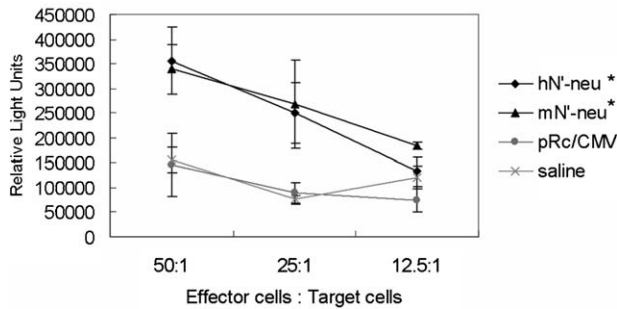


Fig. 4. The role of cellular immunity in immunological defense. Lysis of MBT-2 cells with splenocytes derived from mice inoculated with various vaccines or saline. Splenocytes were incubated with serial dilution of MBT-2 cells expressing luciferase. The release of luciferase upon lysis of MBT-2 cells was measured by means of a luminometer. The symbol (*) indicates a statistically significant difference when compared with the control saline mice ($P < 0.01$).

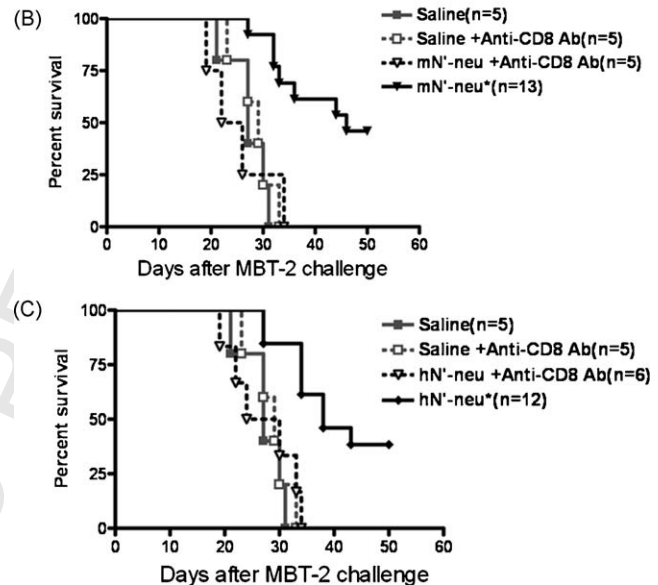
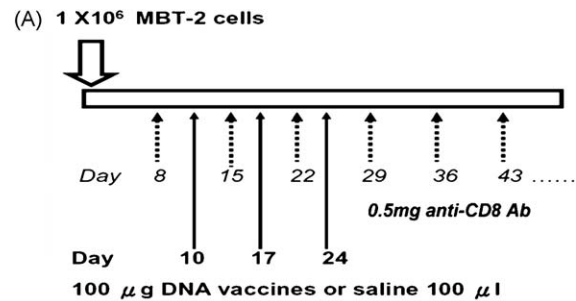


Fig. 5. $CD8^+$ T cells are essential for the therapeutic effect. (A) Protocol for depletion of $CD8^+$ T cells *in vivo*. Tumor-bearing mice were injected intraperitoneally with 500 μ g of anti-CD8 antibody at weekly intervals starting from 2 days before the first inoculation of DNA vaccine. Lifespan of C3H mice after subcutaneous challenge with MBT-2 cells is depicted in (B). mN'-neu; and (C) hN'-neu depletion of $CD8^+$ T cells. The survival data were subjected to Kaplan-Meier analysis. The symbol (*) indicates a statistically significant difference ($P < 0.01$), when compared with the vaccinated mN'-neu or hN'-neu mice without depletion of $CD8^+$ T cell.

2.4. Influence of $CD8^+$ T cells on induction of anti-tumor immunity

$CD8^+$ T cells play a major role in defending MBT-2 cells in a C3H mice animal model [28]. To confirm this role, C3H mice were depleted of $CD8^+$ T cells by a regimen of weekly procedures (Fig. 5A). Depletion completely abolished the therapeutic efficacy of mN'-neu (Fig. 5B) and hN'-neu DNA vaccines (Fig. 5C).

2.5. Xenogenic hN'-neu DNA vaccine had better therapeutic efficacy with gene gun delivery

As the vaccination method of DNA vaccine affects the immunological response [22,30], we tested the efficacy of mN'-neu and hN'-neu DNA vaccines applied using a gene gun (Fig. 6A). Human N'-neu DNA vaccine significantly delayed tumor growth (Fig. 6B) and prolonged mouse survival as compared with mN'-neu when administered by gene gun (Fig. 6C).

2.6. Humoral and cellular immunity

Both mN'-neu and hN'-neu groups of mice induced approximately similar amount of specific anti-mouse p185^{neu} antibody (Fig. 7); however, gene gun inoculation induced much more antibody titer than the intramuscular injection (Figs. 3 and 7). Furthermore, we examined the IgG subtype of anti-neu antibody induced by DNA vaccine, the result showed that IgG subtype pattern in gene gun injection of hN'-neu and mN'-neu DNA vaccine were not different (Fig. 7). The gene gun vaccination induces a significant lower IgG2a + IgG2b/IgG1 ratio compare to the intramuscular injection of neu DNA vaccine (Figs. 3 and 7). As for the cellular immunity, the sparse infiltration of NK cells was observed at tumor sites both in the mice vaccinated with mN'-neu or hN'-neu DNA vaccine (Table 4). On the other hand, significant infiltration of $CD8^+$ T cells was

observed in the mice vaccinated with hN'-neu DNA vaccine (Table 2) ($P < 0.01$). Hence, the increased cytotoxic T cells were correlated with the therapeutic efficacy by vaccinating autologous or xenogenic DNA vaccine with gene gun.

Table 2
Infiltrated lymphocytes at tumor sites within cryosectioned samples

Vaccine group	$CD4^+$ T cells	$CD8^+$ T cells	NK cells
Saline (GG)	1 \pm 1	0	0
Vector (GG)	1 \pm 1	1 \pm 1	0
Mouse N'-neu (GG)	13 \pm 4	59 \pm 7	2 \pm 1
Human N'-neu (GG)	21 \pm 6	77 \pm 4*	2 \pm 1

Note: Cell count was performed at 400 \times magnification. Three samples and five randomly chosen fields/sample were evaluated. Results are expressed as mean \pm standard deviation of immunohistochemical positive cells in the cryosection. GG: gene gun. The symbol (*) indicates a statistically significant difference when compared with the mouse N'-neu group ($P < 0.01$).

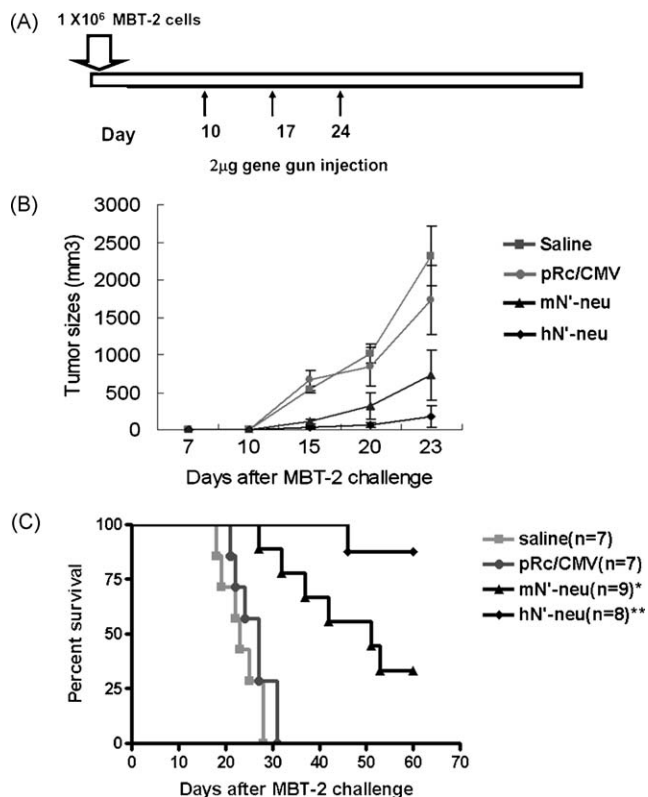


Fig. 6. Human N'-neu has significantly better therapeutic efficacy than mouse N'-neu with gene gun delivery: (A) the protocol used is depicted. Two μg DNA was used in the gene gun approach; (B) tumor volume was measured every third day. Data are means of the animals per group; bars, \pm S.D. (C) Lifespan of C3H mice after subcutaneous challenge with MBT-2 cells. The survival data were subjected to Kaplan-Meier analysis. The digit in the parenthesis is the number of mice in the experiment. The symbol (*) indicates a statistically significant difference when compared with the control saline mice ($P < 0.01$). The symbol (**) indicates a statistically significant difference when compared with the control saline mice ($P < 0.01$) and statistical significant difference when compared with mN'-neu group of mice ($P < 0.05$).

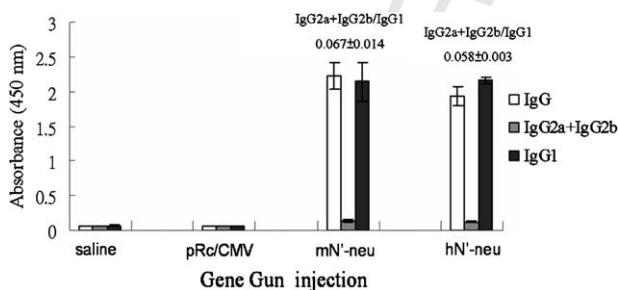


Fig. 7. Neu-specific IgG and IgG subclass titers from mice immunized using the gene gun. The titers of anti-mouse p185^{neu}-specific IgG and IgG subclass in sera of mice were determined with ELISA on dishes coated with the extracellular domain of mouse p185^{neu}. The overall IgG2a + IgG2b/IgG1 ratios (mean \pm standard derivations) for extracellular domain of mouse p185^{neu} antigen are shown above the bars.

3. Discussion

In this report we have examined the therapeutic efficacy of xenogenic and autologous neu DNA vaccines on a mouse tumor model naturally overexpressing p185^{neu}. Autologous neu DNA vaccine had the same therapeutic efficacy as xenogenic neu DNA vaccine upon intramuscular immunization. T-cell depletion experiment indicates that CD8⁺ T cell plays a major role in the immunological defense afforded by either xenogenic or autologous neu DNA vaccine. NK cells and anti-neu antibody may provide additional immune defense based on an increase in the tumor infiltration of NK cells and higher specific anti-mouse neu antibody in the serum. Furthermore, we demonstrate that xenogenic human neu DNA vaccine provides stronger therapeutic efficacy when administered by gene gun. The increased therapeutic efficacy correlates with the significantly enhanced tumor infiltration of CD8⁺ T cells. This confirms our previous work [24] and reinforces the view that CD8⁺ T cells may well be essential for immunological therapeutics for neu DNA vaccine.

Pupa et al. have previously demonstrated that the xenogenic DNA vaccine could inhibit mammary carcinoma development in HER2/neu transgenic mice [19]. In their model, xenogenic human neu DNA vaccine can induce anti-mouse p185^{neu} antibody response which may be responsible for the inhibition of tumor progression. Similar observation was made in our study that xenogenic human neu DNA can induce anti-mouse p185^{neu} antibody. However, cellular immunity including T cells and NK cells may be more important in mediating tumor rejection in our transplantable animal tumor model. The tumor progression in transgenic mice is much more slower than transplantable tumor, and the titer of antibody generated may be sufficient in inhibiting the transition from dysplasia to carcinoma with the targeting of both normal and cancer cells [19]. On the other hand, the apoptosis of tumor cells mediated by cellular immunity is essential in targeting tumor destruction and delay the tumor progression or even eradication in transplantable animal model. The timing of induction of immunity is important for both types of animal model. Inoculation of neu DNA vaccine will have no effect if later than three months in transgenic animal [19], on the other hand, inoculation of DNA vaccine will have little therapeutic effect when the tumor is too large, for example, three weeks after transplantation (unpublished observation).

It is interesting to note that many more NK cells were detected at tumor sites when mice were intramuscular inoculated with autologous mouse neu DNA vaccine. The increase of NK cells may partly explain the equal efficacy observed for autologous and xenogenic neu DNA vaccine with intramuscular injection, since NK cells play an important role in immunological defense. Three factors may determine the infiltration of NK cells at tumor sites. The first is the differential activation toward NK cells by various dendritic cells (DC). For example, monocyte-derived

DCs are more potent stimulators of NK cells than Langerhan cells in the skin [32]. Secondly, CpG motifs in the large amounts of DNA with intramuscular injection may provide stronger signals for activating NK cells [33,34]. Thirdly, specific anti-mouse neu autoantibody at tumor sites may further enhance the adhesion of NK cells [35,36]. We have further studied the subtypes of IgG with xenogenic and autologous DNA vaccine, but the IgG1/IgG2a + IgG2b ratio did not alter. It is possible that the epitopes recognized by anti-p185^{neu} antibody is more important in determining the protection from tumor formation in our animal model.

Biolistic delivery of DNA into skin using gene gun usually directly delivers the DNA into Langerhan cells in the skin, and the activated DCs migrate into lymph node, activating an immune response [37,38]. Direct presentation of DNA vaccines by Langerhan cells may play a major role in eliciting the immune response. On the other hand, DNA vaccine delivered with intramuscular injection may go through direct presentation or cross-presentation. The DNA vaccine may be presented by myocytes, and cross-presented by DCs residing or infiltrating into the muscle site. Cross presentation can cause cross-tolerance or cross-priming [39,40]. Environmental signals, such as inflammatory signals or CpG motifs in the large amounts of DNA with intramuscular injection, may switch the outcome of cross-presentation from cross-tolerance to cross-priming [39]. It is possible that local inflammation induced by intramuscular injection may cause a similar conversion to cross-priming, and thus enhance the therapeutic efficacy of the autologous neu DNA vaccine.

Langerhan cells are more potent stimulators of cytotoxic T lymphocytes than monocyte derived DCs [41]. However, Langerhan cells are less phagocytotic [42], and may be less dependent on cross-presentation. Therefore, xenogenic DNA vaccine induces a very strong immunological response with direct presentation in Langerhan cells. Self-peptide missense mutations enhance the binding of MHC class I molecules and enhance TCR signaling. The stimulation can activate the naïve T cells not only react to the mutated self-peptides and parental non-mutated peptides in tumor cells [43,44]. Xenogenic DNA may employ a similar mechanism to achieve activation of T cells, since xenogenic DNA has a natural missense mutation compared to that of autologous neu DNA.

Recently, Smorlesi et al. [30] have evaluated the therapeutic efficacy of neu DNA vaccine with different immunization routes, and found that the intramuscular injection with electroporation provided the best therapeutic efficacy in transgenic animal model system. On the other hand, gene gun delivery method may provide better therapeutic efficacy when xenogenic DNA vaccine is used in our animal model. The discrepancy may be due to the differences of tumor progression in these two different animal systems: the progression of tumor growth is much more slowly in transgenic mice. The Th1 type antibody response (IgG2a + IgG2b) is important for inhibiting tumor progression in transgenic tumor model [19], and the gene gun method appears to induce a Th2 type (IgG1)

antibody response ([30] and this study). Therefore, intramuscular injection is a better route for slow-progression native tumor. In contrast, to inhibit the fast-growing transplantable tumor may require the high titer IgG1 antibody induced by gene gun method.

In contrast to the present findings, a prior study on EGFR supports the view that xenogenic human DNA is essential for inducing immunological protection or therapeutics with intramuscular administration [25]. This discrepancy may be due to an intrinsic property of self-antigens. EGFR immunological response has only been identified recently in cancer patients [45,46], which suggests that EGFR may be a poorer immunogen than HER2/neu. The conversion from cross-tolerance to cross-priming may be more difficult for EGFR. On the other hand, the MBT-2/C3H mouse tumor model may be more prone to immunological stimulation than the B16 melanoma cells and C57BL/6 animal model. Therefore, autologous neu DNA vaccine can successfully induce immunological therapeutic effects.

Altogether, the present study provides a basis for the clinical application of neu DNA vaccine. The route of immunization affects the selection of xenogenic DNA vaccine or autologous DNA vaccine. It will be of paramount importance to study the immunological interactions between resident DCs in various organs and the inflammatory cytokines induced by vaccines or tumors. This interaction may play an important role in determining the outcome of active immunization of DNA vaccines against neu or other tumor-associated antigens. The efficacy of neu DNA vaccine is only sufficient to delay the tumor progression, but is not sufficient to completely eradicate the existed tumor in our animal system. Further modification of vector and delivery method or combination with other therapeutic module is required to achieve complete response. Synthetic vectors can be modified much more flexibly than viral vectors [47]. Conjugation with cytokines [24], usage of tissue specific promoter [48], or combination of apoptosis-related molecules [49] may provide additional versatile immunological choice for gene therapy in the future.

4. Materials and methods

4.1. Animals, cell lines, and antibodies

Inbred female C3H/HeN mice (6–8 weeks of age) weighing 18–20 g were used. Animal experiments were approved by the National Cheng Kung University animal welfare committee. MBT-2 is a mouse transitional cell carcinoma cell line established by inducing mouse with the carcinogen *N*-[4-(5-nitro-2-furyl)-2-thiazolyl]formamide [24]. Monoclonal antibody (mAb) against the extracellular domain of mouse p185^{neu} (Ab-2; clone 9G6, Oncogene Science, Cambridge, MA) was used to detect surface expression of p185^{neu} in MBT-2 cells, via flow cytometry [24], and to detect the expression of N'-neu DNA vaccine in COS-1 cells.

4.2. Preparation of human and mouse *N'*-neu DNA expression vectors

MBT-2 cells were harvested and total RNA was isolated using a total RNA extraction system (Viogene-Biotek Corp., Hsichih, Taiwan) according to the manufacturer's instructions. The RNA was subjected to reverse transcriptase polymerase chain reaction (RT-PCR) for amplification of the extracellular domain of the mouse neu gene (mN'-neu) using the primers GCAATCGCAAGCTTATGGAGCTG-GCGGCCTGGTG and GCAATCGCGCGGCCGCTACT-GCTCTGCTGGGCAGCCTC. The extracellular domain of the human neu gene (hN'-neu) was generated from the PCR product of pSV2-neu (human) using the primers GCACCCGCAAGCTTATGGAGCTGGCGGCCTTGTG and TAAATATAGCGGCCGCTACTCGGCGGGGCAGC-CCT. The amplified products were cloned into the multiple cloning site of pRc/CMV (Invitrogen, San Diego, CA) to construct the expression vectors, pRc/CMV-mN'-neu and pRc/CMV-hN'-neu. All the constructs were confirmed by DNA sequencing.

4.3. Flow cytometric analysis of the expression of *N'*-neu DNA vaccine in vitro

The expression of DNA vaccine was confirmed in transfected COS-1 cells by flow cytometric analysis [24]. Transfected cells were monodispersed, washed with phosphate-buffered saline (PBS), fixed with 1% paraformaldehyde at room temperature for 10 min, and permeabilized with a buffer containing saponin (1%), NaN₃ (1%), and fetal bovine serum (FBS; 1%) for 10 min on ice. The fixed and permeabilized cells were stained with mAb against the N-terminal domain of mouse p185^{neu} (Ab-2; Oncogene Science, Cambridge, MA) and FITC-conjugated goat against mouse secondary Ab (Chemicon International, Temecula, CA). Normal mouse IgG mAb was used as the negative control.

4.4. Preparation and evaluation of DNA vaccines

Plasmid DNA was purified with Endofree Qiagen Plasmid Mega Kits (Qiagen, Chatsworth, CA) according to the manufacturer's instructions. DNA was then precipitated using isopropanol and resuspended in sterile saline at the concentration of 1 mg/ml. The endotoxin content was less than 20 U/mg of DNA, as determined by the *Limulus* amoebocyte lysate assay (Sigma Chemical Co., St. Louis, MO).

4.4.1. Intramuscular injection

Mice were injected subcutaneously in the flank with 1×10^6 MBT-2 cells in 0.5 ml PBS (day 0). Beginning on day 10 when tumors were palpable, 100 μ g of DNA vaccine in 0.1 ml sterile saline was administered intramuscularly in the upper thigh at weekly interval for three times. Control mice received three injections of only 0.1 ml of saline. Tumor

size was measured using a caliper two times a week. Tumor volume was calculated by the formula of a rational ellipsoid: ($m_1^2 \times m_2 \times 0.5236$), where m_1 represents the shorter axis and m_2 the longer axis. Mice were sacrificed when the tumor volume exceeded 2500 mm³ or the mouse was in poor condition and death was expected shortly. Significant differences were revealed by Kaplan-Meier analysis of survival rates.

4.4.2. Gene gun injection

Plasmid DNA was precipitated onto gold particles (Bio-Rad 1652263, Bio-Rad, Hercules, CA) for gene gun vaccination at the ratio of 1–2 μ g DNA per milligram gold particles. The gold particles and DNA solution were vortexed and sonicated for several seconds before adding 0.05 M spermidine and 2.5 M CaCl₂ solution with vortexing. This solution was placed on ice for 10 min. Gold particles were collected by centrifugation and washed three times with 100% ethanol. The particles were resuspended on in 100% ethanol as bullets with appreciate volume. Plasmid human-neu and mouse-neu DNA-coated gold particles were delivered to the shaved abdominal region of mice at a helium pressure of 50 psi using a low pressure-accelerated gene gun (BioWare Technologies Co. Ltd., Taipei, Taiwan).

4.5. Construction and transfection of *Sec*-mouse *N'*-neu/myc/His (*Sec*-mN-tag)

The extracellular domain of the mouse neu gene containing signal peptide was generated from the PCR product of pRc/CMV-mN'-neu using the primers GCAATCGCAAGCT-TATGGAGCTGGCGGCCTGGTG and GCAATCGCGCG-GCCGCTGCTGCTGGGCAGCCTC. The amplified products were cloned into the multiple cloning site of pcDNATM3.1/myc-His B (Invitrogen, San Diego, CA) to construct the expression vectors, Sec-mN-tag. The constructs were confirmed by DNA sequencing. Lipofectamine 2000 reagent was purchased from Invitrogen Technologies. Cos-7 cells were transfected with Sec-mN-tag plasmid. Transfected cells were passed into medium containing 800 μ g/ml of G418 (Promega) at 24 h after transfection. Positive colonies were further cloned by limiting of dilution.

4.6. Preparation of *secE2* for ELISA

The methods of preparing recombinant Sec-mN-tag protein as previously described [50]. Briefly, the medium was replaced with serum free hybridoma-Max (Gibco BRL) when COS-7-Sec-mN-tag cells were grown to 80% confluence. Cells were cultured for additional 4–5 days. Cell culture supernatants were harvested and filter through molecular-porous membrane (spectrum Laboratories Inc.) 2 days in 4 °C. A 10 \times concentrate of culture supernatants was prepared using freeze dryer (Labconco) according to the manufacturer's guidelines. One unit of recombinant Sec-mN-tag was defined as 1 ml of the 10-fold concentrated cell culture supernatant.

4.7. Determination of serum anti-neu antibody titer

Antibody titers were determined using an enzyme-linked immunosorbant assay (ELISA). A total of 50 U recombinant Sec-mN-tag protein was added to each well. The plate was incubated overnight at 4 °C. Nonspecific binding was blocked with 1% BSA in PBS, followed by three washes with PBS containing 0.05% Tween 20. Test sera were serially diluted (IgG and IgG1, 1:10,000; IgG2a and IgG2b, 1:25) and added to the plates to determine the titer of mouse anti-p185^{neu} antibody. For detection of mouse IgG, HRP-conjugated anti-mouse IgG (Calbiochem, Darmstadt, Germany) was used; detection of mouse IgG1, HRP-conjugated anti-mouse IgG1 (Pharmingen); detection of mouse IgG2a/IgG2b, HRP-conjugated anti-mouse IgG2a + IgG2b (Pharmingen) was used. Color development was facilitated using 3,3',5,5'-tetramethylbenzidine (TMB) as substrate. Absorbance was read at 450 nm with a microplate reader (Dynatech MR5000 plate reader).

4.8. Histological analysis of lymphocyte infiltration

Tumor tissues removed from vaccinated mice one week after the third vaccination were embedded in optimal cutting temperature (OCT) compound (Sakura Finetek Inc., USA) and then frozen in liquid nitrogen. Cryosections (5 µm) were fixed with 3.7% formaldehyde and acetone, washed with PBS three times, and incubated overnight at 4 °C with anti-CD4 (GK 1.5; BD Biosciences Pharmingen, San Jose, CA), anti-CD8 (53-6.7; Pharmingen), anti-macrophage (rm C5-3 for CD14; Pharmingen), or anti-pan-NK (DX5; Pharmingen) antibodies. After an additional reaction with peroxidase-conjugated secondary antibody, an aminoethylcarbazole substrate kit (Zymed Laboratories, San Francisco, CA) was used for color development. Immunohistochemical staining was analyzed independently in a blinded fashion by two observers. For quantification of immune infiltrating cells, we used a light microscope with a 10× eyepiece and a 40× objective lens. The total number of cells in five high-power fields was counted. Three samples from three mice were analyzed.

4.9. Generation and selection of stable transfected MBT-2-luciferase cell lines

The luciferase gene was cloned into the plasmid pCMV vector as previously described [24]. MBT-2 cells were transfected with the plasmid, and selected with G418 at the concentration of 800 µg/ml.

4.10. In vitro CTL induction and activity

Female C3H/HeN mice (6–8 weeks old) were injected with DNA vaccine three times as described above. A week after the third DNA vaccination, spleen cells were harvested and were grown in RPMI 1640 with 25 mM HEPES and L-glutamate (GibcoBRL, Rockville, MD), supplemented with

penicillin (100 U/ml), streptomycin (100 µg/ml), 50 mM 2-mercaptoethanol (ME), 100 U/ml penicillin, and 10% FBS. In addition, 500 U Sec-mN-tag protein were added. After 5 days of incubation, non-adherent cells were harvested as effector cells and plated with MBT-2 luciferase cells as target cells. Target cells of 5×10^3 /well were incubated for 18 h in triplicate at 37 °C with serial dilutions (50:1, 25:1, 12.5:1) of effector cells. After 18 h, cells were recovered by centrifugation and 100 µl of supernatant was obtained. The specific lysis was assessed in the supernatant using a conventional luciferase detection system (Promega, Madison, WI). One hundred microliter of the culture medium was mixed with 100 µl of the substrate (luciferin). The mixture was then placed into an EG & G (Berthold) MiniLumat LB9506 luminometer. Light emission was recorded for 10 s. Triplicate measurements were performed for each sample.

4.11. Depletion of CD8⁺ T cells

To deplete CD8⁺ T cells, murine anti-mouse CD8 (2.43; 500 µg), or control antibody (purified rat IgG; 500 µg) was injected intraperitoneally to mice. The first injection took place 2 days prior to DNA vaccination and at intervals of 7 days thereafter. The efficacy of depletion was evaluated by flow cytometry [24]. Single-cell suspension splenocytes (10^5) were obtained from anti-CD8 mAb-treated mice for immunostaining or PE-conjugated anti-CD8 mAb (53-6.7; Pharmingen), respectively.

Uncited reference

[31].

Acknowledgements

This study is supported by Grants NSC-93-3112-B-006-006 and 94-3112-B-006-011 from National Science Council, Taiwan, Republic of China.

References

- [1] Pupa SM, Tagliabue E, Menard S, Anichini A. HER-2: a biomarker at the crossroads of breast cancer immunotherapy and molecular medicine. *J Cell Physiol* 2005;205(1):10–8.
- [2] Choudhury A, Charo J, Parapuram SK, Hunt RC, Hunt DM, Seliger B, et al. Small interfering RNA (siRNA) inhibits the expression of the HER2/neu gene, upregulates HLA class I and induces apoptosis of HER2/neu positive tumor cell lines. *Int J Cancer* 2004;108(1):71–7.
- [3] Sliwkowski MX, Lofgren JA, Lewis GD, Hotaling TE, Fendly BM, Fox JA. Nonclinical studies addressing the mechanism of action of trastuzumab (Herceptin). *Semin Oncol* 1999;26(4 (Suppl. 12)): 60–70.
- [4] Warburton C, Dragowska WH, Gelmon K, Chia S, Yan H, Masin D, et al. Treatment of HER-2/neu overexpressing breast cancer xenograft models with trastuzumab (Herceptin) and gefitinib (ZD1839): drug combination effects on tumor growth, HER-2/neu and epidermal

- 516 growth factor receptor expression, and viable hypoxic cell fraction.
517 Clin Cancer Res 2004;10(7):2512-24.
- 518 [5] Osoba D, Slamon DJ, Burchmore M, Murphy M. Effects on quality
519 of life of combined trastuzumab and chemotherapy in women with
520 metastatic breast cancer. J Clin Oncol 2002;20(14):3106-13.
- 521 [6] Shak S. Overview of the trastuzumab (Herceptin) anti-HER2 mono-
522 clonal antibody clinical program in HER2-overexpressing metastatic
523 breast cancer. Herceptin Multinational Investigator Study Group. Semin
524 Oncol 1999;26(4 Suppl 12):71-7.
- 525 [7] Crone SA, Zhao YY, Fan L, Gu Y, Minamisawa S, Liu Y, et al. ErbB2
526 is essential in the prevention of dilated cardiomyopathy. Nat Med
527 2002;8(5):459-65.
- 528 [8] Grazette LP, Boecker W, Matsui T, Semigran M, Force TL, Hajjar RJ, et
529 al. Inhibition of ErbB2 causes mitochondrial dysfunction in cardiomyo-
530 cytes: implications for herceptin-induced cardiomyopathy. J Am Coll
531 Cardiol 2004;44(11):2231-8.
- 532 [9] Knutson KL, Almand B, Dang Y, Disis ML. Neu antigen-negative
533 variants can be generated after neu-specific antibody therapy in neu
534 transgenic mice. Cancer Res 2004;64(3):1146-51.
- 535 [10] Disis ML, Gralow JR, Bernhardt H, Hand SL, Rubin WD, Cheever
536 MA. Peptide-based, but not whole protein, vaccines elicit immu-
537 nity to HER-2/neu, oncogenic self-protein. J Immunol 1996;156(9):
538 3151-8.
- 539 [11] Nagata Y, Furugen R, Hiasa A, Ikeda H, Ohta N, Furukawa K, et
540 al. Peptides derived from a wild-type murine proto-oncogene c-erbB-
541 2/HER2/neu can induce CTL and tumor suppression in syngeneic hosts.
542 J Immunol 1997;159(3):1336-43.
- 543 [12] Disis ML, Schiffman K, Guthrie K, Salazar LG, Knutson KL, Goodell
544 V, et al. Effect of dose on immune response in patients vaccinated with
545 an her-2/neu intracellular domain protein-based vaccine. J Clin Oncol
546 2004;22(10):1916-25.
- 547 [13] Disis ML, Goodell V, Schiffman K, Knutson KL. Humoral epitope-
548 spreading following immunization with a HER-2/neu peptide based
549 vaccine in cancer patients. J Clin Immunol 2004;24(5):571-8.
- 550 [14] Rovero S, Amici A, Emma DC, Bei R, Nanni P, Quaglino E, et al.
551 DNA vaccination against rat Her-2/neu p185 more effectively inhibits
552 carcinogenesis than transplantable carcinomas in transgenic BALB/c
553 mice. J Immunol 2000;165(9):5133-42.
- 554 [15] Chen Y, Hu D, Eling DJ, Robbins J, Kipps TJ. DNA vaccines encoding
555 full-length or truncated Neu induce protective immunity against Neu-
556 expressing mammary tumors. Cancer Res 1998;58(9):1965-71.
- 557 [16] Amici A, Smorlesi A, Noce G, Santoni G, Cappelletti P, Capparuccia
558 L, et al. DNA vaccination with full-length or truncated neu induces
559 protective immunity against the development of spontaneous mam-
560 mmary tumors in HER-2/neu transgenic mice. Gene Ther 2000;7(8):
561 703-6.
- 562 [17] Wei WZ, Shi WP, Galy A, Lichlyter D, Hernandez S, Groner B, et al.
563 Protection against mammary tumor growth by vaccination with full-
564 length, modified human ErbB-2 DNA. Int J Cancer 1999;81(5):748-54.
- 565 [18] Pilon SA, Piechocki MP, Wei WZ. Vaccination with cytoplasmic ErbB-
566 2 DNA protects mice from mammary tumor growth without anti-ErbB-
567 2 antibody. J Immunol 2001;167(6):3201-6.
- 568 [19] Pupa SM, Iezzi M, Carlo ED, Invernizzi A, Cavallo F, Meazza R, et al.
569 Inhibition of mammary carcinoma development in HER-2/neu trans-
570 genic mice through induction of autoimmunity by xenogeneic DNA
571 vaccination. Cancer Res 2005;65(3):1071-8.
- 572 [20] Renard V, Sonderbye L, Ebbehøj K, Rasmussen PB, Gregorius K,
573 Gottschalk T, et al. HER-2 DNA and protein vaccines containing potent
574 Th cell epitopes induce distinct protective and therapeutic antitumor
575 responses in HER-2 transgenic mice. J Immunol 2003;171(3):1588-95.
- 576 [21] Curcio C, Di Carlo E, Clynes R, Smyth MJ, Boggio K, Quaglino
577 E, et al. Nonredundant roles of antibody, cytokines, and perforin in
578 the eradication of established HER-2/neu carcinomas. J Clin Invest
579 2003;111(8):1161-70.
- 580 [22] Quaglino E, Iezzi M, Mastini C, Amici A, Pericle F, Di Carlo E, et al.
581 Electroporated DNA vaccine clears away multifocal mammary carcino-
582 mas in HER-2/neu transgenic mice. Cancer Res 2004;64(8):2858-64.
- [23] Gallo P, Dharmapuri S, Nuzzo M, Maldini D, Iezzi M, Cavallo F, et al. 583
Xenogeneic immunization in mice using HER2 DNA delivered by an 584
adenoviral vector. Int J Cancer 2005;113(1):67-77. 585
- [24] Lin CC, Chou CW, Shiau AL, Tu CF, Ko TM, Chen YL, et al. 586
Therapeutic HER2/Neu DNA vaccine inhibits mouse tumor naturally over- 587
expressing endogenous neu. Mol Ther 2004;10(2):290-301. 588
- [25] Lu Y, Wei YQ, Tian L, Zhao X, Yang L, Hu B, et al. Immunogene 589
therapy of tumors with vaccine based on xenogeneic epidermal growth 590
factor receptor. J Immunol 2003;170(6):3162-70. 591
- [26] Pupa SM, Menard S, Andreola S, Colnaghi MI. Antibody response 592
against the c-erbB-2 oncoprotein in breast carcinoma patients. Cancer 593
Res 1993;53(24):5864-6. 594
- [27] Fisk B, Blevins TL, Wharton JT, Ioannides CG. Identification of an 595
immunodominant peptide of HER-2/neu protooncogene recognized 596
by ovarian tumor-specific cytotoxic T lymphocyte lines. J Exp Med 597
1995;181(6):2109-17. 598
- [28] Disis ML, Pupa SM, Gralow JR, Dittadi R, Menard S, Cheever 599
MA. High-titer HER-2/neu protein-specific antibody can be 600
detected in patients with early-stage breast cancer. J Clin Oncol 601
1997;15(11):3363-7. 602
- [29] Peoples GE, Goedegebuure PS, Smith R, Linehan DC, Yoshino I, Eber- 603
lein TJ. Breast and ovarian cancer-specific cytotoxic T lymphocytes 604
recognize the same HER2/neu-derived peptide. Proc Natl Acad Sci 605
USA 1995;92(2):432-6. 606
- [30] Smorlesi A, Papalini F, Amici A, Orlando F, Pierpaoli S, Mancini C, 607
et al. Evaluation of different plasmid DNA delivery systems for immu- 608
nization against HER2/neu in a transgenic murine model of mammary 609
carcinoma. Vaccine 2006;24(11):1766-75. 610
- [31] Drebin JA, Link VC, Greene MI. Monoclonal antibodies specific for 611
the neu oncogene product directly mediate anti-tumor effects in vivo. 612
Oncogene 1988;2(4):387-94. 613
- [32] Ferlazzo G, Tsang ML, Moretta L, Melioli G, Steinman RM, Munz C. 614
Human dendritic cells activate resting natural killer (NK) cells and are 615
recognized via the NKp30 receptor by activated NK cells. J Exp Med 616
2002;195(3):343-51. 617
- [33] Marschner A, Rothenfusser S, Hornung V, Prell D, Krug A, Kerk- 618
mann M, et al. CpG ODN enhance antigen-specific NKT cell acti- 619
vation via plasmacytoid dendritic cells. Eur J Immunol 2005;35(8): 620
2347-57. 621
- [34] Roda JM, Parihar R, Carson 3rd WE. CpG-containing oligodeoxynu- 622
cleotides act through TLR9 to enhance the NK cell cytokine response 623
to antibody-coated tumor cells. J Immunol 2005;175(3):1619-27. 624
- [35] Carson WE, Parihar R, Lindemann MJ, Personeni N, Dierksheide 625
J, Meropol NJ, et al. Interleukin-2 enhances the natural killer cell 626
response to Herceptin-coated HER2/neu-positive breast cancer cells. 627
Eur J Immunol 2001;31(10):3016-25. 628
- [36] Zeng Y, Fest S, Kunert R, Katinger H, Pistoia V, Michon J, et al. 629
Anti-neuroblastoma effect of ch14.18 antibody produced in CHO 630
cells is mediated by NK-cells in mice. Mol Immunol 2005;42(11): 631
1311-9. 632
- [37] Condon C, Watkins SC, Celluzzi CM, Thompson K, Falo Jr LD. DNA- 633
based immunization by *in vivo* transfection of dendritic cells. Nat Med 634
1996;2(10):1122-8. 635
- [38] Porgador A, Irvine KR, Iwasaki A, Barber BH, Restifo NP, Germain 636
RN. Predominant role for directly transfected dendritic cells in antigen 637
presentation to CD8⁺ T cells after gene gun immunization. J Exp Med 638
1998;188(6):1075-82. 639
- [39] Zimmermann VS, Bondanza A, Monno A, Rovere-Querini P, Corti 640
A, Manfredi AA. TNF-alpha coupled to membrane of apoptotic 641
cells favors the cross-priming to melanoma antigens. J Immunol 642
2004;172(4):2643-50. 643
- [40] Ackerman AL, Cresswell P. Cellular mechanisms governing cross- 644
presentation of exogenous antigens. Nat Immunol 2004;5(7):678-84. 645
- [41] Ferlazzo G, Wesa A, Wei WZ, Galy A. Dendritic cells generated 646
either from CD34⁺ progenitor cells or from monocytes differ in 647
their ability to activate antigen-specific CD8⁺ T cells. J Immunol 648
1999;163(7):3597-604. 649

- 650 [42] Ratzinger G, Baggers J, de Cos MA, Yuan J, Dao T, Reagan JL, et
651 al. Mature human Langerhans cells derived from CD34+ hematopoi-
652 etic progenitors stimulate greater cytolytic T lymphocyte activity in
653 the absence of bioactive IL-12p70, by either single peptide presenta-
654 tion or cross-priming, than do dermal-interstitial or monocyte-derived
655 dendritic cells. *J Immunol* 2004;173(4):2780–91.
- 656 [43] Yu Z, Theoret MR, Touloukian CE, Surman DR, Garman SC, Feigen-
657 baum L, et al. Poor immunogenicity of a self/tumor antigen derives
658 from peptide-MHC-I instability and is independent of tolerance. *J Clin*
659 *Invest* 2004;114(4):551–9.
- 660 [44] Houghton AN, Guevara-Patino JA. Immune recognition of self in
661 immunity against cancer. *J Clin Invest* 2004;114(4):468–71.
- 662 [45] Shomura H, Shichijo S, Komatsu N, Matsueda S, Mine T, Rikimaru
663 T, et al. Identification of epidermal growth factor receptor-derived
664 peptides recognised by both cellular and humoral immune responses
665 in HLA-A24+ non-small cell lung cancer patients. *Eur J Cancer*
2004;40(11):1776–86.
- [46] Shomura H, Shichijo S, Matsueda S, Kawakami T, Sato Y, Todo 666
S, et al. Identification of epidermal growth factor receptor-derived 667
peptides immunogenic for HLA-A2(+) cancer patients. *Br J Cancer* 668
2004;90(8):1563–71. 669
- [47] Wolff JA. The “grand” problem of synthetic delivery. *Nat Biotechnol* 670
2002;20(8):768–9. 671
- [48] Sudowe S, Ludwig-Portugall I, Montermann E, Ross R, Reske-Kunz 672
AB. Transcriptional targeting of dendritic cells in gene gun-mediated 673
DNA immunization favors the induction of type 1 immune responses. 674
Mol Ther 2003;8(4):567–75. 675
- [49] Kim TW, Lee JH, He L, Boyd DA, Hardwick JM, Hung CF, et al. 676
Modification of professional antigen-presenting cells with small inter- 677
fering RNA in vivo to enhance cancer vaccine potency. *Cancer Res* 678
2005;65(1):309–16. 679
- [50] Piechocki MP, Pilon SA, Wei WZ. Quantitative measurement of anti- 680
ErbB-2 antibody by flow cytometry and ELISA. *J Immunol Methods* 681
2002;259(1–2):33–42. 682

UNCORRECTED PROOF

Angiotensin II activates myostatin expression in cultured rat neonatal cardiomyocytes via p38 MAP kinase and myocyte enhance factor 2 pathway

Bao-Wei Wang^{1,2}, Hang Chang³, Peiliang Kuan¹ and Kou-Gi Shyu^{1,4}

¹Division of Cardiology, Shin Kong Wu Ho-Su Memorial Hospital, 95 Wen-Chang Road, Taipei 111, Taiwan, ROC

²School of Medicine, Fu-Jen Catholic University, Taipei County 242, Taiwan, ROC

³Department of Emergency Medicine, Shin Kong Wu Ho-Su Memorial Hospital, Taipei, Taiwan, ROC

⁴College of Medicine, Graduate Institute of Clinical Medicine (KGS), Taipei Medical University, Taipei 110, Taiwan, ROC

(Correspondence should be addressed to K-G Shyu; Email: shyukg@ms12.hinet.net)

Abstract

Angiotensin II (AngII) plays a critical role in cardiac remodeling and promotes cardiac myocyte hypertrophy. Myostatin, a negative regulator of muscle growth, is increased in hypertrophied and infarcted heart. The direct effect of AngII on cardiac myocyte myostatin expression has not been previously investigated. We hypothesized that myostatin may act as a cardiac endocrine inhibitor for AngII. AngII-induced myostatin protein expression in cultured rat neonatal cardiomyocytes was dose-dependent. AngII significantly increased myostatin protein and mRNA expression in a time-dependent manner. Addition of losartan, SB203580, or p38 siRNA 30 min before AngII stimulation significantly

blocked the increase of myostatin protein by AngII. AngII significantly increased phosphorylation of p38 while SB203580 and losartan attenuated the phosphorylation of p38 induced by AngII. AngII increased, while myostatin-Mut plasmid, SB203580, losartan, and myocyte enhance factor 2 (MEF-2) antibody abolished the myostatin promoter activity. Co-stimulation with myostatin and AngII significantly inhibited the protein synthesis induced by AngII. In conclusion, AngII enhances myostatin expression in cultured rat neonatal cardiomyocytes. The AngII-induced myostatin is mediated through p38 MAP kinase and MEF-2 pathway.

Journal of Endocrinology (2008) **197**, 85–93

Introduction

Angiotensin II (AngII) plays a critical role in cardiac remodeling and promotes cardiac myocyte hypertrophy (Schnee & Hsueh 2000). Excess of AngII can lead to cardiac dysfunction and failure. Myostatin is a transforming growth factor- β family member that plays an essential role in regulating skeletal muscle growth (McPherron *et al.* 1997, Lee & McPherron 2001). Like other transforming growth factor- β , myostatin is translated into a precursor protein that is proteolytically cleaved to yield the N-terminal, latency-associated peptide (LAP) and the C-terminal, mature processed peptide before secretion from the cell (Thies *et al.* 2001). Myostatin is expressed in fetal and adult hearts and its expression is upregulated in cardiomyocytes after infarction (Sharma *et al.* 1999). Recently, myostatin was found to be dramatically upregulated in hypertrophied hearts with transgenic overexpression of Akt (Cook *et al.* 2002). Since myostatin plays a role in limiting skeletal muscle growth, the upregulation of myostatin in hypertrophic heart may represent a negative feedback mechanism of myostatin in cardiac myocytes to inhibit the overgrowth of cardiac

myocytes. We have demonstrated that the myostatin gene is mechanically responsive in cardiac myocytes (Shyu *et al.* 2005). Mechanical stretch increases the release of AngII from cardiac myocytes (Sadoshima *et al.* 1993, Shyu *et al.* 2001). AngII mediates cardiac myocyte growth and myostatin is secreted by cardiac myocytes and accumulates until it reaches a threshold causing inhibition of cardiac growth. The direct effect of AngII on cardiac myocyte myostatin expression has not been previously investigated. An endocrine inhibitor is secreted by specific tissues and provides a negative feedback mechanism to control the size of the tissue producing it (Gaussin & Depre 2005). We hypothesized that myostatin may act as a cardiac endocrine inhibitor for AngII.

Myocyte enhance factor 2 (MEF-2) transcription factors are critically involved in the regulation of inducible gene expression during myocardial hypertrophy and MEF-2-DNA-binding activity is increased in the rat hearts by pressure or volume overload (Akazawa & Komuro 2003). The transactivation activity of MEF-2A and MEF-2C is stimulated by p38 MAP kinase (Zetser *et al.* 1999, Zhao *et al.* 1999). The myostatin gene upstream region contains MEF-2 site, and muscle-specific expression of myostatin appears to be regulated by MEF-2

(Spiller *et al.* 2002). Mechanical stretch induced myostatin expression via p38 MAP kinase and MEF-2 pathway (Shyu *et al.* 2005). Since AngII is secreted from cardiac myocytes by mechanical stretch, we hypothesized that myostatin-induced by AngII is via p38 MAP kinase and MEF-2 pathway.

Materials and Methods

Primary cardiac myocyte culture

Cardiac myocytes were obtained from Wistar rats, aged 2–3 days old, by trypsinization as previously described (Shyu *et al.* 2001). Cultured myocytes thus obtained were >95% pure as revealed by observation of contractile characteristics with a light microscope and stained with anti-desmin antibody (Dako Cytomation, Glostrup, Denmark). The study conforms to Guide for the Care and Use of Laboratory Animals published by the US National Institutes of Health (NIH Publication No. 85-23, revised 1996). Various concentrations of AngII were added to the culture medium. To determine the roles of c-Jun N-terminal kinase (JNK), p38 MAP kinase, p42/p44 MAP kinase, or phosphatidylinositol-3 (PI-3) kinase in the expression of AngII-induced myostatin expression, myocytes were pretreated with SP600125 (20 μ M, Calbiochem, San Diego, CA, USA), SB203580 (3 μ M, Calbiochem), PD98059 (50 μ M, Calbiochem), or wortmannin (5 nM, Sigma Chemical) for 30 min, respectively, followed by addition of AngII. The SP600125 is a potent, cell-permeable, selective, and reversible inhibitor of JNK. The SB203580 is a highly specific, cell-permeable inhibitor of p38 kinase. The PD98059 is a specific and potent inhibitor of p42/p44 MAP kinase. Wortmannin is a potent and specific inhibitor of PI-3 kinase. In experiments involving the AngII receptor antagonist, losartan at 100 nM was added 30 min before AngII stimulation.

Western blot analysis

Western blot was performed as previously described (Shyu *et al.* 2004). Rabbit polyclonal anti-myostatin antibody (Chemicon, Temecula, CA, USA), polyclonal anti-p38 MAP kinase, monoclonal anti-phospho p38 MAP kinase antibodies (Cell Signaling, Beverly, MA, USA), goat polyclonal antibody against total MEF-2 (Santa Cruz Biotechnol Inc., Santa Cruz, CA, USA), and rabbit polyclonal antibody against phosphorylated MEF-2 (Santa Cruz Biotechnol Inc.) were used. Equal protein loading of the samples was verified by staining monoclonal antibody GAPDH or α -tubulin. All western blots were quantified using densitometry.

Northern blot analysis

Total RNA was prepared by solubilizing myocytes in Ultraspec RNA kit (Biotecx Laboratory Inc., Houston, TX, USA). Aliquots of 20 μ g total RNA were fractionated in formaldehyde agarose gels, transferred to Hybond-N⁺ nylon

membrane, and hybridized with [α ³²-P]dCTP-labeled cDNA probes, generated from mouse myostatin cDNA. The northern blot was performed as previously described (Shyu *et al.* 2001).

Electrophoretic mobility shift assay

Nuclear protein concentrations from cultured cardiomyocytes were determined by Bio-Rad protein assay. Consensus and control oligonucleotides (Santa Cruz Biotechnology Inc., Santa Cruz, CA, USA) were labeled by polynucleotides kinase incorporation of [γ ³²P]-dATP. The oligonucleotides sequences included the MEF-2 consensus 5'-GATCGCTCTAAAAATA-ACCCTGTCG-3'. The MEF-2 mutant oligonucleotides sequences were 5'-GATCGCTGTAAACATAACCCTGTCG-3'. After the oligonucleotide was radiolabeled, the nuclear extracts (4 μ g protein in 2 μ l nuclear extract) were mixed with 20 pmol of the appropriate [γ ³²P]-dATP-labeled consensus or mutant oligonucleotide in a total volume of 20 μ l for 30 min at room temperature. The samples were then resolved on a 4% polyacrylamide gel. Gels were dried and imaged by autoradiography. Controls were performed in each case with mutant oligonucleotides or cold oligonucleotides to compete with labeled sequences.

Promoter activity assay

A-1977 to +32 bp mouse myostatin promoter construct (a gift from Prof WS Yang National Taiwan University, Taiwan) was generated. The myostatin promoter contains MEF-2 conserved sites (CTAAAAAATAA) at -637 to -646 bp. For the mutant, the MEF-2 binding sites were mutated using the mutagenesis kit (Stratagene, La Jolla, CA, USA). Site-specific mutations were confirmed by DNA sequencing. Plasmids were transfected into cardiomyocytes using a low pressure-accelerated gene gun (Bioware Technologies, Taipei, Taiwan, ROC) essentially following the manufacturer's protocol. In brief, 2 μ g plasmid DNA were suspended in 5 μ l PBS and were delivered to the cultured myocytes at a helium pressure of 15 psi. The transfection efficiency using this method is 25%. Following 6 h of AngII stimulation, cell extracts were prepared using Dual-Luciferase Reporter Assay System (Promega) and measured for dual luciferase activity by luminometer (Turner Designs, Sunnyvale, CA, USA).

RNA interference

Neonatal cardiomyocytes were transfected with 800 ng p38 annealed siRNA oligonucleotide according to the manufacturer's instructions (Santa Cruz Biotechnology Inc.). The p38 siRNA is a target-specific 20–25 nt siRNA designed to knock down gene expression of p38 α and p38 β . As a negative control, a non-targeting siRNA (control siRNA) purchased from Dharmacon (Dharmacon Inc., Lafayette, CO, USA) was used. Neonatal cardiomyocytes were transfected with siRNA oligonucleotides using Effectene Transfection Reagent as

suggested by the manufacturer (Qiagen Inc). After incubation at 37 °C for 24 h, cardiac myocytes were stretched for 18 h, and subjected to analysis of western blot. The effect of p38 siRNA transfection was verified by the downregulation of p38 protein when compared with control siRNA.

Protein synthesis assay

Cardiomyocytes were cultured with serum-free medium in ViewPlate for 60 min (Packard Instrument Co., Meriden, CT, USA). AngII (10 nM) and myostatin (100 ng/ml) were added to the medium. The cells were then labeled with 100 μ Ci/ml [³⁵S]-methionine for various periods of time. Losartan, a selective antagonist of the AngII receptor, was added to the medium 30 min before addition of AngII. The cells were washed with PBS twice. Then, 50 μ l MicroScint-20 were added and the plate was read with TopCount (Packard Instrument Co).

Statistical analysis

The data were expressed as mean \pm s.d. Statistical significance was performed with ANOVA (GraphPad Software Inc., San Diego, CA, USA). The Tukey–Kramer comparison test was used for pairwise comparisons between multiple groups after ANOVA. $P < 0.05$ was considered to denote statistical significance.

Results

AngII enhances myostatin protein expression in cardiomyocytes

The western blot showed the three forms of myostatin detected by the polyclonal anti-myostatin antibody and the relative sizes of precursor, LAP, and processed myostatin in cardiomyocytes (Fig. 1). These data indicate that myostatin protein is synthesized in neonatal cardiomyocytes and that the precursor myostatin is processed in cardiomyocytes. AngII induced both precursor and processed myostatin. The levels of processed myostatin were used to represent the myostatin protein expression in the present study. The AngII-induced myostatin protein expression was dose-dependent. AngII at 10 nM showed the maximal effect to enhance myostatin protein expression in neonatal cardiomyocytes. Therefore, the concentration of AngII used for the following experiments is 10 nM. Addition of losartan (100 nM, an antagonist of the AngII receptor), 30 min before AngII treatment completely inhibited the increase of myostatin induced by AngII.

AngII increases myostatin protein and mRNA expression in cardiomyocytes

As shown in Fig. 2, exogenous addition of AngII at 10 nM for 18 h significantly increased the myostatin protein expression and the myostatin expression remained elevated up to 48 h.

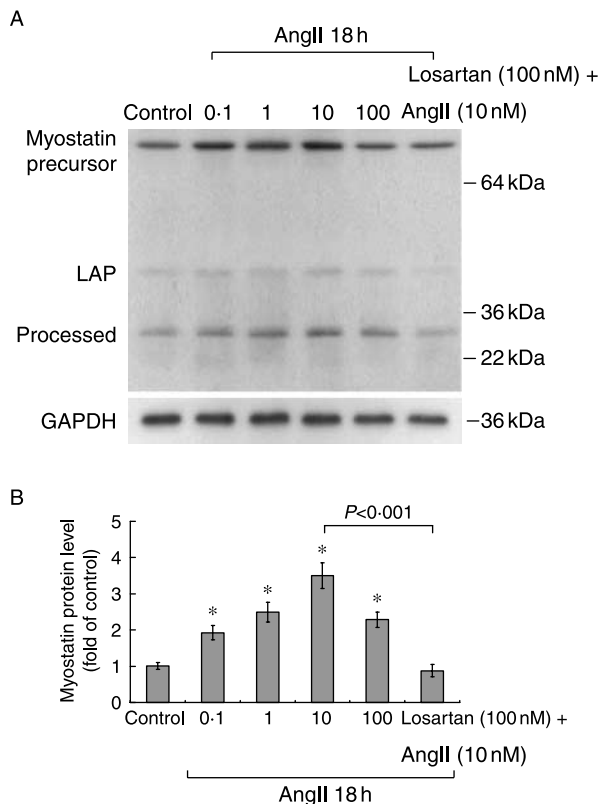


Figure 1 Angiotensin II (AngII) increases myostatin expression in cardiomyocytes. (A) Representative western blots for myostatin in cardiomyocytes treated with different concentrations of AngII for 18 h. Precursor, latency-associated peptide (LAP), and processed forms of myostatin are indicated. (B) Quantitative analysis of myostatin protein levels. The processed myostatin protein was measured. The values from treated myocytes have been normalized to values in control cells ($n = 4$ per group). * $P < 0.001$ versus control.

The northern blots showed that myostatin message to RNAs began to increase as early as 6 h of AngII stimulation at 10 nM, reached a maximum of 3.3-fold over the control by 18 h and remained elevated up to 48 h (Fig. 3).

AngII increases myostatin protein expression mainly through p38 MAP kinase

AngII at 10 nM significantly increased the myostatin protein expression when compared with control ($P < 0.01$, Fig. 4A and B). The western blot demonstrated that the increase of AngII-induced myostatin protein was almost completely attenuated after the addition of SB203580 (a highly specific, cell-permeable inhibitor of p38 kinase), 30 min before AngII stimulation. Addition of PD98059 (a specific and potent inhibitor of p42/p44 MAP kinase) significantly, but partially inhibited the increase of myostatin protein induced by AngII. The myostatin protein induced by AngII was not affected by the addition of SP600125 (a potent, cell-permeable, selective, and reversible inhibitor of JNK) or wortmannin (a potent and

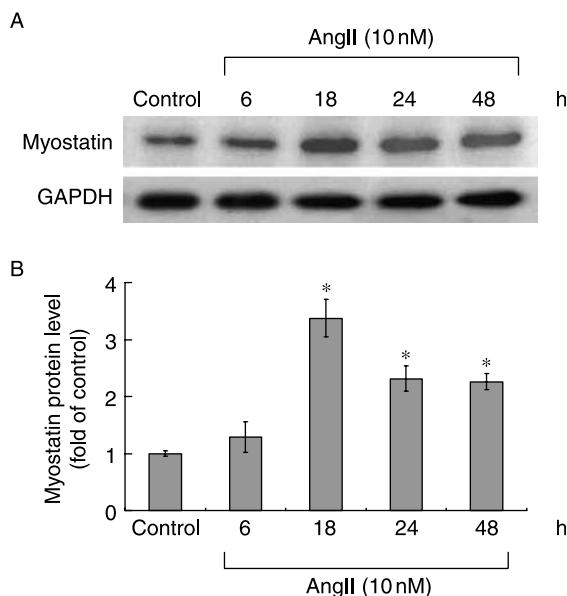


Figure 2 AngII increases myostatin protein expression in cardiomyocytes. (A) Representative western blots for myostatin in cardiomyocytes subjected to 10 nM AngII stimulation for various periods of time. (B) Quantitative analysis of myostatin protein levels. The values from stimulated myocytes have been normalized to values in control cells ($n=4$ per group). * $P<0.001$ versus control.

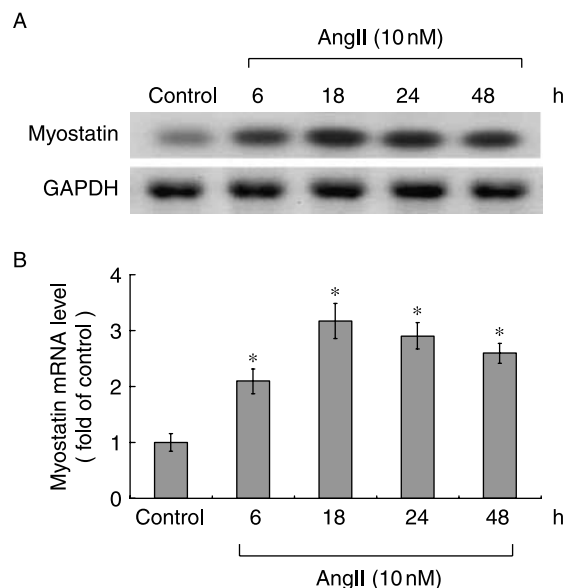


Figure 3 AngII increases myostatin mRNA expression in cardiomyocytes. (A) Representative northern blot for myostatin mRNA in cardiomyocytes subjected to various periods of time of AngII stimulation at 10 nM. (B) Quantitative analysis of myostatin mRNA levels. The values from stimulated myocytes have been normalized to matched GAPDH measurement and then expressed as a ratio of normalized values to mRNA in control cells ($n=4$ per group). * $P<0.001$ versus control.

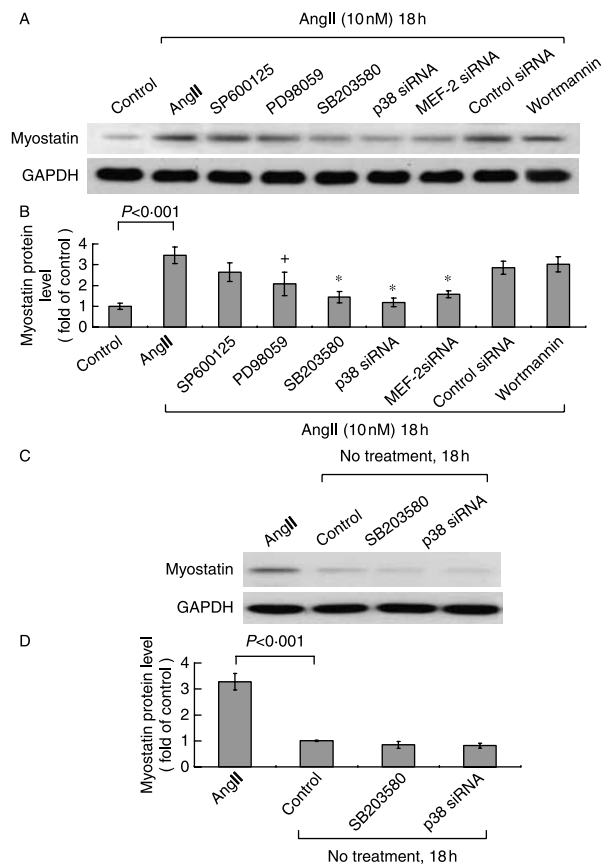


Figure 4 The p38 MAP kinase is an important regulator that mediates AngII-induced myostatin expression in myocytes. (A and C) Representative western blots for myostatin protein levels in myocytes subjected to AngII stimulation for 18 h or control cells without stimulation in the absence or presence of inhibitors, and siRNA. (B and D) Quantitative analysis of myostatin protein levels. The values from stimulated myocytes have been normalized to values in control cells ($n=4$ per group). * $P<0.001$ versus control, + $P<0.01$ versus AngII.

specific inhibitor of PI-3 kinase). To test the specific effect of p38 MAP kinase pathway mediating the expression of myostatin, p38 siRNA was transfected to neonatal cardiomyocytes before AngII stimulation. As shown in Fig. 4A and B, p38 siRNA also completely blocked the myostatin expression induced by AngII ($P<0.001$). The control siRNA did not affect the myostatin protein expression induced by AngII. The SB203580 and p38 siRNA did not affect the myostatin expression in control cells without AngII treatment (Fig. 4C and D). As shown in Fig. 5A and B, phosphorylated p38 protein was induced by AngII stimulation for 6 and 18 h. The phosphorylated p38 proteins induced by AngII was abolished by p38 siRNA, SB203580, and losartan. These findings implicate that p38 MAP kinase is an important regulator that mediates the induction of myostatin protein by AngII in cardiomyocytes. Exogenous addition of p38 MAP kinase activator, anisomycin (50 μ M),

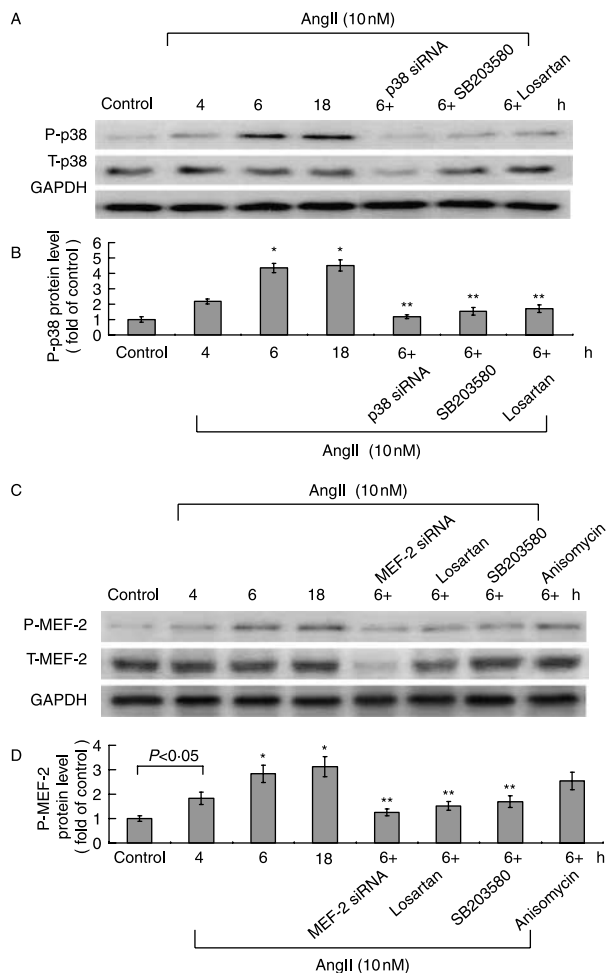


Figure 5 Expression of p38 MAP kinase and MEF-2 in myocytes. (A) Representative western blots for phosphorylated and total p38 MAP in myocytes after treatment with AngII at 10 nM for 6–18 h with or without inhibitor. (B) Quantitative analysis of phosphorylated protein levels. (C) Representative western blots for phosphorylated and total MEF-2 protein in myocytes after treatment with AngII at 10 nM for 6–18 h with or without inhibitor. (D) Quantitative analysis of phosphorylated MEF-2 protein levels. The values from treated myocytes have been normalized to matched GAPDH and corresponding total protein measurement and then expressed as a ratio of normalized values to each phosphorylated protein in control cells ($n=4$ per group). * $P<0.001$ versus control, ** $P<0.001$ versus 6 h.

to the myocytes without any treatment also increased the myostatin protein expression (data not shown). AngII induced the phosphorylated MEF-2 protein in a time-dependent manner (Fig. 5C and D). The MEF-2 siRNA, losartan, and SB203580 attenuated the phosphorylated MEF-2 protein induced by AngII treatment. Addition of anisomycin to the control cells without AngII treatment significantly increased the phosphorylated MEF-2 protein. These data indicate that p38 MAP kinase was activated before the MEF-2 stimulation and p38 MAP kinase stimulated the phosphorylated MEF-2

protein expression, clarifying the sequence of the p38 MAP kinase activation and the MEF-2 stimulation.

AngII increases MEF-2-binding activity

Stimulation of myocytes with AngII at 10 nM for 4–18 h significantly increased the DNA–protein-binding activity of MEF-2 (Fig. 6). An excess of the unlabeled MEF-2 oligonucleotide competed with the probe for binding the MEF-2 protein, whereas an oligonucleotide containing a 2 bp substitution in the MEF-2 binding site did not compete for binding. Addition of SB203580 or losartan 30 min before AngII stimulation abolished the DNA–protein-binding activity induced by AngII. DNA-binding complexes induced by AngII could be supershifted by a specific MEF-2 monoclonal antibody and IgG antibody did not affect the DNA-binding activity, indicating the presence of this protein in these complexes.

AngII increases myostatin promoter activity through MEF-2

To study whether the myostatin expression induced by AngII is regulated at the transcriptional level, we cloned the promoter region of rat myostatin (–1977 ~ +32), and constructed a luciferase reporter plasmid (pGL3-Luc). The myostatin promoter construct contains HIF-1 α , CREB, MEF-2, Myc–Max, Smad3/4, GATA, and Ets-binding sites. As shown in Fig. 7, transient transfection experiment in cardiomyocytes using this reporter gene revealed that AngII stimulation for 6 h significantly caused myostatin promoter activation. This result indicated that myostatin expression is induced at the transcriptional level by AngII. When the MEF-2 binding sites were mutated, the increased promoter activity induced by AngII was abolished. Moreover, addition

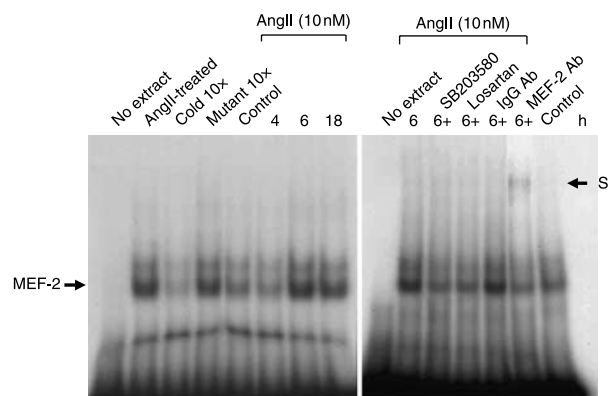


Figure 6 AngII increases MEF-2-binding activity. Representative EMSA showing protein binding to the MEF-2 oligonucleotide in nuclear extracts of cardiomyocytes after AngII treatment in the presence or absence of inhibitors. Arrow indicates the mobility of the complex. Similar results were found in another two independent experiments. Cold oligo means unlabeled MEF-2 oligonucleotides. A significant supershifted complex (S) after incubation with MEF-2 antibody was observed.

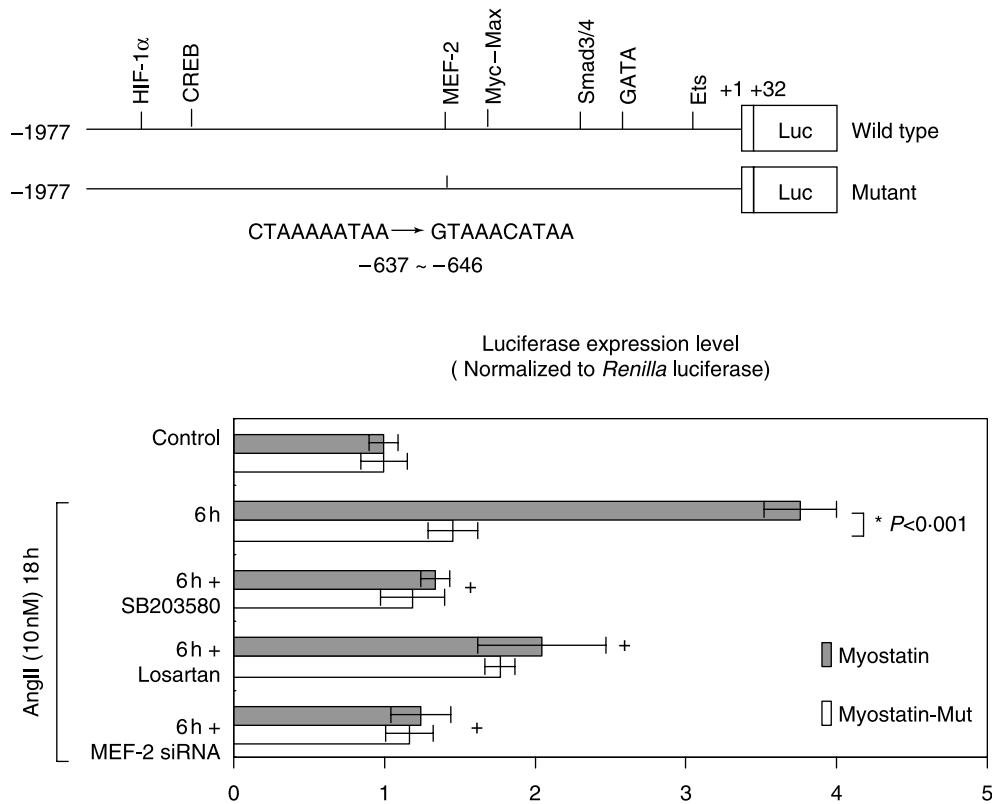


Figure 7 Effect of AngII on myostatin promoter activity in cardiomyocytes. (A) Constructs of myostatin promoter gene. Positive +1 demonstrates the initiation site for the myostatin transcription. (B) Quantitative analysis of myostatin promoter activity. Cardiomyocytes were transiently transfected with pGL3-Luc by gene gun. The luciferase activity in cell lysates was measured and was normalized with *Renilla* activity ($n=3$ per group). * $P<0.001$ versus control, + $P<0.001$ versus 6 h.

of SB203580, losartan, and MEF-2 siRNA caused an inhibition of transcription. These results indicate that MEF-2-binding site in the myostatin promoter, AngII receptor, and p38 pathways are essential for the transcriptional regulation by AngII.

AngII increases and myostatin inhibits protein synthesis

To study the functional consequences of myostatin expression by cardiomyocytes, [35 S]methionine incorporation assay was performed. Stimulation with AngII at 10 nM for 6–48 h increased protein synthesis for 2- and 2.2-fold, respectively, in cardiomyocytes when compared with control cells without treatment (Fig. 8). Exogenous addition of myostatin at 100 ng/ml alone did not increase the protein synthesis. Co-stimulation with myostatin at 100 ng/ml and AngII at 10 nM significantly inhibited the protein synthesis induced by AngII. Addition of losartan 30 min before AngII stimulation significantly attenuated the protein synthesis by AngII. The protein synthesis was similar between addition of SB203580, 30 min before AngII stimulation and AngII stimulation alone. Protein synthesis was lower in the group of co-stimulation of

AngII with myostatin than in the group of AngII with SB203580 ($P<0.05$). This result indicates that the primary effect of the p38 MAP kinase activation is stimulation of myostatin expression, but not stimulation of cell growth. Our data indicate that the catabolic effect might be induced by increased myostatin in cardiomyocytes.

Discussion

In this study, we demonstrated that AngII upregulates myostatin expression in cardiomyocytes, and p38 MAP kinase and MEF-2 transcription factor are involved in the signaling pathway of myostatin induction. AngII plays a critical role in cardiac remodeling and promotes cardiac myocyte hypertrophy (Schnee & Hsueh 2000). Cardiac myocytes respond to increased mechanical load and hormonal stimulation by hypertrophic growth, but mechanical stress or hormonal factor is also an important stimulus for triggering the initial steps toward cardiac myocytes degeneration and death, which play a critical role in the maladaptive myocardial remodeling and heart failure (Torsoni *et al.* 2003). Myostatin has been shown to regulate

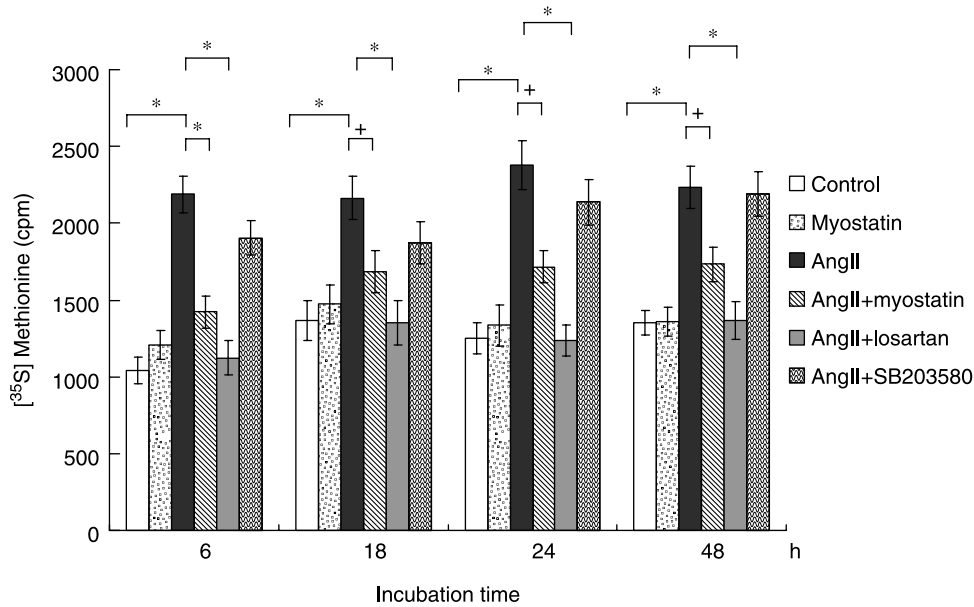


Figure 8 Effect of AngII and myostatin on protein synthesis by [³⁵S]methionine incorporation assay. * $P < 0.001$, + $P < 0.01$ ($n = 3$ per group).

cardiomyocyte growth through the modulation of Akt signaling (Morissette *et al.* 2006). More recently, two studies reported that myostatin is an inhibitor of cardiomyocyte proliferation and reduces cardiac mass (Atraza *et al.* 2007, McKoy *et al.* 2007), while one study reported that myostatin does not regulate cardiac hypertrophy or fibrosis (Cohn *et al.* 2007). Therefore, the effect of myostatin on cardiac hypertrophy is controversial. The functional role of myostatin in cardiac remodeling is unclear and understanding its regulatory mechanism under hormonal stimulation may help to reveal more insights. Given the role of myostatin in limiting skeletal muscle growth, the upregulation of myostatin in AngII-treated cardiomyocytes may represent a negative feedback mechanism to counteract the pathologic hypertrophy effect of AngII. Actually, in the present study, we have demonstrated that the AngII-induced protein synthesis was inhibited by co-stimulation with myostatin. Angiotensin receptor blocker inhibited the cardiac hypertrophy effect of AngII. Without AngII stimulation, exogenous addition of myostatin did not have effect on cardiac hypertrophy. These results indicate that the actions of AngII on hypertrophy and myostatin expression are counter-intuitive.

Sadoshima *et al.* (1993) and our group have demonstrated that mechanical stretch enhances AngII secretion from cardiomyocytes (Shyu *et al.* 2001). In the present study, we have demonstrated that losartan significantly blocked the increase of myostatin protein by AngII. These data indicated that AngII increases myostatin expression in cardiomyocytes through AngII type 1 receptor. The response of myostatin in cardiomyocytes to AngII may strongly suggest that myostatin represents an endocrine inhibitor of the AngII pathway in the heart. Zou *et al.* (2004) have demonstrated that mechanical stress activates

AngII type 1 receptor without the involvement of AngII. However, in that study, short period (5–8 min) of mechanical stress was applied. Previous study and our group used longer period (more than 4 h) of mechanical stress. Different periods of stress may have different activated mechanisms in cardiac hypertrophy. We have demonstrated that mechanical stretch enhances myostatin expression in cultured rat neonatal cardiomyocytes through insulin-like growth factor (IGF-1; Shyu *et al.* 2005). The interaction of AngII and IGF-1 in ventricular myocardium has been previously investigated in animal models (Brink *et al.* 1999, Leri *et al.* 1999). The AngII infusion has been demonstrated to stimulate cardiac IGF-1 gene expression but reduces circulating IGF-1 levels (Brink *et al.* 1999). Constitutive overexpression of IGF-1 in myocytes downregulates AngII formation (Leri *et al.* 1999). IGF-1 is synthesized by almost all tissues and is an important mediator of cell growth, differentiation, and transformation (Delafontaine *et al.* 2004). IGF-1 is an important growth and survival factor for cardiac muscle cell (Wang *et al.* 1998). IGF-1 is induced in pathological myocardium such as left ventricular hypertrophy and myocardial infarction, and in normal myocardium such as mechanical stress (Donohue *et al.* 1994, Loennechen *et al.* 2001, Palmieri *et al.* 2001). Our study confirms the autocrine or paracrine production of cardiomyocytes in response to AngII stimulation. Cachexia has been observed in patients with chronic severe heart failure (Anker *et al.* 2004). The AngII infusion causes weight loss and skeletal muscle wasting in rats (Song *et al.* 2005). Excess myostatin could induce cachexia in mice and myostatin may be involved in human cachexia (Zimmers *et al.* 2002). AngII is implicated in pathophysiological processes associated with cardiac hypertrophy and remodeling,

and the induction of myostatin by AngII may serve to ameliorate the effects of excess hypertrophy. The role of myostatin in human cachexia due to chronic heart failure needs further study.

The MEF-2 transcription factors are critically involved in the regulation of inducible gene expression during myocardial hypertrophy and MEF-2-DNA-binding activity is increased in the rat hearts of pressure or volume overload (Akazawa & Komuro 2003). The myostatin gene upstream region contains MEF-2 site and muscle-specific expression of myostatin appears to be regulated by MEF-2 (Zhao *et al.* 1999). Although p38 MAP kinase is an important transducer of growth and stress stimuli in virtually all eukaryotic cell types, the role of p38 MAP kinase signaling in cardiac hypertrophy is controversial (Liang & Molkentin 2003). The p38 MAP kinase has been shown to play a critical role in stretch-induced cardiomyocyte hypertrophy (Aikawa *et al.* 2002). Our results suggest that AngII is responsible for MEF-2-DNA binding in cardiomyocytes. In this study, we demonstrated that AngII stimulation of MEF-2-DNA-binding activity required at least phosphorylation of the p38 since p38 inhibitor, SB203580, abolished the MEF-2-binding activity. The SB203580, a potent and specific inhibitor of p38 MAP kinase, completely inhibited the myostatin expression induced by AngII, while inhibitor of PI-3 kinase did not have the inhibitory effect and inhibitors of JNK and p42/p44 MAP kinase had partial inhibitory effect. These data implicated that the p38 MAP kinase pathway, but not the JNK, p42/p44 MAP, and PI-3 kinase pathway is an important signaling pathway that mediates the increased transcriptional activity of MEF-2. Recently, Yang *et al.* (2007) reported that myostatin inhibits skeletal muscle proliferation through PI-3 kinase pathway. The regulation pathway for myostatin may be different in different cell types.

In summary, AngII enhances myostatin expression in cultured rat neonatal cardiomyocytes. The AngII-induced myostatin is mediated at least in part, through p38 MAP kinase and MEF-2 pathway.

Acknowledgements

This study was supported in part by Shin Kong Wu Ho-Su Memorial Hospital, Taipei, Taiwan and National Science Council, Taiwan. No conflict of interests for all authors.

References

Aikawa R, Nagai T, Kudoh S, Zou Y, Tanaka M, Tamura M, Kazawa H, Takano H, Nagai R & Komuro I 2002 Integrins play a critical role in mechanical stress-induced p38 MAPK activation. *Hypertension* **39** 233–238.
 Akazawa H & Komuro I 2003 Roles of cardiac transcription factors in cardiac hypertrophy. *Circulation Research* **92** 1079–1088.
 Anker SD, Steinborn W & Strassbourg S 2004 Cardiac cachexia. *Annals of Medicine* **36** 518–529.

Atraza JN, Reisz-Porszasz S, Dow JS, Kloner RA, Tsao J, Bhasin S & Gonzalez-Cadavid NF 2007 Alteration in myostatin expression are associated with changes in cardiac left ventricular mass but not ejection fraction in the mouse. *Journal of Endocrinology* **194** 63–76.
 Brink M, Chrast J, Price R, Mitch WE & Delafontaine P 1999 Angiotensin II stimulates gene expression of cardiac insulin-like growth factor 1 and its receptor through effects on blood pressure and food intake. *Hypertension* **34** 1053–1059.
 Cohn RD, Liang HY, Shetty R, Abraham T & Wanger KR 2007 Myostatin does not regulate cardiac hypertrophy or fibrosis. *Neuromuscular Disorders* **17** 290–296.
 Cook SA, Matsui T, Li L & Bosenzweig A 2002 Transcriptional effects of chronic Akt activation in the heart. *Journal of Biological Chemistry* **277** 22528–22533.
 Delafontaine P, Song YH & Li Y 2004 Expression, regulation, and function of IGF-I, IGF-1R, and IGF-1 binding proteins in blood vessels. *Arteriosclerosis, Thrombosis, and Vascular Biology* **24** 435–444.
 Donohue TJ, Dworkin LD, Lango MN, Fliegner K, Lango RP, Benetein JA, Slater WR & Catanese VM 1994 Induction of myocardial insulin-like growth factor-1 gene expression in left ventricular hypertrophy. *Circulation* **89** 799–809.
 Gaussin V & Depre C 2005 Myostatin, the cardiac chalone of insulin-like growth factor-1. *Cardiovascular Research* **68** 347–349.
 Lee SJ & McPherron AC 2001 Regulation of myostatin activity and muscle growth. *PNAS* **98** 9306–9311.
 Leri A, Liu Y, Wang X, Kajstura J, Malhotra A, Meggs LG & Anversa P 1999 Overexpression of insulin-like growth factor-1 attenuates the myocyte rennin-angiotensin system in transgenic mice. *Circulation Research* **84** 752–762.
 Liang Q & Molkentin JD 2003 Redefining the roles of p38 and JNK signaling in cardiac hypertrophy: dichotomy between cultured myocytes and animal models. *Journal of Molecular and Cellular Cardiology* **35** 1385–1394.
 Loennechen JP, Stoylen A, Beisvang V, Wisloff U & Ellingsen O 2001 Regional expression of endothelin-1, ANP, IGF-1, and LV wall stress in the infarcted rat heart. *American Journal of Physiology* **280** H2902–H2910.
 McKoy G, Bicknell KA, Patel K & Brooks G 2007 Developmental expression of myostatin in cardiomyocytes and its effect on fetal and neonatal rat cardiomyocyte proliferation. *Cardiovascular Research* **74** 304–312.
 McPherron AC, Lawler AM & Lee SJ 1997 Regulation of skeletal muscle mass in mice by a new TGF- β superfamily member. *Nature* **387** 83–90.
 Morissette MR, Cook SA, Foo SY, McKoy G, Ashida N, Novikov M, Scherrer-Crosbie M, Li L, Matsui T, Brooks G *et al.* 2006 Myostatin regulates cardiomyocytes growth through modulation of Akt signaling. *Circulation Research* **99** 15–24.
 Palmieri EA, Benincasa G, Di Rella F, Casaburi C, Monti MG, De Simone G, Chiariotti L, Palombini L, Bruni CB, Sacca L *et al.* 2001 Differential expression of TNF- α , IL-6, and IGF-1 by graded mechanical stress in normal rat myocardium. *American Journal of Physiology* **282** H926–H934.
 Sadoshima JI, Xu Y, Slayter HS & Izumo S 1993 Autocrine release of angiotensin II mediates stretch-induced hypertrophy of cardiac myocytes *in vitro*. *Cell* **75** 977–984.
 Schnee JM & Hsueh WA 2000 Angiotensin II adhesion, and cardiac fibrosis. *Cardiovascular Research* **46** 264–268.
 Sharma M, Kambadur R, Matthews KG, Somers WG, Delvin GP, Conaglen JV, Fowke PJ & Bass JJ 1999 Myostatin, a transforming growth factor- β superfamily member, is expressed in heart muscle and is upregulated in cardiomyocytes after infarct. *Journal of Cellular Physiology* **180** 1–9.
 Shyu KG, Chen CC, Wang BW & Kuan P 2001 Angiotensin II receptor antagonist blocks the expression of connexin43 induced by cyclical mechanical stretch in cultured neonatal rat cardiac myocytes. *Journal of Molecular and Cellular Cardiology* **33** 691–698.
 Shyu KG, Wang BW, Yang YH, Tsai SC, Lin S & Lee CC 2004 Amphetamine activates connexin43 gene expression in cultured neonatal rat cardiomyocytes through JNK and AP-1 pathway. *Cardiovascular Research* **63** 98–108.
 Shyu KG, Ko WH, Yang WS, Wang BW & Kuan P 2005 Insulin-like growth factor-1 mediates stretch-induced upregulation of myostatin expression in neonatal rat cardiomyocytes. *Cardiovascular Research* **68** 405–414.

- Song YH, Li Y, Du J, Mitch WE, Rosenthal N & Delafontaine P 2005 Muscle-specific expression of IGF-1 blocks angiotensin II-induced skeletal muscle wasting. *Journal of Clinical Investigation* **115** 451–458.
- Spiller MP, Kambadur R, Jeanplong F, Thomas M, Martyn JK, Bass JJ & Sharma M 2002 The myostatin gene is a downstream target gene of basic helix-loop-helix transcription factor MyoD. *Molecular and Cellular Biology* **22** 7066–7082.
- Thies RS, Chen T, Davies MV, Tomkinson KN, Pearson AA, Shakey QA & Wolfman NM 2001 GDF-8 propeptide binds to GDF-8 and antagonizes biological activity by inhibiting GDF-8 receptor binding. *Growth Factors* **18** 251–259.
- Torsoni AS, Constancio SS, Nadruz W, Hanks SK & Franchini KG 2003 Focal adhesion kinase is activated and mediates the early hypertrophic response to stretch in cardiac myocytes. *Circulation Research* **93** 140–147.
- Wang L, Ma W, Markovich R, Lee WL & Wang PH 1998 Insulin-like growth factor 1 modulates induction of apoptotic signaling in H9C2 cardiac muscle cells. *Endocrinology* **139** 1354–1360.
- Yang W, Zhang Y, Li Y, Wu Z & Zhu D 2007 Myostatin induces cyclin D1 degradation to cause cell cycle arrest through a phosphatidylinositol 3-kinase/AKT/GSK-3 β pathway and is antagonized by insulin-like growth factor-1. *Journal of Biological Chemistry* **282** 3799–3808.
- Zetser A, Gredinger E & Bengal E 1999 p38 mitogen-activated protein kinase pathway promotes skeletal muscle differentiation. *Journal of Biological Chemistry* **274** 5193–5200.
- Zhao M, New L, Kravchenko VV, Kato Y, Gram H, di Padova F, Olson EN, Ulevitch RJ & Han J 1999 Regulation of the MEF2 family of transcription factors by p38. *Molecular and Cellular Biology* **19** 21–30.
- Zimmers TA, Davies MV, Koniaris LC, Haynes P, Esquela AF, Tomkinson KN, McPherron AC, Wolfman NM & Lee SJ 2002 Induction of cachexia in mice by systemically administered myostatin. *Science* **296** 1486–1488.
- Zou Y, Akazawa H, Qin Y, Sano M, Takano H, Minamino T, Makita N, Iwanaga K, Zhu W, Kudoh S *et al.* 2004 Mechanical stress activates angiotensin II type 1 receptor without the involvement of angiotensin II. *Nature Cell Biology* **6** 499–506.

Received in final form 2 February 2008

Accepted 4 February 2008

Made available online as an Accepted Preprint

4 February 2008

Bao-Wei Wang, Huei-Fong Hung, Hang Chang, Peiliang Kuan and Kou-Gi Shyu

Am J Physiol Heart Circ Physiol 293:2305-2312, 2007. First published Jun 15, 2007;

doi:10.1152/ajpheart.00361.2007

You might find this additional information useful...

Supplemental material for this article can be found at:

<http://ajpheart.physiology.org/cgi/content/full/00361.2007/DC1>

This article cites 31 articles, 15 of which you can access free at:

<http://ajpheart.physiology.org/cgi/content/full/293/4/H2305#BIBL>

Updated information and services including high-resolution figures, can be found at:

<http://ajpheart.physiology.org/cgi/content/full/293/4/H2305>

Additional material and information about *AJP - Heart and Circulatory Physiology* can be found at:

<http://www.the-aps.org/publications/ajpheart>

This information is current as of December 30, 2007 .

Mechanical stretch enhances the expression of resistin gene in cultured cardiomyocytes via tumor necrosis factor- α

Bao-Wei Wang,^{1,2} Huei-Fong Hung,¹ Hang Chang,³ Peiliang Kuan,¹ and Kou-Gi Shyu^{1,4}

¹Division of Cardiology and ³Department of Emergency Medicine, Shin Kong Wu Ho-Su Memorial Hospital; ²School of Medicine, Fu-Jen Catholic University; and ⁴Graduate Institute of Medical Sciences, College of Medicine, Taipei Medical University, Taipei, Taiwan

Submitted 22 March 2007; accepted in final form 7 June 2007

Wang B-W, Hung H-F, Chang H, Kuan P, Shyu K-G. Mechanical stretch enhances the expression of resistin gene in cultured cardiomyocytes via tumor necrosis factor- α . *Am J Physiol Heart Circ Physiol* 293: H2305–H2312, 2007. First published June 15, 2007; doi:10.1152/ajpheart.00361.2007.—The heart is a resistin target tissue and can function as an autocrine organ. We sought to investigate whether cyclic mechanical stretch could induce resistin expression in cardiomyocytes and to test whether there is a link between the stretch-induced TNF- α and resistin. Neonatal Wistar rat cardiomyocytes grown on a flexible membrane base were stretched by vacuum to 20% of maximum elongation at 60 cycles/min. Cyclic stretch significantly increased resistin protein and mRNA expression after 2–18 h of stretch. Addition of PD-98059, TNF- α antibody, TNF- α receptor antibody, and ERK MAP kinase small interfering RNA 30 min before stretch inhibited the induction of resistin protein. Cyclic stretch increased, whereas PD-98059 abolished, the phosphorylated ERK protein. Gel-shift assay showed a significant increase in DNA-protein binding activity of NF- κ B after stretch, and PD-98059 abolished the DNA-protein binding activity induced by cyclic stretch. DNA binding complexes induced by cyclic stretch could be supershifted by p65 monoclonal antibody. Cyclic stretch increased resistin promoter activity, whereas PD-98059 and p65 antibody decreased resistin promoter activity. Cyclic stretch significantly increased TNF- α secretion from myocytes. Recombinant resistin protein and conditioned medium from stretched cardiomyocytes reduced glucose uptake in cardiomyocytes, and recombinant small interfering RNA of resistin or TNF- α antibody reversed glucose uptake. In conclusion, cyclic mechanical stretch enhances resistin expression in cultured rat neonatal cardiomyocytes. The stretch-induced resistin is mediated by TNF- α , at least in part, through ERK MAP kinase and NF- κ B pathways. Glucose uptake in cardiomyocytes was reduced by resistin upregulation.

cyclic stretch; glucose uptake

CARDIOMYOCYTES HAVE BEEN IDENTIFIED as a principal target of the proinflammatory actions of TNF- α (14). TNF- α can be induced in stretched myocytes and in hemodynamic-overloaded myocardium (9, 13, 18, 22). TNF- α is recognized as a significant contributor to myocardial dysfunction (11). In neonatal cardiomyocytes, TNF- α activates NF- κ B (15). TNF- α can also modulate resistin expression in adipocytes and peripheral blood mononuclear cells (4, 11, 15). The link between TNF- α and resistin in cardiomyocytes has not been reported.

More recently, the heart was shown to be a resistin target tissue (12). In cardiomyocytes, mouse and human resistins directly impair glucose transport (12). Many studies demon-

strated that isolated cardiomyocytes are insulin responsive and share many characteristics of adipocytes and skeletal muscle in terms of insulin stimulation of glucose transport (1, 3, 10, 19). Murine resistin is expressed not only in adipose tissue but, also, in the gastrointestinal tract, adrenal gland, skeletal muscle, brain, and pituitary gland (20, 21). There have been no reports, however, on resistin expression in cardiomyocytes. Since the heart is a resistin target tissue and can function as an autocrine organ, we hypothesize that cardiomyocytes express resistin gene. In diseased heart, glucose transport in the myocardium may be impaired. Left ventricular end-diastolic pressure is elevated in most of the diseased heart. The elevated end-diastolic pressure will stretch the myocardium. Whether mechanical stretch can induce resistin expression in cardiomyocytes has not been reported. Therefore, we sought to investigate whether cyclic mechanical stretch could induce resistin expression in cardiomyocytes and test whether there is a link between the stretch-induced TNF- α and resistin. Furthermore, we also tried to seek possible molecular mechanisms and signal pathways mediating resistin expression in cardiomyocytes by cyclic mechanical stretch.

MATERIALS AND METHODS

Primary cardiomyocyte culture. Cardiomyocytes were obtained from 2- to 3-day-old Wistar rats by trypsinization, as previously described (27). Cultured myocytes thus obtained were >95% pure as revealed by observation of contractile characteristics with a light microscope and stained with anti-desmin antibody (Dako Cytomation, Glostrup, Denmark). Cardiomyocytes were seeded on a flexible membrane base of six culture wells at a density of 1.6×10^6 cells/well in Ham's F-10 containing 10% horse serum and 10% fetal calf serum. After 2 days in culture, cells were transferred to serum-free medium (Ham's F-12-DMEM, 1:1) and maintained for another 2 days. The enriched myocytes were then subjected to cyclic stretch. The study conforms with the National Institutes of Health (NIH) *Guide for the Care and Use of Laboratory Animals* (NIH Publication No. 85-23, Revised 1996). The study was reviewed and approved by the Institutional Animal Care and Use Committee of Shin Kong Wu Ho-Su Memorial Hospital.

In vitro cyclic stretch on cultured cardiomyocytes. Cardiomyocytes cultured on the flexible membrane base were subjected to cyclic stretch produced by a Flexcell FX-2000 strain unit with computer-controlled application of sinusoidal negative pressure at a frequency of 1 Hz (60 cycles/min) for 2–24 h. The roles of JNK, p38 MAP kinase, or ERK kinase in stretch-induced resistin expression were determined by pretreatment of the myocytes with 20 μ M SP-600125, 3 μ M SB-203580, or 50 μ M PD-98059 (all from Calbiochem, San

Address for reprint requests and other correspondence: K. G. Shyu, Div. of Cardiology, Shin Kong Wu Ho-Su Memorial Hospital, 95 Wen-Chang Rd., Taipei 111, Taiwan (e-mail: shyukg@ms12.hinet.net).

The costs of publication of this article were defrayed in part by the payment of page charges. The article must therefore be hereby marked "advertisement" in accordance with 18 U.S.C. Section 1734 solely to indicate this fact.

Diego, CA) for 30 min before cyclic stretch. SP-600125 is a potent, cell-permeable, selective, and reversible inhibitor of JNK. SB-203580 is a highly specific, cell-permeable inhibitor of p38 kinase. PD-98059 is a specific and potent inhibitor of ERK kinase.

Real-time RT-PCR. Total RNA from rat abdominal fat, cardiomyocytes, skeletal muscle, liver, and kidney was extracted using the single-step acid guanidinium thiocyanate-phenol-chloroform extraction method (8). Real-time RT-PCR was performed as described previously (8). The rat resistin primers were 5'-ACTTCAGCTC-CCTACTG-3' and 5'-GTCTATGCTTCCGCACT-3'.

Western blot analysis. Western blot was performed as previously described (29). Rabbit anti-resistin rat polyclonal antibody was obtained from Chemicon (Temecula, CA), anti-rat TNF- α and anti-rat TNF- α receptor antibodies from R & D Systems (Minneapolis, MN), and polyclonal anti-ERK and monoclonal anti-phosphorylated ERK kinase antibodies from Cell Signaling (Beverly, MA).

RNA interference. Neonatal cardiomyocytes were transfected with 800 ng of ERK-annealed small interfering RNA (siRNA; Dharmacon, Lafayette, CO) or resistin siRNA oligonucleotide (Invitrogen, Carlsbad, CA). ERK and resistin siRNAs are target specific 20- to 25-nt siRNAs designed to knock down gene expression. siRNA sequences were 5'-GACCGAUGUUAACCUUUAAU (sense) and 5'-PUA-AAGGUUAACAUCGUCUU (antisense) for ERK and ACA-CAUUGUAUCCUCACGGACGUCCC (sense) and GGACGUCC-GUGAGGATACAAUGUGU (antisense) for resistin. As a negative control, a nontargeting (control) siRNA (Dharmacon) was used. For transfection of neonatal cardiomyocytes with siRNA oligonucleotides, Effectene transfection reagent was used according to the manufacturer's instructions (Qiagen, Valencia, CA). After incubation at 37°C for 24 h, cells were stretched for 18 h and analyzed by Western blot.

EMSA. Nuclear protein concentrations from cultured myocytes were determined by Bio-Rad protein assay. Consensus and control oligonucleotides (Research Biolabs, Singapore) were labeled by polynucleotide kinase incorporation of [γ -³²P]dATP. The consensus oligonucleotide sequence of NF- κ B was 5'-AGTTGAGGGGACTT-TCCAGGC-3'. The NF- κ B mutant oligonucleotide sequence was 5'-AGTTGAGGCGACTT-TCCAGG-3'. EMSA was performed as previously described (8). In each case, mutant or cold oligonucleotide was used as control to compete with labeled sequences.

Chromatin immunoprecipitation assay. Chromatin immunoprecipitation (CHIP) assays were carried out with the CHIP assay kit (Upstate Biotech, Temecula, CA) according to the manufacturer's instructions. One-third of the cell lysate from a stretched cardiomyocyte was immunoprecipitated by anti-NF- κ B p65 monoclonal antibody (Santa Cruz Biotechnology, Santa Cruz, CA) and then analyzed by PCR of the resistin promoter, and the remaining two-thirds of the cell lysate was added with anti-acetylated histone H3 antibody and analyzed by PCR of the resistin promoter. The primers for the resistin promoter were 5'-GAAGGAGCTGTGGGAC-3' and 5'-GCAGT-AGGGAGCTGAAG-3'. The primers for GAPDH were 5'-CATC-ACCATCTTCCAGGAGC-3' and 5'-GGATGATGTTCTGGGCTG-CC-3'. The PCR products of the resistin promoter and GAPDH (210 and 359 bp, respectively) were separated by agarose gel electrophoresis.

Promoter activity assay. A -741- to +22-bp rat resistin promoter construct was generated as follows. Rat genomic DNA was amplified with forward (ACGCGTCTCAGCGGTAGAGCTCTTG) and reverse (AGATCTGGAGAAATGAAAGTTCTTCATC) primer. The amplified product was digested with *Mlu* I and *Bgl* II restriction enzymes and ligated into pGL3-basic luciferase plasmid vector (Promega, Madison, WI) digested with the same enzymes. The resistin promoter contains NF- κ B conserved sites (GGGACTT) at -285 to -279 bp. For the mutant, the NF- κ B binding sites were mutated using the mutagenesis kit (Stratagene, La Jolla, CA). Site-specific mutations were confirmed by DNA sequencing. Plasmids were transfected into cardiomyocytes using a low-pressure accelerated gene gun (BioWare

Technologies, Taipei, Taiwan) essentially according to the manufacturer's protocol. Two micrograms of test plasmid and 0.02 μ g of control plasmid (pGL4-*Renilla* luciferases) were cotransfected with the gene gun in each well and then replaced by normal culture medium. After 6 h of cyclic stretching, cell extracts were prepared using the Dual-Luciferase Reporter Assay System (Promega), and dual-luciferase activity was measured using a luminometer (Turner Designs).

Measurement of TNF- α concentration. Conditioned medium from stretched myocytes and control (unstretched) cells was collected for TNF- α measurement. The level of TNF- α was measured by a quantitative sandwich enzyme immunoassay technique (R & D Systems). The lower limit of detection of rat TNF- α was 5 pg/ml. Intra- and interobserver coefficients of variance were <10%.

Glucose uptake in cardiomyocytes. Cardiomyocytes were seeded on ViewPlate (Packard Instrument, Meriden, CT) for 60 min at a density of 5×10^3 cells/well in serum-free medium with transferrin (5 μ g/ml) and insulin (5 μ g/ml) and incubated overnight. Recombinant mouse resistin (20 μ g/ml; R & D Systems), resistin siRNA, TNF- α antibody, or conditioned medium was added to the plate. Glucose uptake was studied by addition of 0.1 mmol/l glucose and 500 nCi/ml D-[3-³H]glucose (Perkin Elmer, Boston, MA) for 2–8 h. Cells were washed twice with PBS. Nonspecific uptake was studied in the presence of 10 μ M cytochalasin B and subtracted from the measured value. MicroScint-20 (50 μ l) was added, and the plate was read with TopCount (Packard Instrument, Meriden, CT).

Rat model of aorta-caval shunt. On the day of surgery, 290- to 320-g Wistar rats were anesthetized with pentobarbital sodium (80 mg/kg), and aorta-caval shunt was induced as described previously (28). The animals were killed 17 days after aorta-caval shunt, and blood was obtained from the right ventricle for measurement of circulating resistin levels.

Statistical analysis. Values are means \pm SE. Statistical significance was performed with Student's *t*-test or ANOVA (GraphPad Software, San Diego, CA) where appropriate. Dunnett's test was used to compare multiple groups with a single control group. The Tukey-Kramer comparison test was used for pairwise comparisons between multiple groups after ANOVA. *P* < 0.05 was considered to denote statistical significance.

RESULTS

Cardiomyocytes express resistin gene. RT-PCR was performed to investigate whether cardiomyocytes express resistin gene. Resistin mRNA was expressed most intensely in fat tissue (see supplemental Fig. 1 in the online version of this article at the *American Journal of Physiology-Heart and Circulatory Physiology* website). Cardiomyocytes and skeletal muscle expressed resistin mRNA, whereas liver and kidney did not.

Cyclic stretch enhances resistin protein and mRNA expression in cardiomyocytes. The levels of resistin protein shown by Western blot analysis began to increase as early as 2 h after stretch at 20% of maximum elongation, reached a maximum of 3.7-fold (*P* < 0.01) over the control by 6 h, and remained elevated up to 18 h (Fig. 1). Resistin protein returned to the baseline level after 24 h of stretch. Stretch-induced resistin protein expression was load dependent (Fig. 1). Stretch at 10% of maximum elongation increased resistin protein expression from 18 to 24 h.

Real time-PCR showed a significant increase in resistin messages from 2 to 18 h of stretch at 20% of maximum elongation (Fig. 1C). Resistin mRNA, similar to protein expression, returned to the baseline level after 24 h of stretch. Addition of the angiotensin type 1 receptor antagonist losartan

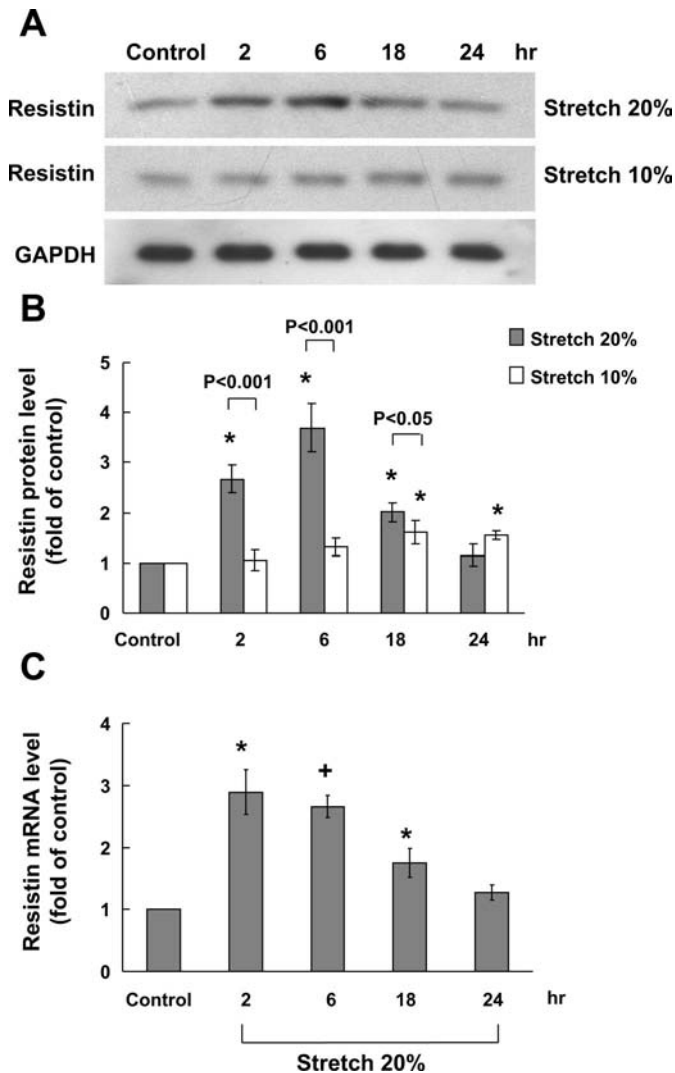


Fig. 1. Cyclic stretch increases resistin protein and mRNA expression in cardiomyocytes. *A*: representative Western blots of resistin in cardiomyocytes subjected to cyclic stretch to 20% or 10% of maximum elongation for 2–24 h. *B*: quantitative analysis of resistin protein levels. Values from stretched myocytes have been normalized to values in control cells, and data from 4 independent experiments are shown. * $P < 0.01$ vs. control. *C*: fold increases in resistin mRNA as a result of 20% cyclic stretch for 2–24 h. Values from stretched myocytes have been normalized to GAPDH and then expressed as a ratio of normalized values to mRNA in control cells ($n = 3$ –4 per group). * $P < 0.05$ vs. control. + $P < 0.05$ vs. control.

(100 nM) 30 min before stretch did not significantly attenuate stretch-induced resistin mRNA expression (data not shown).

Stretch-induced resistin protein expression in myocytes is mediated by TNF- α and ERK kinase. Western blot demonstrated a significant reduction in the stretch-induced increase of resistin protein after addition of TNF- α antibody (5 μ g/ml), TNF- α receptor antibody (5 μ g/ml), or PD-98059 30 min before stretch (Fig. 2, *A* and *B*). The stretch-induced increase in resistin protein was not affected by SP-600125. The stretch-induced increases in resistin protein were also completely blocked after addition of U-0126 (25 μ mol/l), a specific and potent inhibitor of ERK kinase, 30 min before stretch (data not shown). SB-203580 partially decreased stretch-induced resistin protein expression. ERK siRNA also completely blocked the

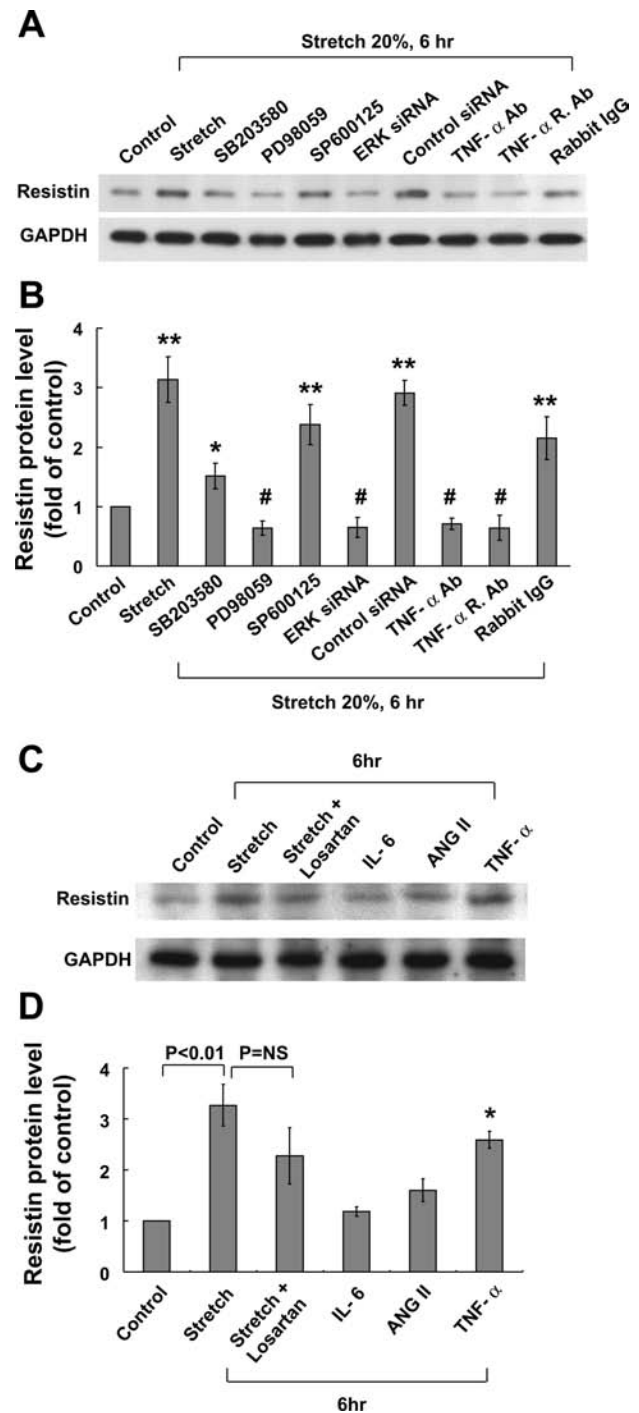


Fig. 2. Stretch-induced resistin protein expression in myocytes is mediated by TNF- α and ERK kinase. *A*: representative Western blots of resistin protein levels in myocytes subjected to cyclic stretch to 20% of maximum elongation for 6 h in the absence or presence of TNF- α antibody (Ab), TNF- α receptor antibody (TNF- α R. Ab), inhibitors, or small interfering RNA (siRNA). *B*: quantitative analysis of resistin protein levels. Values from stretched myocytes have been normalized to values in control cells, and data from 4 independent experiments are shown. * $P < 0.05$ vs. control. ** $P < 0.01$ vs. control. # $P < 0.001$ vs. stretch. *C*: effect of exogenous addition of proinflammatory cytokines on resistin expression. *D*: quantitative analysis of resistin protein levels. Data are from 4 independent experiments. * $P < 0.01$ vs. control.

resistin expression induced by cyclic stretch ($P < 0.001$). ERK siRNA knocked down the ERK protein expression. The control siRNA did not affect the resistin expression induced by cyclic stretch. The inhibitor used in the study did not affect basal resistin gene expression (data not shown). These findings

imply that the ERK pathway and TNF- α mediated the induction of resistin protein by cyclic stretch in myocytes. Exogenous addition of other proinflammatory cytokines, such as interleukin-6 (10 ng/ml) and angiotensin II (10 nM), did not induce resistin protein expression (Fig. 2, C and D) in cultured cardiomyocytes. This finding confirms the specificity of TNF- α in stretch-induced resistin expression. Addition of losartan before stretch also did not significantly attenuate the stretch-induced resistin protein expression.

Phosphorylated ERK protein was induced by cyclic stretch to 20% of maximum elongation (Fig. 3). The stretch-induced increase in phosphorylated ERK protein occurred slightly earlier than the stretch-increase in resistin protein. The phosphorylated ERK was abolished by PD-98059 and ERK siRNA. Addition of TNF- α antibody (5 μ g/ml) or TNF- α receptor antibody (5 μ g/ml) attenuated the phosphorylation of ERK protein induced by cyclic stretch. Addition of losartan before stretch did not abolish the stretch-induced phosphorylated ERK.

Cyclic stretch increases NF- κ B binding activity. Cyclic stretch of myocytes for 2–24 h significantly increased the DNA-protein binding activity of NF- κ B (Fig. 4A). An excess of unlabeled NF- κ B oligonucleotide competed with the probe for binding NF- κ B protein, whereas an oligonucleotide containing a 2-bp substitution in the NF- κ B binding site did not compete for binding. Addition of PD-98059 30 min before stretch abolished the DNA-protein binding activity induced by cyclic stretch. DNA binding complexes induced by cyclic stretch could be supershifted by a specific p65 antibody (a specific antibody for NF- κ B), indicating the presence of this protein in these complexes. After immunoprecipitation with p65 antibody, CHIP assay showed a resistin promoter band (Fig. 4B). This implies that NF- κ B binds to resistin promoter and confirms the specificity of DNA-protein binding activity of NF- κ B by gel-shift assay.

Cyclic stretch increases resistin promoter activity. The rat resistin promoter construct contains signal transducer and activator of transcription (Stat-3), activator protein-1, NF- κ B, and hypoxia-inducible factor-1 α binding sites. Cyclic stretch for 6 h significantly increased the resistin promoter activity by 2.3-fold compared with control without stretch (Fig. 5). When the NF- κ B binding sites were mutated, the increased promoter activity induced by cyclic stretch was abolished. Addition of PD-98059 and NF- κ B p65 antibody 30 min before stretch abolished the increased resistin promoter. This finding indicates that cyclic stretch regulates resistin in cardiomyocytes at the transcriptional level and that NF- κ B binding sites in the resistin promoter are essential for transcriptional regulation.

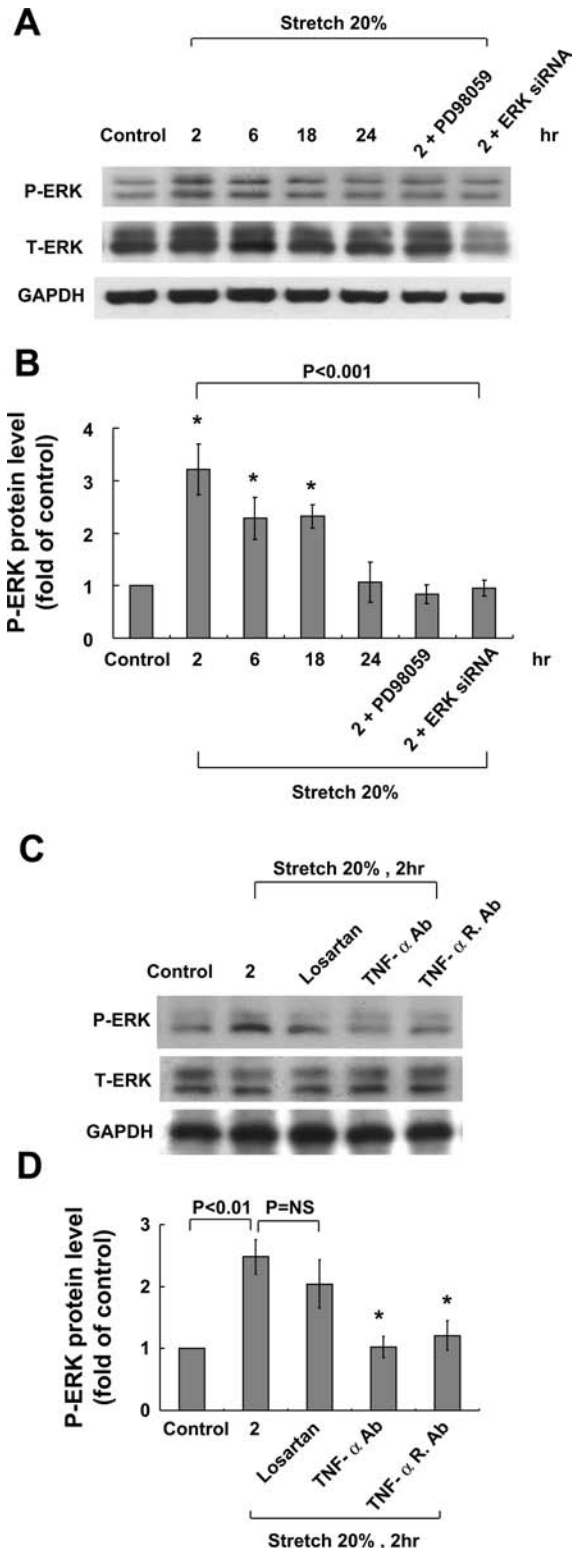


Fig. 3. Effect of cyclic stretch on expression of ERK kinase in myocytes. *A*: representative Western blot of phosphorylated and total ERK kinases (P-ERK and T-ERK, respectively) in myocytes after stretch to 20% of maximum elongation for 2–24 h. *B*: quantitative analysis of phosphorylated protein levels. Values from stretched myocytes have been normalized to GAPDH and corresponding total protein measurement and are expressed as a ratio of normalized values to each phosphorylated protein in control cells. Data are from 4 independent experiments. * $P < 0.01$ vs. control. *C*: representative Western blot of phosphorylated and total ERK kinases in myocytes after 20% stretch for 2 h and in the presence of losartan, TNF- α antibody, or TNF- α receptor antibody. *D*: quantitative analysis of phosphorylated ERK protein levels. Data are from 3 independent experiments. * $P < 0.05$ vs. 2 h of stretch.

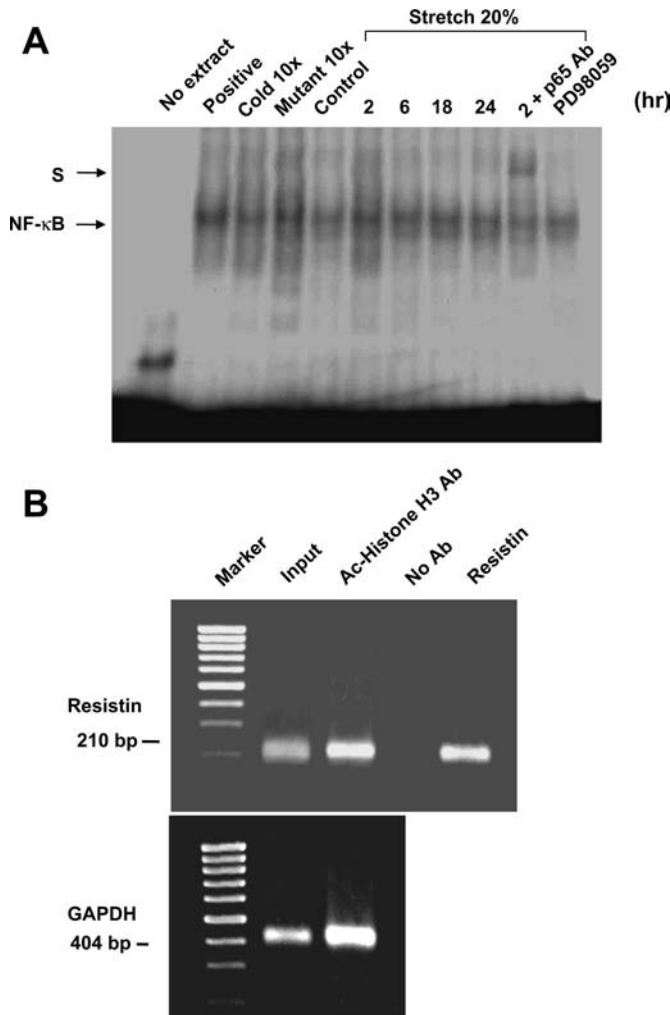


Fig. 4. *A*: cyclic stretch increases NF-κB-binding activity. Representative EMSA shows protein binding to the NF-κB oligonucleotide in nuclear extracts of cardiomyocytes after cyclic stretch in the presence and absence of inhibitors. Arrow indicates mobility of the complex. Similar results were found in 2 other independent experiments. Cold, unlabeled NF-κB oligonucleotides. A significant supershifted complex (S) was observed after incubation with p65 antibody. *B*: chromatin immunoprecipitation assay shows acetylation of histones with resistin promoter in cardiomyocytes after stretch. Input indicates amount of DNA in each sample. Immunoprecipitations were performed without p65 antibody (No Ab) as a negative control and with anti-acetyl (Ac) histone H3 antibody as a positive control.

Cyclic stretch stimulates secretion of TNF-α from myocytes. The increase in TNF-α secretion from myocytes induced by cyclic stretch began 2 h after stretch and continued for 18 h (see supplemental Fig. 2 in the online version of this article). The mean concentration of TNF-α rose from 36.5 ± 1.7 pg/ml before stretch to 98.9 ± 5.1 pg/ml after 2 h of stretch ($P < 0.01$). The increased resistin expression levels in cultured myocytes upon stretch were associated with TNF-α secretion.

Recombinant resistin reduces glucose uptake. Recombinant mouse resistin (20 μg/ml) and conditioned medium from stretched cardiomyocytes significantly reduced glucose uptake over 2–8 h of incubation compared with control untreated cardiomyocytes (Fig. 6). The dose of recombinant mouse resistin was based on the study by Graveleau et al. (12). Addition of resistin siRNA or TNF-α antibody before recom-

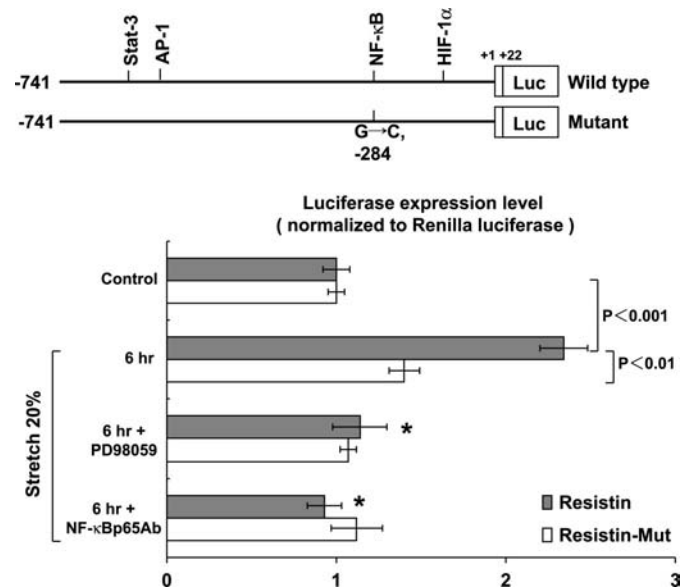


Fig. 5. Cyclic stretch increases rat resistin promoter activity. *Top*: construct of wild-type and mutant (Mut) resistin promoter. AP-1, activator protein-1; Stat-3, signal transducer and activator of transcription-1; HIF-1α, hypoxia-inducible factor-1α; Luc, luciferase. *Bottom*: quantitative analysis of promoter activity expressed as ratio of luciferase expression in stretched myocytes to luciferase expression in control (unstretched) cells. Data are from 4 independent experiments. $*P < 0.01$ vs. 6 h of stretch.

binant resistin reversed the glucose uptake to baseline levels. Resistin siRNA also reversed the glucose-lowering effect of conditioned medium. After an overnight incubation, the insulin in the medium measured by enzyme immunoassay (CRYSTAL CHEM, Downers Grove, IL) was still measurable (700 pg/ml). Use of serum-free medium without insulin and resistin resulted in glucose uptake by cardiomyocytes of 150 ± 10 counts/min, whereas addition of resistin reduced glucose uptake to 110 ± 8 counts/min ($P < 0.05$, $n = 3$).

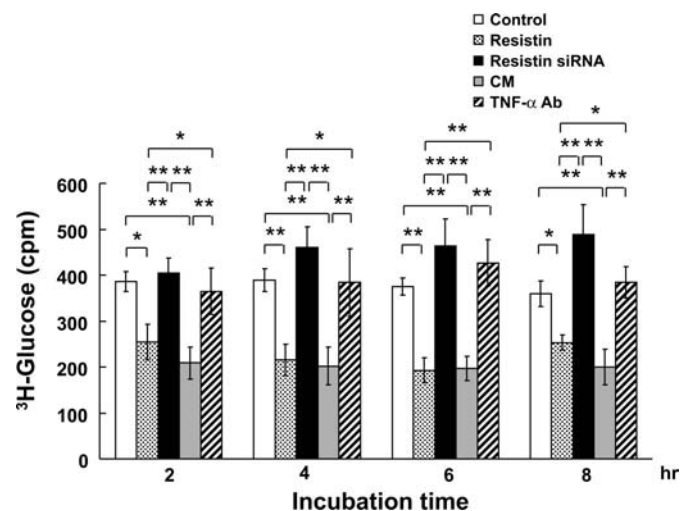


Fig. 6. Effect of recombinant resistin on glucose uptake [counts/min (cpm)] in cardiomyocytes. Glucose uptake was measured in cardiomyocytes treated for 90 min with 20 μg/ml recombinant mouse resistin with or without siRNA or TNF-α antibody or conditioned medium (CM) from stretched cardiomyocytes. $*P < 0.01$. $**P < 0.001$. Data are from 4 independent experiments.

In vivo aorta-caval shunt increases resistin protein expression. Resistin protein and mRNA expression significantly increased 1 and 3 days after induction of aorta-caval shunt and tended to decrease 5 and 7 days after shunt (Fig. 7). The left ventricular end-diastolic dimension increased from 6.1 ± 0.3 to 6.5 ± 0.4 mm after 3 days of aorta-caval shunt. Aorta-caval shunt resulted in a pulmonary-to-systemic flow ratio of 1.7. The circulating resistin levels increased from 1 to 5 days after aorta-caval shunt and returned to baseline 7 days after shunt (see supplemental Fig. 3 in the online version of this article). The circulating TNF- α also significantly increased ($P < 0.05$, $n = 3$) from 1 day (140 ± 7 pg/ml) to 5 days (122 ± 9 pg/ml) after shunt compared with the sham group (80 ± 5 pg/ml). Although the circulating TNF- α level remained elevated 7 days after shunt (115 ± 5 pg/ml), the difference did not reach statistical significance compared with the sham group.

DISCUSSION

In the present study, we demonstrated several significant findings: 1) cardiomyocytes express resistin gene; 2) cyclic stretch upregulates resistin expression in cardiomyocytes; 3) TNF- α acts as an autocrine factor to mediate the increased resistin expression induced by cyclic stretch; 4) ERK kinase and NF- κ B transcription factor are involved in the signaling pathway of resistin induction; 5) resistin impairs glucose uptake in cardiomyocytes; and 6) the *in vivo* aorta-caval shunt acutely increases resistin protein expression. The aorta-caval shunt is the animal model for cardiac volume overload. Resistin in cardiomyocytes was upregulated in a time- and a load-dependent manner by cyclic stretch. Our data clearly indicate that hemodynamic forces play a crucial role in the modulation of resistin expression in cardiomyocytes. Our data also demonstrated that a functional consequence of resistin upregulation by stretch was reduction of glucose uptake.

The induction of resistin protein by cyclic stretch was largely mediated by the ERK kinase pathway, because the specific and potent inhibitors of an upstream ERK kinase, PD-98059 and U-0126, inhibited the induction of resistin protein. This signaling pathway of ERK was further confirmed by the finding that ERK siRNA inhibited the induction of resistin protein by cyclic stretch. In the present study, stretched myocytes secreted TNF- α , and TNF- α monoclonal antibody and TNF- α receptor antibody blocked the increases of resistin protein induced by cyclic stretch. These results provide the first evidence for TNF- α mediation of cyclic stretch-induced expression of resistin in cardiomyocytes. These results further confirm the autocrine or paracrine production of cardiomyocytes in response to cyclic stretch.

Previous studies showed that obesity and atherosclerosis are increasingly viewed as inflammatory states. Biomarkers that integrate metabolic and inflammatory signals are attractive candidates for defining risk of atherosclerotic cardiovascular disease (30). Rodent resistin is derived almost exclusively from fat tissue, and adipose expression and serum levels are elevated in models of obesity and insulin resistance (16, 25, 23). Hyperresistinemia impairs glucose tolerance and induces hepatic insulin resistance in rodents (2), whereas resistin-deficient mice are protected from obesity-associated insulin resistance (26). The present study using an isolated cardiomyocyte culture system demonstrated that glucose transport was impaired by resistin. The glucose uptake in cardiomyocytes was reduced by resistin upregulation. Resistin has been demonstrated to impair insulin-mediated GLUT4 translocation in cardiomyocytes (12). Thus, impairment of glucose transport may explain the potential mechanism of resistin induction of insulin resistance. In hemodynamic overload, especially volume overload, stretched myocytes may impair glucose uptake and contractile function. The present study suggests that resistin is a metabolic link between mechanical stress and hypertrophic heart. Therefore, the transient increase in resistin gene expression after cyclic stretch or acute volume overload may be important in patients with hemodynamic overload. Recently, using an isolated perfused rat heart model, Rothwell et al. (26) demonstrated that resistin impaired cardiac recovery after ischemia-reperfusion injury. Their study showed no significant effect of resistin on myocardial glucose uptake. The different findings may be explained by the difference in glu-

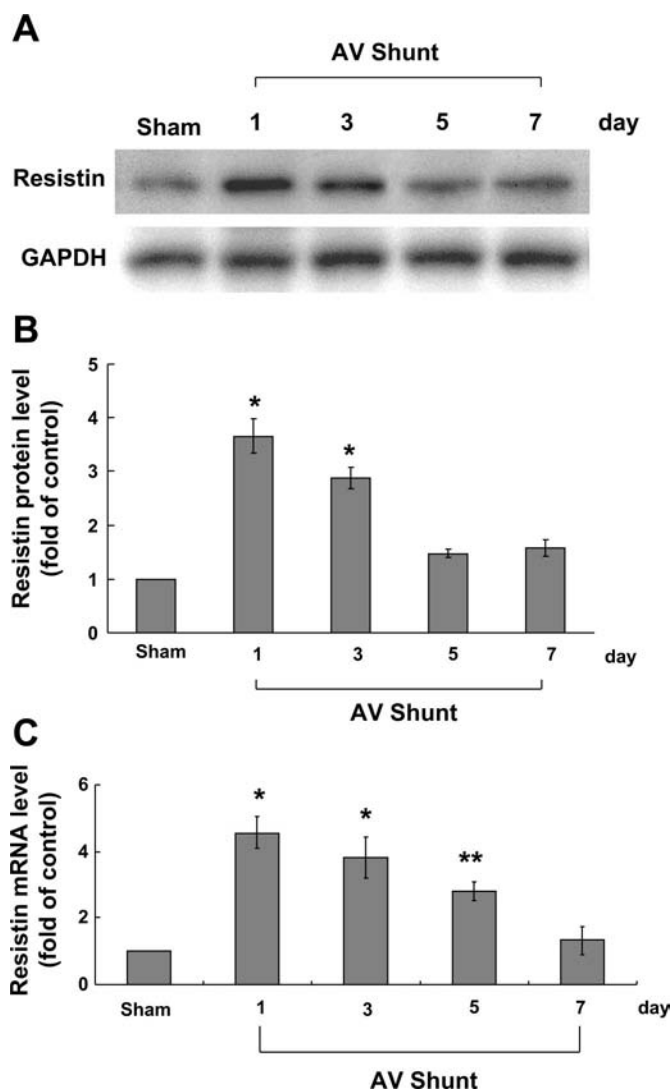


Fig. 7. Effect of *in vivo* model of aorta-caval (AV) shunt on myocardial resistin expression. *A*: representative Western blots of resistin in rat myocardium after short-term induction of AV shunt. *B*: quantitative analysis of resistin protein levels. Values have been normalized to GAPDH and are expressed as ratio of normalized values to resistin protein in sham group. Data are from 3 independent experiments. * $P < 0.01$ vs. sham. *C*: fold increases in resistin mRNA as a result of AV shunt. Data are from 3 independent experiments. * $P < 0.01$ vs. sham. ** $P < 0.001$ vs. sham.

cose metabolism between whole myocardium and cultured cardiomyocytes. Therefore, the role of resistin in dilated ventricle with contractile dysfunction needs further investigation.

TNF- α is recognized as a significant contributor to myocardial dysfunction (13). Cardiomyocytes have been identified as a principal target of the proinflammatory actions of TNF- α and cause a series of pathological changes in cardiomyocytes. In neonatal cardiomyocytes, TNF- α activates NF- κ B (9). Resistin was also shown to have potent proinflammatory properties (4). Resistin promotes endothelial cell activation (17) and causes endothelial dysfunction of porcine coronary arteries (5). Recently, resistin was found to have a potential role in atherosclerosis, because resistin increases monocyte chemoattractant protein-1 and soluble vascular cell adhesion molecule-1 expression in vascular endothelial cells (7) and promotes vascular smooth muscle cell proliferation (6). The link between TNF- α and resistin in cardiomyocytes may indicate that resistin plays a role as a downstream protein of TNF- α to contribute to cardiomyocyte dysfunction. The present study confirms that heart is a resistin target tissue as well as a resistin autocrine organ.

The role of TNF- α on the effect of resistin is controversial. Fasshauer et al. (11) reported that TNF- α is a negative regulator of resistin gene expression in adipocytes, whereas Kaser et al. (15) and Bokarewa et al. (4) reported that TNF- α is a positive regulator of resistin gene expression in peripheral blood mononuclear cells. In the present study, TNF- α was found to be a positive regulator of resistin gene expression in stretched cardiomyocytes. Taken together, the effect of TNF- α on the regulation of resistin gene expression is different in different cell types.

NF- κ B is a proinflammatory master switch that controls the production of several inflammatory markers and mediators. Cae et al. (6) demonstrated that hepatic activation of NF- κ B caused local and systemic insulin resistance. In the present study, we demonstrated that cyclic stretch-stimulated NF- κ B-DNA binding activity required at least phosphorylation of ERK, since ERK inhibitor abolished the NF- κ B binding activity. The p65 monoclonal antibody, a specific antibody for NF- κ B, shifted the NF- κ B-DNA binding complex, indicating the specificity of the cyclic stretch-induced NF- κ B-DNA binding activity. In the present study, we used CHIP assay to confirm that the resistin gene upstream region contains an NF- κ B site. We further demonstrated that cyclic stretch increased resistin promoter activity and that the binding site of NF- κ B in the resistin promoter is essential for the transcriptional regulation. Taken together, our results indicate that cyclic stretch may increase NF- κ B transcriptional activity in cardiomyocytes.

In summary, our study is the first report of cyclic mechanical stretch enhancement of resistin expression in cultured rat neonatal cardiomyocytes. The stretch-induced resistin is mediated by TNF- α , at least in part, through the ERK kinase and NF- κ B pathway. Glucose uptake in cardiomyocytes was reduced by resistin upregulation.

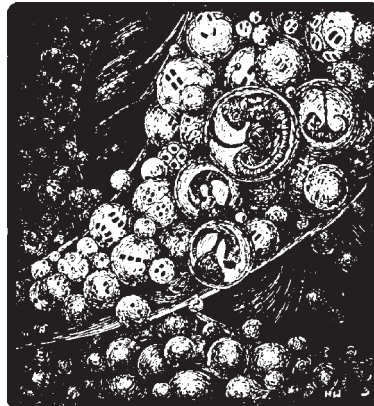
GRANTS

This study was sponsored in part by a grant from the New Century Health Care Promotion Foundation (Taipei, Taiwan).

REFERENCES

- Abel ED, Graveleau C, Betuing S, Pham M, Reay PA, Kandror V, Kupriyanova T, Xu Z, Kandror KV. Regulation of insulin-responsive aminopeptidase expression and targeting in the insulin-responsive vesicle compartment of glucose transporter isoform 4-deficient cardiomyocytes. *Mol Endocrinol* 18: 2491–2501, 2004.
- Banerjee RR, Rangwala SM, Shapiro JS, Rich AS, Rhoades B, Qi Y, Wang J, Rajala MW, Poci A, Scherer PE, Stepan CM, Ahima RS, Obici S, Rossetti L, Lazar MA. Regulation of fasted blood glucose by resistin. *Science* 303: 1195–1198, 2004.
- Belke DD, Betuing S, Tuttle MJ, Graveleau C, Young ME, Pham M, Zhang D, Cooksey RC, McClain DA, Litwin SE, Taegtmeier H, Severson D, Kahn CR, Abel ED. Insulin signaling coordinately regulates cardiac size, metabolism, and contractile protein isoform expression. *J Clin Invest* 109: 629–639, 2002.
- Bokarewa M, Nagaev I, Dahlberg L, Smith U, Tarkowski A. Resistin, an adipokine with potent proinflammatory properties. *J Immunol* 174: 5789–5795, 2005.
- Burnett MS, Lee CW, Kinnaird TD, Stabile E, Durrani S, Dullum MK, Devaney JM, Fishman C, Stamou S, Canos D, Zbinden S, Clavijo LC, Jang GJ, Andrews JA, Zhu J, Epstein SE. The potential role of resistin in atherogenesis. *Atherosclerosis* 182: 241–248, 2005.
- Cae D, Yuan M, Frantz DF, Melendez PA, Hansen L, Lee J, Shoelson SE. Local and systemic insulin resistance resulting from hepatic activation of I κ B and NF- κ B. *Nat Med* 11: 183–190, 2005.
- Calabro P, Samudio I, Willerson JT, Yeh ETH. Resistin promotes smooth muscle cell proliferation through activation of extracellular signal-regulated kinases 1/2 and phosphatidylinositol 3-kinase pathways. *Circulation* 110: 3335–3340, 2004.
- Chang H, Shyu KG, Wang BW, Kuan P. Regulation of hypoxia-inducible factor 1- α by cyclical mechanical stretch in rat vascular smooth muscle cells. *Clin Sci (Lond)* 105: 447–456, 2003.
- Condorelli G, Morisco C, Latronico MVG, Claudio PP, Dent P, Tschichlis P, Condorelli G, Frati G, Drusco A, Croce CM, Napoli C. TNF- α signal transduction in rat neonatal cardiac myocytes: definition of pathways generating from the TNF- α receptor. *FASEB J* 16: 1732–1737, 2002.
- Eckel J, Reinauer H. Glucose uptake in isolated heart cells: studies on the role of insulin. *Basic Res Cardiol* 80: 103–106, 1985.
- Fasshauer M, Klein J, Neumann S, Eszlinger M, Paschke R. Tumor necrosis factor- α is a negative regulator of resistin gene expression and secretion in 3T3-L1 adipocytes. *Biochem Biophys Res Commun* 288: 1027–1031, 2001.
- Graveleau C, Zaha VG, Mohajer A, Banerjee RR, Duedley-Rucker N, Stepan CM, Rajala M, Scherer PE, Ahima RS, Lazar MA, Abel ED. Mouse and human resistins impair glucose transport in primary mouse cardiomyocytes, and oligomerization is required for this biological action. *J Biol Chem* 280: 31679–31685, 2005.
- Hall G, Singh IS, Hester L, Hasday JD, Rogers TB. Inhibitor- κ B kinase- β regulates LPS-induced TNF- α production in cardiac myocytes through modulation of NF- κ B p65 subunit phosphorylation. *Am J Physiol Heart Circ Physiol* 289: H2103–H2111, 2005.
- Kapadia SR, Oral H, Lee J, Nakano M, Taffet GE, Mann DL. Hemodynamic regulation of tumor necrosis factor- α gene and protein expression in adult feline myocardium. *Circ Res* 81: 187–195, 1997.
- Kaser S, Kaser A, Sandhofer A, Ebenbichler CF, Tilg H, Patsch JR. Resistin messenger-RNA expression is increased by proinflammatory cytokine in vitro. *Biochem Biophys Res Commun* 309: 286–290, 2003.
- Kim KH, Lee K, Moon YS, Sul HS. A cysteine-rich adipose tissue-specific secretory factor inhibits adipocyte differentiation. *J Biol Chem* 276: 11252–11256, 2001.
- Kougas P, Chai H, Lin PH, Lumsden AB, Yao Q, Chen C. Adipocyte-derived cytokine resistin causes endothelial dysfunction of porcine coronary arteries. *J Vasc Surg* 41: 691–698, 2005.
- Li M, Georgakopoulos D, Lu G, Hester L, Kass DA, Hasday J, Wang Y. p38 MAP kinase mediates inflammatory cytokine induction in cardiomyocytes and extracellular matrix remodeling in heart. *Circulation* 111: 2494–2502, 2005.
- Mazumder PK, O'Neill BT, Roberts MW, Buchanan J, Yun UJ, Cooksey RC, Boudina S, Abel ED. Impaired cardiac efficiency and increased fatty acid oxidation in insulin-resistant *ob/ob* mouse hearts. *Diabetes* 53: 2366–2374, 2004.

20. **Morash BA, Ur E, Wiesner G, Roy J, Wilkinson M.** Pituitary resistin gene expression: effects of age, gender and obesity. *Neuroendocrinology* 79: 149–156, 2004.
21. **Nogueiras R, Gallego R, Gualillo O, Caminos JE, Garcia-Caballero T, Casanueva FF, Dieguez C.** Resistin is expressed in different rat tissues and is regulated in a tissue- and gender-specific manner. *FEBS Lett* 548: 21–27, 2003.
22. **Palmieri EA, Benincasa G, Di Rella F, Casaburi C, Monti MG, De Simone G, Chiariotti L, Palombini L, Bruni CB, Sacca L, Cittadini A.** Differential expression of TNF- α , IL-6, and IGF-1 by graded mechanical stress in normal rat myocardium. *Am J Physiol Heart Circ Physiol* 282: H926–H934, 2002.
23. **Rajala MW, Obici S, Scherer PE, Rossetti L.** Adipose-derived resistin and gut-derived resistin-like molecule- β selectively impair insulin action on glucose production. *J Clin Invest* 111: 225–230, 2003.
24. **Rajala MW, Scherer PE.** The adipocyte: at the crossroads of energy homeostasis, inflammation, and atherosclerosis. *Endocrinology* 144: 3765–3773, 2003.
25. **Rajala MW, Qi Y, Patel HR, Takahashi N, Banerjee R, Pajvani UB, Sinha MK, Gingerich RL, Scherer PE, Ahima RS.** Regulation of resistin expression and circulating levels in obesity, diabetes, and fasting. *Diabetes* 53: 1671–1679, 2004.
26. **Rothwell SE, Richards AM, Pemberton CJ.** Resistin worsens cardiac ischemia-reperfusion injury. *Biochem Biophys Res Commun* 349: 4000–4007, 2006.
27. **Shyu KG, Chen CC, Wang BW, Kuan P.** Angiotensin II receptor antagonist blocks the expression of connexin43 induced by cyclical mechanical stretch in cultured neonatal rat cardiac myocytes. *J Mol Cell Cardiol* 33: 691–698, 2001.
28. **Shyu KG, Lu MJ, Chang H, Sun HY, Wang BW, Kuan P.** Carvedilol modulates the expression of hypoxia-inducible factor-1 α and vascular endothelial growth factor in a rat model of volume-overload heart failure. *J Card Fail* 11: 156–165, 2005.
29. **Shyu KG, Wang BW, Yang YH, Tsai SC, Lin S, Lee CC.** Amphetamine activates connexin43 gene expression in cultured neonatal rat cardiomyocytes through JNK and AP-1 pathway. *Cardiovasc Res* 63: 98–108, 2004.
30. **Steppan CM, Bailey ST, Bhat S, Brown EJ, Banerjee RR, Wright CM, Patel HR, Ahima RS, Lazar MA.** The hormone resistin links obesity to diabetes. *Nature* 409: 307–312, 2001.
31. **Verma S, Li SH, Wang CH, Fedark PWM, Li RK, Weisel RD, Mickle DAG.** Resistin promotes endothelial cell activation. Further evidence of adipokine-endothelial interaction. *Circulation* 108: 736–740, 2003.



Delivery of noncarrier naked DNA vaccine into the skin by supersonic flow induces a polarized T helper type 1 immune response to cancer

Chi-Chen Lin¹
Meng-Chi Yen^{1,2}
Chiu-Mei Lin³
Shih-Shien Huang¹
Huei-Jiun Yang¹
Nan-Haw Chow⁴
Ming-Derg Lai^{1,2,5*}

¹Department of Biochemistry and Molecular Biology, College of Medicine, National Cheng Kung University, Tainan, Taiwan

²Institute of Basic Medicine, College of Medicine, National Cheng Kung University, Tainan, Taiwan

³School of Medicine, College of Medicine, Taipei Medical University, Tainan, Taiwan

⁴Department of Pathology, College of Medicine, National Cheng Kung University, Tainan, Taiwan

⁵Center for Gene Regulation and Signal Transduction Research, National Cheng Kung University, Tainan, Taiwan

*Correspondence to: Ming-Derg Lai, Department of Biochemistry and Molecular Biology, College of Medicine, National Cheng Kung University, Tainan, Taiwan. E-mail: a1211207@mail.ncku.edu.tw

Received: 20 September 2007

Revised: 18 January 2008

Accepted: 21 January 2008

Abstract

Background DNA vaccine is a new and powerful approach to generate immunological responses against infectious disease and cancer. The T helper type (Th)1 immune response is usually required for generating effective anti-tumor responses. A microparticulate bombardment system can induce an immune response using very low amounts of DNA. Using nozzle aerodynamics, a low pressure gene gun has been developed to decrease the noise associated with high pressure gene guns. Particles are propelled by supersonic flow through this novel nozzle. To test whether this gun could inoculate a DNA vaccine that stimulates an anti-tumor Th1 immune response, we examined the effect of direct delivery of naked DNA (i.e. without any carrier) on the anti-tumor immune response of mice.

Methods The luciferase reporter plasmid DNA was delivered using a low-pressure biolistic device and expressed in C3H/HeN, BALB/c, and C57BL/6 mice.

Results Plasmid DNA expression was mainly in the epidermis. Noncarrier naked neu DNA vaccine and gold particle-coated neu DNA vaccine (at 1 µg per mouse) had similar anti-tumor effects in C3H mice. However, cytokine profile examination showed the Th1-bias of the response induced by naked DNA vaccine and the Th2-bias of the response induced by coated DNA vaccine.

Conclusions A shift in the immune response to favour enhanced tumor rejection can be achieved by skin delivery of naked DNA vaccine. Copyright © 2008 John Wiley & Sons, Ltd.

Keywords biolistic; cancer; DNA vaccine; gene gun; neu; Th1 immune response

Introduction

Advances in molecular biology have made it possible to sequence the genomes of primates and infectious agents. This achievement allowed us to identify targets for gene therapy and vaccine development. However, our primary concern is the development of effective and safe methods of delivering gene-based drugs. Although highly efficient viral vectors have been used, their use has many negative consequences (including induction of host immune responses, random integration, and risks of wild-type virus contamination) [1,2]. Non-viral gene transfer provides a safe, superior alternative. Nonviral delivery methods include gene-gun injection, liquid jet injection, intramuscular direct injection, and electroporation, among others [3–5]. Of these methods, the

gene gun, also named the biolistic device, has been demonstrated to deliver genes in an effective and homogeneous fashion. The gene-gun delivery method was originally designed to propel DNA-coated gold particles (using exploding gunpowder as an accelerant) through plant cell walls [6]. High pressure helium replaced gunpowder in most particle-mediated delivery devices [7]. The method is also applied to deliver genes into mammalian cells [8], and may be superior to the lipofectamine method for certain cell lines. In addition, the successful introduction of DNA via skin has been demonstrated *in vivo* [9].

Plasmid DNA vaccine was shown to elicit humoral and cellular immunity [10–12]. The simplicity and stability of DNA vaccines confer advantages over certain current immunological manipulations. DNA vaccines are usually delivered by intramuscular injection or particle-mediated gene-gun transfer. Intramuscular injection induces a predominantly T helper type 1 (Th1) response, whereas gene-gun delivery elicits predominantly T helper type 2 (Th2) responses [13–16]. The difference may be influenced by the amount of DNA, the associated CpG motifs, the nature of the antigen, and the particle used in delivery [17–20]. The advantage of gene-gun delivery over intramuscular injection is that less DNA is used. The Th1 response is usually needed to clear infection and cancer cells [21].

To decrease the noise and cell damage caused by high-pressure (200–400 Psi) gene guns, a low-pressure (30–60 Psi) gene gun was developed (US patent 6436709B1). This low pressure biolistic device can introduce gold particle-coated DNA into animal cells using supersonic flow generated by a rocket nozzle [22,23]. Since supersonic air flow can shoot low density particles through cell walls, we wished to determine whether it could introduce naked DNA into animal skin. Our results demonstrate that this device can deliver naked DNA into mouse skin and thereby provoke Th1-biased immune responses that are effective for cancer therapy.

Materials and methods

Mice

Female C3H/HeN, BALB/c, and C57BL/6, mice were obtained from the laboratory animal center at National Cheng Kung University. All animal studies were approved by the animal welfare committee at National Cheng Kung University.

Gene-gun injection

One to 10 μg of naked DNA was dissolved in 20 μl of double-distilled water and added to the loading hole near the nozzle. Pushing the trigger of the low pressure Gene Gun (BioWare Technologies Co. Ltd, Taipei, Taiwan) released the DNA-containing water, which was directly

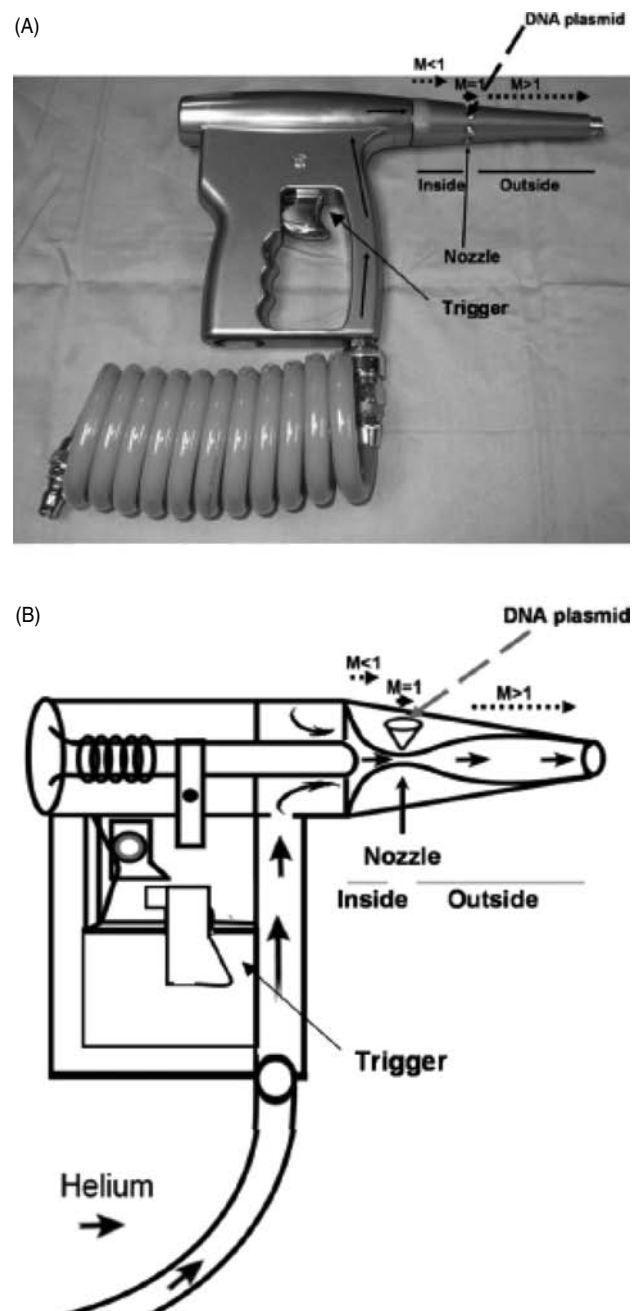


Figure 1. Low-pressure biolistic device. (A) Photograph showing the exterior of the gene delivery device. The plasmid sample is applied through the upper hole. Helium is supplied through an inlet at the bottom. (B) Schematic showing the internal features of the gene delivery device. M, Mach; $M < 1$, subsonic flow; $M > 1$, supersonic flow

propelled by helium at a pressure of 60 psi into the shaved abdomen of the mouse (Figure 1). To avoid the cross-contamination between each shot, water and ethanol were added sequentially to wash the loading well and the gun was fired to clear the nozzle. Plasmid DNA was precipitated onto gold particles (Bio-Rad, Hercules, CA, USA) at the ratio of 1–2 μg of DNA per mg of gold particles. The total volume (50 μl) was vortexed and sonicated for several seconds before adding equal volumes of 0.05 M spermidine and 2.5 M CaCl_2 solution

with vortexing, and then placed on ice for 10 min. The gold particles were collected by centrifugation at 9000 g for 1 min, washed three times with 100% ethanol, resuspended in 20 μ l of 100% ethanol, and used as bullets (at a 40 psi pressure of helium) in the same low pressure gene gun used to deliver the naked DNA plasmid.

The efficiency of delivery

The CMV promoter was subcloned from pRc/CMV empty vector (Invitrogen, Carlsbad, CA, USA) by polymerase chain reaction (PCR). Primers were: forward: 5'-GCAATCGGTACCCGATGTACGGGCCAGATATAC-3'; reverse: 5'-GCAATCAAGCTTAATTTTCGATAAGCCAGTTAAGC-3'. pCMV-luciferase plasmid was generated by inserting a *KpnI/HindIII* fragment of CMV promoter into the pGL3-basic vector upstream of the luciferase gene. The luciferase activity on mouse skin was detected 48 h after bombardment with pCMV-luciferase. The distribution of luciferase activity in treated mice was visualized using a Night Owl imaging unit (Berthold Technologies, Bad Wildbad, Germany) consisting of a Peltier cooled CCD slow-scan camera mounted on a light-tight specimen chamber. Images were acquired and processed using WinLight software (Berthold Technologies). Just before imaging, the skin was shaved, and 100 μ l of D-luciferin (Synchem OHG, Altenburg, Germany) in saline was injected at a dose of 100 mg/kg. Mice then were placed in the chamber, and a gray-scale image was taken with dimmed light. Photon emission was then integrated over a period of 10 min. Luminescence measurements are expressed as the integration of the average brightness/pixel unit expressed as photon counts emitted per second.

Locating sites of gene-gun delivery

Mice were sacrificed 48 h after bombardment with pCMV-EGFP-N1 (Clontech, Palo Alto, CA, USA). Abdominal skin was removed, embedded in paraffin, sectioned (5 μ m), and directly observed under an IX71 fluorescence microscope (Olympus, Tokyo, Japan).

Detection of CD11c+ GFP-positive cells in inguinal lymph nodes from vaccinated mice

The protocol is modified from that previously reported [24]. In brief, C3H/HeN mice were inoculated with different doses of pCMV-EGFP plasmid (pEGFP-N1; Clontech) via gene-gun bombardment. Inguinal lymph nodes were harvested 48 h later. CD11c+ cells were further enriched from single cell suspensions of isolated inguinal lymph node by CD11c (N418) microbeads (Miltenyi Biotec, Auburn, CA, USA). To increase the purity of the enriched CD11c+ cells, the magnetic separation

procedure was repeated using a new column. The purity of the populations was at least 90% as determined by staining with monoclonal anti-CD11c-PE antibody. FACSCalibur flow cytometry (BD Bioscience, Mountain View, CA, USA) was used to determine percentage of GFP positive CD11c+ cells in a gated population (electronic gates set for monocytes according to their forward and side scatter characteristics).

Therapeutic efficacy of DNA vaccine with/without coating

Mice were injected subcutaneously in the flank with 1×10^6 MBT-2 cells in 0.5 ml of phosphate-buffered saline (PBS) (day 0). Beginning on day 10, when tumors were palpable, pCMV-human *N'*-neu DNA vaccine [23] or pRc/CMV DNA (Invitrogen) was delivered by gene gun on skin in the shaved abdominal region three times at weekly intervals. Control mice received three injections of water. Tumor size was measured using a caliper twice each week. Tumor volume was calculated using the formula for a rational ellipse: ($m_{12} \times m_2 \times 0.5236$), where m_1 represents the shorter axis and m_2 the longer axis. Mice were sacrificed when the tumor volume exceeded 2500 mm³ or the mouse was in poor condition and death was expected shortly. Significance of differences in survival were tested by Kaplan–Meier analysis.

Determination of the expression of extracellular domain of p185neu protein in skin

A 96-well plate was coated with 0.2 μ g of rabbit-anti-ErbB-2 antibody (Neomarker, Fremont, CA, USA) in 100 μ l of PBS (pH 7.4) and incubated overnight at 4 °C. Nonspecific binding was blocked with PBS containing 1% bovine serum albumin (BSA), followed by three washes with 0.05% Tween 20 in PBS. Skin samples were homogenized 48 h after pCMV-human-*N'*-neu bombardment, while 100 μ l of each prepared sample was added to duplicate coated wells and incubated at 37 °C for 2 h. After washing them three times, the following was added to the wells: mouse-anti-ErbB-2 antibody (Ab-20) (Neomarker) (incubated at 37 °C for 90 min), Horseradish peroxidase (HRP)-conjugated anti-mouse IgG (Calbiochem, Darmstadt, Germany) (incubated for 45 min at 37 °C), and 3,3',5,5'-tetramethylbenzidine (TMB) substrate (eBioscience, San Diego, CA, USA) for color development. Absorbance was measured at 450 nm with a microplate reader.

Determination of serum anti-neu antibody titer

Recombinant human-ErbB2 protein (0.2 μ g/100 μ l; R&D Systems, Minneapolis, MN, USA) was added to 96-well flat-bottom plate, which was incubated overnight

at 4°C, blocked with PBS buffer containing 1% BSA (room temperature 1–2 h), and washed with PBS containing 0.05% Tween 20 for three to five times. Mouse anti-ErbB-2 antibody (Ab-20) was used to generate the standard curve, and the background value calculated from absorbance read in control wells containing an irrelevant antibody (i.e. anti-SV40 large T antigen; Oncogene Science, Cambridge, MA, USA). The titer of human anti-p185neu antibody in test sera was determined by serial dilution and addition to the plates. HRP-conjugated anti-mouse IgG (Calbiochem) was used to detect total mouse IgG and TMB substrate was for colour development. Absorbance was read at 450 nm with a microplate reader.

Spleen cell-mediated cytotoxicity assay for targeting MBT-2 cells

The protocol is modified from that previously reported [23,25]. Female C3H/HeN mice (6–8 weeks old) were injected with DNA vaccine three times as described above. A week after the third DNA vaccination, spleen cells were harvested and grown in RPMI 1640 with 25 mM Hepes and L-glutamate (GibcoBRL, Rockville, MD, USA), supplemented with penicillin (100 U/ml), streptomycin (100 µg/ml), 50 mM 2-mercaptoethanol, 100 U/ml penicillin, and 10% fetal bovine serum (FBS). In addition, 10 µg/ml of recombinant extracellular domain of neu protein, amino acids 1–652 (R&D Systems) was added. After 5 days of incubation, non-adherent cells were harvested as effector cells and plated with MBT-2 luciferase cells as target cells [23]. Target cells of 5×10^3 cells/well were incubated for 18 h in triplicate at 37°C with effector cells serially diluted 50:1, 25:1, or 12.5:1. After 18 h, cells were recovered by centrifugation and 100 µl of supernatant was obtained. The specific lysis was assessed in the supernatant using a conventional luciferase detection system (Promega, Madison, WI, USA). One hundred µl of the culture medium was mixed with 100 µl of the substrate luciferin (dual luciferase reporter system; Promega). The mixture was then placed into an EG & G MiniLumat LB9506 luminometer (Berthold Technologies). Light emission was recorded for 10 s, with triplicate measurements being performed for each sample. The percentage-specific lysis was calculated using the following formula:

$$\begin{aligned} \% \text{ lysis} &= (\text{test RLU} [\text{relative light units}] \\ &\quad - \text{spontaneous RLU} / \text{max RLU} \\ &\quad - \text{spontaneous RLU}) \times 100. \end{aligned}$$

Cytokine enzyme-linked immunosorbent assay (ELISA)

Lymphocytes (5×10^6) obtained from peripheral lymph nodes 1 week after the last vaccination were cultured for 48 h in a 24-well plate containing 10 µg/ml of

recombinant human ErbB2 protein (R&D Systems) in 1 ml of RPMI 1640 with 10% FBS. The supernatants were harvested and assayed for the presence of cytokines using the mouse ELISA Ready-SET-Go kits (eBioscience) according to the manufacturer's instructions.

Reverse transcriptase (RT)-PCR

Total RNA was extracted from lymphocytes by TRIZOL (Invitrogen). cDNA was synthesized from 2 µg of RNA using MMLV-Reverse Transcriptase according to the manufacturer's directions. Primers were: IL-12p40 forward: 5'-TGC TGG TGT CTC CAC TCA TGG C-3'; IL-12p40 reverse: 5'-TTT CAG TGG ACC AAA TTC CAT T-3'; IFN- γ forward: 5'-AAC GCT ACA CAC TGC ATC TTG G-3'; IFN- γ reverse: 5'-CAA GAC TTC AAA GAG TCT GAG G-3'; IL-4 forward: 5'-GAA TGT ACC AGG AGC CAT ATC-3'; IL-4 reverse: 5'-CTC AGT ACT ACG AGT AAT CCA-3'; IL-10 forward: 5'-CGG GAA GAC AAT AAC TG-3'; IL-10 reverse: 5'-CAT TTC CGA TAA GGC TTG-3'; hypoxanthine phosphoribosyltransferase (HPRT) forward: 5'-GTT GGA TAC AGG CCA GAC TTT GTT G-3'; HPRT reverse: 5'-GAT TCA ACT TGC GCT CAT CTT AGG C-3'. cDNA was amplified by Protaq (Protech, Taipei, Taiwan). PCR amplifications were carried out in 50 µl volumes containing 20–60 pmol of each primer, Protaq buffer (Protech), 200 µM each of dNTP, and 5 U of ProTaq polymerase. PCR was performed on a PCR thermal cycler (MJ Research, Watertown, MA, USA). The PCR reaction commenced at 94°C for 2 min, followed by 30–40 cycles at 94°C for 30 s, 55°C for 30 s, and 72°C for 30 s. The PCR products were subjected to electrophoresis on 1.5% agarose gels and visualized by ethidium bromide staining under ultraviolet light.

Determination of DNA degradation by gene-gun firing

One µg of naked pCMV-Her-2/neu DNA or gold particles coated with 1 µg of pCMV-Her-2/neu DNA was shot into a circular region, equal in area to the area at the exit of the gene-gun nozzle, on 6-µm-pore-size filter paper (Advantec, Tokyo, Japan) at a pressure of 60 or 40 psi, respectively. The DNA on the bombarded filter paper was recovered by placing the paper in a PD column (Geneaid, Taiwan) and immersing it in 100 µl of ddH₂O for 5 min. The DNA was eluted by centrifuging (15300g for 5 min) the column. After agarose gel electrophoresis of 0.3 µg of the eluted DNA, DNA integrity was evaluated from video images by densitometry using Visionworks LS software (UVP, Upland, CA, USA).

Statistical analysis

SE values were calculated from each triplicate set and *t*-tests were performed using GraphPad Prism 4 software (GraphPad Software; San Diego, CA, USA). A

p -value <0.05 was considered statistically significant. Kaplan–Meier analysis was carried out and the graphs plotted using GraphPad Prism 4, and curves were compared using the log-rank test.

Results

Biolistic gene delivery device

A photograph of the low-pressure gene delivery device is shown in Figure 1A. Low pressure helium is supplied through the bottom inlet. The DNA sample is applied to the top hole and propelled into the target tissue via a nozzle. The internal features are illustrated in Figure 1B. The inner nozzle is convergent, whereas the outer nozzle is divergent. The trigger momentarily releases helium gas. A supersonic flow is generated when the pressure difference between the inner and outer nozzle is greater than 1.9 atm and can accelerate particles to extremely high speed. Previous results from our group and others indicated that supersonic flow can safely and effectively deliver gold particle-coated DNA into animals and generate immune responses delaying tumor growth [22,23].

Novel biolistic gene gun can deliver noncarrier naked DNA into mouse epidermis

Initially, we investigated whether naked DNA could be delivered into the skin of C3H/HeN mice, BALB/c mice, and C57BL/6 mice. Luciferase was used as a reporter gene to monitor the expression of the DNA vaccine plasmid; imaging detected luciferase activity *in vivo* after delivery of 1 μ g of naked DNA plasmid in the three strains of mice. However, the activity was significantly higher after vaccination with 1 μ g of coated DNA than with 1, 5, or 10 μ g of naked DNA in C3H/HeN, BALB/C, and C57BL/6 mice (Figure 2A). Quantification of luciferase expression is shown in Figure 2B. To further examine the localization of the plasmid, the coated pCMV-EGFP DNA or naked pCMV-EGFP DNA was used to inoculate C3H/HeN mice. Their skins were sectioned 48 h after inoculation and examined by immunofluorescence microscopy. Coated or naked pCMV-EGFP DNA was mainly detected in the epidermis (Figure 2C). Several studies have demonstrated that, following intradermal immunization, dendritic cells migrate to draining lymph nodes where they play a major role in priming and stimulating antigen-specific T cells [26–28]. Therefore, it is important to determine whether dendritic cells express the reporter genes in draining lymph nodes when naked DNA is administered. The numbers of CD11c+ and GFP-positive cells in the inguinal lymph nodes are similar whether vaccination is with gold particles coated with 1 μ g of pCMV-EGFP DNA or 1 μ g of naked pCMV-EGFP DNA. Interestingly, we observed a greater percentage of GFP-positive CD11c+

cells in lymph nodes from mice injected with 5 and 10 mg of naked DNA than in lymph nodes from mice vaccinated with either 1 mg gold particles-coated pCMV-EGFP DNA or 1 mg of naked pCMV-EGFP DNA (Figure 2D).

Cancer therapy with naked DNA delivered by a low-pressure biolistic device

To examine whether noncarrier DNA vaccine had a cancer therapeutic effect, MBT-2 bladder tumor cells in C3H/HeN mice were used as a tumor model [29]. Overexpression of endogenous p185neu was observed in MBT-2 cells. We had previously demonstrated that low-pressure gene-gun propelled, skin delivery of gold particles coated with DNA encoding the extracellular portion of p185neu (pCMV-human-*N'*-neu) inhibited MBT-2 tumor growth in C3H/HeN syngeneic mice [23]. One million MBT-2 tumor cells were implanted subcutaneously at day 1. Gold particle-coated or noncarrier naked pCMV-human-*N'*-neu DNA (1 μ g) was inoculated three times at weekly intervals after the tumors became palpable (day 10). The tumor volume was measured (Figure 3A) and the survival data were subjected to Kaplan–Meier analysis (Figure 3B). One μ g of pCMV-human-*N'*-neu DNA could delay tumor progression and extend lifespan. In addition, 1 μ g of naked DNA vaccine had the same therapeutic efficacy as 1 μ g of the coated DNA vaccine. ELISA was used to detect the extracellular portion of p185neu in skin. The amount of the *N*-terminal portion of human p185neu produced by 1 μ g of naked DNA vaccine was much lower than that produced by 1 μ g coated DNA vaccine (Figure 4A). The amount of anti-p185neu antibody in serum was the measure of humoral immunity. The antibody response was weaker to naked DNA vaccine than to coated DNA vaccine, which is consistent with the expression of pCMV-human-*N'*-neu (Figure 4B). Cell-mediated toxicity to MBT-2 targets was the measure of anti-tumor cellular immunity in the spleen cell population. Both vaccines elicited similar cell-mediated cytotoxic immune responses (Figure 4C). Therefore, we hypothesized that the naked DNA vaccine may activate a Th1-biased immune reaction and lead to cellular immune responses. RT-PCR assay of the Th1/Th2 cytokine profile of mice inoculated with naked versus coated DNA vaccine revealed significant induction of IFN- γ by the naked DNA vaccine but not by the coated DNA vaccine. By contrast, interleukin (IL)-4 and IL-10 was significantly induced by the coated DNA vaccine, suggesting a Th2 immune response (Figure 4D). ELISA of IL-4 and IFN- γ protein expression reflected the RT-PCR results; however, there was less of a difference in IFN- γ (Figure 4E). These results suggest that compared to the coated vaccine, the naked vaccine induces more of a Th1-type immune response.

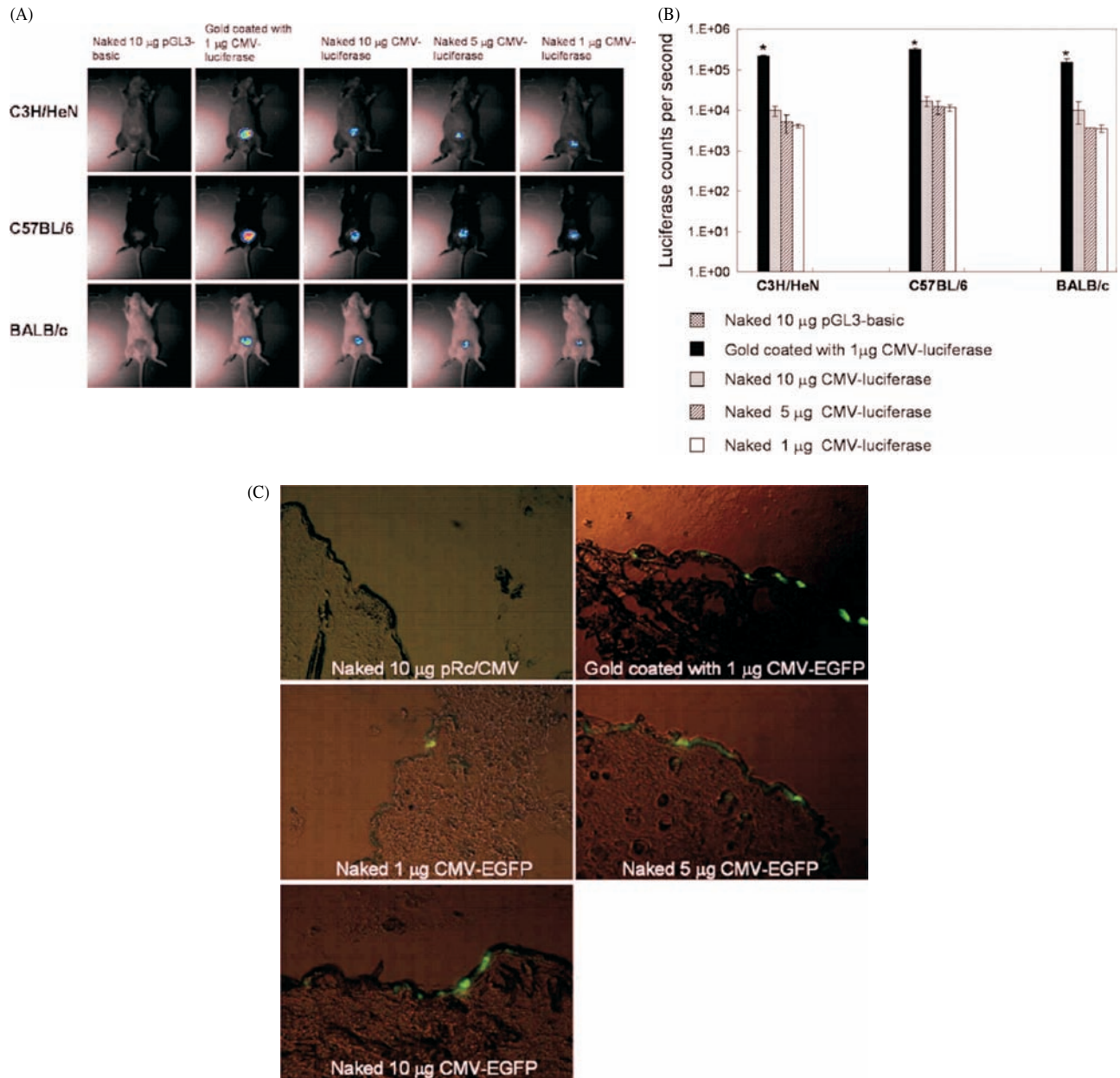


Figure 2. Naked DNA can be delivered into mouse skin. (A) Expression of luciferase in skin. Mice were inoculated with 1 μ g of gold particle-coated pCMV-luciferase DNA or 1, 5, 10 μ g of naked pCMV-luciferase DNA. *In vivo* images showing luciferase activity at 48 h after inoculation (taken with a Night Owl imaging unit). (B) Histogram showing the quantification of luciferase activity. *Statistically significant difference compared to the 10- μ g naked CMV-luciferase group ($p < 0.05$) (C) Expression of GFP in the epidermis. C3H/HeN mice were inoculated with 1 μ g of gold particle-coated pCMV-EGFP DNA or 1, 5, or 10 mg of naked pCMV-EGFP DNA. The mouse skin was removed 48 h later, fixed, paraffin-embedded, and sectioned for green fluorescence observation. (D) Migration of GFP-positive CD11c+ dendritic cells into lymph node. Mice were inoculated with 1 μ g of gold particle-coated pCMV-EGFP DNA or 1–10 μ g of naked pCMV-EGFP DNA, and the inguinal lymph nodes were removed 48 h later. The ratio of GFP positive to total CD11c+ dendritic cells was measured using flow cytometry. The CD11c+ dendritic cell population was first enriched using CD11c (N418) microbeads and then by flow cytometry gated for monocyte-like cells. *Statistically significant difference compared to the control DNA plasmid ($p < 0.05$)

Influence of gene-gun firing on DNA plasmid integrity

Finally, we monitored the integrity of DNA plasmids before and after supersonic flow (i.e. coated or naked pCMV-human-HER-2/neu DNA propelled by supersonic flow onto filter paper at 40 or 60 psi, respectively). The DNA was recovered from the filter paper and evaluated by

gel electrophoresis. Compared with the control (DNA simply spotted on filter paper), DNA propelled by supersonic flow was somewhat degraded at air pressures of 40 psi (coated DNA) or 60 psi (naked DNA). Semi-quantitative analysis of video images revealed 65–70% shearing of the naked DNA and 20–25% shearing of the coated DNA (Figure 5). However, approximately one-third of the DNA remained apparently intact. The residual intact

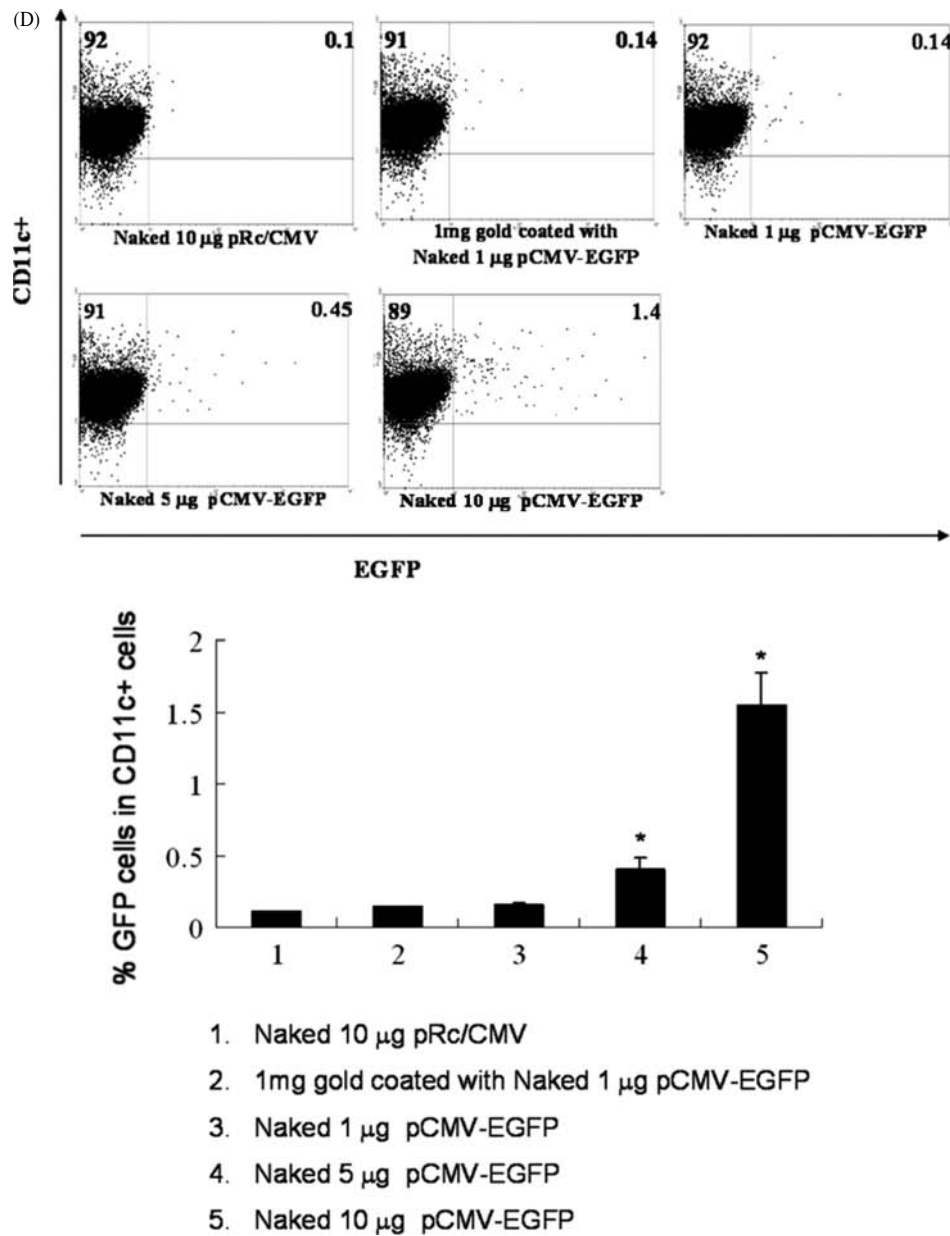


Figure 2. (Continued)

nucleic acid might be quantitatively and qualitatively sufficient to generate a Th1-biased immune response in the skin.

Discussion

In the present study, we demonstrate that naked DNA can be delivered via supersonic flow into mouse skin using a low-pressure biolistic device. The naked DNA can induce Th1-biased immunity and be used as a cancer therapeutic agent. The expression of DNA-encoded protein was DNA dose-dependent, as demonstrated by luciferase imaging *in vivo*, and was mainly in the epidermis. Furthermore, the noncarrier naked pCMV-human-*N'*-neu DNA vaccine and gold particle-coated pCMV-human-*N'*-neu DNA vaccine had comparable therapeutic value as demonstrated by

the significant delay in tumor progression and extension of mouse lifespan. Less antigen was expressed in response to the naked DNA vaccine than to the coated DNA vaccine, and the antibody response induced by the naked DNA vaccine was weak. By contrast, both vaccines elicited comparable cell-mediated cytotoxicity responses of spleen cells to MBT-2 cells. The reason both vaccines have comparable anti-tumor effects might be that eradication of MBT-2 tumor overexpressing p185neu is mainly through CD8+ T cells [23,29], with the antibody response apparently playing only a minor role.

The Th1/Th2 profile was influenced by multiple factors including the method, route, amount of gene-gun delivered DNA, and the nature of the antigen. The Th1 type response is mainly attributed to immunostimulatory DNA sequences containing the CpG motif. Although DNA

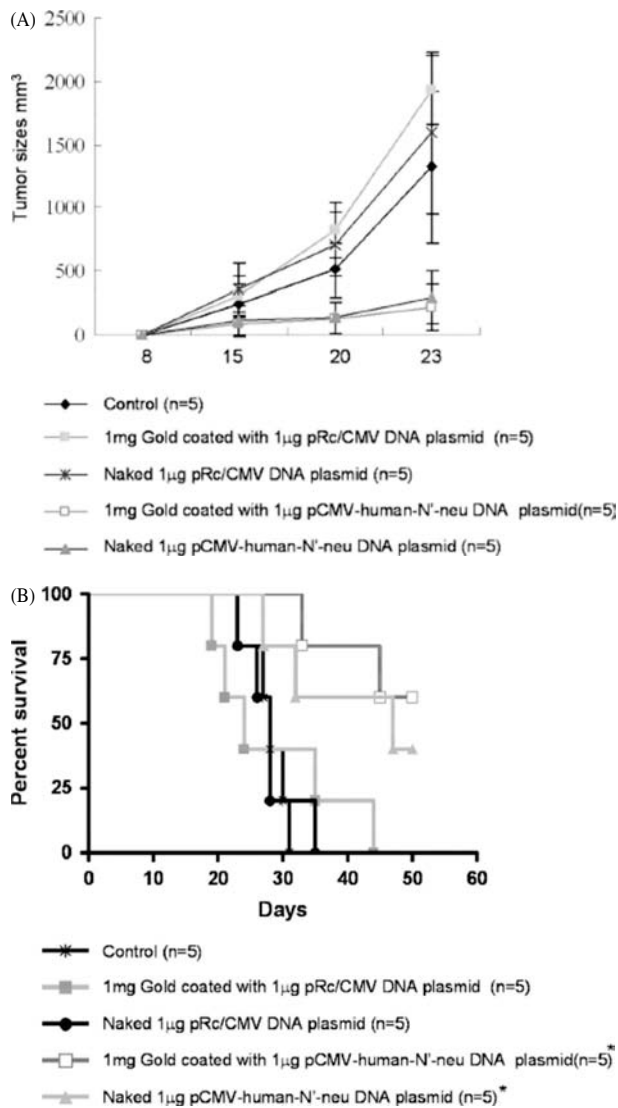


Figure 3. Cancer therapy with gene-gun delivery of naked or coated pCMV-human-N'-neu DNA vaccine. (A) Time course of tumor volume change. The average tumor volume was measured until sacrifice due to excess tumor burden. (B) Lifespan of C3H/HeN mice after subcutaneous challenge with MBT-2 cells. The number of mice in the experiment are in parenthesis. *Statistically significant difference compared to the control saline mice ($p < 0.05$). The survival data were subjected to Kaplan–Meier analysis

dose as low as 1 μ g can stimulate Th1 responses by muscle injection [28], this low dose (1 μ g) may not be enough to induce a Th1 response by skin vaccination using a gene gun. On the other hand, gold particle DNA vaccines were demonstrated to have mainly Th2-promoting effects [30,31]. In this report, we demonstrated that 1 μ g of gene-gun inoculated naked DNA might be sufficient to produce a Th1-biased response, suggesting that the amount of DNA plays only a minor role in Th1/Th2 biasing and that the carrier of the DNA may have a greater role.

Evidence indicates that Th1 immunity is critical for the induction of specific cell-mediated cytotoxic cells such as tumor-specific cytotoxic T lymphocytes

in tumor-bearing mice [32,33]. In the present study, naked DNA vaccine induced a stronger Th1-biased response than coated DNA vaccine, but the spleen cell-mediated cytotoxic responses to naked and coated DNA were similar (Figure 4C). One explanation for this result is that coated DNA may more efficiently transfect skin keratinocytes, which affect the magnitude of immune response by presenting the protein products of transfected genes through a process [34] that culminates in the induction of antigen-specific CD8+ T cells

In the spleen cell-mediated cytotoxic response to MBT-2 tumor cells, lymphocytes are activated by recombinant HER-2/neu protein, suggesting that the cytotoxic response is probably directed towards those MBT-2 cells overexpressing HER-2/neu. However, we cannot exclude nonspecific immune cells such as natural killer cells or macrophages in the spleen from playing a role in the anti-MBT-2 cell response. Hence, whether nonspecific immune cells contribute to tumor cell killing and whether the DNA formulation can affect this role should be examined.

In the present study, skin delivery of 1 μ g of gold particle-coated or naked pCMV-EGFP DNA generated similar numbers of GFP-positive CD11c+ dendritic cells in lymph nodes. Interestingly, the percentage of these cells in lymph nodes is much higher when the naked pCMV-EGFP-DNA dose is 10 μ g. The result could be attributed to two possible factors. Results indicating DNA vaccine coadministered with plasmids carrying anti-apoptotic factors can increase the percentage of dendritic cells migrated from epidermis to lymph node [24] suggest that the survival (after bombardment with naked DNA versus coated DNA) and migration of dendritic cells into lymph nodes may be increased because the dendritic cells are less damaged by gene-gun transfer of naked DNA than by gene-gun transfer of coated DNA. The second possibility is that naked DNA may be more easily taken up by dendritic cells in the epidermis than coated DNA. Uptake of coated DNA might be less efficient because, when introduced into the epidermis, the DNA is in the proximity of, but not injected directly into, the dendritic cells. Uptake is therefore dependent on endocytosis and related processes, which may be more efficient for naked DNA than coated DNA. Since the gold coating limits the amount of DNA uptake and not all 10 μ g of gold-coated DNA is taken up [35], we cannot exclude the possibility that delivery of 10 μ g of coated DNA would not elevate the percentage of GFP-positive cells to a similar extent. The mechanism of this interesting phenomenon requires further investigation.

The mechanism by which DNA penetrates the skin barrier is unknown. First, the force of supersonic flow may cause transient skin permeability to large molecules such as plasmid DNA. Second, the DNA (rather than penetrate) may first adhere to the skin surface and subsequently be absorbed through the skin barrier. The latter possibility is less likely because treatment of skin

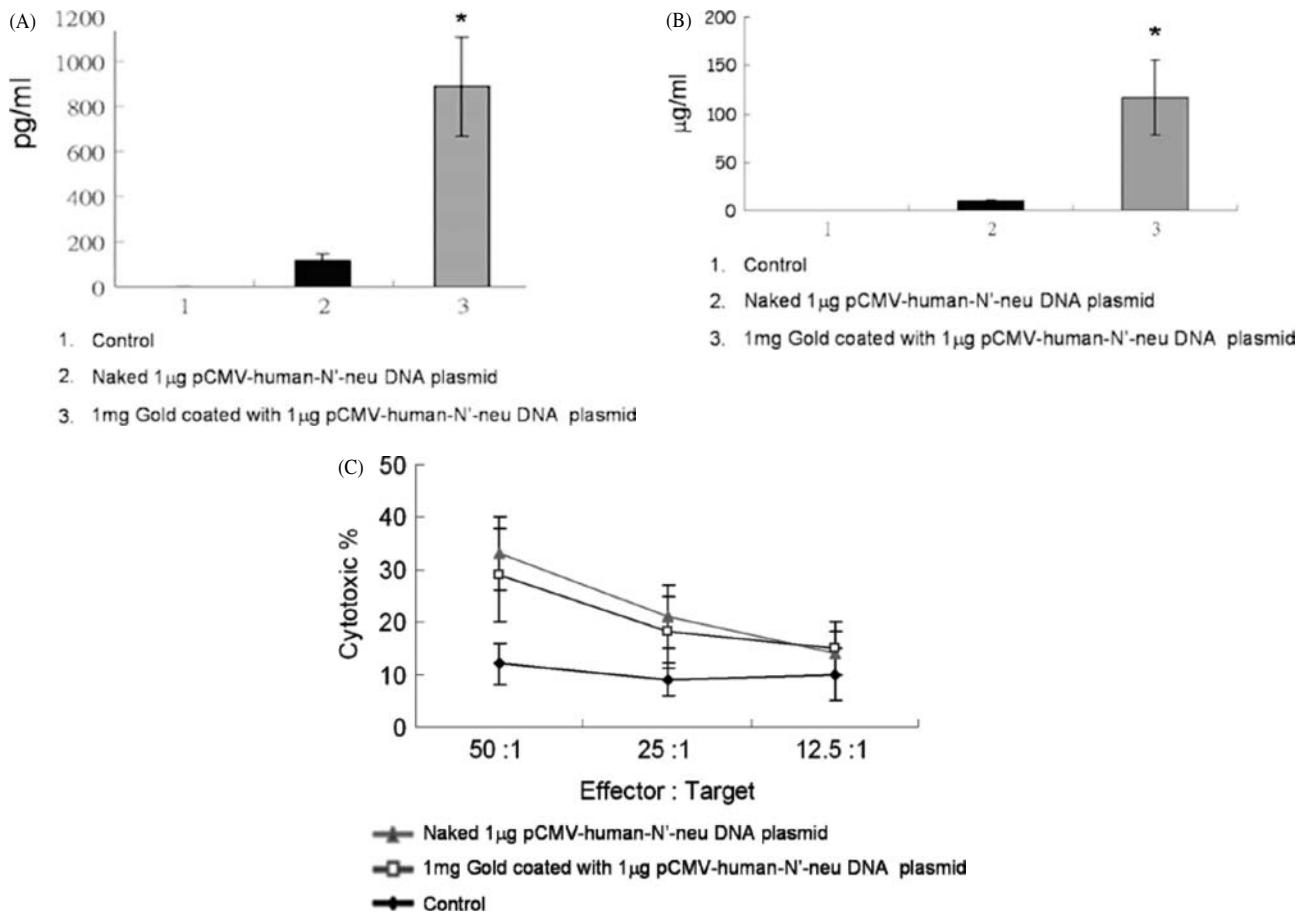


Figure 4. The immune responses to naked or coated pCMV-human-N'-neu DNA vaccine. (A) The expression of the extracellular domain of p185neu in skin measured with ELISA. (B) Anti-p185neu antibody titers in sera measured with ELISA. The data are average titers in the sera of three mice. (C) Spleen cell-mediated cytotoxicity assay for targeting MBT-2 cells in inoculated mice. Target cells were MBT-2-luciferase cells cultured *in vitro*. Effector cells were lymphocytes from mice treated with naked or coated N'-neu DNA vaccine. Cytotoxicity was determined by the luciferase release. Each point represents the average of triplicate wells. (D) Pooled splenocytes from each group were stimulated with p185neu antigen. RNA was extracted and RT-PCR was performed to assess cytokine mRNA levels. Hypoxanthine phosphoribosyltransferase (HPRT) was used as an internal control. (E) Supernatants were collected 2 days after stimulation and the concentration of IFN- γ and IL-4 were measured with ELISA. *Statistically significant difference compared to the 1- μ g naked pCMV-human-N'-neu DNA vaccine group ($p < 0.05$)

with DNase immediately after bombardment had no effect on luciferase expression (data not shown). A recent report on gene-gun transfer of naked DNA [36] suggested that the shockwave generated by a gene gun can cause transient permeability to outside substances, which is similar to our first proposed mechanism.

Our results demonstrate that naked DNA can be introduced through the skin in sufficient quantity to generate a cellular response capable of delaying tumor progression. Naked DNA vaccines may have several advantages over coated DNA vaccines, including ease of development, minimal preparation costs, and reduced skin damage. The level of antigen expression in the skin and the antibody response indicate that naked DNA is less efficiently delivered than coated DNA. Therefore, naked DNA may be useful in treating cancer or diseases that depend on the cell-mediated immune response, but not the antibody-mediated response. In addition, naked DNA may be useful in treating diseases, such as Dengue virus infection, where preventing inadvertent antibody

responses is desirable. The development of severe dengue hemorrhagic fever/dengue shock syndrome after vaccination suggests that anti-virion antibodies induced by current Dengue virus vaccines may enhance infection [37].

Our experiments further extend the use of biolistic technology to deliver naked DNA into skin. The key feature of this low-pressure gene gun is the converging-diverging nozzle, which is used in rocket engines. The force generated by the nozzle is determined by three parameters: (i) the gas speed; (ii) length of the terminal spray tube; and (iii) type of gas used. Alteration of these parameters may further expand the range of gene-gun usage. For example, naked DNA may be delivered into surgically exposed organs in the future. Furthermore, since supersonic flow apparently caused approximately three-fold more damage to naked DNA than coated DNA, finding ways to protect DNA molecules may further enhance its laboratory or clinical use.

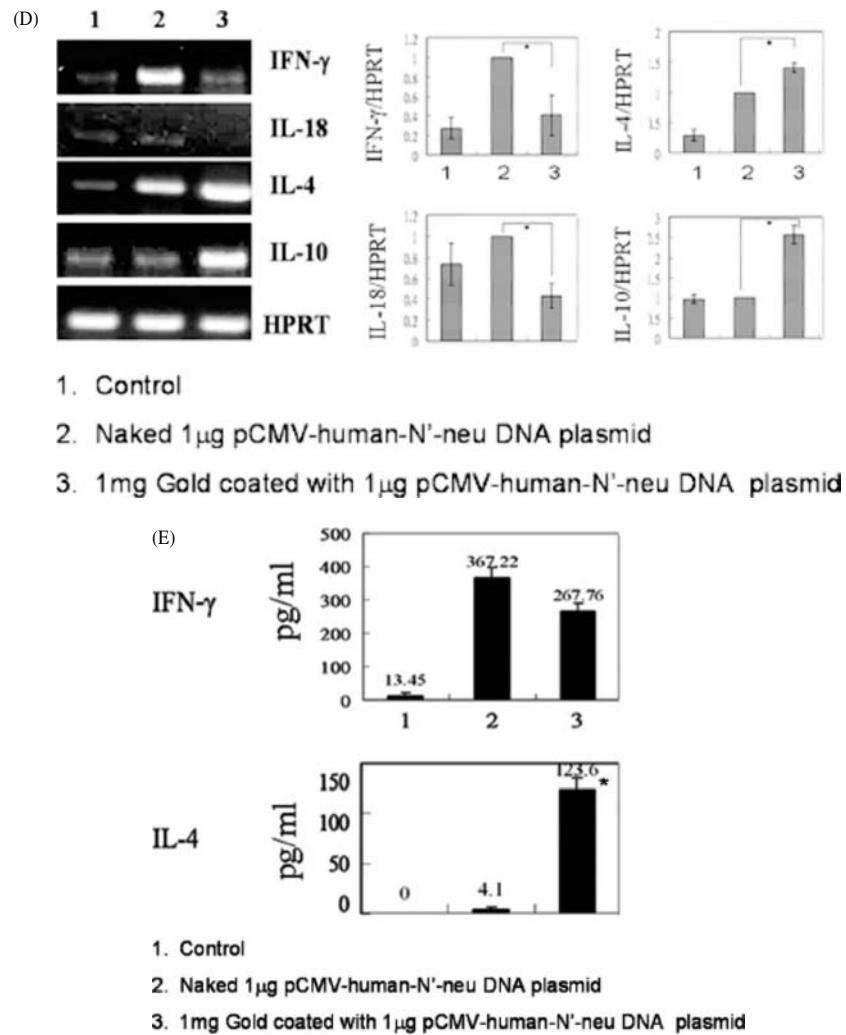


Figure 4. (Continued)

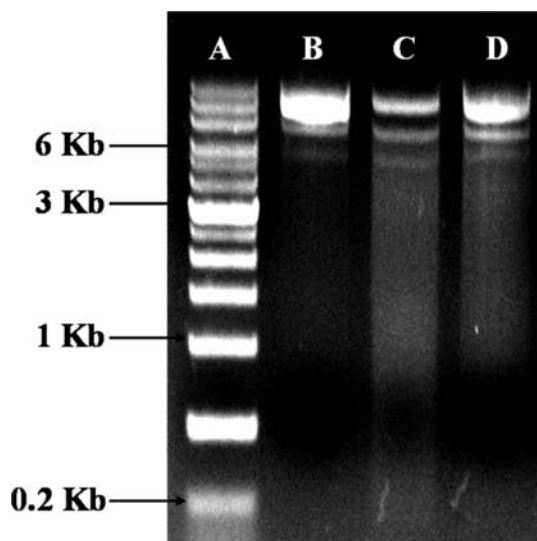


Figure 5. Influence of supersonic flow on plasmid DNA integrity. The integrity of plasmid DNA after gene-gun delivery was analysed by electrophoresis through a 1% agarose gel. Lane A: molecular weight marker; lane B: HER-2/neu DNA plasmid before delivery by gene gun; lane C: Naked HER-2/neu DNA plasmid after delivery by gene gun (60 psi); lane D: Gold particle coated with HER-2/neu DNA plasmid after delivery by gene gun (40 psi). 0.3 μg of DNA was loaded per lane

Acknowledgements

This study is supported by Grants NSC-93-3112-B-006-006 and NSC-94-3112-B-006-011 from National Science Council, Taiwan, Republic of China.

References

- VandenDriessche T, Collen D, Chuah MK. Biosafety of onco-retroviral vectors. *Curr Gene Ther* 2003; **3**: 501–515.
- Klein RM, Wolf ED, Wu R, *et al.* High-velocity microprojectiles for delivering nucleic acids into living cells. *Biotechnology* 1992; **24**: 384–386.
- Liu F, Huang L. A syringe electrode device for simultaneous injection of DNA and electrotransfer. *Mol Ther* 2002; **5**: 323–328.
- Chen WC, Huang L. Non-viral vector as vaccine carrier. *Adv Genet* 2005; **54**: 315–337.
- Foldvari M, Babiuk S, Badea I. DNA delivery for vaccination and therapeutics through the skin. *Curr Drug Deliv* 2006; **3**: 17–28.
- Oard JH. Physical methods for the transformation of plant cells. *Biotechnol Adv* 1991; **9**: 1–11.
- Yang NS, Burkholder J, Roberts B, *et al.* In vivo and in vitro gene transfer to mammalian somatic cells by particle bombardment. *Proc Natl Acad Sci USA* 1990; **87**: 9568–9572.
- Heiser WC. Gene transfer into mammalian cells by particle bombardment. *Anal Biochem* 1994; **217**: 185–196.

9. Macklin MD, McCabe D, McGregor MW, *et al.* Immunization of pigs with a particle-mediated DNA vaccine to influenza A virus protects against challenge with homologous virus. *J Virol* 1998; **72**: 1491–1496.
10. Tang DC, Devit M, Johnson SA. Genetic immunization is a simple method for eliciting an immune response. *Nature* 1992; **356**: 152–154.
11. Ulmer JB, Donnelly JJ, Parker SE, *et al.* Heterologous protection against influenza by injection of DNA encoding a viral protein. *Science* 1993; **259**: 1745–1749.
12. Lollini PL, De Giovanni C, Pannellini T, *et al.* Cancer immunoprevention. *Future Oncol* 2005; **1**: 57–66.
13. Barry MA, Johnston SA. Biological features of genetic immunization. *Vaccine* 1997; **15**: 788–791.
14. Feltquate DM, Heaney S, Webster RG, *et al.* Different T helper cell types and antibody isotypes generated by saline and gene gun DNA immunization. *J Immunol* 1997; **158**: 2278–2284.
15. Schirmbeck R, Reimann J. Modulation of gene-gun-mediated Th2 immunity to hepatitis B surface antigen by bacterial CpG motifs or IL-12. *Intervirology* 2001; **44**: 115–123.
16. Cohen AD, Boyer JD, Weiner DB. Modulating the immune response to genetic immunization. *FASEB J* 1998; **12**: 1611–1626.
17. Zhou X, Zheng L, Liu L, *et al.* T helper 2 immunity to hepatitis B surface antigen primed by gene-gun-mediated DNA vaccination can be shifted towards T helper 1 immunity by codelivery of CpG motif-containing oligodeoxynucleotides. *Scand J Immunol* 2003; **58**: 350–357.
18. Haddad D, Liljeqvist S, Stahl S, *et al.* Differential induction of immunoglobulin G subclasses by immunization with DNA vectors containing or lacking a signal sequence. *Immunol Lett* 1998; **61**: 201–204.
19. Aberle JH, Aberle SW, Allison SL, *et al.* A DNA immunization model study with constructs expressing the tick-borne encephalitis virus envelope protein E in different physical forms. *J Immunol* 1999; **163**: 6756–6761.
20. Weiss R, Scheiblhofer S, Freund J, *et al.* Gene gun bombardment with gold particles displays a particular Th2-promoting signal that over-rules the Th1-inducing effect of immunostimulatory CpG motifs in DNA vaccines. *Vaccine* 2002; **20**: 3148–3154.
21. Ikeda H, Chamoto K, Tsuji T, *et al.* The critical role of type-1 innate and acquired immunity in tumor immunotherapy. *Cancer Sci* 2004; **95**: 697–703.
22. Cheng WF, Lee CN, Chang MC, *et al.* Antigen-specific CD8+ T lymphocytes generated from a DNA vaccine control tumors through the Fas-FasL pathway. *Mol Ther* 2005; **12**: 960–968.
23. Tu CF, Lin CC, Chen MC, *et al.* Autologous neu DNA vaccine can be as effective as xenogenic neu DNA vaccine by altering administration route. *Vaccine* 2007; **25**: 719–728.
24. Kim TW, Hung CF, Ling M, *et al.* Enhancing DNA vaccine potency by coadministration of DNA encoding antiapoptotic proteins. *J Clin Invest* 2003; **112**: 109–17.
25. Giovarelli M, Musiani P, Modesti A, *et al.* Local release of IL-10 by transfected mouse mammary adenocarcinoma cells does not suppress but enhances antitumor reaction and elicits a strong cytotoxic lymphocyte and antibody-dependent immune memory. *J Immunol* 1995; **15**: 3112–23.
26. Klinman DM, Sechler JM, Conover JM, *et al.* Contribution of cells at the site of DNA vaccination to the generation of antigen-specific immunity and memory. *J Immunol* 1998; **160**: 2388–2392.
27. Torres CA, Iwasaki A, Barber BH, *et al.* Differential dependence on target site tissue for gene gun and intramuscular DNA immunizations. *J Immunol* 1997; **158**: 4529–4532.
28. Ji H, Wang TL, Chen CH, *et al.* Targeting human papillomavirus type 16 E7 to the endosomal/lysosomal compartment enhances the antitumor immunity of DNA vaccines against murine human papillomavirus type 16 E7-expressing tumors. *Hum Gene Ther* 1999; **10**: 2727–2740.
29. Lin CC, Chou CW, Shiau AL, *et al.* Therapeutic HER2/Neu DNA vaccine inhibits mouse tumor naturally overexpressing endogenous neu. *Mol Ther* 2004; **10**: 290–301.
30. Feltquate DM, Heaney S, Webster RG, *et al.* Different T helper cell types and antibody isotypes generated by saline and gene gun DNA immunization. *J Immunol* 1997; **158**: 2278–2284.
31. Weiss R, Scheiblhofer S, Freund J, *et al.* Gene gun bombardment with gold particles displays a particular Th2-promoting signal that over-rules the Th1-inducing effect of immunostimulatory CpG motifs in DNA vaccines. *Vaccine* 2002; **20**: 3148–3154.
32. Nishimura T, Iwakabe K, Sekimoto M, *et al.* Distinct role of antigen-specific T helper type 1 (Th1) and Th2 cells in tumor eradication in vivo. *J Exp Med* 1999; **190**: 617–628.
33. Germann T, Gately MK, Schoenhaut DS, *et al.* Interleukin-12/T cell stimulating factor, a cytokine with multiple effects on T helper type 1 (Th1) but not on Th2 cells. *Eur J Immunol* 1993; **23**: 1762.
34. Shirota H, Petrenko L, Hong C, *et al.* Potential of transfected muscle cells to contribute to DNA vaccine immunogenicity. *J Immunol* 2007; **179**: 329–36.
35. van Drunen S, den Hurk LV. Novel methods for the non-invasive administration of DNA therapeutics and vaccines. *Curr Drug Deliv* 2006; **3**: 3–15.
36. Lian WN, Chang CH, Chen YJ, *et al.* Intracellular delivery can be achieved by bombarding cells or tissues with accelerated molecules or bacteria without the need for carrier particles. *Exp Cell Res* 2007; **313**: 53–64.
37. Green S, Rothman A. Immunopathological mechanisms in dengue and dengue hemorrhagic fever. *Curr Opin Infect Dis* 2006; **19**: 429–436.

A low-pressure gene gun for genetic transformation of maize (*Zea mays* L.)

Chien-Yuan Kao · Shin-Hui Huang ·
Chiu-Mei Lin

Received: 24 June 2008 / Accepted: 1 August 2008
© Korean Society for Plant Biotechnology and Springer 2008

Abstract We have successfully used the low-pressure BioWare gene gun, developed for gene transfer in animal cells, for plant tissues. The BioWare device is easy to manipulate. Just 50 psi helium pressure was sufficient to transfer foreign genes into the aleurone layer and embryo of maize without causing tissue damage in the impact area. As shown by expression signals from invasive histochemical β -glucuronidase (GUS) activity, the foreign reporter gene expressed well in bombarded tissues. This successful GUS-transient expression extends the application of this low-pressure gene gun from animal cells to plant tissues.

Keywords Maize · Gene gun · GUS ·
Transient expression · BioWare

Introduction

The stable integration of foreign genes into plant genome represents one of the most significant developments in plant biology and crop improvement. The first transgenic tobacco plant was produced by using *Agrobacterium tumefaciens* (Horsch et al. 1985). Several years later, the high-velocity microprojectile, or gene-gun technology, was invented by John Sanford and his colleagues (Klein

et al. 1987; Sanford 2000). Both methods have been used extensively for genetic transformation of plants, leading to the commercialization of biotech crops. The biolistics system can be used with intact tissues and is not restricted to any particular plant group. It has revolutionized plant genetics by producing most of the world's biotech crops and has also been used extensively in transient expression assays for studying gene regulation and function (Christou 1992; Kao et al. 1996; Sambrook and Russel 2001; Vasil 2003). A number of modifications of the original biolistics device have been developed to improve its performance (Gray and Finer 1993; Kikkert 1993; McCabe and Christou 1993; Oard 1993; Sautter 1993; Vain et al. 1993). One of the major problems with all biolistic devices developed so far is the use of high pressure, which causes severe damage to target cells. They also suffer from several other disadvantages: (1) low transformation efficiency, (2) need to use large amounts of deoxyribonucleic acid (DNA), (3) laborious to use, (4) high noise level, (5) large size and design makes it less portable, (6) and the high cost of the basic instrument and disposable supplies needed for operation.

The low-pressure BioWare gene gun has been used for genetic transformation of animal cells and human tumor cell lines only (Chang et al. 2008; Cheng et al. 2005a, b; Tu et al. 2007; Lin et al. 2008). By gene delivery and expression in the aleurone layer and embryos of maize (*Zea mays* L.) we show for the first time that it can be equally effective in plant transformation. We found the BioWare device to be safe and flexible to use, as well as light and handy. We used it obtain 18 stable transgenic plants of the orchids *Mormodes lawrence* and *Zygopetalum mackayi*, transformed with three different plasmid constructs (manuscript in preparation).

C.-Y. Kao (✉) · S.-H. Huang
Department of Horticulture, National I-Lan University,
Yilan 26047, Taiwan
e-mail: cykao@niu.edu.tw

C.-M. Lin
School of Medicine, College of Medicine,
Taipei Medical University, Taipei 110, Taiwan

Materials and methods

Tissue preparation

Sweet corn (*Zea mays* L.) ears of 25 days after pollination were surface-sterilized by immersion for 1 min in 70% ethanol and 5 min in 5% commercial Clorox, followed by two rinses with sterile water. The kernels were cut horizontally, and the pericarp was peeled off to expose the aleurone layer. The developing embryos were then removed from the kernel. The kernels with exposed aleurones and isolated embryos were placed on a gelrite solidified Murashige Skoog (MS) medium (Sigma, M5519) containing 20 g/l sucrose prior to bombardment.

Particle bombardment

The preparation of the pCambia 1301 plasmid DNA/gold mixture was modified from the methods described previously (Taylor and Vasil 1991). Briefly, 37 μ l of a 40 mg/ml gold stock solution (1.6 μ m diameter, Biorad Inc.) was mixed in order with 25 μ l water and 5 μ g plasmid DNA in a 250- μ l Eppendorf tube. The tubes were vortexed briefly before and after each addition. Twenty microliters of 100 mM free-base spermidine and 50 μ l of 2.5 M calcium chloride (CaCl_2) were placed in separate drops on the side of the tube to avoid premature mixing of either solution with the DNA/gold solution. The tubes were then immediately mixed by vortexing for 10 s. At that time, the plasmid DNA was precipitated and attached to the gold particle. The tubes were centrifuged for 5 s and the supernatant fluid removed. Two hundred microliters of 100% ethanol were added and sonicated briefly. After brief centrifugation to pellet the gold/DNA, the supernatant fluid was removed. One hundred microliters of 100% ethanol were added and the tubes placed on ice. A 10- μ l volume of sonicated gold/DNA mixture was used for each bombardment. The gun was pointed longitudinally to the sample under a funnel-shaped steel net (3 cm high) with a helium pressure of 50 psi. The BioWare low-pressure gene gun with its accessory parts (Fig. 1a; BioWare Technologies Co. Ltd., Taipei, Taiwan) was used for these experiments.

Histochemical localization of GUS activity

Bombarded aleurone kernels and embryos were incubated overnight at 37°C in the presence of 1 mM 5-bromo-4-chloro-3-indolyl-b-D-glucuronide (X-Gluc) and 0.5 mM potassium ferricyanide. Photographs were taken under low magnification with a light microscope (Jefferson et al. 1987).

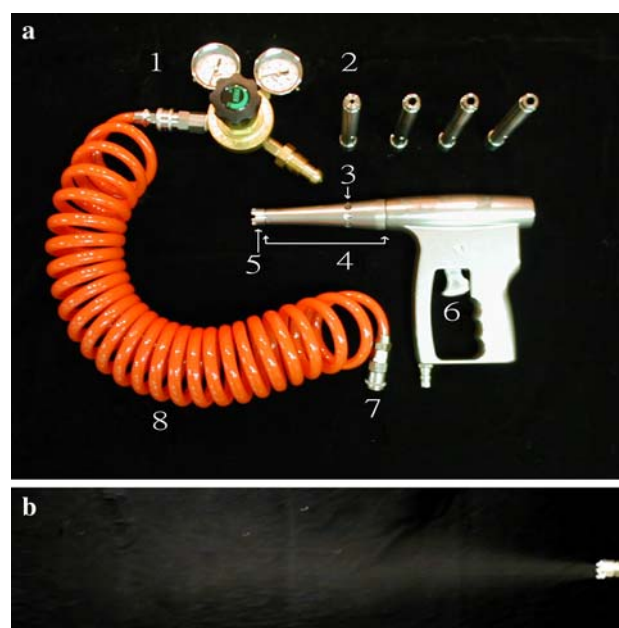


Fig. 1 BioWare low-pressure gene gun and image of sample explosion from the gun. **a** Low-pressure gene gun and its accessory parts, 1 regulator; 2 barrels with different inside diameter; 3 loading aperture; 4 sleeve; 5 spacer; 6 trigger; 7 quick coupling; 8 PU coil tube. **b** Pattern of bursting mist from the gun at 50 psi helium pressure in 20 μ l distilled water simulation

Results and discussion

The direction and extent of exploding mist at the time of the explosion is shown in Fig. 1b. One of the major concerns for the application of the BioWare device for plant tissues has been the low pressure (maximum 75 psi) that is used to propel microprojectiles coated with DNA, and whether it would generate enough force to penetrate the rigid wall that surrounds plant cells. Two features incorporated in the design of the instrument overcame this limitation: (1) helium gas directly propels the DNA-coated particles, and (2) the distance between the gun hole and target tissues can be adjusted to nearly zero (Fig. 1). Without previous experience in plant tissues with this gun, we observed that edible brown pigment as loading buffer gave the best result with the filter set at 50 psi pressure and 3 cm from target tissue (Fig. 2). We then used this condition for aleurone and embryos tissue transformation.

Maize aleurone and embryo have been extensively used as ideal plant transient expression systems (Kao et al. 1996; Hattori et al. 1992; Hoecher et al. 1995; McCarty et al. 1991). In our study, 30 exposed aleurone kernels used in ten separate bombardments and 18 embryos in six separate bombardments with the pCambia 1301 construct showed strong positive β -glucuronidase (GUS) blue stain (Fig. 3). Indeed, the staining was intense. Therefore, we reduced the length of time used for incubation and GUS

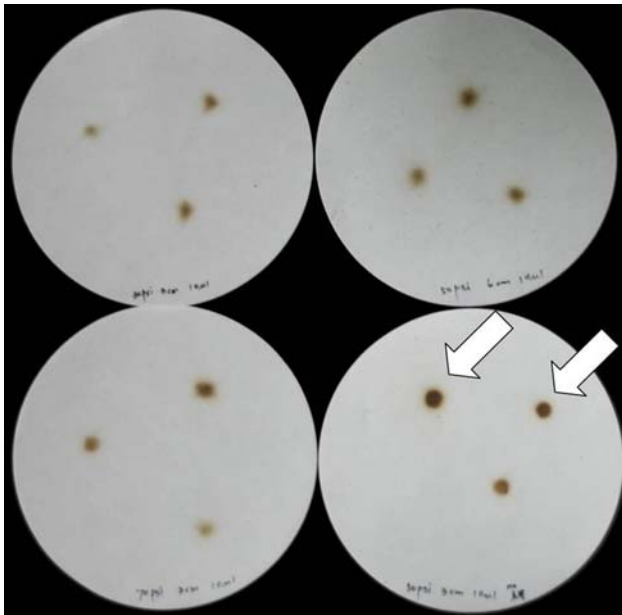


Fig. 2 Ten microliters of brown pigment as loading buffer generates the best impact area with 50 psi, with the target at 3 cm (*bottom right; arrow*). Other conditions tested were 30 psi, 3 cm (*upper left*); 70 psi, 3 cm (*bottom left*), and 50 psi, 6 cm (*upper right*)



Fig. 3 Strong β -glucuronidase (GUS) expression on the surface of maize aleurone layer and embryos after low-pressure gene-gun bombardment. Appearance of GUS stain on the **a** aleurone layer and **b** embryos bombarded with pCambia 1301 in contrast to no blue stain in DNA-free control on the *left*

staining to create well-defined blue spots. From the longitudinal free-hand sections of the embryo and kernels, the GUS blue stain could be seen beyond the outer surface layers of the embryo in contrast to aleurone (Fig. 4). This indicates that even at the low pressure of 50 psi, DNA-coated gold particles can penetrate several cells layers and be expressed in the inner layers of the embryo. Although the possible diffusion of β -glucuronidase and/or its blue cleavage products cannot be ruled out. It should be pointed



Fig. 4 β -glucuronidase (GUS) staining in longitudinal free-hand sections of maize embryo and kernel with exposed aleurone layer. *Deep blue* GUS stain can be seen beyond the outer surface of embryo (*bottom left*) in contrast to *deep blue* in the outer layer of endosperm (*bottom right*) and their no-DNA control, respectively (*upper left and right*)

out that we obtained similar results with a privately owned green fluorescent protein (GFP) plasmid under fluorescent microscope. Positive GUS histochemical staining in the aleurone layer and embryos (Figs. 3, 4) indicated the successful delivery and expression of foreign DNA by the low-pressure BioWare gene gun. We show that helium gas pressure as low as 50 psi is sufficient to drive DNA/gold particles through several layers of cells in plant tissues and successfully express the introduced gene. Compared with the 1,300 psi used for transient assays in the same material (Kao et al. 1996), and 1,100–1,350 psi used in orchid transformation (Yu et al. 1999; Davina et al. 2007) with the Biolistics device, 50 psi helium pressure is exceptionally low. Bombardment of noncarrier naked DNA (without gold particles) at 50 or 70 psi, and shorter distance to the embryo and aleurone samples, gave only negative results. However, noncarrier naked DNA bombardment at low pressure has been successfully used for transformation in animal systems (Lin et al. 2008). This suggests that the rigid plant cell wall is indeed a penetration barrier and the gold particles play an indispensable role in plant tissue transformation.

High-velocity bombardment of DNA-coated microprojectiles allows direct delivery of genes of interest into regenerable plant tissues, bypassing the complexities and limitations of *Agrobacterium* transformation. It appears to be the best method for plant transformation (Christou 1992). The biolistics device has been used for the production of most of the world's major transgenic crops and also in extensive transient expression investigations. The low-pressure gene gun used by us was invented to circumvent the many problems associated with the use of existing devices in transforming live mice. We have shown that it is also efficient in delivering DNA constructs into plant cells and has several advantages over the traditional biolistics devices used previously.

Acknowledgments The authors thank Dr. Indra K. Vasil (Associate Director, Genetics Institute, University of Florida) for his critical reading of and helpful suggestions for the manuscript.

References

- Chang ML, Chen JC, Yeh CT, Chang MY, Liang CK, Chiu CT, Lin DY, Liaw YF (2008) Gene gun bombardment with DNA-coated gold particles is a potential alternative to hydrodynamics-based transfection for delivering genes into superficial hepatocytes. *Hum Gene Ther* 19:391–395
- Cheng WF, Hung CF, Chen CA, Lee CN, Su YN, Chai CY, Boyd DA, Hsieh CY, Wu TC (2005a) Characterization of DNA vaccines encoding the domains of calreticulin for their ability to elicit tumor-specific immunity and antiangiogenesis. *Vaccine* 23(29):3864–3874
- Cheng WF, Lee CN, Chang MC, Su YN, Chen CA, Hsieh CY (2005b) Antigen-specific CD8+T lymphocytes generated from a DNA vaccine control tumors through the Fas-FasL pathway. *Mol Ther* 12:960–968
- Christou P (1992) Genetic transformation of crop plants using microprojectile bombardment. *Plant J* 2:275–281
- Davina C, Lee SM, Ng JH, Yu H (2007) L-methionine sulfoximine as a novel selection agent for genetic transformation of orchids. *J Biotechnol* 131:466–472
- Gray DJ, Finer JJ (1993) Development and operation of five particle guns for introduction of DNA into plant cells. *Plant Cell Tissue Organ Cult* 33:219
- Hattori T, Vasil V, Rosenkrans L, Hannah LC, McCarty DR (1992) The *viviparous-1* gene and abscisic acid activate the *C1* regulatory gene for anthocyanin biosynthesis during seed maturation in maize. *Genes Dev* 6:609–618
- Hoecker U, Vasil IK, McCarty DR (1995) Integration control of seed maturation and germination programs by activator and repressor functions of *viviparous-1* of maize. *Genes Dev* 9:2459–2469
- Jefferson RA (1987) Assaying chimeric genes in plants: the GUS gene fusion system. *Plant Mol Biol Rep* 5:387–405
- Horsch RB, Fry JE, Hoffmann N, Wallroth M, Eichholtz D, Rogers SG, Fraley RT (1985) Transferring genes into plants. *Science* 227:1229–1331
- Kao CY, Cocciolone SM, Vasil IK, McCarty DR (1996) Localization and interaction of the *cis*-acting elements for abscisic acid, VIVIPAROUS1, and light activation of the *C1* gene of maize. *Plant Cell* 8:1171–1179
- Kikkert JR (1993) The biolistic PDS-1000/He device. *Plant Cell Tissue Organ Cult* 33:221–226
- Klein TM, Wolf ED, Wu R, Sanford JC (1987) High-velocity microprojectiles for delivering nucleic acids into living cells. *Nature* 327:70–73
- Lin CC, Yen MC, Lin CM, Huang SS, Yang HJ, Chow NH, Lai MD (2008) Delivery of noncarrier naked DNA vaccine into the skin by supersonic flow induces a polarized T helper type 1 immune response to cancer. *J Gene Med* 10:679–689
- McCabe D, Christou P (1993) Direct DNA transfer using electric discharge particle acceleration (ACCELL™ technology). *Plant Cell Tissue Organ Cult* 33:227–236
- McCarty DR, Hattori T, Carson CB, Vasil V, Lazar M, Vasil IK (1991) The *viviparous-1* developmental gene of maize encodes a novel transcriptional activator. *Cell* 66:895–905
- Oard J (1993) Development of an airgun device for particle bombardment. *Plant Cell Tissue Organ Cult* 33:247–250
- Sambrook J, Russel DW (2001) DNA transfection by biolistics. In: *Molecular cloning: a laboratory manual*, 3rd edn. Cold Spring Harbor, New York
- Sanford JC (2000) The development of the biolistic process. *In Vitro Cell Dev Biol Plant* 36:303–308
- Sautter C (1993) Development of a microtargeting device for particle bombardment of plant meristems. *Plant Cell Tissue Organ Cult* 33:251–257
- Taylor LP, Vasil IK (1991) Histology of and physical factors affecting transient GUS expression in plant millet (*Pennisetum glaucum* (L.) R. Br.) embryos following microprojectile bombardment. *Plant Cell Rep* 10:120–125
- Tu CF, Lin CC, Chen MC, Ko TM, Lin CM, Wang YC, Lai MD (2007) Autologous neu DNA vaccine can be as effective as xenogenic neu DNA vaccine by altering administration route. *Vaccine* 25(4):719–728
- Vain P, Keen N, Murillo J, Rathus C, Nemes C, Finer JJ (1993) Development of the particle inflow gun. *Plant Cell Tissue Organ Cult* 33:237–246
- Vasil IK (2003) The science and politics of plant biotechnology—a personal perspective. *Nat Biotechnol* 21:849–851
- Yu H, Chen M, Nie L, Lu X, Ming X, Zheng H, Qu LJ, Chen Z (1999) Recovery of transgenic orchid plants with hygromycin selection by particle bombardment to protocorms. *Plant Cell Tissue Organ Cult* 58:87–92